Next Generation Risk Assessment of Organophosphate Pesticides

Thijs M.J.A. Moerenhout

Propositions

1. Next generation risk assessment for humans and test animals quantifies interspecies toxicological differences. (this thesis)

2. Animal free risk assessment requires human-derived in vivo validation data. (this thesis)

3. Writing and publishing papers is an inefficient way of disseminating information.

4. Code of computational projects in science needs to be open source and include a user interface.

5. Use of proprietary software by government funded institutions limits software innovation and accessibility.

6. Learning a programming language helps to develop a framework for structured thinking.

Propositions belonging to the thesis, entitled
Next Generation Risk Assessment of Organophosphate Pesticides

Thijs M.J.A. Moerenhout
Wageningen, 11 september 2026

Next Generation Risk Assessment of Organophosphate Pesticides

Thijs M.J.A. Moerenhout

Thesis committee

Promotor

Dr Nynke I. Kramer
Associate professor in Toxicology
Wageningen University & Research

Co-promotor

Prof. Dr *ir.* Hans Bouwmeester
Professor in Toxicology
Wageningen University & Research

Other members

Prof. Dr *ir.* P.J. van de Brink, Wageningen University & Research
Prof. Dr R. Gehring, Utrecht University
Prof. Dr *ir.* A.J. Hendriks, Radboud University, Nijmegen
Prof. Dr M. Luijten, Leiden University

This research was conducted under the auspices of the Graduate School VLAG (Biobased, Biomolecular, Chemical, Food and Nutritional Sciences)

Next Generation Risk Assessment of Organophosphate Pesticides

Thesis

submitted in fulfilment of the requirements for the degree of doctor
at Wageningen University
by the authority of the Rector Magnificus,
Prof. Dr C. Kroeze,
in the presence of the
Thesis Committee appointed by the Academic Board
to be defended in public
on Friday 11 September 2026
at 3.30 p.m. in the Omnia Auditorium.

Thijs M.J.A. Moerenhout

Next Generation Risk Assessment of Organophosphate Pesticides,

157 pages.

PhD thesis, Wageningen University, Wageningen, the Netherlands (2026)

With references, with summary in English

DOI: 10.18174/681718

ISBN: 978-94-6534-510-9

Table of contents

Chapter 1 **7**
General introduction

Chapter 2 **21**
Development of a generic physiologically based kinetic model for the prediction of internal exposure to organophosphate pesticides

Chapter 3 **39**
Next generation risk assessment of acute neurotoxicity from organophosphate exposures using the in vitro–in silico derived dietary comparator ratio

Chapter 4 **57**
The effect of glutathione-mediated metabolism of organophosphate pesticides on rat and human *in vivo* toxicokinetics investigated using physiologically based kinetic modelling

Chapter 5 **75**
Application of new approach methodologies for point of departure prediction in organophosphate pesticide hazard assessment

Chapter 6 **109**
General discussion

References 123

Summary 147

Acknowledgements 149

Biography 154

List of publications 155

Overview of training activities 156

Funding 157

1

General introduction

1. Pesticide use and pollution

In the last decades, the world has seen a significant increase in population growth. Currently in 2025, the world population is estimated at about 8 billion and surpassing 10 billion within in 40 years (1). At the same time, human pollution causes climate change, putting strain on populations worldwide, not only because of natural disasters, but also by limiting agricultural efficiency and therefore crop yield and food availability. Various methods are used to maintain adequate yields and protect local and global food chains. While earlier methods focused on planning and optimization, half way through the 20th century the use of pesticides took over. Initially organochlorines were popular insecticides. Later, organochlorines were replaced by organophosphate and carbamate pesticides, since these are less persistent in the environment (2). Studies have estimated crop loss due to pests was reduced by 35-42% due to pesticide use (Pimentel D. 1997, via (3)). Pesticides can be subdivided in rodenticides, insecticides, fungicides, bactericides and herbicides, which are compounds that protect crops from rodents, insects, fungi, bacteria and weeds respectively. While pesticide use increased until, and stagnated after, 2007, overall insecticide use has declined. Between 2010 and 2014, the global average of pesticide use was 2.78 kg per hectare. While Japan, China and Mexico had the highest pesticide use in the same period, using between 8-19 kg per hectare (3). In current day agriculture, an estimated 1/3 of crops are treated with pesticides. To prevent excessive application of pesticides, these compounds are heavily regulated in some parts of the world. Meanwhile, excessive use in other, less regulated parts of the world results in environmental pollution, poisoning local flora and fauna, and potentially humans. To minimize environmental pollution and effects in/on non-target species, it is advised to limit the use of chemical pesticides and increase the use of bio-pesticides, use pesticide mixtures to lower resistance and apply precision pesticide use methods to lower pesticide use and limit off-target effects (3). Biopesticides are either chemicals with pesticidal activity derived from plants, or microbial, viral, biochemical entities used to deter or kill pests. While these methods are being developed and their adoption is limited for now, chemical pesticides are still very popular up to this day. Organophosphate pesticides remained the most used type of chemical insecticides used in 1995 and 2014 (3,4) and are still extensively used today.

2. Organophosphate pesticides

2.1 Compound and chemistry

Organophosphate (OP) pesticides are a subgroup of organophosphorus compounds and contain a central phosphorus atom, which is usually bound by four oxygen atoms, but for some OP pesticides, one or two of these oxygens are substituted by sulfur atoms; this is different from organophosphorus compounds, which can be bound to other types of atoms as well, like carbon or nitrogen (5). One of these oxygen or sulfur atoms shares a double bond with the central phosphor atom, while the other three are also bound to other atoms. In case the phosphate has a double bond with a sulfur atom, it is called a(n organo-) phosphorothioate or thiophosphate, subsequently referred to as an OTP. If the central phosphorus atom has a double bond to an oxygen, the compound is called a phosphate or (organophosphate-) oxon (OPO). The other three oxygen or sulfur atoms

are usually also bound to alkyl or aryl carbon structures (5). Classical OP pesticides contain one aryl (rest) structure and two ethyl or methyl groups (see **figure 1**). The rest structure is designed to be a good leaving group, optimizing it's reaction with various esterases.

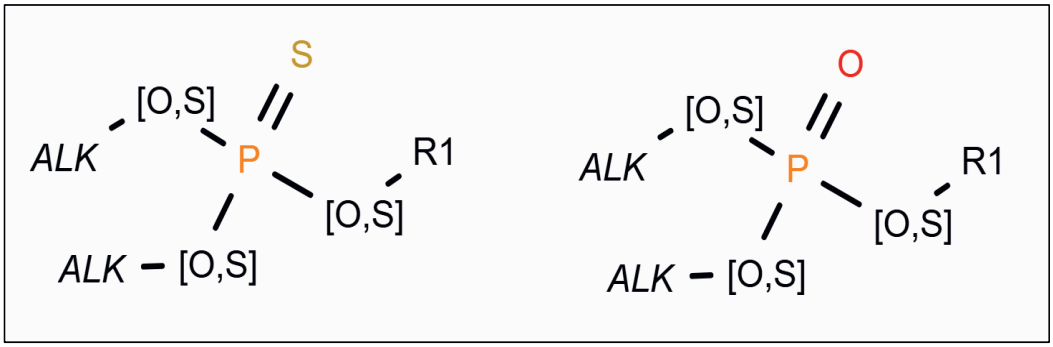


Figure 1: Chemical structures of organothiophosphate (OTP; left) and organophosphate oxon (OPO; right) pesticides. Usually these compounds have two or less sulfur atoms bound to the phosphor atom. Alkyl groups (ALK) are often methyl or ethyl groups, however other alkyl groups are possible as well. The rest group (R1) often has a group containing a resonance structure, like phenols or amides. Structures were visualized with Ketcher 3.4.

2.2 Toxicity

The toxicological effects of organophosphates are mostly caused by OPOs. OPOs are known to interact with acetylcholinesterase (AChE), buturylcholinesterase (BuChE), neuropathy target esterase (NTE) and carboxylesterases (CES). Of these enzymes, the inhibition of AChE is most studied and is considered to be the primary mechanism of action of organophosphate pesticides.

AChE is a naturally occurring enzyme in nearly all tissues of most animals, ranging from insects to fishes and from birds to mammals (6–11). It is highly concentrated in neuronal and muscle tissue, where it breaks down the neurotransmitter acetylcholine. As a neurotransmitter, acetylcholine is mostly present in synapses in the central nervous system, as well as in neuromuscular junctions. However, it can also be found on the membranes of red blood cells (12). Controlled release and breakdown of acetylcholine is essential for normal functioning of the body. Acetylcholine is released by presynaptic neurons, after which it activates the postsynaptic structure, being another neuron or a muscle fibre. AChE then breaks down acetylcholine to prevent overstimulation of this postsynaptic structure. The oxon (OPO) subtype of organophosphate pesticides is able to bind efficiently to AChE in the same binding pocket as acetylcholine (13,14). Here, the OPO can phosphorylate the enzyme by binding covalently to a serine residue of the enzyme (reaction 1 in **figure 2**), replacing and releasing the rest group (R1 in **figure 1**). Having a rest group that is easily released will therefore increase the potency of the organophosphate pesticide. The covalent bond between the enzyme and the OPO results in inhibition of the enzyme. However, the enzyme-OPO complex can undergo further hydrolysis. Depending on where in the molecule the hydrolysis reaction occurs, the enzyme can either be reactivated or it can become permanently inactivated. (13,14). If the OPO-enzyme bond is cleaved, the enzyme is reactivated (reaction 2 in **figure 2**) (15,16). If one of the rest or alkyl groups (ALK in **figure 1**) of the OPO part of the OPO-enzyme complex is cleaved, the enzyme is permanently inactivated (reaction 3 in **figure 2**) (17–19). This process is called

'aging'. This means that to regain the function lost from AChE inhibition, the aged enzyme needs to be replaced by a new AChE molecule. Similar mechanisms are thought to affect BuChE, NTE and CES inhibition, (20–23) where initial inhibition can be reversed or made permanent by further hydrolysis of the OPO moiety in the OPO-enzyme complex.

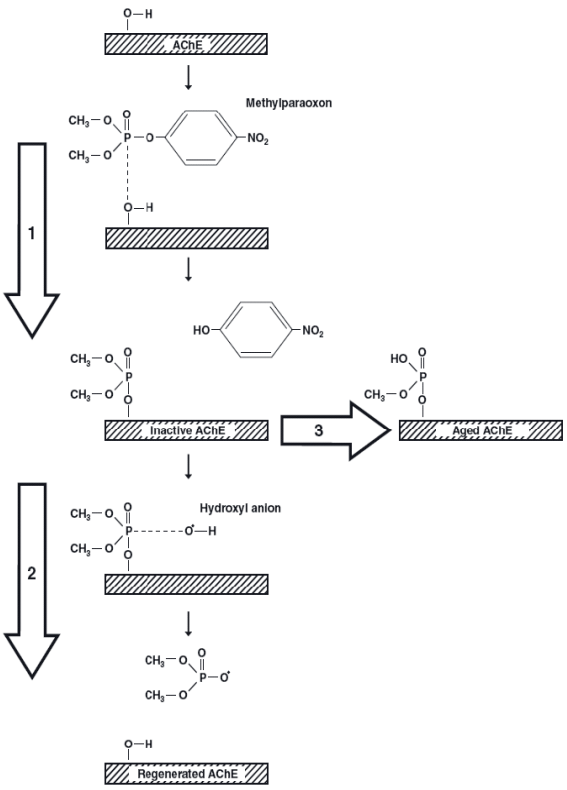


Figure 2: Binding, reactivation and aging of acetylcholinesterase (AChE) by the organophosphate methyl-paraoxon. Reaction 1: Covalent binding of organophosphate pesticide (methylparaoxon) to AChE. In this reaction, the rest group (ring structure; R1 in figure 1) is released. Reaction 2: Regenerated/reactivated of the enzyme by breaking the covalent bond between the phosphate and AChE. Hydroxyl anions, formed from normal temporary dissociation of water molecules, can bind to the phosphate, releasing it from the enzyme. Reaction 3: Irriversible binding of the organophosphate pesticide to AChE (aging). Alternatively to reaction 2, one of the alkyl groups (ALK in figure 1) is broken instead of the bond between the organophosphate pesticide and AChE. Figure taken from Eddleston et al. (24).

Butyrylcholinesterase is located in nearly all tissues in the body. However, the most prevalent locations are the liver, intestine and the plasma. (10,25) BuChE is produced in the liver and released into plasma, where, according to a limited amount of data, it might be associated with lipoprotein particles (26,27). The endogenous biological function of BuChE is not clear, however studies show relations between BuChE function and lipid metabolism and obesity (25,26,28,29). Inhibition of BuChE by OP pesticides has not been directly associated with any direct implications.

Neuropathy target esterase has mostly been found in the nervous system, placenta, kidney and the testes, where it is localized in the endoplasmic reticulum and lipid droplets (30). Here it acts as a phospholipase with high affinity for (lyso)phosphatidylcholine (31,32). NTE is important for proper neuronal development, axonal and myelin maintenance and membrane homeostasis. Inhibition or loss of function mutations of the enzyme are associated with neurodegenerative diseases (33).

Carboxylesterases can be found in most tissues, but are highly expressed in the liver (CES1) and intestine (CES2) (34). In some species, but not in humans, CES can also be found in plasma (35,36). The enzyme is strongly associated with lipid metabolism, and has endogenous ligands such as

cholesterol esters, triglycerides and other glycerides. Inhibition of CES by OP pesticides (37–39) was indirectly associated with atherosclerosis (40).

The physiological symptoms of organophosphate intoxication are summarized in **table 1**, along with their associated references. Most of the physiological symptoms are associated with AChE inhibition, which leads to cholinergic syndrome and potentially intermediate syndrome. Organophosphate induced delayed neuropathy (OPIDN) is thought to be caused by inhibition of NTE, while the mechanism of organophosphate-induced chronic neurotoxicity (OPICN), a collection of various long term behavioral changes, is poorly understood. Lastly, some neurodegenerative diseases have been associated with organophosphate exposure. One study showed 53% higher Alzheimer's disease incidence in individuals occupationally exposed to OP pesticides (41). A limited number of studies, found a consistent association of increased risk of Parkinson's disease in OP pesticide exposed individuals (42–46). While associations with neurodegenerative diseases have been found, their mechanism of action is currently not understood. Organophosphate pesticides can cause many symptoms and types of neurotoxicities. However, which specific pesticides causes what toxicity can depend on how the compound is absorbed, distributed and cleared by the body (i.e. its kinetics), and how it reacts with its target enzymes (i.e. its dynamics).

2.3 Exposure and toxicokinetics

Exposure to organophosphate pesticides can be subdivided into four exposure scenarios: passive exposure of the general population, occupational exposures, environmental exposures, and high dose exposures. Since organophosphate pesticides are often used in agricultural setting, the general public is mainly exposed to these compounds via foods, such as vegetables and fruits. While most foods are washed thoroughly before they end up in the supermarket, pesticide residues will always be present to some extent (72). Therefore, passive exposure of the general population to organophosphate pesticides mainly occurs via the oral route. Other routes of exposure that are of concern are respiratory (inhalation) and dermal exposures. These routes of exposure are of interest occupational and environmental exposures (73). Occupational exposures generally occur when people synthesize or apply the pesticides. Such exposures would result in comparatively high dose exposures when pesticides come into contact with the skin or are inhaled. Meanwhile, environmental exposures occur when people live or get close to areas where pesticides are used or produced. In these areas pesticides can become airborne, in the form of (spraying) droplets or gasses, and/or can be deposited on foliage nearby. Furthermore, wind and rain can carry the pesticide away from the field and into it's surroundings. Living or getting close to these areas can result in medium to low dose exposure via skin or inhalation routes. Lastly, high dose exposure can occur, for example, when a person accidentally ingest pure pesticide formulation, resulting in very high oral exposure.

Table 1: Overview of neurotoxic effects of organophosphate pesticides.

Neurotoxic effect	Time	Organophosphorus type	Symptoms	Mechanism	References
Cholinergic syndrome	Minutes to hours after exposure	Most OP and organophosphorus compounds	Sweating, cyanosis, lacrimation, salivation, miosis and ataxia, dyspnea, wheezing, bradycardia, vomiting, involuntary defecation and urination, nausea, headache, dizziness, confusion. In extreme cases: seizures and convulsions, coma and respiratory failure.	Due to inhibition of AChE, neurotransmitter acetylcholine is not broken down and keeps activating post synaptic neurons or muscles. General overstimulation of cholinergic nervous system.	(47–49)
Intermediate syndrome	24-96 hours after exposure	Mostly dimethyl OPs, however other OPs and organophosphorus compounds have also been reported	Respiratory weakness and paralysis, and weakness in muscles throughout the body.	Overstimulation of cholinergic receptors at postsynaptic structure causes the cells to adapt and reduce cholinergic receptor density. Overstimulation of presynaptic cholinergic receptors might reduce acetylcholine release.	(50–54)
Organophosphate induced delayed neuropathy	10-20 days after exposure	Phosphonates and phosphoramidates OPs with longer alkyl chain lengths and hydrophobic rest groups, not containing thioethers or nitrophenols.	Weakness in muscles and loss of sensation in extremities.	Effects of inhibition of neuropathy target esterase result in degeneration of the myelin sheath of axons of long/peripheral neurons. This causes neuronal signal transduction to become disrupted and induces denervation of muscles. Autoantibodies against neuronal proteins.	Johnson 1982 via (55) (56–65)
Organophosphate-induced chronic neurotoxicity	repeated, chronic exposure Long term	Not specified	Neurobehavioral and neuropsychological effects: learning, memory, attention, response speed, coordination and orientation, mood, fine motor control. Not all may apply.	Specific mechanism not known. Often not correlated with AChE inhibition. Effects could be both positive and negative and can vary a lot per pesticide.	(66–71)

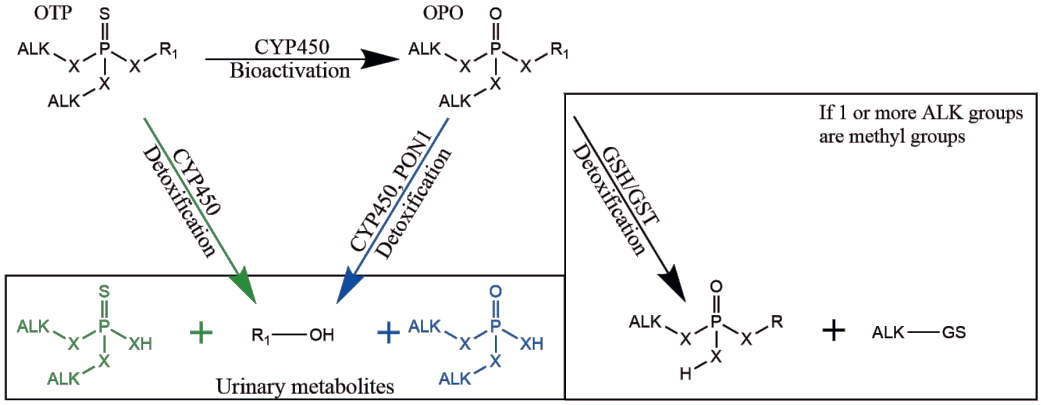


Figure 3: Metabolic scheme of organothiophosphate (OTP) and organophosphate-oxon (OPO) pesticides. In the structures, X can be a sulfur or an oxygen atom, and, usually, no more than two sulfur atoms are bound to the phosphor atom. OTPs and OPOs contain a sulfur or an oxygen atom, respectively, which is connected via a double bond to the central phosphate. ALK are alkyl groups, typically methyl or ethyl, and sometimes propyl groups. R1 can be aromatic or aliphatic. In the liver, OTPs can be detoxified to urinary metabolites by CYP450-mediated oxidative cleavage of the ring structure, or they can be bioactivated to OPOs by CYP450-mediated oxidative desulfuration. OPOs can be detoxified to urinary metabolites by CYP450-mediated oxidative cleavage of the ring structure in the liver or hydrolysis by paraoxonase 1 (PON1) enzymes in the plasma and liver. Glutathione-mediated (GSH/GST) detoxification only takes place if at least one of the alkyl groups (A1 or A2) is a methyl group.

Once exposed, absorption of organophosphate pesticides via the oral route occurs rapidly and, based on their lipophilicity and charge (74,75), are distributed throughout organs and tissues. In the liver OTPs and OPOs rapidly metabolized (see **figure 3**). OTPs are bioactivated to OPOs as well as detoxified by cleavage of the rest group (R1 in **figure 3**). For OTPs, both these reactions are performed by cytochrome P450 (CYP450) enzymes (76–81). OPOs can also be detoxified by cleavage of the rest group. This reaction can be performed by CYP450 enzymes and paraoxanase-1 (PON1) in the liver, as well as PON1 associated with high density lipoprotein particles in plasma (82–84). Furthermore, for di-methyl-organophosphates, a subclass of organophosphate pesticides, the methyl-moieties attached to the phosphate are also able to react with glutathione. In this detoxification reaction, glutathione-S-methyl as well as the de-methylated organophosphate are formed and glutathione-S-transferase (GST) might be required for this reaction to occur (85–97).

Renal excretion of organophosphates and their metabolites is largely dependent on their ability to bind plasma proteins, where higher plasma protein binding is correlated to lower renal excretion. Most organophosphate pesticides, with some exceptions, bind extensively to plasma proteins and are therefore mostly cleared via metabolic processes as opposed to excretion via the kidneys. However, detoxification products (cleaved rest group and de-methylated organophosphate) of organophosphate pesticides are usually extensively cleared via the kidney, either as glucuronidated or sulfonidated conjugates or in unconjugated form.

3. Chemical risk assessment

Up until the current day, traditional chemical risk assessment relies largely on animal toxicity studies. Data from these animal experiments often consist of doses at which no or low adverse

effects are detected in animals and are appropriately named the no- and low-observed-adverse-effect-levels (NOAEL and LOAEL, respectively). The NOAEL and LOAEL are often used to determine the highest safe dose, which is often termed as the point of departure (PoD). Any exposure to a dose higher than the point of departure is assumed to possibly cause adverse effects. Another method to derive the point of departure is by fitting statistical models to dose-effect data, which is known as benchmark dose modelling (BMD). BMD modelling is preferred for point of departure determination in risk assessment since it is able to incorporate data variation, does not depend on the specific doses tested, and can be adjusted based on how strong of an effect is considered to be adverse. (98) The point of departure is used to determine the dose that does not cause adverse effects during a lifetime in a species for a specific route of exposure. This is called the reference dose (RfD). The reference dose in humans is derived from the point of departure determined in animal experiments. The animal point of departure is divided by an uncertainty factor of 10 for differences in physiology between humans and experimental animals (species differences) and divided by an uncertainty factor of 10 again for differences between the average and most sensitive humans in a population (interindividual differences) (99). Other uncertainty factors can be applied as well, for example, when translating points of departure from acute exposure studies to chronic exposure situations (100,101).

For traditional risk assessment, large numbers of animals are exposed to increasing doses of a chemical, after which the animals are killed and studied for any adverse effects (102). While for a long time, this was the best available method and golden standard for risk assessment, this approach has been scrutinized in the past years based on both ethical, scientific and economic grounds. The scientific reasoning being that various lab animal species do not properly represent the human physiology and therefore toxicity measured in those animals does not properly translate to humans (103). Furthermore, the uncertainty factors used to translate points of departure from animal studies to humans lack a scientific basis. Economic reasoning is based on the high costs in both time and money to perform animal testing, limiting companies in both the ability and the speed of developing new drugs and chemicals.

The first initiative to step away from animal testing was started by Russel and Birch, who published their famous book about the replacement, reduction and refinement (3Rs) of animal testing and proposed an initial framework to minimize and steer away from animal testing (104). In the current day, this framework has been refined under next generation risk assessment (NGRA). NGRA focusses on the use of novel assessment methodologies (NAMs), which are in vitro, in silico or in chemico methods and tools to derive human centric toxicity and risk assessment data (105–107). Physiologically based kinetic modelling and in vitro toxicity testing are essential tools in next generation risk assessment.

4. Physiologically based kinetic modelling

Physiologically based kinetic (PBK) modelling is a mathematical modelling approach that enables predictions of concentrations in specific tissues and organs in the body (108). This allows for the estimation of internal exposure at target tissues for a specific external exposure. This approach initially evolved from compartmental modelling, in which the body was described in one to three compartments for which simple equations were fitted to in vivo data. Meanwhile, PBK modelling uses differential equations to describe the change in a variable (for example the amount of moles of compound present in the liver) over time. While this approach has the potential to more

mechanistically predict exposures in an organism, it requires thorough knowledge of what physiological and kinetic processes are at play to accurately predict internal exposures (109). Examples of such processes are transport and absorption of the compound through the gastrointestinal tract; metabolism in the liver, or active transport by transporter proteins in the blood-brain-barrier, kidneys or other tissues; specific binding to cell/tissue components (DNA, proteins). In most cases, much of this information is lacking, which often leads to parameter fitting. While this introduces significant uncertainty in the predictions of internal concentrations at other exposure levels/scenarios than for which the model was optimized, it will usually allow for reliable predictions for similar exposures.

Since PBK modelling provides a mechanistic and modular platform for internal exposure prediction, it can be expanded upon to allow for different situations or outcomes. Different types of PBK models include: deterministic, population and probability models. While deterministic models are specifically for one individual and one chemical (with it's metabolites), population models use distributions to describe the variation in each physiological or physicochemical parameter. This way the model is parameterized for a population of individuals. Probability models are similar to population models in terms of including variation of parameters, however these models also include parameter variation for or uncertainty in chemical parameters; like the octanol:water partition coefficient (logP or $\log K_{o/w}$). These three types of PBK models can be adapted for many different situations, like pregnancy, life-stage or disease models, and can be adapted for specific organisms. While all these kinds of models are theoretically possible, they strongly depend on the availability of the required parameters.

The main parameters required for PBK models are physiological, chemical and kinetic (or physicochemical) parameters. Physiological parameters mainly consist of weights and blood flows of organs and tissues (110) and describe those organs and tissues in a mathematical way. Meanwhile kinetic parameters describe the interaction between physiology and a compound. Many of the essential kinetic parameters can be estimated in silico using algorithms or quantitative structure property relationships (QSPRs), for which chemical parameters, like the logP and pKa are required. Kinetic parameters that can be estimated using in silico methods are intestinal absorption rate constants (111–114), tissue:plasma or tissue:blood partition coefficients (75,115–118), the unbound fraction in plasma (119) and the blood:plasma ratio (120). Some of these parameters can also be determined in vitro. For example, intestinal absorption rate constants can be derived from apparent permeability (P_{app}) values measured in vitro in the caco-2 permeability assay (121) or the parallel artificial membrane permeability assay (PAMPA) (122). Furthermore, the unbound fraction in plasma (fu_p) can be determined using in vitro assays like the rapid equilibrium dialysis (RED) (123) and solid phase microextraction (SPME) (124). Other kinetic parameters can only be predicted using in vitro experiments. This is especially true for processes like metabolism or active transport, which are essential for modelling most compounds. Metabolism is usually quantified using in vitro experiments using (liver) subcellular fractions, namely: microsomes, cytosol, S9; which contain phase I, phase II and both phase I and II enzymes, respectively (125,126). Other approaches include the use of recombinant enzymes and hepatocytes, of which the latter also includes the effects of transport into or out of the cell. These assays provide clearance rates or Michaelis-Menten parameters (V_{max} and K_m) (127), which can be scaled to the in vivo situation (128,129). Meanwhile, active transport is not yet easy to incorporate, since transporter specific parameters are hard to determine reliably in vitro, and scaling to the in vivo situation is currently not possible. Therefore, active transport parameters are often fitted. While the physiological and

kinetic parameters describe a relatively simple PBK model, it can be expanded upon by including submodels for specific exposure routes, like inhalation, dermal or oral exposures. Furthermore, dynamic (effect) interactions, like activating or inhibiting a specific enzyme, can be included as well. For example, for organophosphates specifically, parameters describing the binding interactions with AChE and BuChE can be determined in the lab and used to model their binding, aging and reactivation as well (130,131).

While PBK models have been around for more than 65 years (132), there is still not enough trust in initial PBK model predictions to allow them to replace animal testing for regulation purposes. This is mainly due to the lack of compound specific parameter data and proper understanding of all significant kinetic processes, like metabolic and/or active transport reactions. Therefore, it is important to validate the model against in vivo data. While thorough validation compares predicted to in vivo measured concentration-time profiles of an exposure, it is also possible to validate against pharmacokinetic or toxicokinetic parameters like C_{max}, T_{max} and the area under the curve (AUC). For compound specific models, predictions are considered accurate if they are within a 2-fold difference from in vivo data (133). For generic models, which are PBK models that can be used to model internal concentrations of a group or spectrum of compounds, currently no criterion is generally accepted, however a criterion of a 5-fold difference has been proposed (112). These criteria are based on variation due to interindividual differences and differences in study design and compound quantification.

5. Translating in vitro toxicity data to in vivo situations

In vitro experiments are performed using cells or proteins, and have the benefit of using species specific material to test on. This removes the need for interspecies extrapolation and gives a quantitative indication of species differences. In vitro experiments for investigation of kinetic processes have been discussed in the section above. However, in vitro experiments can also be used for toxicity testing.

There is a multitude of in vitro assays that can be performed to asses various kinds of toxicity endpoints. Toxicity testing can be performed for very general endpoints, or for functional (specific) endpoints. Cell death/viability can be considered a general endpoint and is often measured by LDH, CFDA, Alamar blue or MTT assays (134). There are many more cell viability assays that give specific information in the mechanism of cell death (134) of which apoptosis, autophagy, necrosis, are most well known, but various other mechanisms exist (135). Other general effects can be investigated using any kinds of omics approach (proteomics, transcriptomics, genomics, metabolomics, lipidomics and epigenomics), which gain insight into changes in gene transcription and translation, and cellular metabolites and lipids (136). More functional assays associated with receptor/enzyme binding or inhibition. Reporter gene assays give quantitative information on receptor activation and subsequent gene activation. An example of a reporter gene assay is the Chemically Activated LUciferase eXpression (CALUX) assay. This is a cell-based assay which enables quantitative correlation between receptor activation and gene expression, as was done for the estrogen receptor for example (137). Other functional assays rely on measuring enzyme activity, providing information about the stimulatory or inhibitory effect of a compound on the enzyme. For example, the Ellman assay (138) can be used for investigating the inhibition of AChE by organophosphate pesticides for example (12). All of these in vitro assays, for general and functional endpoints, provide data in the form of a

concentration-effect relation, which needs to be translated to the in vivo situation in order to be useful for chemical risk assessment.

While PBK modelling can be used to gain more insight into how a compound is absorbed, distributed, metabolized and excreted, it can also be used for translating concentration-effect data from in vitro experiments to the in vivo situation. This approach is called quantitative in vitro to in vivo extrapolation (QIVIVE) and combines in vitro experiments with PBK modelling by translating in vitro determined concentration-effect curves to in vivo dose-response curves. The PBK model can be used to investigate what dose is needed to reach the concentrations at which these effects, measured in vitro, occur in the target organ in vivo. Once a QIVIVE based dose-response curve has been obtained for the in vivo situation, benchmark dose modelling can be used to define a point of departure (139,140). Alternatively, the dietary comparator ratio (DCR) approach could be used to determine a dose at which no adverse effects are expected (141). In this approach, a ratio is calculated between the in vitro derived 50% effect concentration (EC_{50}) and lower limit of the 5% effect concentration of a well researched compound. This ratio is considered safe. For other exposures and compounds (within the same class as the well researched compound) a ratio is calculated between the compound specific in vitro determined EC_{50} and PBK-predicted internal concentration. This ratio is compared to the safe ratio of the well researched compound. Ratios higher than the safe ratio are considered dangerous, likely resulting in toxic effects (141). The QIVIVE and DCR approaches could be used to determine from what dose a chemical can be toxic. This in turn can be used to guide regulatory safe values and therefore legislation.

6. Thesis aim and outline

In this thesis we aim to evaluate the QIVIVE and DCR approaches for application in chemical class specific next generation risk assessment, based on new assessment methodologies, using organophosphate pesticides as a model compound class. In the next chapters it is shown how these methods can be implemented for use in next generation risk assessment.

In **chapter 2** the development and evaluation of a physiologically based kinetic model is described in detail. This model can be used to predict blood and plasma concentrations of eight organophosphate pesticides and their metabolites after oral exposure.

Safety evaluation of organophosphate pesticides was performed using the Dietary Comparator Ratio method in **chapter 3**. Here the developed physiologically based kinetic model is used to determine blood concentrations of reported in vivo exposures to organophosphate pesticides. These concentrations are used in the DCR method to predict if exposures to organophosphate pesticides will result in adverse effects or not.

Findings in chapter 2 and 3 showed that predicted blood concentrations and safety evaluations were less accurate for dimethyl-organophosphate pesticides compared to other organophosphate pesticides. In **chapter 4** glutathione dependent metabolism of dimethyl-organophosphate pesticides was characterized using in vitro metabolism experiments. Glutathione dependent metabolism was implemented in the physiologically based kinetic model developed in chapter 2 to improve blood concentration predictions for dimethyl-organophosphate pesticide exposures.

In **chapter 5** hazard characterization was performed for eight organophosphate pesticides. Concentration dependent AChE inhibition data was derived using in vitro experiments for each pesticides and active metabolite. Quantitative in vitro to in vivo extrapolation (QIVIVE) and benchmark dose modelling was then used to predict in vivo AChE inhibition in blood.

Lastly, in **chapter 6** all results are summarized, and suggestions and recommendations for future organophosphate pesticide research and physiologically based kinetic modelling efforts are discussed.

2

Development of a generic physiologically based kinetic model for the prediction of internal exposure to organophosphate pesticides

Thijs M.J.A. Moerenhout, Jiaqi Chen, Hans Bouwmeester,
Ivonne M.C.M. Rietjens and Nynke I. Kramer

Environ. Sci. Technol. 2024, 58, 42, 18834–18845

Abstract

Since their introduction in agriculture, the toxicity of organophosphate (OP) pesticides has been widely studied in animal models. However, next generation risk assessment (NGRA) intends to maximize the use of novel approach methodologies (NAMs), based on in vitro and in silico methods. Therefore, this study describes the development and evaluation of a generic physiologically based kinetic (PBK) model for organophosphate pesticides in rats and humans using quantitative structure property relationships (QSPRs) and data from published in vitro-studies. The models were evaluated using in vivo studies from literature for chlorpyrifos, diazinon, fenitrothion, methyl-parathion, ethyl-parathion, dimethoate, chlorfenvinphos and profenofos. Model evaluation was performed by comparing simulated and in vivo observed time profiles for blood, plasma or urinary concentrations, and other toxicokinetic parameters. Of simulated concentration-time profiles, 87% and 91% were within a 5-fold difference from observed toxicokinetic data from rat and human studies, respectively. Only for di-methyl-organophosphates further refinement of the model is required. It is concluded that the developed generic PBK model provides a new tool to assess species differences in rat and human kinetics of organophosphate pesticides. This approach provides a means to perform NGRA for these compounds and could be adopted for other classes of compounds as well.

1. Introduction

Although numerous organophosphate (OP) pesticides have been banned in various countries (142), OPs are still a widely used class of pesticides (143). Two major classes of OP pesticides can be distinguished: organothiophosphates (OTPs) and organophosphate-oxons (OPOs; **figure 1**). Many OP pesticides are OTPs, which can be bioactivated to OPOs by oxidative desulfuration. Both OTPs and OPOs can also be detoxified by cytochromes P450 (CYP450)-mediated oxidative cleavage to hydrophilic metabolites (**figure 1**) that are excreted in urine. The mechanism of action of OP pesticides is based on inhibition of the enzyme acetylcholinesterase (AChE) by OPOs (13,14). AChE normally hydrolyses the neurotransmitter acetylcholine in the synaptic cleft. Inhibition of this enzyme results in an accumulation of acetylcholine in the synapse and subsequent overactivation of the cholinergic nervous system. While blocking of AChE in pest animals is very effective, and therefore works well for crop protection, concern has been raised with regards to exposure in non-target species, including humans. OPs and their metabolites have been repeatedly found in human blood, milk and urine (144–148). In addition, recent studies suggest a correlation between chronic exposure to OP pesticides and neurological complications in the form of neurodegenerative diseases like Parkinson's and Alzheimer's disease, possibly mediated by inhibition of AChE (149,150). Together, these studies raise questions about the adequacy of current pesticide regulations and the general safety of these compounds.

In the field of chemical risk assessment, there is a push towards developing and implementing non-animal test methods or so-called novel approach methodologies (NAMs). The use of these NAMs in risk assessments is termed Next Generation Risk Assessment (NGRA) (105,107,151). NAMs include *in silico* and *in vitro* approaches aimed at providing a molecular understanding of the kinetics, toxic mode of action and potency of chemicals. Last decades, NAMs, have also been used for risk assessment of individual OPs (131,152–158). These models were specifically designed for individual OPs, they have been helpful, not only in risk assessment for these specific compounds, but also in gaining general understanding of kinetic processes, in pushing for *in silico* modelling as an alternative to animal experiments and in elucidating interspecies differences in toxicity. However, to compare kinetics and predict (neuro)toxic potencies of different OPs in humans from *in vitro* data, a more generic approach would be of great value.

In the present study, we aim to develop a generic PBK model for OP pesticide exposure in rats and humans to predict tissue concentrations of OTPs and OPOs, the latter representing either the parent compound or the active metabolite of an OTP. To ensure adequate accuracy in the prediction of blood concentrations, the model was evaluated using *in vivo* experimentally obtained rat and human concentration-time profiles in blood and plasma or urinary excretion profiles found in literature for six OTPs (chlorpyrifos, diazinon, dimethoate, fenitrothion, methyl-parathion and ethyl-parathion) and two OPOs (chlorfenvinphos and profenofos) (**figure 1**) and their metabolites.

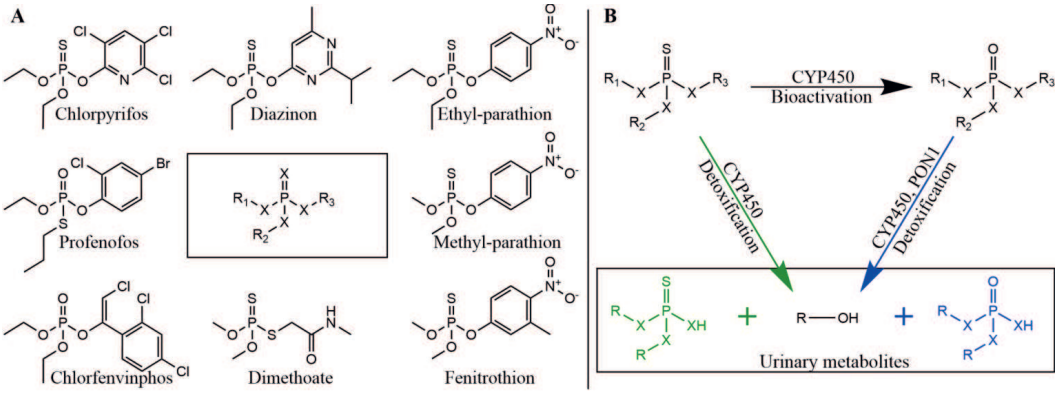


Figure 1: Structures and generalized metabolic pathway of organophosphate pesticides considered in this study. A: The central structure represents the general structure for organophosphate pesticides, where X can be a sulfur or an oxygen atom and usually no more than two sulfur atoms are bound to the phosphor atom. Organothiophosphates (OTP) and organophosphate-oxons (OPO) contain a sulfur or an oxygen atom, respectively, which is connected via a double bond to the central phosphate. R_1 and R_2 are alkyl groups, typically methyl or ethyl, and sometimes propyl groups. R_3 can be aromatic or aliphatic (**SI table S1**). **B:** Metabolic scheme of OTP and OPO pesticides. In the liver, OTPs can be detoxified to urinary metabolites by CYP450-mediated oxidative cleavage, or they can be bioactivated to OPOs by CYP450-mediated oxidative desulfuration. OPOs can be detoxified to urinary metabolites by CYP450-mediated oxidative cleavage in the liver, or hydrolysis by paraoxonase 1 (PON1) enzymes in the plasma and liver.

2. Materials and methods

2.1 PBK model development

The PBK models were developed for the simulation of blood and plasma concentrations as well as urinary excretion of OPs and their metabolites in rats and humans after a single intravenous (IV) and oral dose. The rat and human models were evaluated by comparing model simulations with observed *in vivo* concentration-time profiles in blood, plasma and urine of rats and humans.

2.1.1 PBK model structure

The generic PBK models were developed based on literature describing PBK models for individual OPs (131,153–155,157,158) and contain a gastrointestinal absorption model and three submodels (**figure 2; SI PBK model**).

Absorption

For the general public, oral exposure via food is considered the main route of exposure to OP pesticides. Therefore, OP oral absorption was modelled using a compartmentalized stomach and intestinal model (114,159), since it more accurately predicts the temporal absorption profile compared to a mixed-tank model (114,159). The model consists of a stomach compartment, seven small intestine (SI) compartments, one large intestine compartment and a fecal compartment (114). Since most OPs are highly lipophilic, it was assumed that these compounds need bile acids to be dissolved and absorbed. Therefore OPs were assumed to only be absorbed in the small intestine, where bile acids are active (160). All orally absorbed OTP or OPO was assumed to enter the liver, where it can be metabolized or partition into the blood. Meanwhile unabsorbed OPs enter the colon and are excreted in the feces.

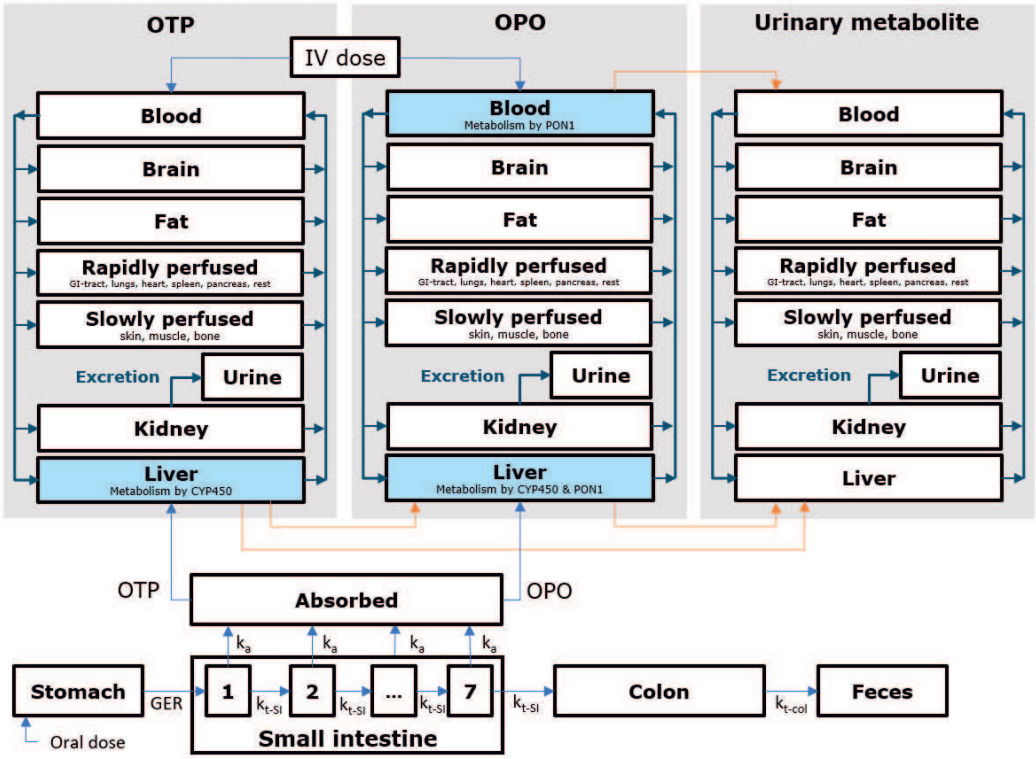


Figure 2: Schematic representation of the PBK model structure. Compounds are absorbed in the small intestine (bottom) and subsequently enter the liver of either the OTP or OPO sub-model. Metabolism by CYP450 is incorporated in the liver compartment of both the OTP and OPO submodels. For the OPO submodel, PON1 metabolism is also incorporated in the liver and blood compartments. Urinary excretion by glomerular filtration is incorporated in all sub-models. Metabolites from liver and blood are transferred to their respective submodels. This is represented by orange arrows, while distribution is represented by blue arrows. GER is the gastric emptying rate, $k_{t\text{-}SI}$ is the transit rate in the small intestine, k_a is the absorption rate constant, and $k_{t\text{-}col}$ is the transit time from colon to feces.

Distribution

Tissue distribution of OTPs, OPOs and urinary metabolites was described by their respective submodels, each containing eight compartments representing bodily tissues and urine. Distribution was assumed to be blood flow limited. Liver and kidney tissues are parametrized as individual compartments, since they are clearing organs. The brain is a target organ for OP pesticide toxicity and fat tissues act as reservoir for lipophilic OTP and OPO compounds. Therefore, these tissues modelled separately as well. Skin, muscle and bone tissues are lumped together in a slowly perfused compartment and the remaining tissues (lungs, heart, gastrointestinal, rest) are lumped together in a rapidly perfused compartment. All tissue compartments are connected by a single blood compartment. Distribution between blood and plasma is determined using the blood plasma ratio. Urinary metabolites were included in the model, since most of the available *in vivo* data consists of urinary excretion-time data and blood concentration-time profiles for OP urinary metabolites, which were used for model evaluation.

Metabolism and excretion

In the generic PBK model, the main metabolic reactions for OTPs and OPOs (**figure 1B**) are included. For OTPs, these consist of CYP450-mediated oxidative cleavage to the urinary metabolites, and oxidative desulfuration to the bioactive OPOs, both taking place in the liver. PON1 metabolism of OTPs has not been reported (or negligible) (161) and was therefore not included in the model. For OPOs, hepatic CYP450-mediated oxidative cleavage, as well as hepatic and plasma PON1-mediated hydrolysis are included (162). Passive renal excretion into the urine was described using a species-specific glomerular filtration rate.

2.1.2 PBK model parameterization

The averages of male and female physiological parameters for adult rats and humans were taken from literature (110) and scaled to body weight. For rats, the data are expected to have a tendency towards male physiology, since they are based on data from control animals in experimental studies, for which mostly male rats are used (110). For human parameters, a tendency towards Caucasian physiology is expected for similar reasons. Passage through the gut model is described by the gastric emptying rate, and the small intestinal and colonic transfer rates, respectively (114,163). Body weight corrected cardiac output and glomerular filtration rates were taken from literature (164). Scaling factors for liver and plasma metabolism were obtained from various sources and are reported in **SI table S2**, together with all physiological parameters.

Compound specific parameters

In this study, eight OP pesticides were used to evaluate the model: six OTPs chlorpyrifos, diazinon, fenitrothion, methyl-parathion, ethyl-parathion and dimethoate, and two OPOs chlorfenvinphos and profenofos. For these compounds and their metabolites, physicochemical parameters (log P and pKa) and their sources are shown in **SI table S3**.

For the determination of tissue:plasma partition coefficients, several QSPRs reported in literature (74,75,165,166) were considered. For OTPs and OPOs, the QSPR reported by Berezhhovsky (165) was used. The QSPR by De Jongh et al. was excluded since it inadequately predicted partition coefficients for ethyl-parathion (166). The QSPR by Rodgers and Roland (75) was only used for urinary metabolites, since it was the only QSPR including the charge of a molecule, while the predictive power of this QSPR diminishes for lipophilic compounds with a log P > 3 (167,168). All tissue:plasma partition coefficients were calculated using R code published previously (169). In an effort to keep the model as simple as possible, an 'average physicochemical entity' was created to represent both unconjugated and conjugated urinary metabolites together. This was done by taking the weighted average of the calculated fraction unbound in plasma (fu_p) and tissue:plasma partition coefficients for each derivative, based on the reported fraction of the respective chemical derivative found in urine (**SI table S4**). This enabled the simulation of distribution and excretion of all the derivatives at once. It must be noted that the current implementation assumes the ratios of different chemical derivatives to be independent of species and dose, and that all derivatives are produced in the liver.

Since previous studies showed that microsomal and blood metabolism of OP pesticides followed Michaelis-Menten kinetics (154,157,158), the maximum reaction rate (V_{max}) and the Michaelis-Menten constant (K_m) were used to describe CYP450- and PON1-mediated metabolism in the liver and plasma. These parameters were derived from *in vitro* experiments performed in the

present study (chlorfenvinphos), used from a similar compound (read-across from fenitrothion to methyl-parathion) or from literature (all other OPs; **SI table S5**). The data from literature were derived using pooled male rat, or pooled mixed gender human plasma, microsomal fractions and, in case of profenofos, cytosolic fractions (see references in **SI table S5**). For chlorfenvinphos, microsomal incubations were performed to determine the Michaelis-Menten parameters for CYP450-mediated dealkylation. No plasma incubations were performed, since multiple studies show minimal PON1-mediated metabolism of chlorfenvinphos in rats and humans (170,171). Since the primary metabolite des-ethyl-chlorfenvinphos was not commercially available, an analytical method for its identification and quantification was developed without the reference compound. Materials and methods for this experiment are described in the supporting information. When implementing metabolism in the model, the V_{max} was scaled by tissue weight using scaling factors (**SI table S2** and **SI PBK model**), while K_m was assumed to be similar *in vitro* and *in vivo*.

For the parent compounds (chlorpyrifos, diazinon, fenitrothion methyl-parathion, ethyl-parathion, chlorfenvinphos, dimethoate and profenofos), the absorption rate constant (k_a) was calculated for rats based on the method proposed in literature (112) and corrected using *ex vivo* absorption data for chlorpyrifos (172). The calculated values can be found in the supporting information (**SI: Calculation of absorption rate constant)**. For humans, predicted k_a values resulted in significant overpredictions of internal concentrations. Therefore, a k_a value was derived from fitting the parameter to the urinary excretion of 3,5,6-trichloropyridinol (TCP) in human exposure studies to chlorpyrifos of Timchalk et al. 2002 and Brzak et al. 2000 (131,173). This resulted in a k_a of 0.1, which was also used for other OPs in the human model. With this, minimal interindividual differences are assumed. This fixed k_a approach was used because incorporating the effects of food, formulation and interindividual differences on absorption into the current model fell outside the scope of this study.

2.1.3 PBK model corrections

During development, the model showed some deviations when comparing model simulations with reported *in vivo* profiles. Some of these deviations could be explained and corrected for. This was done for chlorpyrifos, diazinon, chlorfenvinphos, and the urinary metabolites of fenitrothion and profenofos: 3-methyl-4-nitrophenol (MNP) and 4-bromo-2-chlorophenol (BCP), respectively.

For chlorpyrifos and diazinon, some of the rat oral exposure studies showed a delay in absorption (131,174). Therefore, for these simulations, absorption was delayed by the same amount of time as the *in vivo* data indicated (1-2.5 hours; **SI figures S3, S5 and S10**). Furthermore, model simulations of the oral chlorpyrifos exposure studies in humans by Nolan et al. (175) (**SI figure S6**) were corrected by fitting the k_a as described above (see section 2.1.2).

Differences between simulated and *in vivo* profiles of chlorfenvinphos in rat (**SI figure S16**) were attributed to low recovery of the analytical method used in the exposure studies of Ikeda et al. (176,177). However, results from another study (178) showed that a similar analytical method, had low recovery (13%) at 1 µM, but less so at higher concentrations. Moreover, Boyer mentioned very strong plasma protein binding for the di-methyl-derivative of chlorfenvinphos (179). Since protein was not denatured in the analytical method, this explains the low recovery in the aforementioned *in vivo* studies. Therefore, *in vivo* blood and plasma concentrations after

oral exposure (all below 1µM), but not following IV exposure (all below 6 µM) were compared to the simulated unbound concentrations instead.

For MNP and BCP, active renal excretion was used, since literature suggests that phenol glucuronide- and sulfate-phenol conjugates are excreted actively at about 1.6 and 5.5 times the glomerular filtration rate in rainbow trout (180), and these compounds are extensively conjugated (**SI table S4**). Using cross-species extrapolation, these values were used to simulate the active excretion of the respective conjugates in rats and humans as well (adjusted for the ratio of conjugate present).

Lastly, *in vivo* data for 2-isopropyl-4-methyl-6-hydroxypyrimidine (IMHP) excretion in urine after exposure to diazinon was assumed to be only free, unconjugated IMHP, since another study reported IMHP being unstable during the acidic hydrolysis step to release IMHP from its conjugate molecule during sample preparation (174). Since the human *in vivo* IMHP data used here were taken from a risk assessment report, and the original study was not available in the literature, there was no information available on the specific analytical methods, thus the assumption could not be checked. The data used for evaluation of the model, reported in the results section, include the discussed corrections.

2.2 PBK model evaluation

Model performance was evaluated using available *in vivo* blood and plasma concentration-time and urinary excretion-time profiles after intravenous and oral OP exposure of rats and humans. Importantly, data of intravenous exposures allowed for evaluation of the distribution and clearance predictions, without being affected by variation in the absorption process or inaccuracies in the used *in vivo* studies. Only studies mentioning the route of exposure, the dose and the (average) bodyweight of the animals/volunteers were considered for evaluation (**SI table S6**). Blood and plasma concentration and urine excretion-time profiles for rats and humans were simulated and were compared to observed *in vivo* profiles. This was done qualitatively, by visually inspecting the overall fit and shape of the simulated concentration-time profile against *in vivo* profiles, and quantitatively, based on observed vs predicted plots and comparison of simulated and *in vivo* T_{max}, C_{max} and area under the concentration time curve (AUC) values. Predictions were considered adequate when simulated blood and plasma concentration-time or urinary excretion-time profiles were within a 5-fold difference from the respective *in vivo* profiles and the overall shape was visually similar. While the WHO states that model predictions of 2-fold difference from *in vivo* data are considered good predictions (181), high variability in observed studies with small sample sizes, combined with the development of a generic instead of a compound-specific PBK model, allows for acceptance of a larger difference (182). Therefore, predictions within a 5-fold difference from *in vivo* data, were considered adequate in this work.

2.3 Sensitivity analysis

Using the FME R package (183), a local sensitivity analysis was performed to determine the impact of individual parameters on the simulated maximum free concentration of OPO in blood. Sensitivity coefficients (SC) were calculated following the formula: $SC = \frac{\Delta C}{\Delta P} * \frac{P}{C}$ (183). Where C is the maximum free concentration of OPO in blood and P is the model parameter value. Input parameters were changed by 1% and the relative effect on the maximum free concentration of

OPO in blood was reported. Sensitivity analysis was performed at a dose of 1 mg/kg bodyweight for both rats and humans. This dose was selected to represent a dose that is close to the doses used in both rat and human *in vivo* studies. Using the same dose also allows for better comparison between the two species.

2.4 Software and data analysis

The R programming language (version 4.1.0) and R studio (version 1.4.1717) were used to develop the model. Several packages were used for modelling and data analysis. The *RxODE2* package (184) was used to solve the ordinary differential equations of the model. *Tidyverse* and *dplyr* were used to for data handling and *Readxl* and *xlsx* were used to read and write Excel files for in- and output, respectively. The *FME* package was used for sensitivity analysis. Microsoft Excel (version 16.0.14931.20764) and GraphPad Prism (version 5.04) and the R packages *ggplot2* and *patchwork* were used to analyse and visualize the data. GraphPad Prism was also used to derive the Michaelis-Menten parameters from data from incubation studies. WebPlotDigitizer (https://automeris.io/WebPlotDigitizer/) was used to extract *in vivo* concentration-time data from graphs in literature.

3. Results

To develop the PBK model, physiological, chemical and metabolic data are required. Physiological and chemical data were retrieved from literature or predicted using QSPRs (**SI tables S2 and S3**). Metabolic parameters were available in literature for all OPs (**SI table S5**) except for chlorfenvinphos, for which the metabolic parameters were determined experimentally in the present study.

3.1 Chlorfenvinphos metabolic incubation experiments

Microsomal incubations were performed with both rat and human liver microsomes to define the PBK model parameters for hepatic clearance of chlorfenvinphos. Des-ethyl-chlorfenvinphos was the only metabolite detected in the incubations. It was not produced if the incubations were performed without NADPH. Parameters describing the Michaelis-Menten kinetics of chlorfenvinphos metabolism were 0.46 and 0.57 nmol/min/mg microsomal protein for V_{max}, and 5.91 and 6.36 µM for the K_m for rat and human liver microsomes, respectively (**SI figure S1**). The catalytic efficiencies (calculated as V_{max}/K_m) were 78.0 and 88.9 µL/min/mg microsomal protein for rat and human liver microsomes respectively. The V_{max} and K_m were used to describe the metabolism of chlorfenvinphos in the human and rat models.

3.2 PBK model evaluation

Once all parameters for all eight OP pesticides (chlorpyrifos, diazinon, fenitrothion, methyl-parathion, ethyl-parathion, dimethoate, chlorfenvinphos, profenofos and metabolites) were collected, the generic model was developed (**SI PBK model**) and evaluated. The model was found to have an adequate mass balance, with the mass error of around $1e^{-12}$ µmol for runs using doses of 1 to 100 mg/kg body weight. Very low doses of 0.001 mg/kg bodyweight gave mass errors of $1e^{-9}$ µmol (data not shown), which are considered acceptable.

The studies considered for model evaluation are listed in **SI table S6.** The PBK model was evaluated by means of comparison of concentration-time plots (**figure 3A-C**), by plotting observed versus predicted concentrations (**figures 3D-F, 4, and 5**) and by comparison of predicted and *in vivo* observed toxicokinetic parameters (T_{max}, C_{max}, AUC; **SI table S7**). Data used for these comparisons included literature reported *in vivo* rat and human blood and plasma concentration-time profiles and urinary excretion profiles after intravenous and oral exposures. Toxicokinetic parameters were calculated for model simulations, as well as *in vivo* data that consisted of four or more datapoints. All simulated exposures are graphed separately in **SI figures S2-S19**.

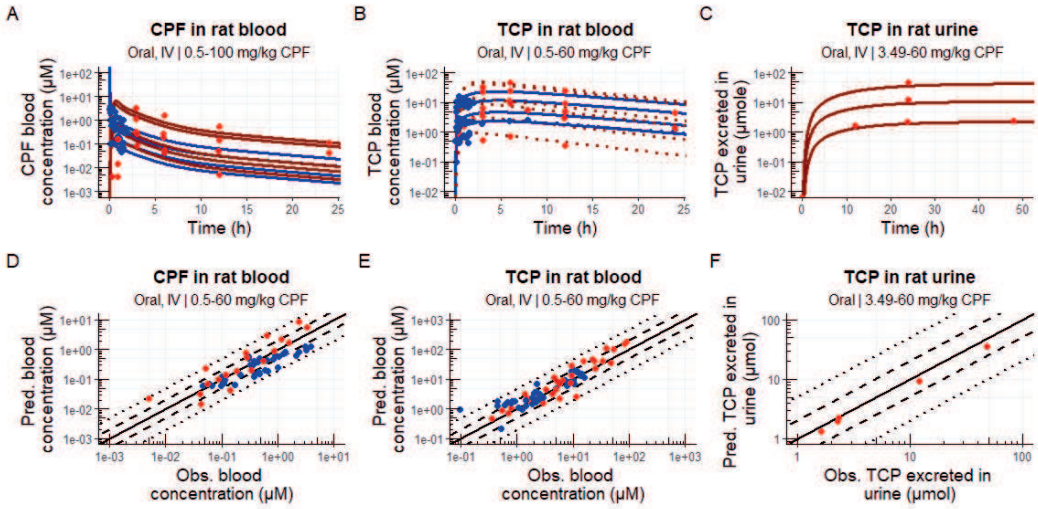


Figure 3: Simulated blood concentration- and urinary excretion-time profiles (A-C), and predicted versus observed data plots (D-F) for chlorpyrifos exposures in rats. Blue and red dots represent means of observed in vivo values after intravenous or oral doses, respectively, and similarly coloured solid and dotted lines represent simulated profiles (at different doses) of the total and unconjugated blood concentration, respectively. Unconjugated concentrations were based on conjugate ratios reported in **SI table S5**. In predicted versus observed data plots (D. E and F), lines representing perfect prediction (solid line), 2-fold difference (dashed lines) and 5-fold difference (dotted lines) are shown in black. See materials and methods for included corrections. Abbreviations: CPF: chlorpyrifos; TCP: 3,5,6-trichloropyridinol.

3.2.1 Simulations for OP exposures in rats

Simulations of OP exposures in rats were evaluated using predicted versus observed plots (**figures 3D-F and Figure 4**). *In vivo* data were well predicted by the rat model, with the exception of fenitro-oxon and methyl-paraoxon. For all simulations combined, 88% and 57% of simulated concentrations fell within 5-fold and 2-fold difference from *in vivo* data, respectively. These percentages were higher for IV (91.1% and 64.2%) than for oral exposures (85% and 46%). For each compound individually, excluding fenitro-oxon and methyl-paraoxon, at least 60% of predicted *in vivo* blood and plasma concentrations fell within a 5-fold difference for IV exposures. This was 40% for oral exposures. For fenitro-oxon and methyl-paraoxon all predictions fell outside the 5-fold difference from *in vivo* data.

Next, simulated and *in vivo* observed toxicokinetic parameters (T_{max}, C_{max} and AUC) were compared (**SI table S7**). All but one of the predicted T_{max} values, were predicted within a 5-fold

difference. Furthermore, for 37 out of 40 data sets, *in vivo* C_{max} and AUC values were predicted within a 5-fold difference from *in vivo* data. The three data sets for which the predicted C_{max} and AUC fell outside a 5-fold difference were for chlorpyrifos, diazinon and methyl-parathion. Predictions with a large fold difference compared to *in vivo* data were often explained by the low number of *in vivo* data points in the experimental concentration time curve.

3.2.2 Simulations for OP exposures in humans

The rat model was adjusted using human parameters and used to simulate human blood and plasma concentration-time profiles and urinary excretion-time profiles after oral exposures. Human *in vivo* exposure data were only available for oral exposures to chlorpyrifos, diazinon and fenitrothion. Therefore, these compounds were used for evaluation of the human model.

Figure 5 shows that human data were well predicted, with 91% and 43% of simulated concentrations being predicted within 5- and 2-fold difference from *in vivo* data, respectively. For chlorpyrifos, TCP, diazinon, IMHP and fenitrothion individually, each was predicted with more than 80% of the predicted blood and plasma concentrations and urinary excretion within 5-fold difference from *in vivo* data. Meanwhile, 60% of the predicted amounts of MNP excreted in urine fell within the 5-fold difference limit.

Predicted toxicokinetic parameters could only be compared to those of TCP and fenitrothion due to data availability. For TCP, the T_{max} was well predicted with 1.1-fold difference compared to *in vivo* data. Meanwhile, the predicted C_{max} and AUC were 3.19- and 2.45-fold different from *in vivo* data, respectively. Similar accuracy was found for fenitrothion: the T_{max}, C_{max} and AUC were predicted with 1.1-, 2.3- and 3.3-fold difference from *in vivo* data respectively.

3.3 Sensitivity analysis

Sensitivity coefficients were calculated to quantify the effect of individual parameters on the predicted maximum free blood concentration of OPOs. Besides body weight, the most sensitive parameters were related to metabolism, absorption or blood flow and blood partitioning (**SI figures S20-27**). Overall, for the generic human model, the predictions for diazinon, ethyl-parathion and chlorpyrifos show the highest number of sensitive parameters, with 17, 13 and 11 input parameters with a sensitivity coefficient of 0.5 or higher, respectively. Furthermore, when comparing the sensitivity coefficients of rats and humans, diazinon showed the least, and fenitrothion the most interspecies differences in the sensitivity analysis.

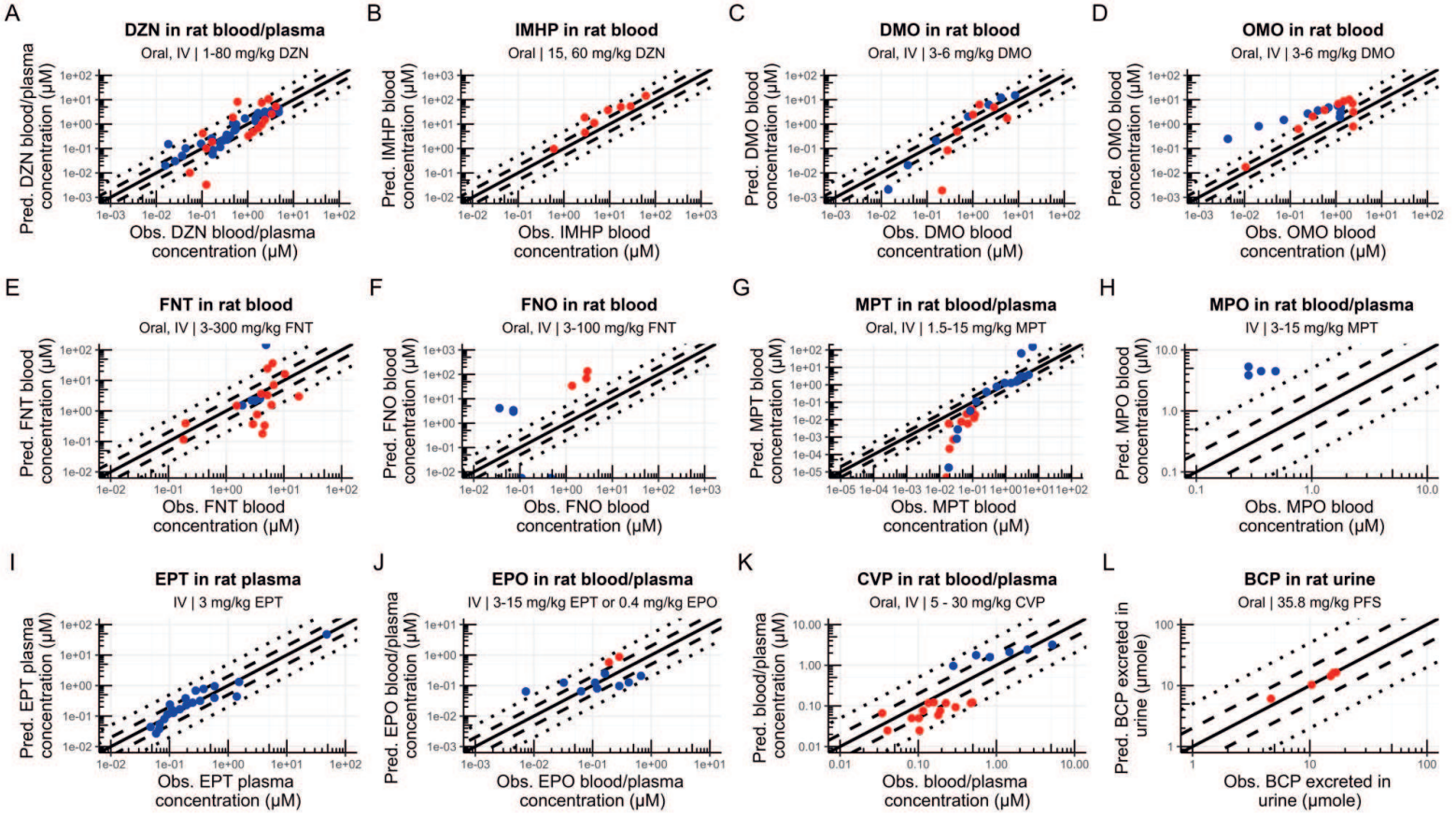


Figure 4: Predicted versus observed data plots for oral (red) and intravenous (blue) OP exposures in rats. Rats were exposed to: diazinon (DZN; A, B), dimethoate (DMO; C, D), fenitrothion (FNT; E, F), methyl-parathion (MPT; G, H) and ethyl-parathion (EPT; I, J), chlorfenvinphos (CVP; K) and profenofos (PFS; L). Lines for perfect prediction (solid line), 2-fold difference (dashed lines) and 5-fold difference (dotted lines) are shown in black. See materials and methods for included corrections. Metabolite abbreviations: IMHP: 2-isopropyl-4-methyl-6-hydroxypyrimidine; OMO: omethoate; FNO: fenitro-oxon; MPO: methyl-paraoxon; EPO: ethyl-paraoxon; BCP: 4-bromo-2-chlorophenol.

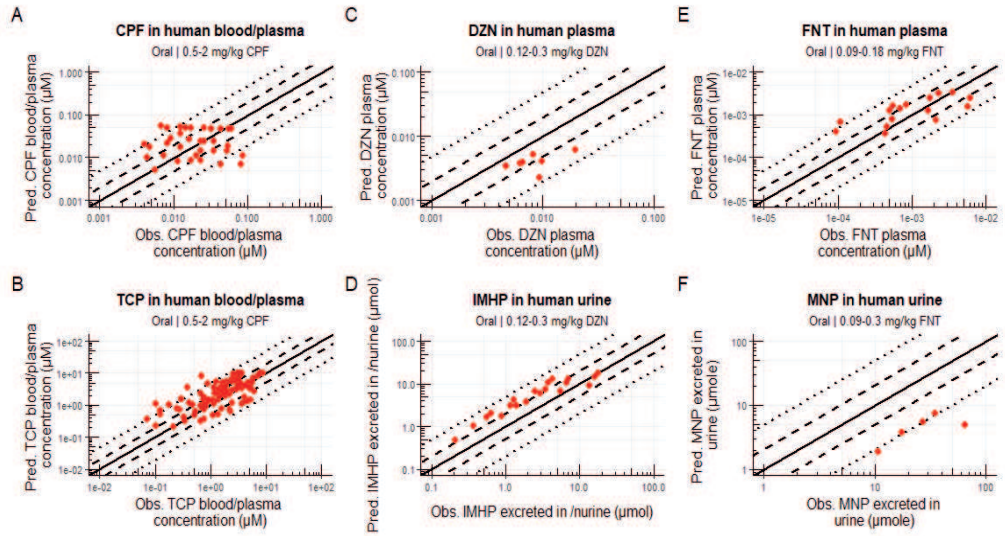


Figure 5: Predicted versus observed data plots for oral exposure to OPs in humans. Humans were exposed to chlorpyrifos (CPF; A, B), diazinon (DZN; C, D) and fenitrothion (FNT; E, F). Lines for perfect prediction (solid line), 2-fold difference (dashed lines) and 5-fold difference (dotted lines) are shown in black. See materials and methods for included corrections. Metabolite abbreviations: TCP: 3,5,6-trichloropyridinol; IMHP: 2-isopropyl-4-methyl-6-hydroxypyrimidine; MNP: 3-methyl-4-nitrophenol.

4. Discussion

The aim of this study was to develop a generic PBK model for OP pesticides which can be used to predict and compare blood concentrations of OPs and their bioactive metabolites after acute exposures in rats and humans. The model was evaluated for rats and humans using the respective available *in vivo* data for eight OP pesticides. When considering all simulations, the rat model was shown to predict 88% and 57% of the simulated blood and plasma concentrations within a 5- and 2-fold difference from *in vivo* data respectively. For humans these values were 91% and 43%, respectively, when considering only simulations for chlorpyrifos, diazinon and fenitrothion. Similar trends were seen for the predicted toxicokinetic parameters. With these results, the model was considered to adequately predict blood and plasma concentrations of OP pesticides and their metabolites, with the exception of predictions for the di-methyl-organophosphates methyl-parathion and fenitrothion. Looking at individual pesticides, the blood and plasma concentration-time and urinary excretion-time profiles, and toxicokinetic parameters were well predicted for chlorpyrifos, diazinon, dimethoate, ethyl-parathion, chlorfenvinphos, profenofos, and their metabolites. While for fenitrothion and methyl-parathion rat blood and plasma concentration-time and urinary excretion-time profiles, and toxicokinetic parameters were well predicted, simulated blood and plasma concentrations of their oxon metabolites differed by more than 10-fold from *in vivo* data. In humans, however, the fenitrothion exposures were well predicted within a 5-fold difference compared to available *in vivo* data. While almost all of the compounds were predicted well by the final model, initial simulations revealed that some corrections were needed.

Some of the corrections were needed due to errors in the analytical methods used in the *in vivo* studies, like those mentioned earlier for chlorfenvinphos (see section 2.1.3). The quality of reporting of *in vivo* data affected the reliability of some specific datasets. Namely, plotting concentration-time profiles non-logarithmically hampered accurate extraction of data for timepoints that are close to the x-axis, as was the case for methyl-parathion and dimethoate (**figure 4C, D and G**). Since this could not be corrected for, low concentrations of *in vivo* data for these compounds are less reliable.

Further corrections were related to physiological aspects and were especially relevant for predicting data upon oral exposure, since there was some odd trends in *in vivo* oral exposure data, especially in rats. Firstly, in some studies a delay in oral absorption was visible (**SI figures S3, S5 and S10**), while in default simulations absorption starts immediately after exposure. Predictions were improved when incorporating a 1 to 2.5 hour delay in absorption. In rats, such a delay in absorption might be explained by the presence of a forestomach, which is able to store food for up to three hours (185). Secondly, while the current model accounts for a temporal aspect of absorption by simulating transit through the intestine, differences are found in the k_a between *in vivo* studies. In this study, the k_a was predicted using a set of QSPRs (112), in combination with intestinal permeability data (172) (**SI: Calculation of absorption rate constant**). For rats, these predictions worked very well for those studies that used oil as the dosing vehicle, while for humans the predicted k_a's resulted in overpredictions of blood and plasma concentration-time profiles. It is often quite clear that, when the pesticides were dosed with food or oils from biological origin, a high k_a was found, while absorption seems to be lower and slower when synthetic oils were used. For human studies, this is apparent when comparing the studies of Nolan et al. (175), Timchalk et al. (131) and Brzak et al. 2000 (via EPA, 2009). In the study of Nolan et al., dosing was accompanied by a meal and a k_a of 0.6 was found after fitting to *in vivo* urinary excretion of TCP, while in the study of Timchalk et al. there was no mentioning of food or fasting state and the k_a was found to be around 0.1. If these volunteers in the latter study indeed did not eat when ingesting chlorpyrifos, food effects facilitating the oral absorption of these lipophilic compounds may explain the difference between these studies. In the current study, it is hypothesized that the higher bioavailability of OPs, when ingested with food, is mediated by bile acids. Due to their lipophilicity, OP pesticides easily pass the membranes of the intestinal wall. However, these compounds are poorly soluble in intestinal fluids, making dissolution the rate limiting step in intestinal absorption. Bile acids significantly increase the solubility of lipophilic compounds and therefore increase the rate at which they are absorbed. Bile acids are released when free fatty acids are detected in duodenal fluids, which is induced by the presence of food or oils of biological origin in the intestinal lumen. While humans have a gallbladder that releases bile when needed, rats do not have this organ and continuously secrete bile (186). This in itself might, in part, explain why the k_a for intestinal absorption of OPs in rats is generally higher compared to that in humans. However, according to Vonk et al. (187), when rats are fasted, bile secretion rates are about half of those in a fed state, potentially affecting the k_a for intestinal uptake. Implementing bile mediated intestinal dissolution is therefore expected to improve predictions, especially in humans.

While the k_a is the main absorption parameter in the model, if it is derived from *in vivo* data, it represents various physiological and kinetic processes that take place in the intestine. Not all of these processes might be captured using *in vitro* or QSPR models. This includes distribution by chylomicrons through the lymphatic system. Once absorbed, lipophilic compounds might be

distributed via the lymphatic system, packaged in chylomicrons and lipoproteins, since these particles have a lipid core (188). While fatty acids will be extracted from these particles by various tissues, the particle itself, its lipophilic core and potentially OP pesticides, will almost completely be taken up by the liver and the spleen as a chylomicron remnant particle (189,190). This is different from more hydrophilic compounds, which are usually distributed via the portal vein after absorption and for which passive diffusion into the liver is generally quite low due to their hydrophilicity. Currently, to our knowledge, there is no reported *in vitro* or *in silico* method to quantitatively predict to what extend a compound is distributed via chylomicrons after oral absorption. Such a method could potentially improve PBK predictions for lipophilic compounds, since these differences in distribution after absorption influence the concentration in the liver, and therefore the extend of metabolism.

Metabolic clearance was predicted well for six of eight of the modelled compounds. Only fenitro-oxon and methyl-paraoxon blood concentrations were predicted with over a 10-fold difference from *in vivo* data. This difference might be explained by an additional metabolic process for di-methyl-OPs that is not included in the model: glutathione transferase mediated O-dealkylation. Several studies suggest that glutathione transferases, located in the soluble fraction of the liver, are able to extensively cleave the alkyl groups (usually R_1 and R_2 in **figure 1 and SI table S1**) of di-methyl-organophosphates (90,91,97). This might explain the overpredictions of the oxon metabolites and urinary metabolites of di-methyl-organophosphates like fenitrothion and methyl-parathion. Addition of metabolism and sub-models for dealkylated metabolites would likely make the model more accurate for dimethoate, fenitrothion and methyl-parathion, but also increases model complexity.

Overall, the presented generic PBK models for rat and human were shown to predict OP pesticide and metabolite concentrations in blood, plasma and urine within generally a 5-fold and often even 2-fold difference from *in vivo* data. Deviations could be explained by lack of dealkylation metabolism in the models, and food/oil effects on absorption. The evaluated model can be used to simulate blood and plasma concentrations for OP pesticides that are metabolized via CYP450-mediated desulfuration and oxidative cleavage, and PON1-mediated hydrolysis. With regard to NGRA, to remove all reliance on animal experiments, the model could be further combined with *in vitro* or *in silico* absorption models to determine the k_a for a specific OP formulation. The general approach described in this study could also be applied to other classes of compounds, providing further insights into their toxicokinetics and aiding in NGRA. In a future study the model will be used for quantitative-*in*-*vitro*-to-*in*-*vivo*-extrapolation (QIVIVE) to determine PODs for acute neurotoxicity after exposure to OP pesticides, supporting animal alternative risk assessment and providing tools for elucidating the association of OP exposure and neurodegenerative diseases.

Acknowledgement

This work is part of the VHP4Safety project and funded is funded by the Netherlands Research Council (NWO; NWA-ORC 1292.19.272) and a grant from the China Scholarship Council (no. 202009370057 to J.C.). Through the contribution of H.B., I.M.C.M.R. and N.I.K. to this research, this research was co-funded by the European Union through Horizon Europe project "European Partnership for the Assessment of Risk from Chemicals (PARC) under grant agreement No. 101057014. This publication reflects only the authors' view and does not necessarily reflect those of the funding bodies. The European Union is not responsible for any use that may be made of the information it contains.

Supporting information

The supporting information can be found at https://doi.org/10.1021/acs.est.4c06534.

3

Next Generation Risk Assessment of Acute Neurotoxicity from Organophosphate Exposures Using the In Vitro–In Silico Derived Dietary Comparator Ratio

Jiaqi Chen, Thijs M. J. A. Moerenhout, Nynke I. Kramer and Ivonne M. C. M. Rietjens

Environ. Sci. Technol. 2025, 59, 12, 6106–6114

Abstract

Organophosphate (OP) pesticides are common environmental contaminants, of which the resulting acetylcholinesterase (AChE) inhibition and concomitant neurotoxic effects following exposure remain a global concern. To evaluate the safety upon acute exposure to OP pesticides, the Dietary Comparator Ratio (DCR) approach was used for the first time for this class of chemicals. Six OPs including chlorpyrifos, diazinon, fenitrothion, methyl parathion, profenofos, and chlorfenvinphos were selected as model compounds. Seventy-four reports of human exposures were collected, and a DCR value at each defined exposure level was calculated with in vitro determined AChE inhibition potency and in silico simulated internal exposures. Results indicate that the DCR outcomes are comparable to the actual knowledge on the presence or absence of in vivo AChE inhibition and adverse effects for the respective exposure scenarios. Of all collected scenarios, only four false positives but no false negatives were obtained. No safety concern on acute neurotoxicity appears to be raised for the evaluated environmental exposure scenarios to OPs. To conclude, the described DCR approach provides an adequate evaluation of the OP-induced adverse outcomes for humans, shedding light on its utility for 3Rs-compliant safety assessment of chemicals with different toxicity mechanisms especially for which in vitro bioassays are available.

1. Introduction

Organophosphate (OP) pesticides have been used for pest control since the 1940s. (73,191) In spite of the ban on several OP pesticides in various countries and regions, extensive application of OP pesticides results in residues being continuously found in food products and the environment. (192–194) In addition, OP pesticides and related metabolites have also been detected in human urine and breast milk as reported in biomonitoring investigations. (195–197) Dietary ingestion of OP pesticides via food and drinking water, along with accidental and intentional OP exposures among the general population remain a global public health issue, (198,199) demanding a risk evaluation for such exposure scenarios. OP pesticides can be broadly categorized into two groups as organothiophosphates and organophosphate-oxons, containing a phosphoryl-sulfur double bond (P=S) or a phosphoryl-oxygen double bond (P=O), respectively (Figure 1). With an oxidative desulfuration of the thiophosphate group mediated primarily by hepatic cytochromes P450 (CYP450), an organothiophosphate can be bioactivated to the corresponding organophosphate-oxon analogue. (200) Different from organophosphate-oxons, organothiophosphates themselves exert limited inhibition towards acetylcholinesterase (AChE) in humans. (12,200) Therefore, the OP-induced acute neurotoxicity is mainly attributed to the irreversible binding between neuronal AChE and the organophosphate-oxon, hindering the breakdown of acetylcholine at the synaptic cleft and causing cholinergic toxidrome in mammals. (201)

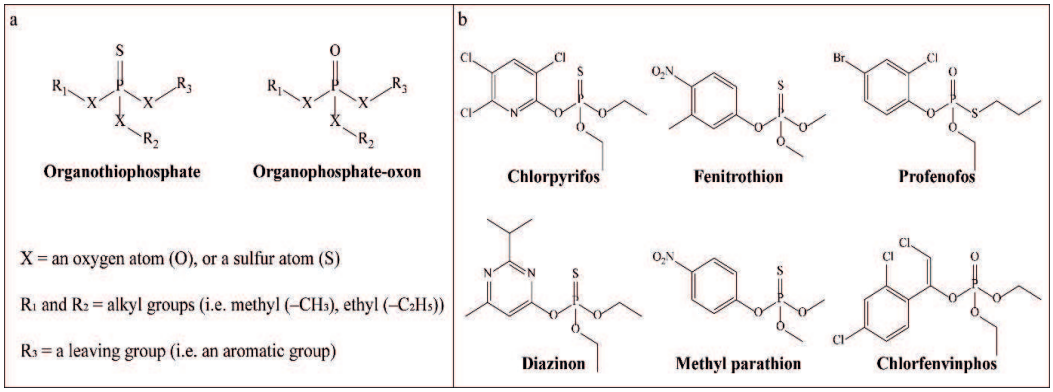


Figure 1: Chemical structures of organophosphate pesticides. The generic structure of organothiophosphates and organophosphate-oxons are shown in panel a, and the structures of OP pesticides selected as model compounds in this work are shown in panel b.

For chemical risk assessment, large strides have been made in the past decades in developing *in vitro* toxicity testing to accelerate the transformation from the conventional means that depend heavily on animals to Next Generation Risk Assessment minimizing reliance on *in vivo* testing. (202,203) While *in vitro* toxicity assays, such as the *in vitro* AChE inhibition assay, are powerful tools to develop mechanistic insights into the chemical potency, (204) implementation of these assays in risk assessment still remains elusive due to a gap between *in vitro* toxicity datasets and *in vivo* adverse outcomes. To bridge the gap, the Dietary Comparator Ratio (DCR) approach has been proposed for chemical risk assessment, considering mode of action, toxicity potency, and exposure context. (141) This approach is based on the use of a dietary compound with a history of safe consumption as a point of reference (the comparator). However, in essence every compound can serve as a comparator compound as long as a safe *in vivo* exposure level can be defined.

The DCR approach works for chemicals with the same mode of action, and evaluates the Exposure Activity Ratio (EAR) of an exposure scenario for a test substance (EAR_{test}) along with the EAR of a safe human exposure to a comparator compound ($EAR_{comparator}$). Calculated as the ratio of the EAR_{test} against the $EAR_{comparator}$, the resultant DCR is then used to evaluate the safety of the exposure scenario for the test compound, where a DCR value below 1 indicates a safe exposure scenario. (205–207) The EARs can be defined with *in vitro* derived toxicity information and *in silico* simulated internal exposure data, (141) hence no animal testing is required when employing the DCR approach for chemical risk evaluation. This approach has been proved as adequate for safety assessment of chemically-induced anti-androgenicity and estrogenicity, (205–207) and it is of interest to explore its utility for chemicals with other modes of action.

The aim of the current study is to investigate the feasibility of applying the DCR approach for safety evaluation of acute human exposure to OP pesticides. Six OPs including four organothiophosphates (chlorpyrifos, diazinon, fenitrothion, and methyl parathion) and two organophosphate-oxons (profenofos and chlorfenvinphos) (Figure 1b) were selected as model compounds. For the model OPs, relevant data on available human exposures and the resulting effects were collected from literature. Because of the high sensitivity and accessibility, erythrocyte AChE inhibition was used as a surrogate endpoint to the inhibition of neuronal AChE, (208) and an *in vitro* assay with human blood samples was performed to assess the inhibitory potential of the selected compounds and/or the active oxon metabolites. Together with the scenario-specific internal oxon levels predicted by a recently developed generic human physiologically based kinetic (PBK) model, (209) the EAR_{test} and $EAR_{comparator}$ were defined and used for DCR calculations at the defined exposure levels. The obtained DCR outcomes were compared to the actual knowledge on health outcomes (AChE inhibition and adverse health effects) reported for the respective exposure scenarios, enabling the evaluation of the DCR approach and providing insights into its utility for predicting safe thresholds of human exposure to OP pesticides.

2. Materials and Methods

2.1. Chemical and biological materials

Methyl paraoxon, profenofos, chlorfenvinphos, acetylthiocholine iodide (ATC), 5,5'-dithiobis (2-nitrobenzoic acid) (DTNB), ethopropazine, NaH_2PO_4, Na_2HPO_4, and Triton-X 100 were purchased from Sigma-Aldrich (Amsterdam, The Netherlands). Chlorpyrifos-oxon and diazoxon were ordered from TRC-Canada (Toronto, Ontario, Canada). Ethanol (UPLC/MS grade) was ordered from Biosolve (Valkenswaard, The Netherlands). Ultrapure water used for experiments was prepared with a Sartorius Arium® Pro ultrapure water system (Göttingen, Germany). Human whole peripheral blood with K_2EDTA as an anticoagulant was used for the *in vitro* erythrocyte AChE inhibition assay. K_2EDTA acts as an inhibitor to the paraoxonase 1 (PON1) enzyme,[23] preventing the underestimation of the inhibition potential of organophosphate-oxons due to the nontarget clearance by PON1 present in the blood samples.

2.2. Preparation and application of the DCR approach

The workflow of the DCR approach employed in the present study for risk assessment of acute exposure to OP pesticides was modified based on the previous applications for anti-androgens and estrogens, (205–207) and is described step by step in the following sections.

2.2.1. Step 1: Selection of model compounds

OP pesticides, including both organothiophosphates and organophosphate-oxons, were selected as model compounds, based on the availability of literature data on human exposure and of a generic human PBK model for predicting internal concentrations following exposure, (209) as these are necessary for the application of the DCR approach. (205–207)

2.2.2. Step 2: Collection of in vitro concentration-response data using the AChE inhibition assay

Inhibition of erythrocyte AChE by the organophosphate-oxon or the corresponding oxon metabolite of an organothiophosphate was measured *in vitro* using the method previously described. (12) The ethanolic stock solution of the test oxon was first diluted 100 times with sodium phosphate buffer (100 mM, pH 7.4), and 10 µL of the diluted solution was added to 90 µL human whole blood sample in a 48-wells flat-bottom transparent plate (Greiner Bio-One, The Netherlands). After a 30-min incubation at room temperature, the blood samples were then diluted 20 times with ultrapure water containing 0.03% Triton-X 100 (*v*/*v*), and 20 µL of the Triton-diluted blood was incubated for 20 min following the addition of 460 µL DTNB and 20 µL ethopropazine (an inhibitor to plasma butyrylcholinesterase (BuChE)). After that, 100 µL ATC was added (final concentrations of ethopropazine, DTNB, and ATC were 20 µM, 1 mM, and 1 mM, respectively), and the absorbance at 436 nm was measured continuously to detect the remaining AChE activity. Controls were carried out by replacing the test compound with sodium phosphate buffer to correct for any background absorbance. Assays were conducted in triplicate, and the obtained data were analyzed using a nonlinear regression of Log(inhibitor) vs. response – variable slope (four parameters) model in GraphPad Prism (version 5.04, San Diego, CA, USA) to define the concentration resulting in 50% erythrocyte AChE inhibition (IC_{50}).

Additionally, for the comparator compound, the lower 95% confidence limit of the benchmark concentration associated with a 5% erythrocyte AChE inhibition ($BMCL_{05}$) was determined by performing a benchmark concentration (BMC) analysis on the obtained *in vitro* AChE inhibition data. The benchmark response (BMR) of 5% for erythrocyte AChE inhibition is a conservative endpoint for deriving an effect level, since regulatory bodies usually use a higher BMR (i.e. 10% or 20%) for risk assessment of acute OP pesticide exposure. (210,211) The European Food Safety Authority (EFSA) web-tool (https://efsa.openanalytics.eu/) integrated with the R package PROAST (version 70.0) was employed for the BMC analysis (see Supporting Information).

2.2.3. Step 3: Collection of available exposure scenarios and relevant adverse health effects

Acute exposure scenarios where human individuals were orally exposed to one of the model OPs were gathered from literature. The collected scenarios could be broadly classified into two categories: human volunteer studies at relatively low dose levels, where adverse effects might not be observed; and intentional and/or accidental exposures, for which usually a relatively high OP pesticide dose was ingested and the resulting AChE inhibition and/or adverse health effects were reported. Data on the first oral administration in repeated dose studies were also collected and

considered to represent an acute exposure scenario. Based on the information on erythrocyte AChE inhibition and the resultant adverse health effects at respective exposure scenarios, it could be concluded whether the respective dose levels induced a positive, negative, or unknown (unreported) adverse effect in humans. This enabled the evaluation of the obtained DCR outcomes in Step 7 (see section 2.2.7).

2.2.4. Step 4: Prediction of internal concentrations for collected exposure scenarios

A newly developed generic human PBK model for OP pesticides was used to predict the maximum blood oxon concentration (CB_{max}oxon) for the collected exposure scenarios, (209) considering that this value is relevant to the erythrocyte AChE inhibition induced by acute exposure to an OP pesticide. (152,212) No corrections for differences in *in vivo* and *in vitro* protein binding are necessary, since the *in vitro* AChE inhibition assay was performed with human blood samples (see section 2.2.2).

When predicting CB_{max}oxon with the generic PBK model, (209) dose levels and oral absorption rate constants were needed as model inputs. Generally, in volunteer studies the tested dose levels (in mg/kg BW) are explicitly reported, while this information is unclear for most accidental and intentional exposures. For such scenarios, the exposure level was estimated with the ingested amount (in mg) assuming a body weight of 70 kg regardless of age, sex and ethnicity, unless a specific body weight was reported. With regard to the oral absorption rate constant (in hr^{-1}), OP-specific values calculated based on quantitative structure–activity relationships (QSARs) are available, (112,209) and are summarized in Table S1 (see Supporting Information). For CB_{max}oxon prediction, both the established rat and human generic PBK models have been reported to adequately predict internal exposure of OP pesticides, while it is important to note that the rat model has been reported to overpredict the blood oxon concentration for dimethyl-organothiophosphates including fenitrothion and methyl parathion by about one order of magnitude. (209) Since no relevant data on the blood oxon profile following exposure to fenitrothion or methyl parathion are available to evaluate the human model, the assumption of the same overprediction magnitude (10-fold) was made in this work. Therefore, the CB_{max}oxon predictions from the generic human PBK model for fenitrothion and methyl parathion were divided by 10 to correct for the probable overestimation.

2.2.5. Step 5: Selection of a comparator compound

Single oral chlorpyrifos exposure scenarios that did not result in notable adverse health effects in humans are available and well-described, (208) making this organothiophosphate an adequate comparator. The generic human PBK model was used to predict the CB_{max}oxon under a safe chlorpyrifos dose level, and the *in vitro* derived $BMCL_{05}$ was compared with this predicted value to determine if the $BMCL_{05}$ could indeed represent a safe scenario to define the $EAR_{comparator}$.

2.2.6. Step 6: DCR calculation for collected exposure scenarios

The DCR value for an exposure scenario was calculated as the ratio of EAR_{test} and $EAR_{comparator}$ (Eq 1). The EAR_{test} is scenario-specific, and was defined with the IC_{50} of the tested organophosphate-oxon for *in vitro* erythrocyte AChE inhibition and the PBK model-simulated CB_{max}oxon at the defined exposure level (Eq 2). Chlorpyrifos was selected as the comparator compound, and the $EAR_{comparator}$ was calculated using the $BMCL_{05}$ and IC_{50} derived from *in vitro* AChE inhibition assay for chlorpyrifos-oxon (Eq 3).

$$DCR = \frac{EAR_{test}}{EAR_{comparator}} \quad \text{(Eq 1)}$$

$$EAR_{test} = \frac{Predicted\ CB_{max}\ oxon\ at\ a\ defined\ exposure\ level\ (test\ substance)}{IC_{50}\ (test\ substance)} \quad \text{(Eq 2)}$$

$$EAR_{comparator} = \frac{BMCL_{05}\ (comparator)}{IC_{50}\ (comparator)} \quad \text{(Eq 3)}$$

2.2.7. Step 7: Evaluation and application of the DCR approach

The DCR-based predictions were evaluated by comparing the obtained DCR results with the actual knowledge on the adverse health effects reported for the respective exposure scenarios. Adverse effects cannot be ruled out for human exposure scenarios with a DCR result greater than 1, while exposure scenarios with a DCR result less than or equal to 1 are considered to raise no safety concern. (205–207) Once validated as an adequate predicting tool, the DCR approach was applied for evaluating the safety of exposure scenarios for which no information on the resulting toxic outcomes was reported at the defined dose levels for humans.

3. Results

3.1. Step 1: Selection of model compounds

Six OP pesticides were selected as model compounds, including two diethyl-organothiophosphates (chlorpyrifos and diazinon), two dimethyl-organothiophosphates (fenitrothion and methyl parathion), and two organophosphate-oxons (profenofos and chlorfenvinphos) (Figure 1b).

3.2. Step 2: Collection of *in vitro* concentration-response data using the AChE inhibition assay

In vitro concentration-based erythrocyte AChE inhibition was determined for the relevant organophosphate-oxons (Figure 2). The derived IC_{50} values are 0.14, 0.38, 0.84, 1.82, 27.7, and 94.5 μM for methyl paraoxon, chlorpyrifos-oxon, fenitrooxon, diazoxon, chlorfenvinphos, and profenofos, respectively. Additionally, for the comparator compound chlorpyrifos, the derived $BMCL_{05}$ value for its oxon metabolite (chlorpyrifos-oxon) is 0.015 μM (detailed results of the BMC analysis are provided in Supporting Information).

3.3. Step 3: Collection of available exposure scenarios and relevant adverse health effects

Seventy-four human cases reporting single oral exposure to one of the selected OP pesticides were collected, with the corresponding information on the occurrence or absence of adverse health effects (Table S2). Toxic signs and symptoms like weakness, vomiting, headache, dizziness, coma, and even death have been observed in accidental and/or intentional exposure scenarios, where the erythrocyte AChE was substantially inactivated due to the ingestion of large amounts of an OP pesticide. (213–215) In volunteer studies, abnormal signs and symptoms were usually absent at the relatively low test doses, and erythrocyte AChE activity was monitored as a surrogate endpoint. (216) Because of the high sensitivity of erythrocyte AChE, dose levels that resulted in erythrocyte

AChE inhibition without concomitant signs and symptoms in the respective participants, as observed for example upon a dose of 2 mg/kg BW chlorpyrifos or 1 mg/kg BW chlorfenvinphos, (208,217) were still considered safe.

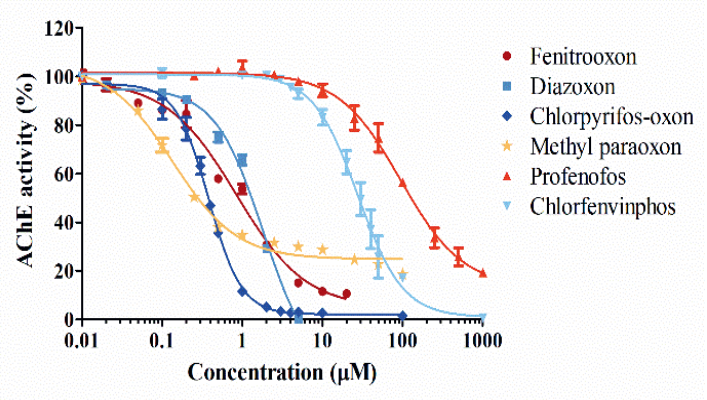


Figure 2: Erythrocyte AChE inhibition determined via *in vitro* incubations with human blood. AChE inhibition was determined for six organophosphate pesticides: fenitrooxon, (152) diazoxon, chlorpyrifos-oxon, methyl paraoxon, profenofos, and chlorfenvinphos. Results are presented as means ± SEM from three independent experiments.

Of the collected cases, there were eleven, thirteen, twenty-two, nine, one, and three different dose levels collected for chlorpyrifos, diazinon, fenitrothion, methyl parathion, profenofos, and chlorfenvinphos, respectively (Table 1). Analysis of these datasets indicated that toxic effects were present (positive outcome) for twenty-nine, and absent (negative outcome) for twenty-seven of them (Table 1). Meanwhile, three dose levels that had unreported (unknown) health outcomes in humans were also found. Specifically, no information on AChE inhibition and concomitant adverse effects was provided for chlorfenvinphos at 0.18 mg/kg BW; while for diazinon, conflicting opinions on erythrocyte AChE inhibition were reported by the Australian Pesticides and Veterinary Medicines Authority (218) and the US Environmental Protection Agency (219) after reviewing the human volunteer study (220), of which the description on toxic signs following a single oral DZN administration was also equivocal at dose levels of 0.21 and 0.30 mg/kg BW.

Table 1: CB_{max}oxon predictions and EAR_{test} and DCR calculations. Calculations were performed for the respective exposure levels collected for chlorpyrifos, diazinon, fenitrothion, methyl parathion, profenofos and chlorfenvinphos.

Exposure level (mg/kg BW) [a]	Predicted CB_{max}oxon (µM) [b]	Calculated EAR_{test} value	Calculated DCR value	Reported or expected adverse health outcome [a]
Chlorpyrifos				
0.01	6.8×10^{-5}	1.8×10^{-4}	4.6×10^{-3}	Negative
0.012	8.2×10^{-5}	2.2×10^{-4}	5.0×10^{-3}	Negative
0.014	9.6×10^{-5}	2.5×10^{-4}	6.4×10^{-3}	Negative
0.03	2.1×10^{-4}	5.4×10^{-4}	0.014	Negative
0.1	6.9×10^{-4}	1.8×10^{-3}	0.046	Negative
0.5	3.5×10^{-3}	9.2×10^{-3}	0.23	Negative
1	7.2×10^{-3}	0.019	0.48	Negative
2	0.015	0.040	1.0	Negative
214	0.57	1.50	38	Positive
286	0.60	1.57	40	Positive

Exposure level (mg/kg BW) [a]	Predicted CB_{max}oxon (μM) [b]	Calculated EAR_{test} value	Calculated DCR value	Reported or expected adverse health outcome [a]
300	0.60	1.58	40	Positive
Diazinon				
0.011	1.5×10^{-5}	8.3×10^{-6}	2.1×10^{-4}	Negative
0.03	4.1×10^{-5}	2.3×10^{-5}	5.7×10^{-4}	Negative
0.12	1.6×10^{-4}	9.1×10^{-5}	2.3×10^{-3}	Negative
0.20	2.8×10^{-4}	1.5×10^{-4}	3.8×10^{-3}	Negative
0.21	2.9×10^{-4}	1.6×10^{-4}	4.0×10^{-3}	Unknown
0.30	4.1×10^{-4}	2.3×10^{-4}	5.8×10^{-3}	Unknown
200	0.15	0.084	2.1	Positive
214	0.15	0.085	2.2	Positive
293	0.16	0.089	2.3	Positive
323	0.16	0.090	2.3	Positive
357	0.17	0.091	2.3	Positive
429	0.17	0.093	2.3	Positive
643	0.17	0.095	2.4	Positive
Fenitrothion				
0.042	5.7×10^{-3}	6.8×10^{-3}	0.17	Negative
0.06	8.2×10^{-3}	9.7×10^{-3}	0.25	Negative
0.083	0.011	0.013	0.34	Negative
0.09	0.012	0.015	0.37	Negative
0.17	0.023	0.028	0.70	Negative
0.18	0.025	0.029	0.74	Negative
0.25	0.034	0.041	1.0	Negative
0.33	0.045	0.054	1.4	Negative
0.36	0.049	0.059	1.5	Negative
36	5.79	6.89	174	Positive
71	11.47	13.66	346	Positive
143	20.24	24.10	610	Positive
214	26.90	32.03	811	Positive
286	33.34	39.69	1005	Positive
357	39.42	46.93	1189	Positive
429	45.24	53.86	1364	Positive
500	50.60	60.24	1526	Positive
536	53.18	63.31	1604	Positive
571	55.60	66.18	1677	Positive
714	64.64	76.95	1949	Positive
1714	100.71	119.90	3037	Positive
1786	102.06	121.49	3078	Positive
Methyl parathion				
0.003	5.1×10^{-4}	3.6×10^{-3}	0.092	Negative
0.029	4.9×10^{-3}	0.035	0.89	Negative
0.057	9.7×10^{-3}	0.069	1.8	Negative
0.30	0.051	0.36	9.2	Negative
26	5.12	36.59	927	Positive
171	28.50	203.58	5157	Positive
286	40.69	290.61	7362	Positive
714	71.03	507.39	12854	Positive
1143	84.26	601.86	15247	Positive
Profenofos				
1600	1015.56	10.75	272	Positive
Chlorfenvinphos				
0.04	4.1×10^{-3}	1.5×10^{-4}	3.8×10^{-3}	Negative
0.18	0.019	6.8×10^{-4}	0.017	Unknown
1	0.11	3.9×10^{-3}	0.098	Negative

a: See Table S2 for more details and references of original studies; **b:** Predicted with a generic human PBK model. (209) The values for fenitrothion and methyl parathion were corrected by dividing the original model predictions by 10 (see section 2.2.4 for more details).

3.4. Step 4: Prediction of internal concentrations for collected exposure scenarios

The CB_{max}oxon for the collected exposure scenarios was predicted for all selected model compounds with a generic human PBK model (209) and is presented in Table 1. For acute exposure to an organothiophosphate like chlorpyrifos, diazinon, fenitrothion, and methyl parathion, the CB_{max}oxon was simulated for the corresponding oxon analogue, namely chlorpyrifos-oxon, diazoxon, fenitrooxon and methyl paraoxon. The original CB_{max}oxon simulations from the model for dimethyl-organothiophosphates (fenitrothion and methyl parathion) was corrected for the overprediction (see section 2.2.4), and for the purpose of comparison, the results without correction are presented in Table S3. For single exposure to an organophosphate-oxon (profenofos or chlorfenvinphos), the CB_{max}oxon was simulated for the parent compound itself.

3.5. Step 5: Selection of a comparator compound

Chlorpyrifos was chosen as the comparator compound. Toxicity testing following single exposure to this organothiophosphate was investigated with human volunteers, who were fasted overnight and given an oral dose next morning. (208,221) It was found that 1 mg/kg BW was a dose level where no erythrocyte AChE inhibition took place, and that 2 mg/kg BW was the no-observed-adverse-effect level (NOAEL) for toxic signs and symptoms, with a 28% inhibition of erythrocyte AChE reported at this level in one of the participants causing no abnormalities. (208,221) At the NOAEL of 2 mg/kg BW, the CB_{max}oxon predicted by the generic human PBK model was 0.015 µM, which was equal to the *in vitro* derived $BMCL_{05}$ for chlorpyrifos-oxon. This indicates that the $BMCL_{05}$ can indeed be considered to represent a safe concentration where no adverse effects occur and hence can be used to define the $EAR_{comparator}$.

3.6. Step 6: DCR calculation for collected exposure scenarios

With the predicted CB_{max}oxon of the test substances (Table 1) and the *in vitro* derived IC_{50} values (see section 3.2), the EAR_{test} values for the collected exposure scenarios were calculated and are listed in Table 1. The $EAR_{comparator}$ was defined with the *in vitro* derived $BMCL_{05}$ and IC_{50} values for chlorpyrifos-oxon, and the resulting value was 0.039. By dividing the EAR_{test} by the $EAR_{comparator}$, a DCR for each exposure scenario was obtained (Table 1).

3.7. Step 7: Evaluation and application of the DCR approach

To evaluate the performance of the obtained DCR-based predictions, a comparison was made between the DCR outcomes and the reported or expected health outcomes for each exposure scenario. Dose levels causing toxic signs and symptoms due to a substantial erythrocyte AChE inactivation are considered to result in positive outcomes, and the DCR approach well predicted the occurrence of the adverse effects for these exposure scenarios with no false negatives (Figure 3). Also, safe (negative) exposure scenarios inducing no adverse health effects were adequately predicted, except for the false positive results obtained for fenitrothion at 0.33 and 0.36 mg/kg BW,

and for methyl parathion at 0.057 and 0.30 mg/kg BW, respectively (Figure 3b). These scenarios were considered as safe (negative), because no significant erythrocyte AChE inhibition and/or no abnormal signs and symptoms were observed (Table S2). A DCR result close to 1 has been obtained for these false positive exposure scenarios (Figure 3b). With a less conservative $EAR_{comparator}$ than the one currently defined based on the $BMCL_{05}$ for erythrocyte AChE inhibition, these false positive scenarios would have been correctly predicted to be negative (DCR ≤ 1), however this is not preferred, because by doing so the chance of false negative predictions also increases.

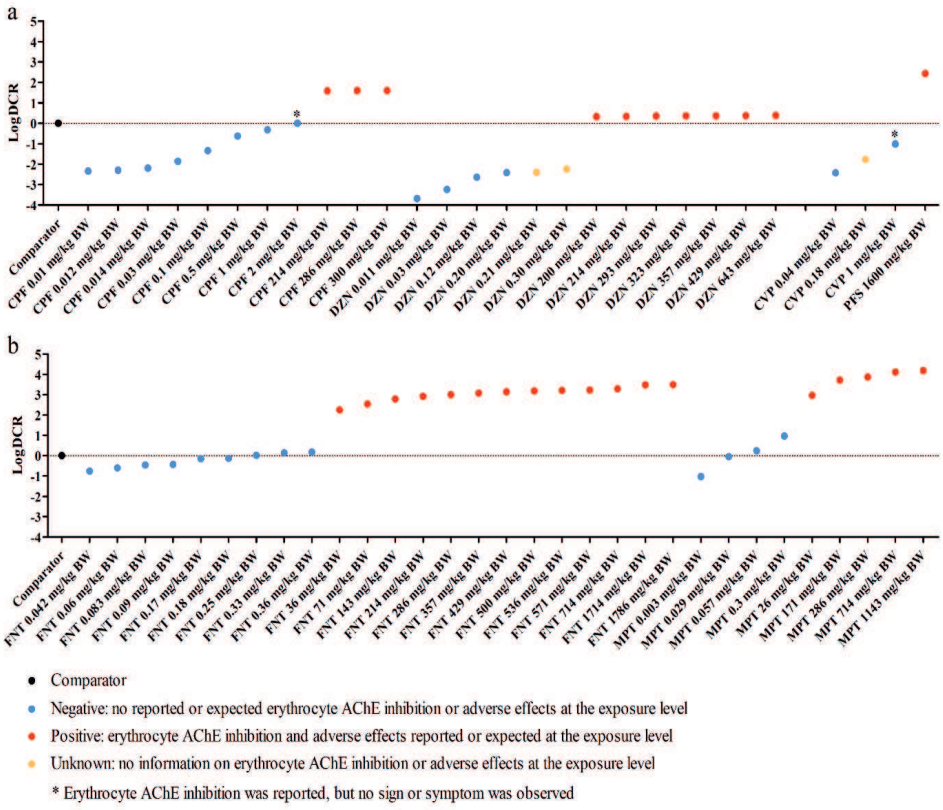


Figure 3: The DCR outcomes of collected human cases upon a single oral administration to the selected OP pesticides. Collected OP pesticides include (a) chlorpyrifos (CPF), diazinon (DZN), profenofos (PFS) and chlorfenvinphos (CVP), and (b) fenitrothion (FNT) and methyl parathion (MPT). The dotted horizontal lines display the DCR of 1 (LogDCR = 0). Calculated DCR results are shown in Table 1. Details on the evaluation of an exposure scenario as positive, negative, or unknown with respect to the occurrence of erythrocyte AChE inhibition and/or adverse effects are summarized in Table S2.

Given that no false negatives were obtained, it was concluded that the DCR approach can provide adequate safety evaluation for the acute OP pesticide exposure scenarios by incorporating *in vitro* derived AChE inhibition potentials with relevant exposure data. The DCR approach was then applied for three exposure scenarios, of which the occurrence of toxic outcomes was unreported (unknown) upon acute exposure to diazinon at 0.21 or 0.30 mg/kg BW, or to chlorfenvinphos at 0.18 mg/kg BW. The obtained DCR values for these exposure scenarios are all below 1 (Figure 3a), indicating that these scenarios are predicted to be safe.

4. Discussion

In the present study, the use of the DCR approach was evaluated as an alternative to animal testing for human health risk assessment of acute OP pesticide exposure. To this end, the EAR_{test} of OP exposure scenarios of interest and the $EAR_{comparator}$ of chlorpyrifos were defined based on toxicity data derived from the *in vitro* AChE inhibition assay, along with internal exposure data predicted using a newly developed generic human PBK model for OP pesticides (209). With the EAR values, the DCR was calculated for the respective exposure scenarios, and was then compared with the actual knowledge on the occurrence or absence of *in vivo* AChE inhibition and adverse effects, enabling the evaluation of the DCR-based predictions.

Four organothiophosphates (chlorpyrifos, diazinon, fenitrothion and methyl parathion) and two organophosphate-oxons (profenofos and chlorfenvinphos) were chosen as model compounds in this work (Figure 1b). All these selected pesticides act as AChE inhibitors after absorption (and metabolic activation to the corresponding oxon analogue) in humans. The inhibition potential of these substances on AChE was determined *in vitro* with human blood samples (Figure 2), and the erythrocyte AChE inhibition was considered as an adequate surrogate endpoint for the neuronal AChE inactivation. This surrogate endpoint is widely adopted in scientific studies (152,158) and also by regulatory bodies, (222) given that erythrocyte AChE is more sensitive and easy to sample as compared to the neuronal AChE. (208) Though the physiological function of erythrocyte AChE is currently unclear, a good correlation has been noted between the severity of clinical signs and symptoms and the degree of erythrocyte AChE inhibition, where approximately 40% remaining erythrocyte AChE activity has been linked with only mild symptoms. (73,215) For the risk assessment of acute OP pesticide exposure, both 10% and 20% inhibition levels in erythrocyte AChE have been employed by regulatory bodies to define points of departure for setting health-based guidance values. (210,211,223) In this work, a 5% *in vitro* erythrocyte AChE inhibition was used as a conservative threshold to define the $EAR_{comparator}$. Using a 10% or 20% inhibition would result in a higher $EAR_{comparator}$ and lower DCR predictions, and would hence be less protective.

Instead of making comparisons between the predicted CB_{max}oxon for a given OP exposure and the OP-specific $BMCL_{05}$, the DCR approach that divides an EAR_{test} by a well-defined $EAR_{comparator}$ adds an extra dimension of conservatism to the safety evaluation, since the EAR_{test} is compared to the $EAR_{comparator}$ for a safe exposure level of the comparator compound, taking into account a margin between the predicted blood level and the $BMCL_{05}$ for exposure to the comparator that can be considered safe. Chlorpyrifos was chosen as the comparator compound, because compared with other OPs, relevant single exposure studies and NOAELs for humans were well-documented and reviewed by the United States Environmental Protection Agency as a useful assessment for potential erythrocyte AChE inhibition induced by chlorpyrifos. (224) This enables the validation of the assumption that the *in vitro* derived $BMCL_{05}$ value resembles a safe internal concentration where no *in vivo* adverse effect occurs, and hence can be used to define an appropriate $EAR_{comparator}$. It is noteworthy that the NOAELs of chlorpyrifos were tested with a limited number of adult participants, (208,221,224) who may not represent the whole population including susceptible individuals like pregnant women and children. Also, most of the human exposure cases reported (Table S2) and the PBK model used for CB_{max}oxon predictions (209) were for adults. Therefore, the EAR and DCR values in the current study are in the first place applicable for the general adult population. Their

use for susceptible individuals may require the consideration of an uncertainty factor. For example, one could consider adapting the cut-off DCR value from 1 to 0.1 by applying the commonly used uncertainty factor of 10 accounting for human variability in risk assessment. In so doing, confidence would be increased with the negative predictions (DCR ≤ 0.1). However, one could also argue that for a sensitive individual the EAR_{test} and $EAR_{comparator}$ might be affected to the same extent so that their higher sensitivity can be expected to cancel out when calculating the DCR.

The half maximum activity concentration, for example the IC_{50} determined in this study, is considered as the most appropriate metric for EAR_{test} and $EAR_{comparator}$ calculations. (141,205) This is because the DCR approach (also being referred to as the exposure:activity profiling method) was initially applied for prioritizing chemicals with estrogenic activity. (141) The estrogenic activity was determined based on various *in vitro* assays measuring events at different points downstream of receptor binding, and the concentration at half maximal activity was regarded as the most reliable measurement from different assays to quantify chemical potency. (141) In this study, the *in vitro* erythrocyte AChE inhibition of six model OP compounds was tested with the same assay system (human whole blood samples), displaying substrate-specific location and steepness of the concentration-response data (Figure 2). Given that an IC_{50} is the least variable metric and thus provides greater reliability than other metrics along the concentration-response curve, (141) the IC_{50} values for the model OP compounds were derived from the obtained curves (Figure 2) to determine the inhibition potential, and were used as the activity component for calculating EARs (Eq 2 and 3).

The results of the DCR-based safety evaluation reveal that the approach provides adequate predictions for the collected human exposure scenarios of OP pesticides with no false negatives (Figure 3). Still, this approach has uncertainties and limitations, and understanding these is helpful for interpreting the obtained DCR results and making further safety decisions. First, current DCR outcomes might be conservative with regard to the exposure level estimation. The exposure level might be overestimated especially for accidental and intentional scenarios, where vomiting could happen following OP pesticide poisoning. Besides, the *in vitro* bioassay (see section 2.2.2) solely measured the inhibition potential of test OPs on AChE using human whole blood that contains no carboxylesterase, (35) and the influence of plasma BuChE was also excluded by adding the inhibitor ethopropazine. (12) In fact, both BuChE and carboxylesterase in the human body (i.e. liver) are able to bind organophosphate-oxons, (225–227) while such protection on AChE is not taken into account in the current DCR calculations. Furthermore, the CB_{max}oxon was predicted with a generic human PBK model that needs further improvement. (209) Except for a 10-fold overestimation in CB_{max}oxon for dimethyl-organothiophosphates (see section 2.2.4), this deterministic PBK model does not take into account interindividual variations in the (formation and) clearance of organophosphate-oxons following administration to OP pesticides. (76,156,228) Further refinement of the PBK model by correcting the overestimation and by integrating interindividual variabilities in physiological and toxicokinetic parameters would greatly increase confidence in the model predictions. Third, the current $EAR_{comparator}$ was built with an *in vitro* derived $BMCL_{05}$ instead of the predicted CB_{max}oxon at safe exposure levels. This is based on the consideration of the probable uncertainty in these *in vivo* dose levels, (208,221) and also because the relevant internal oxon concentration under the safe dose levels was not reported and using a model-predicted CB_{max}oxon to define the $EAR_{comparator}$ might introduce more uncertainties. Furthermore, using an *in vitro* derived

$BMCL_{05}$ value instead of *in vivo* data to define the $EAR_{comparator}$ is in line with the principle of the DCR approach as a 3Rs-compliant methodology. It has previously been demonstrated that using a $BMCL_{05}$-defined $EAR_{comparator}$ is adequate in DCR-based safety evaluations for estrogens and anti-androgens, (206,207) and the results in this work provide a further proof-of-concept for using an *in vitro* defined $EAR_{comparator}$ in a DCR-based human safety assessment for acute OP pesticide exposures. Once *in silico* tools are available for predicting internal concentrations of more OP pesticides, the datasets collected in this work can be extended for a further evaluation on the performance of the current $EAR_{comparator}$.

Of note, the currently collected exposure scenarios are from human volunteer studies and acute poisoning cases (Table S2), for which the exposure dose levels are either very low or high, and hence resulting in explicitly negative or positive DCR outcomes. In the context of environmental exposure to OP pesticides, the OP concentrations commonly measured in human blood samples have been reported to range from 1×10^{-6} to 2×10^{-4} μM. (229) Comparing the upper value to the predicted CB_{max}oxon for six model OPs (Table 1), it indicates that environmental exposure to OP pesticides appears not to raise safety concern with respect to AChE inactivation and the following acute neurotoxicity. However, AChE inhibition alone cannot account for the adverse effects (i.e., impaired neurobehavioral performance) induced by repeated low-level OP exposures occurring in an environmental context. (149,150,230) Although data on internal exposure following repeated exposure can be predicted via computational toxicokinetic modeling, to apply the DCR approach for evaluating the safety from chronic exposure to OP pesticides, information on the underlying mechanism, available *in vitro* bioassays that can well characterize toxicity, as well as safe chronic exposure scenario are required.

To conclude, the present study investigated the applicability of the DCR approach for Next Generation Risk Assessment of OP pesticide exposure. Toxicity and internal exposure data used for the EAR and DCR calculations were derived *in vitro* and *in silico*. The results suggest that in addition to its application for anti-androgens and estrogens, this DCR-based strategy can also be of use to evaluate the *in vivo* adverse effects caused by acute exposure to environmental toxicants like OP pesticides, providing another proof-of-principle for applying this approach for human safety assessment based on the consideration of mode of action, toxicity potency, and exposure context. To further extend the applicability domain of the DCR strategy for more environmental pollutants, available data on the toxic mechanism, toxicity potency and internal exposure of the compounds of interest, as well as an adequate comparator compound with the same mode of action and a known safe exposure level are prerequisites.

Acknowledgement

This work was funded by a grant from the China Scholarship Council (no. 202009370057) to J.C. Through the contribution of T.M.J.A.M. to this work, this work was co-funded by the Netherlands Research Council (NWO; NWA-ORC 1292.19.272) to the VHP4Safety project. Through the contribution of N.I.K. and I.M.C.M.R. to this work, this work was co-funded by the European Union through Horizon Europe project "European Partnership for the Assessment of Risk from Chemicals (PARC)" under a grant agreement no. 101057014. This publication reflects only the authors' view and does not necessarily reflect those of the funding bodies. The European Union is not responsible for any use that may be made of the information it contains. The authors would like to thank Nynke Vermazeren and Dongxin Zhai for their assistance with data collection, and Hans Bouwmeester (Wageningen University and Research) for providing comments on the first draft of the manuscript. The graphic for Table of Contents was created with BioRender.com by J.C.

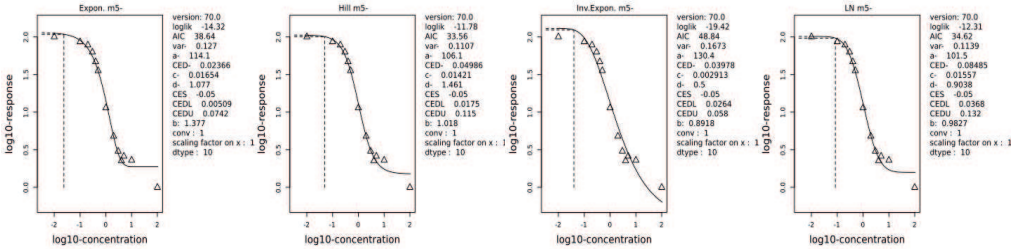
Supporting information

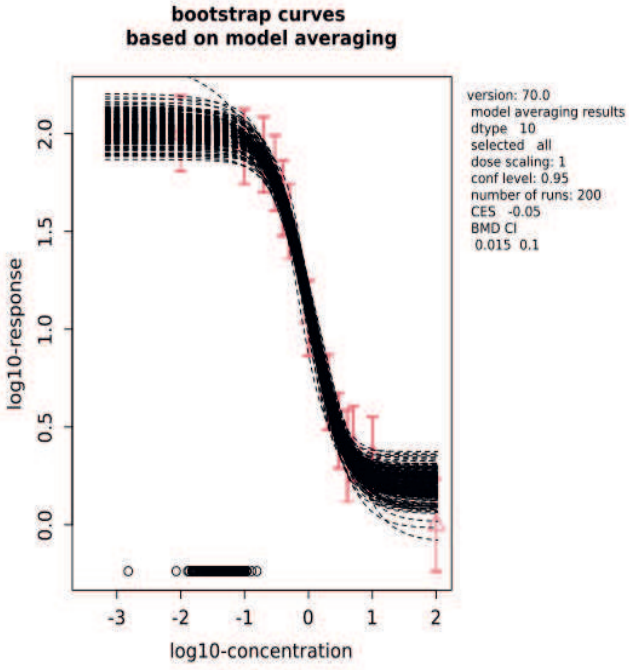
Methods from the supporting information are shown below. The full supporting information including all data tables can be found at https://doi.org/10.1021/acs.est.5c00220.

BMC analysis for chlorpyrifos-oxon

The EFSA web-tool (https://efsa.openanalytics.eu/) integrated with the R package PROAST (version 70.0) was employed for the BMC analysis. Briefly, the continuous data (the obtained erythrocyte AChE activity in human blood upon *in vitro* incubations with increasing concentrations of chlorpyrifos-oxon) were fitted to a set of models (Exponential, Hill, Inverse Exponential, and Log-Normal family models), and all fitted models excluding the FULL and NULL models were used for model averaging via a weighted average model. More weight was given to the models with lower Akaike's Information Criterion (AIC), and an averaged confidence interval was estimated using the recommended defaults. The table and figures present the characteristics of fitted models, the weights for model averaging, and the benchmark concentration for 5% erythrocyte AChE inhibition with the 95% lower–upper confidence limits (BMCL–BMCU).

Model	**Converged**	**loglik**	**npar**	**AIC**	**Weights**	**Final BMC values (µM)**	
full	NA	NA	NA	NA	-	$BMCL_{05}$	$BMCU_{05}$
null model	yes	-70.36	2	144.72	-	0.015	0.10
Expon. m3-	yes	-46.83	4	101.66	-		
Expon. m5-	yes	-14.32	5	38.64	0.05		
Hill m3-	yes	-45.81	4	99.62	-		
Hill m5-	yes	-11.78	5	33.56	0.60		
Inv.Expon. m3-	yes	-37.99	4	83.98	-		
Inv.Expon. m5-	yes	-19.42	5	48.84	0		
LN m3-	yes	-40.79	4	89.58	-		
LN m5-	yes	-12.31	5	34.62	0.35		




bootstrap curves
based on model averaging
version: 70.0
model averaging results
dtype 10
selected all
dose scaling: 1
conf level: 0.95
number of runs: 200
CES -0.05
BMD CI
0.015 0.1
log10-response
0.0
0.5
1.0
1.5
2.0
-3
-2
-1
0
1
2
log10-concentration

4

The effect of glutathione-mediated metabolism of organophosphate pesticides on rat and human in vivo toxicokinetics investigated using physiologically based kinetic modelling

Thijs M.J.A. Moerenhout, Wouter Bakker, Hans Bouwmeester and Nynke I. Kramer

Manuscript in preparation

Abstract

Organophosphates have been widely used as pesticides in agricultural practices. Consequently, the general public is exposed to these pesticides via food. Upon absorption, organophosphates can be bioactivated and inhibit acetylcholinesterase, affecting neurological functioning. Metabolism of these pesticides has been investigated mostly with respect to cytochrome P450 and paraoxonase-1 enzymes. However, recent PBK modelling studies, along with qualitative metabolism studies, suggested dimethyl organophosphates can be metabolized by glutathione-mediated pathways. Therefore glutathione-mediated metabolism of the dimethyl organophosphates methyl-paraoxon and omethoate was investigated using in vitro incubations with rat and human liver S9 subcellular fractions. For methyl-paraoxon, demethylation was dependent on the presence of both S9 protein and glutathione and had clearance rates of 1.60 ± 0.007 and 0.43 ± 0.036 L/hour/gram liver were found for rats and humans, respectively. For omethoate, the reaction was only dependent on GSH and the chemical clearance rate was 0.800 ± 0.012 mL/hour. Implementing these clearance rates in a PBK model significantly improved the predictions of methyl-paraoxon and fenitro-oxon (read-across), and reduced the 10-fold difference in predicted blood concentrations to within 2- and 5-fold difference, respectively, compared to *in vivo* experimental data. For omethoate, implementation of its chemical demethylation did not have a significant effect on its simulated plasma profile. The consequences of glutathione-mediated metabolism on risk assessment and potential correlation between lipophilicity and glutathione mediated clearance are discussed.

1. Introduction

Organophosphate pesticides have been extensively used in agricultural practice as an important tool in sustaining agricultural yields and support the food production chain. While some specific organophosphates have been banned because of risks to human and environmental health (142), organophosphate pesticides are still widely used in many countries (3). Organophosphate pesticides efficiently inhibit the enzyme acetylcholinesterase (AChE), an enzyme that is crucial for normal neurological functioning, in both target and non-target species (13,14).

Organophosphate pesticides can be subdivided into organothiophosphates (OTPs) and organophosphate(oxon)s (OPOs). While OTPs generally poorly inhibit AChE, they become potent inhibitors when bioactivated by cytochrome P450 (CYP450) enzymes to OPOs (see **figure 1**). Both OTPs and OPOs are known to be extensively detoxified via CYP450 enzymes in the liver (76–81). Besides CYP450-mediated metabolic pathways, OPOs are also detoxified by the paraoxonase 1 (PON1) enzyme in the liver and plasma (82–84). While both CYP450- and PON1-mediated reactions occur in rats and humans, large differences in metabolic rates of these species have been found (209).

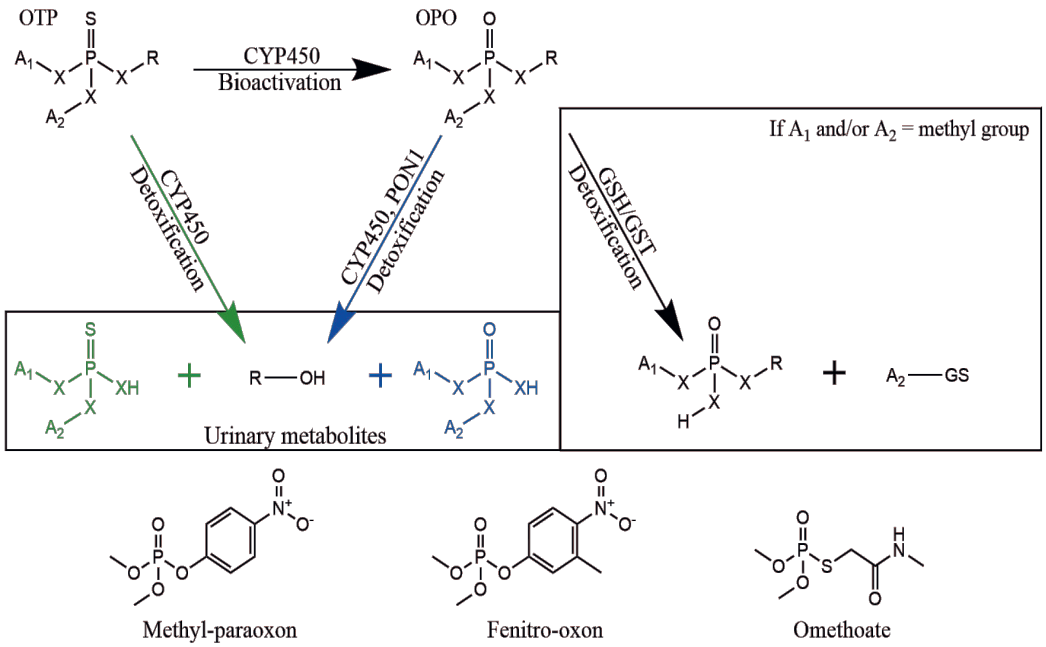


Figure 1: Metabolic scheme of organothiophosphate (OTP) and organophosphate-oxon (OPO) pesticides. In the structures, X can be a sulfur or an oxygen atom, and, usually, no more than two sulfur atoms are bound to the phosphor atom. OTPs and OPOs contain a sulfur or an oxygen atom, respectively, which is connected via a double bond to the central phosphate. A1 and A2 are alkyl groups, typically methyl or ethyl, and sometimes propyl groups. R can be aromatic or aliphatic. In the liver, OTPs can be detoxified to urinary metabolites by CYP450-mediated oxidative cleavage of the ring structure, or they can be bioactivated to OPOs by CYP450-mediated oxidative desulfuration. OPOs can be detoxified to urinary metabolites by CYP450-mediated oxidative cleavage of the ring structure in the liver or hydrolysis by paraoxonase 1 (PON1) enzymes in the plasma and liver. Glutathione-mediated (GSH/GST) detoxification only takes place if at least one of the alkyl groups (A1 or A2) is a methyl group. The OPs structures of OPs investigated in this study are shown below.

However, while PON1 and CYP450-mediated reactions are well characterized, some organophosphates are also metabolized by the less well studied glutathione S transferases (GSTs) (231). Of OP pesticides, predominantly dimethyl-OPOs seem to be metabolized by GST, while diethyl-OPOs are only slightly metabolized via this route (85–97). Up until now, GST-mediated metabolism of organophosphate pesticides has mostly been investigated in a qualitative manner. Quantitative data, like clearance rates or Michaelis-Menten parameters, are still lacking, despite its importance in the development of physiologically based kinetic (PBK) models. PBK models are sets of mathematical equations that describe the physiology of an organism, as well as how a chemical is absorbed, distributed, metabolized and excreted in that organism. These models can be used for estimating internal tissue concentrations and study species variability in toxicokinetics and toxicity. PBK models can also be used in combination with a quantitative in vitro to *in vivo* extrapolation (QIVIVE) approach to derive a point of departure (POD) for risk assessment of organophosphates (154,157,158).

The aim of this study is to investigate and quantify the contribution of GSH-mediated metabolism of dimethyl organophosphates, using S9 subcellular fractions to derive species specific clearance rates. These rates can be used to incorporate the GSH-mediated metabolism in a generic PBK model for organophosphate pesticides which in turn can be used to investigate the influence of GSH-mediated metabolism on the toxicokinetic profiles for rats and humans. This study follows up on a previous study (209), where it was found that internal concentrations of the dimethyl organophosphates pesticides, methyl-paraoxon (MPO), fenitro-oxon (FNO) and omethoate (OMO), are not well predicted by a PBK model incorporating only CYP450- and PON1-mediated metabolism. Work in the current study focused on the GSH-mediated metabolism of the same three dimethyl organophosphates, since the other kinetic parameters and *in vivo* validation data for the PBK model are already available.

2. Materials and methods

2.1 Chemicals and Reagents

Methyl-paraoxon (MPO; >98%), omethoate (OMO; >95%), 4-nitrophenol (4NP; >99%), L-glutathione reduced (GSH, >98%), ethylenediaminetetraacetic acid (EDTA; >99%), formic acid, ammonium formate, hydrochloric acid (HCl) and Trizma base (>99.9%) were obtained from Merck Life Sciences N.V. (Amsterdam, The Netherlands). Tetraisopropyl pyrophosphoramide (iso-OMPA; 95%) was obtained from BOC Sciences (Germany). Ethanol (absolute), methanol (UPLC/MS grade) and acetonitrile (ACN; UPLC/MS grade) were obtained from Biosolve (Valkenswaard, The Netherlands) and Ultrapure water was produced using a Sartorius Arium® Pro ultrapure water system (Göttingen, Germany). Pooled male Sprague-Dawley rat liver S9 cellular fractions (20 mg/mL) were obtained from BioIVT (West Sussex, United Kingdom) and pooled human liver S9 cellular fraction from 150 donors (20 mg/mL) was obtained from Corning (Amsterdam, The Netherlands).

2.2 S9 subcellular fraction incubations

GSH-mediated metabolism of the dimethyl-OPOs MPO and OMO was investigated in vitro using rat and human liver subcellular fractions. Since this type of reaction can be catalyzed by GST, which is present in both microsomal and cytosolic fractions (232), S9 subcellular fractions are used for metabolism studies.

Selection of solvents and reagents

To minimize the effect of solvents and inhibitors, used in these experiments, on the determination of GSH-mediated metabolic rates, chemicals were carefully selected. Clarke et al. (231) suggested that ethanol resulted in the least interference with GST mediated metabolism compared to other solvents. Therefore, ethanol was used as a solvent for stock solutions of the OPOs investigated. Next, EDTA, an ion chelator, was used to inhibit PON1 and CYP mediated metabolism (233,234), as well as minimize oxidizing effects (e.g. lipid peroxidation) during longer (optimization) incubations (235). The presence of EDTA or availability of metal ions was reported to have no effect on the GST dependent metabolism (95). The CYP cofactor nicotinamide adenine dinucleotide phosphate (NADPH) was also intentionally left out to further minimize CYP activity. Lastly, iso-OMPA was added to inhibit butyrylcholinesterase (BuChE) activity (236). To investigate if iso-OMPA itself is metabolized by GST, and therefore interferes by competitive inhibition during incubations, incubations with only this compound were performed. While Iso-OMPA could not be measured directly using LC-MS/MS, incubations with iso-OMPA showed a minimal change in GSH concentration compared to controls (data not shown). Therefore, it is assumed that iso-OMPA is not significantly metabolized by GSTs.

Methods S9 incubations

Optimal incubation time and S9 protein concentration were determined by finding the linear range for metabolite formation and at which not more than 20% of the initial concentration was cleared. Final incubations were performed in glass tubes in a water bath at 37°C and a final volume of 200 µL containing 50 µM of iso-OMPA, 1 mM of EDTA, 5 mM of GSH, 0.5 mg/mL S9 protein and 0, 1, 2, 5, 10, 20, 50, 100 and 200 µM of the methyl paraoxon or omethoate. The incubation was performed in Tris-HCl buffer (50mM; pH 7.4) with a final concentration of 1% ethanol, being the solvent of the OPO stocks. In control samples, GSH or S9 was replaced with Tris HCl buffer. After pre-incubating for 1 minute, the reaction was started by the addition of the optimized amount (5 µL of 20 mg/mL) of S9 protein. After the optimized amount of time had passed, reactions were stopped by precipitating protein using 400 µL of ice-cold ACN. Samples were centrifuged at 4000 g for 20 minutes at 4°C, after which the supernatant was poured over in glass vials and left at room temperature for 20 minutes. Next, the samples were vortexed and transferred to LC-MS vials for measurement.

2.3 GSH incubations

If an organophosphate was found to be metabolized in the presence of GSH, but did not require S9 protein, it was assumed to be a chemical reaction. Chemical incubations with only GSH and the compound of interest were performed in glass reaction tubes in a water bath at 37°C and a final

volume of 1200 µL containing 5mM of GSH and 0, 1, 2, 5, 10, 20, 50, 100 and 200 µM of the compound of interest. The incubation was performed in Tris-HCl buffer (50mM; pH 7.4) with a final ethanol concentration of 1%, being the solvent of the pesticide stocks. After pre-incubating for 1 minute, the reaction was started by the addition of the compound of interest. The mixture was incubated for 2 hours to ensure that the concentration of the formed product was high enough to be measured on LC-MS/MS. Reactions were stopped by transferring the incubation mixture to LC-MS vials. These vials were prepared the prior day by adding 0.8 mL of milliQ water to LC-MS vials before adding the LC-MS inserts. Next, the vials with empty inserts were capped and frozen overnight at -20°C. During the experiments the ice cooled LC-MS vials were transferred to a container with ice when needed. When samples were taken from the reaction mixtures the reaction was stopped by transferring the sample to the ice-cold LC-MS vials. Samples were measured on LC-MS/MS with the autosampler set to 4°C.

2.4 Chemical generation of desmethyl-OPOs

For verification and optimization of the LC-MS/MS methods for the dealkylated forms of the OPOs, the alkaline hydrolysis method of Plapp & Casida (237) was used to generate desmethyl OPOs in a clean sample, containing a high amount of expected metabolites/reaction products. In short, the OPO of interest was dissolved in 1, 2 or 4 molar equivalents of potassium hydroxide in ethanol. The mixture was incubated at around 28°C until the solvent was evaporated. The residue was redissolved in water as much as possible and the supernatant was taken for optimization/verification of the LC-MS/MS method for detecting desmethyl OPOs. This reaction produces desmethyl OPOs as well as cleaved rest groups (237–239).

2.5 Chemical analysis

Organophosphate pesticides and their metabolites were detected using a Shimadzu LC-MS/MS 8040 system using a Shim-pack Velox Biphenyl column (2.1 x 100 mm, 2.7 µm), a Shim-pack Velox - guard column holder and a Shim-pack Velox Biphenyl guard column. The flow was set to 0.4 ml/min with the column oven at 35°C and the autosampler at 4°C. Nebulizing and drying gas flows were 3 L/min and 10 L/min, respectively. Mobile phase A and B consisted of water and methanol, respectively, both containing 2 mM of ammonium formate as well as 0.002% formic acid. The gradient method for mobile phase A started at 97%, and between t=0 and t=1 min it was decreased to 90%. Mobile phase A further decreased to 45% at between t=1 and t=3 min, and to 0% between t=3 and t=6 min. Mobile phase A was kept at 0% between t=6 and t=12 min, and from t=12 to the end of the method (t=16 min), it was increased to 97%. Detection on the LC-MS/MS was done according to the settings shown in **table 1**.

Lacking the reference compounds for the de-alkylated organophosphates, it was not possible to directly quantify these metabolites. Due to the small changes in structure, it was assumed that the metabolites had similar sensitivity to the parent compounds, which were used to quantify the metabolites. A similar approach was used by Abass et al. (240).

2.6 PBK model

The model of Moerenhout et al. (209) was used, since it is able to simulate kinetics upon oral and intravenous exposures of various organophosphate pesticides in rats and humans. This model (see **figure 2**) consists of a compartmental absorption model for oral exposures and three subcompartments representing the body for OTP, OPO and urinary metabolite distribution. In this case, the urinary metabolite is the cleaved ring structure (see **figure 1**). All CYP450 and PON1 metabolic reactions shown in **figure 1** are included. The model was further adapted to include GSH-mediated metabolism for OPOs in liver (see **figure 2**) as well. The GSH mediated human and rat clearance rates, determined experimentally in this study, were scaled based on mg S9 protein per gram of liver. Incubations were performed at GSH levels assumed to be present in the liver (5mM; ranging from 3.6 to 8.57 (242–247)). Therefore, no scaling for GSH concentrations was deemed necessary. For the simulations of FNO, the GSH-mediated clearance rates of MPO were used since these compounds are very similar and differ only by one methyl group in the ring structure of the compounds and is therefore expected to minimally affect demethylation in the phosphate part of the molecule.

Table 1: Detection of organophosphate-oxons methyl-paraoxon (MPO) and omethoate (OMO), and their desmethyl (dm) metabolites, glutathione-S-methyl (GS-methyl) and reduced glutathione (GSH).

	MW	Polarity	MRM	Q1	CE	Q3	RT (min)	LOD (µM)
Methyl paraoxon	247.14	+	248.00>202.00 248.00>109.00	-15 -26	-35 -35	-15 -15	6.45	0.2
dmMPO	233.01	-	232.00>138.00 232.00>108.05 232.00>92.05	16 16 16	17 34 46	11 16 30	4.46	Assumed same as MPO
4NP	139.11	-	138.10>108.00 138.10>92.05 138.10>46.00	15 15 16	21 23 37	16 17 13	5.56	<0.1
Omethoate	213.19	+	231.10>214.05 231.10>124.95 231.10>182.95	-26 -27 -12	-7 -27 -15	-10 -13 -21	0.49	<0.1
dmOMO*	199.1	-	197.90>103.90 197.90>166.90 197.90>72.90	24 18 40			0.77	Assumed same as OMO
GSH	307.32	+	307.95>76.10 307.95>179.10	-14 -14	-29 -11	-29 -12	0.67	0.1
GS-methyl	321.35	+	322.00>76.10 322.00>179.10 322.00>84.00	-35 -35 -35			0.82	0.1

*Detection settings for dmOMO were taken from EU reference laboratories (241).

If demethylation occurred in presence of GSH, but not dependent on S9 protein fraction, it was considered a chemical reaction. In that case, the reaction was scaled to total body water, assuming most tissues contain high concentrations of GSH (see **SI table S2**). For both chemical and S9-dependent reactions, it was assumed that only the unbound fraction is able to participate in GSH mediated reactions. The evaluation of the PBK model was performed in the same way as for the initial model (209). In short, the predicted blood concentration-time profiles were qualitatively evaluated based on the shape of the curve and quantitatively based on the fold difference between predicted and *in vivo* observed values. Predicted concentrations up to a 5-fold difference from observed concentrations were considered adequate for a generic PBK model (209) as this one. Since no human in vivo blood concentration-time profiles were available, C_{max} values were compared between simulations with and without GSH-mediated metabolism for a range of exposures.

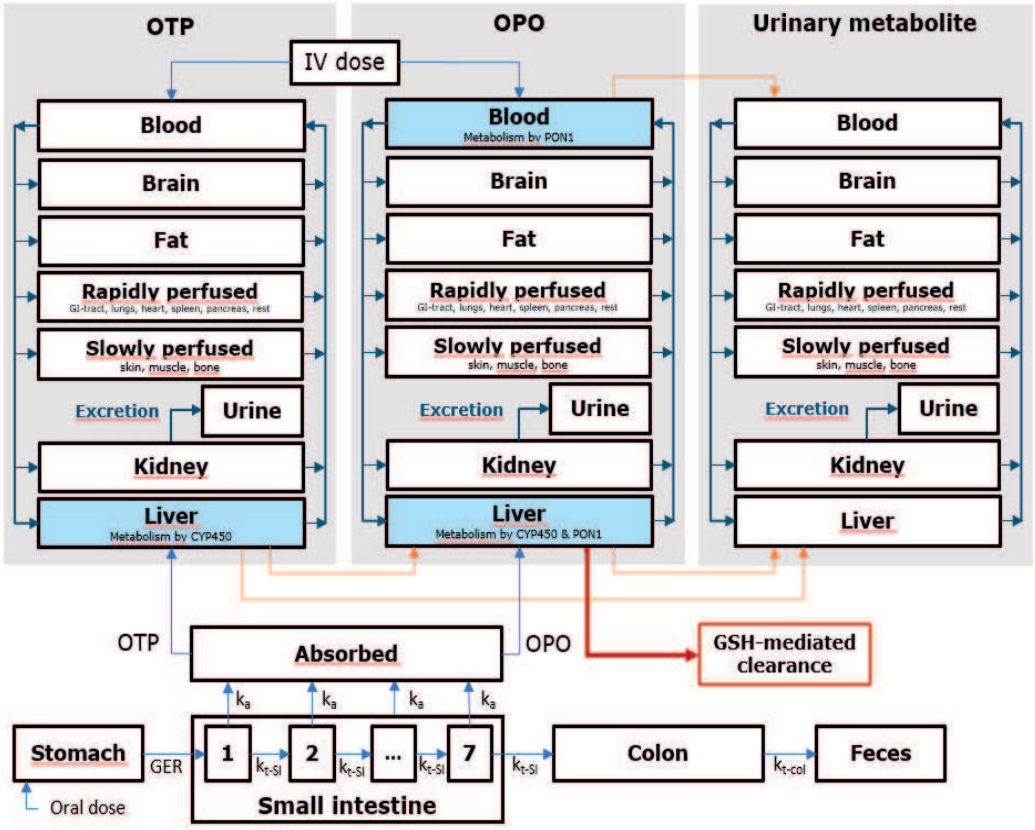


Figure 2: Schematic representation of the PBK model structure. Compounds are absorbed in the small intestine (bottom) and subsequently enter the liver of either the OTP or OPO submodel. Metabolism by CYP450 is incorporated in the liver compartment of both the OTP and OPO submodels. For the OPO submodel, PON1 metabolism is incorporated in the liver and blood compartments. Urinary excretion by glomerular filtration is incorporated in all submodels. Metabolism is represented by orange arrows (CYP450 and PON1) and red arrows (GSH-mediated), while distribution is represented by blue arrows. GER is the gastric emptying rate, kt-SI is the transit rate in the small intestine, ka is the absorption rate constant, and kt-col is the transit time from the colon to feces. Figure adjusted from Moerenhout et al. (209).

2.7 Data analysis

LabSolutions (version 5.114) was used to process LC-MS/MS data. Microsoft Excel and GraphPad Prism (version 5.04) were used to process and visualize incubation data, respectively. The R programming language (version 4.4.2) and R studio (version 2024.09.1 build 394) were used to implement the PBK model. RxODE2 was used to run the PBK model. Tidyverse and dplyr were used for data handling and the Readxl and xlsx packages were used to read and write Excel files for input and output, respectively. For statistics, mean and standard deviation (SD) were used.

3. Results

3.1 Formation of desmethylated organophosphates

Both MPO and OMO were incubated with and without GSH and S9 fractions to investigate GSH-mediated metabolism of these pesticides. DmMPO formation was found to be dependent on both S9 and GSH, suggesting the reaction is enzymatic. The rate of dmMPO formation was quantified for rats and humans and the reaction was not saturated at the concentrations tested (see **figure 3a**). A 4-fold difference was observed in formation rate of dmMPO between the two species (0.237 vs 0.059 nmol/min/mg S9 protein/µM MPO for rat and human, respectively). To determine the storage stability of dmMPO, dmMPO was measured in the same samples, stored at 5°C for 3 days in a row. No significant change in concentration was observed, suggesting the metabolite to be stable for at least 3 days at that temperature (data not shown).

DmOMO formation was found to be dependent on GSH, but not on presence of the S9 fraction (figure 3b). This suggests that the formation of dmOMO is a chemical reaction and not mediated by enzymes. The rate of dmOMO formation was 0.0133 nmol/min/µM OMO in the presence of 5 mM of GSH. It is assumed that tissue GSH levels are similar in rat and human and therefore the rate of demethylation is considered same in both species. The stability of dmOMO could not be assessed since samples containing dmOMO always contained GSH as well.

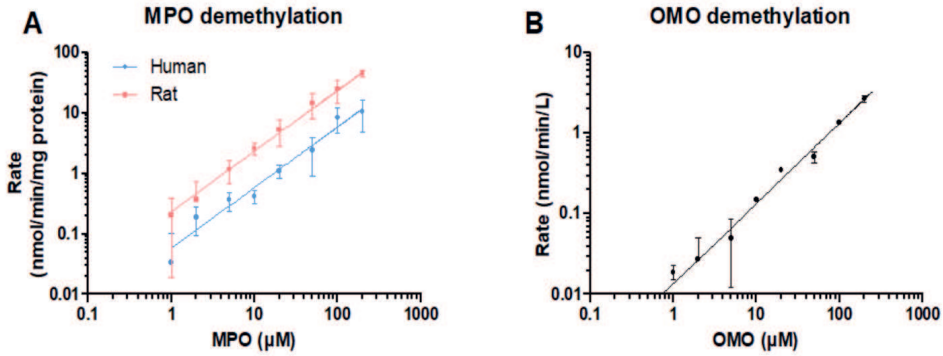


Figure 3: MPO and OMO GSH-mediated demethylation rates derived from incubations with rat and human liver S9 fractions, and GSH. MPO demethylation (**A**) was dependent on both GSH and S9 fraction, while OMO demethylation (**B**) was only dependent on GSH and independent of S9 protein fraction. Fitted lines were forced through the origin. Datapoints represent the mean ± SD of 3 and 2 replicates for MPO and OMO respectively.

Table 2: Formation of dmMPO in MPO-liver S9 incubations and formation of dmOMO in OMO-GSH chemical reactions. Data for dmMPO and dmOMO formation represents the mean ± SD and consist of 3 and 2 replicates respectively. For scaling the formation rate per S9 protein to a gram of liver, the species specific scalars (248–250) for microsomal protein and cytosolic protein were added together, resulting in the values 112.7 and 122 mg S9 protein/gram of liver for rats and humans respectively.

Pesticide	Reaction type	Rat	Human	Units
MPO > dmMPO	Enzymatic	0.2369 ± 0.0010 1.602 ± 0.0068	0.0591 ± 0.0049 0.4326 ± 0.0359	nmol/min/mg S9 protein/µM MPO L/hour/gram liver
OMO > dmOMO	Chemical	0.01334 ± 0.0002 0.8004 ± 0.012		nmol/min/L/µM OMO mL/hour

3.2 Evaluation of adapted PBK model

To investigate the effect of GSH-mediated metabolism on PBK model predictions and accuracy, GSH-mediated clearance of OPOs was incorporated in a previously published PBK model for organophosphate pesticides (209). The organophosphate pesticides methyl-parathion, fenitrothion and dimethoate were used to evaluate this addition, by comparing model outputs with and without GSH-mediated metabolism to *in vivo* experimental data. Given the similar molecular structure of FNO and MPO, where the metabolites differ only by one methyl group, it was assumed that glutathione mediated clearance of FNO is the same as measured for MPO.

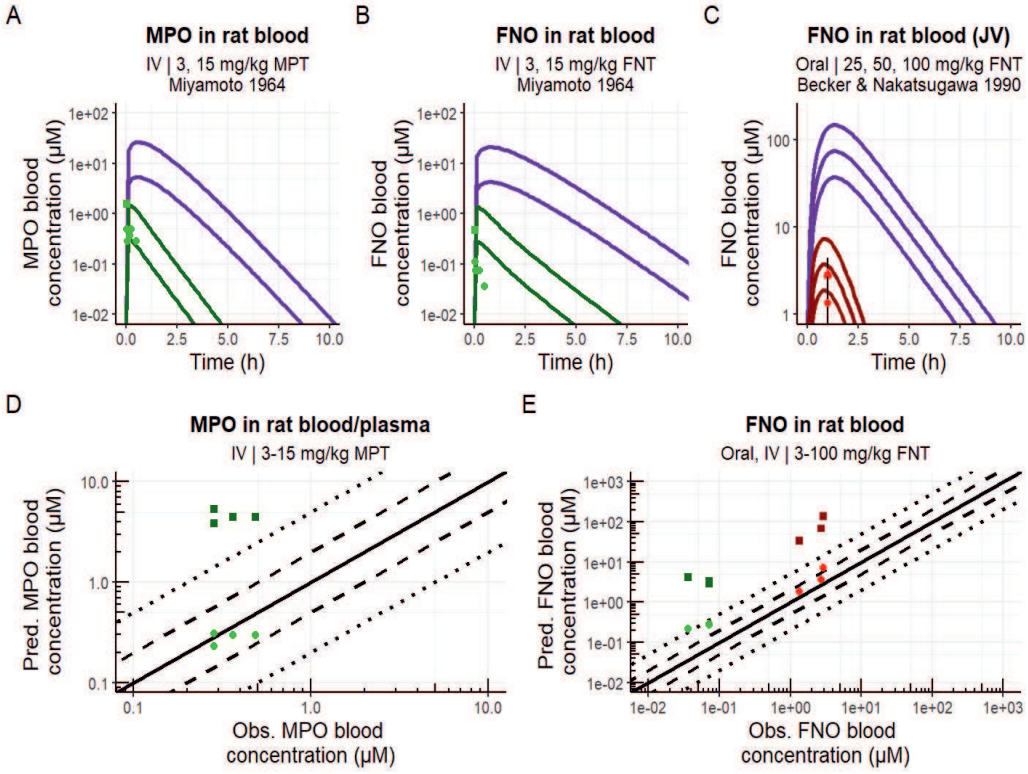


Figure 4: Simulated and *in vivo* rat blood concentration-time plots and observed vs predicted plots for methyl-parathion (MPT) and fenitrothion (FNT) exposures. Improvements of PBK model predictions of blood concentrations in rats by incorporation of GSH mediated metabolism for methyl paraoxon (MPO; A, D) and fenitro-oxon (FNO; via read across; B, C, E) in the PBK model are shown. Solid, dashed and dotted lines represent 1-, 2- and 5-fold difference (D, E). Light green and red shapes are intravenous and oral exposures, respectively, simulated with GSH-mediated clearance included, while dark shapes and purple lines are simulated without GSH-mediated clearance. *In vivo* data was taken from the study of Miyamoto as well as the study of Becker & Nakatsugawa. (251,252).

For both methyl-paraoxon and fenitro-oxon predictions of blood concentrations in rats improved by incorporating GSH mediated metabolism (see **figure 4** and **SI figures S1-S3**). For both chemicals, blood concentrations were poorly simulated, with *in vivo* experimental blood concentrations more

than 10-fold lower than simulated when GSH-mediated metabolism was not incorporated. For methyl-paraoxon, only IV exposure data was available (252), which were predicted within a 2-fold difference of *in vivo* observed blood concentrations when GSH metabolism was included. For fenitro-oxon, data for both IV and oral exposures were available. Here, IV exposures were predicted with about a 5-fold difference, while oral data was predicted with about a 2-fold difference when GSH metabolism was included.

For humans, no *in vivo* data was available to validate the simulations. That said, without GSH-mediated metabolism, methyl-paraoxon and fenitro-oxon were cleared slowly. Inclusion of GSH-mediated metabolism significantly changed the blood concentration-time profile of these metabolites. For methyl-paraoxon and fenitro-oxon, C_{max} values were 15.5- and 11.9-fold lower when GSH was included for the tested doses (0.01, 0.1 and 1 mg/kg body weight) of the respective parent compounds (**figure 5**).

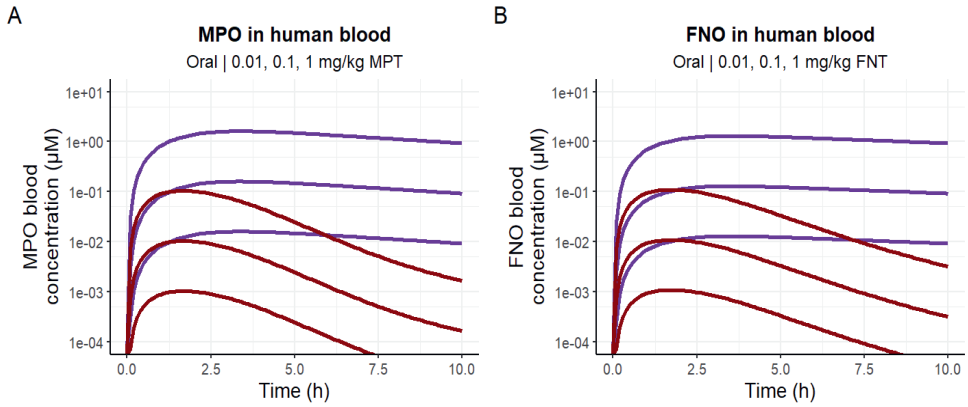


Figure 5: Simulated human blood concentrations-time profiles of methyl-paraoxon and fenitrothion after oral exposures. Methyl-paraoxon (MPO; A) and fenitro-oxon (FNO; B) after oral exposures (three dosages) of parent compounds methyl-parathion (MPT) and fenitrothion (FNT) in humans, with (red) and without (purple) GSH-mediated metabolism. No *in vivo* data was available to validate these simulations.

For OMO, oral and IV exposure data in rats was available from the study of Nallani et al. (79). Without GSH-mediated metabolism omethoate blood concentrations in rats were overpredicted with a 5-fold difference compared to *in vivo* observed concentrations. However, this did not change when implementing GSH mediated metabolism for OMO, as the chemical demethylation of OMO minimally affects the overall plasma concentration-time profile in rats. Therefore the data was not shown.

4. Discussion

GSH-mediated reactions, are often overlooked in in vitro clearance studies, while essential for understanding kinetic and internal exposure profiles, as well as risk assessment using animal-data free testing methods. The investigations performed here have confirmed that dimethyl organophosphates can be metabolized by GSH-mediated reactions and quantified GSH-mediated reaction kinetics for the organophosphates methyl-paraoxon and omethoate.

For methyl-paraoxon, it was found that GSH-mediated demethylation was enzymatic and the formation rate of the demethylated metabolites was 4-fold higher in rats compared to humans (0.237 vs 0.059 nmol/min/mg S9 protein/μM for rat and human, respectively). Meanwhile, GSH-metabolism of omethoate was found to be nonenzymatic and was therefore expected to be the same for rat and human (0.01334 nmol/min/L/μM OMO). When implementing these reactions in the rat PBK model, predicted blood concentrations of omethoate did not change, however, predictions for methyl-paraoxon improved from over 10-fold (i.e. without GSH-mediated metabolism) to less than 2-fold difference when compared to *in vivo* rat experimental data. Furthermore, when GSH-mediated clearance data from methyl-paraoxon was used for read-across modelling of fenitro-oxon, oral exposure simulations in rats improved to a similar degree as for methyl-paraoxon, while intravenous exposures improved from 15- to 20-fold to about 5-fold difference when compared to *in vivo* experimental data. In human model simulations, simulated C_{max} values in blood in the dose range of 0.01-1 mg/kg body weight changed by 12- to 16-fold when GSH-mediated metabolism was implemented. These data show the importance taking into account GSH-mediated metabolism in risk assessment of organophosphate pesticides, since it exposes differences between human and rat metabolism. While the species difference for the GSH-mediated reaction is only 4-fold, other metabolic reactions in the liver and plasma for organophosphates showed significant differences as well (209).

In risk assessment an uncertainty factor of 10 is often used to translate rodent toxicity data to the human situation. In turn, this uncertainty factor is built up of uncertainty factors of 4 and 2.5 for species differences in kinetic and dynamic processes, respectively (99). Since only the GSH-mediated metabolic reaction already shows a 4-fold difference between rat and humans, while CYP450 and PON1 mediated reactions were also shown to be of a higher rate in rats, this raises the question if the standard uncertainty factors for species differences are enough for safely translating rat toxicity data to humans for dimethyl organophosphate pesticides.

4.1 Potential effects on dimethyl organophosphate toxicity

The findings in this paper raise some questions about the toxicity of dimethyl organophosphate pesticides. Specifically the effect of GSH on irreversible binding mechanism (also known as 'aging') of dimethyl organophosphates to AChE as well as effects of chronic exposure on GSH levels.

Organophosphates (oxons) normally bind covalently to a serine residue in the catalytic center of various esterases (AChE, butyrylcholinesterase, carboxylesteras) (13,14). This bond is manifested by releasing the rest group of the organophosphate molecule (the non-methyl or non-ethyl group, usually a ring structure). While this inhibits the enzyme, the phosphate-enzyme bond can still be hydrolyzed, freeing and reactivating the enzyme (15,16). However, it is also possible that one of the methyl or ethyl groups is hydrolyzed instead. If this happens, the enzyme is permanently inactivated, also known as 'aged' (17–19). While demethylated organophosphates on their own are expected to be significantly less toxic (253), the interaction of the esterase-bound dimethylphosphate group with GSH could potentially affect the reversibility of dimethylphosphate-esterase binding. Since GSH is able to react with the methyl groups of dimethyl (organo)phosphates by itself, it might also induce further aging of the (organo)phosphate-enzyme complex by reacting

with one of the methyl groups of the dimethylphosphate-enzyme complex. Since inhibition kinetics experiments are often performed with isolated or pure enzyme, GSH that is normally present in the blood is not, or minimally, present in these kinetics experiments. Therefore, the effect of GSH on aging has never been appropriately investigated. More research needed to reveal if GSH has an effect on aging kinetics of dimethyl organophosphate pesticides.

Besides inhibition of AChE, interaction of dimethyl organophosphate pesticides, like omethoate, with GSH raises concern regarding the possibility of lowering GSH concentrations during chronic exposure. Direct and GST-mediated reactions with GSH suggests dimethyl organophosphate pesticides are able to lower cellular GSH levels and therefore their anti-oxidant status. It needs to be stressed here that (especially chronic) exposure to mixtures of pesticides and other compounds that influence GSH levels, may lower GSH concentrations and anti-oxidant status, for longer periods of time. If the body is not able to counter this, the affected tissue becomes more vulnerable to other sources of oxidative stress, like inflammation, metabolism, UV exposure etc., potentially resulting in tissue and DNA damage in the long term.

4.2 Conclusion

Dimethyl organophosphates methyl-paraoxon and omethoate were shown to undergo GSH-mediated metabolism, in the form of enzymatic or chemical (nonenzymatic) reactions, respectively. Other dimethyl-organophosphate are expected to undergo GSH-mediated metabolism as well. When implementing GSH-mediated metabolism in a rat PBK model significantly improved simulations of *in vivo* kinetics for methyl-paraoxon and fenitrothion (read-across) for rats. Predictions for omethoate, which reacted only nonenzymatically with GSH, did not change. The interactions of dimethyl organophosphate pesticides with GSH raise concerns about its influence on irreversible binding as well as the long term exposure effects on the anti-oxidant status, which could be of importance in future risk assessments of dimethyl-organophosphate pesticides.

Supporting information

Since the model code was almost identical to the model developed in chapter 2 (code can be found here: https://doi.org/10.1021/acs.est.4c06534). Only the parts that were added to include glutathione-mediated metabolism are shown below:

1. In the metabolism scaling part, the following lines of code were added:

```
OPOVmax4  <- OPOVmax4c / 1000 * 60 * (MPL+CPL) * 1000 * VLi; # umol/h/mg S9 protein * mg S9 protein = umol/h
# OPOVmax4  <- OPOVmax4c / 1000 * 0.75*BW; #used for chemical degradation of OMO in rat, assuming 75% body water
```

2. In the liver metabolism part the following line was added:

```
AMR6    <- (OPOVmax4 * fupOPO*CVLiOPO*BPROPO) # Amount metabolized from OPO to OPM in liver S9 by GST
```

3. In the differential equations for the liver, the bold code was added:

```
if(TOP == 1 ){
  d/dt(ALiTOP) <- (ka*Ain1 + ka*Ain2 + ka*Ain3 + ka*Ain4 + ka*Ain5 +
                   ka*Ain6 + ka*Ain7) + QLi * (CBlTOP - CVLiTOP) - AMR1 - AMR2;
  d/dt(ALiOPO) <- QLi * (CBlOPO - CVLiOPO) + AMR1 + AMR3 - AMR4 - AMR6;
  d/dt(ALiOPM) <- QLi * (CBlOPM - CVLiOPM) + AMR2 + AMR3 + AMR4 + AMR6;
}else{
  d/dt(ALiTOP) <- QLi * (CBlTOP - CVLiTOP) - AMR1 - AMR2;
  d/dt(ALiOPO) <- (ka*Ain1 + ka*Ain2 + ka*Ain3 + ka*Ain4 + ka*Ain5 +
                  ka*Ain6 + ka*Ain7) + QLi * (CBlOPO - CVLiOPO) + AMR1 - AMR3 - AMR4 - AMR6;
  d/dt(ALiOPM) <- QLi * (CBlOPM - CVLiOPM) + AMR2 + AMR3 + AMR4 + AMR6;
}
```

Supporting figures: Comparison of in vivo observed and in silico predicted blood concentrations

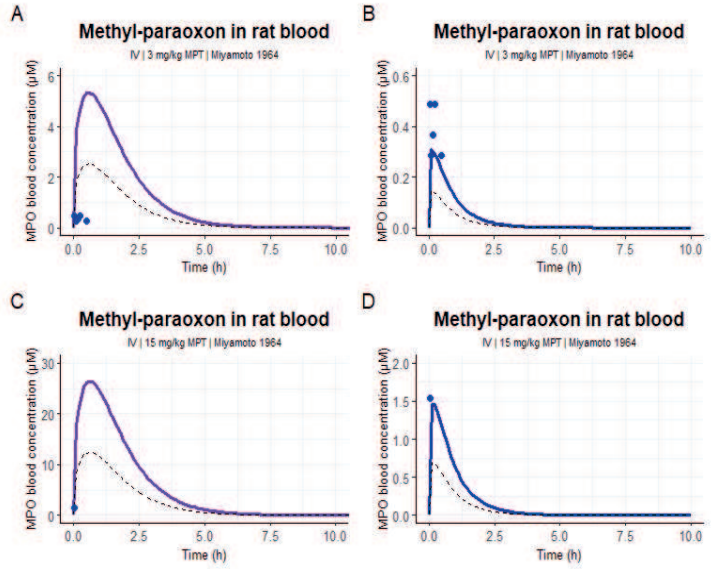


Figure S1: Predictions of rat blood concentrations of methyl paraoxon after exposure to methyl parathion with (blue solid line) and without (purple solid line) GSH mediated metabolism. The dashed line shows the free, unbound concentration. In vivo observed blood concentrations in rats form the methyl parathion exposure study of Miyamoto (252) (blue dots).

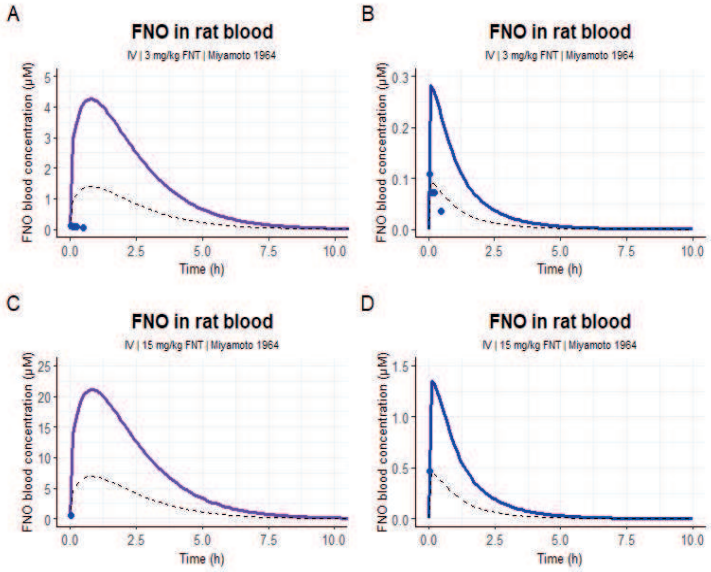


Figure S2: Predictions of rat blood concentrations of fenitro-oxon after exposure to fenitrothion with (blue solid line) and without (purple solid line) GSH mediated metabolism. The dashed line shows the free, unbound concentration. In vivo observed blood concentrations in rats form the fenitrothion exposure study of Miyamoto (252) (blue dots).

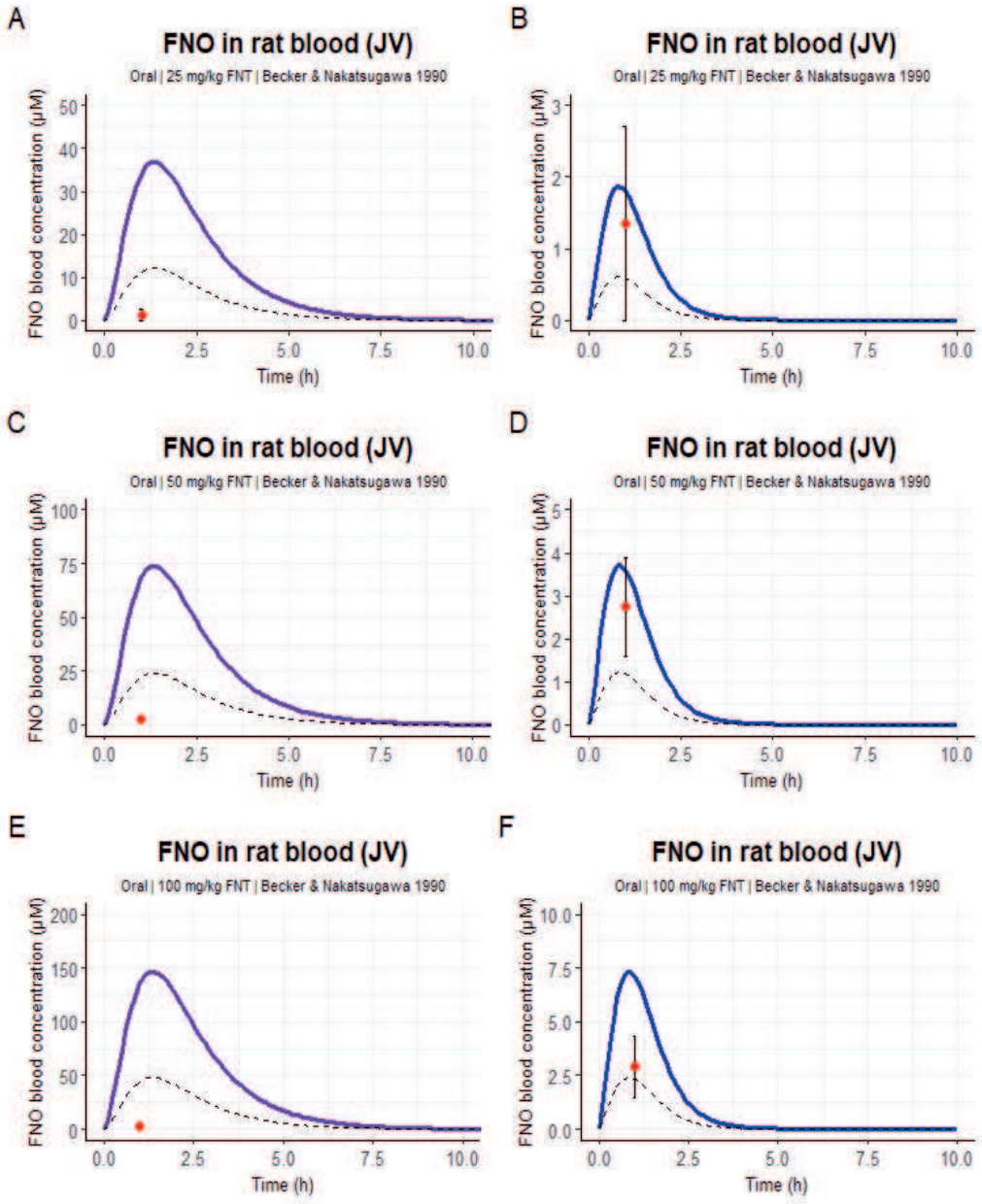


Figure S3: Predictions of rat blood concentrations of fenitro-oxon after exposure to fenitrothion with (blue solid line) and without (purple solid line) GSH mediated metabolism. The dashed line shows the free, unbound concentration. In vivo observed blood concentrations in rats form the fenitrothion exposure study of Becker & Nakatsugawa (251) (red dots).

5

Application of new approach methodologies for point of departure prediction in organophosphate pesticide hazard assessment

Thijs M.J.A. Moerenhout, Wouter Bakker, Hans Bouwmeester and Nynke I. Kramer.

Manuscript in preparation

Abstract

Organophosphate pesticides are able to inhibit the enzyme acetylcholinesterase (AChE) potentially resulting in neurotoxic effects. Due to their common use in agricultural practice, the general public is mainly exposed to these compounds via their diet. Traditional risk assessment determines safe dose levels for humans based on animal experiments. Recently, ethical concerns and concerns about species differences have been raised stimulating research into animal-free methods supporting risk assessment. Here, an animal free approach to predict a safe point of departure determination is used for oral exposure to eight organophosphate pesticides in rat and human. Concentration effect data for these eight OP pesticides was derived from AChE inhibition assays. A physiologically based kinetic (PBK) model was used for quantitative *in vitro* to *in vivo* extrapolation (QIVIVE) of concentration-effect in vitro data to predicted human dose-effects. This data was used to determine $BMDL_{10}$ values by using benchmark dose modelling. Predicted $BMDL_{10}$ values were compared to reported *in vivo* points of departure. Points of departure for nearly all investigated organophosphate pesticides were predicted to be within 4-fold from reported LOAEL values and higher than reported NOAEL values. The use of PBK modelling in combination with *in vitro* toxicity assays was shown to be a viable strategy for organophosphate point of departure derivation for AChE inhibition endpoints in an animal free manner.

1. Introduction

Organophopshate compounds have been used as pesticides since the late 1940s (254) and are still in use today (3). Multiple types of organophosphate pesticides can be grouped in two classes: organophosphate-oxons and organothiophosphates. Organophosphate-oxon compounds, containing a P=O bond, are effective inhibitors of acetylcholinesterase (AChE) and therefore highly toxic (13,14). On the other hand, organothiophosphates, containing a P=S bond, are usually not very toxic by themselves, but can be bioactivated to organophosphate-oxon compounds (76–81). organothiophosphates s and organophosphate-oxons can be further subdivided into di-methyl- and di-ethyl-organophosphates, which have two methyl or two ethyl groups attached to the central phosphate moiety respectively. While only a few organophosphate pesticides are still used in Europe, many organophosphate pesticides are still used in large volumes in other parts of the world (3).

Risk assessment of organophosphate pesticides and other chemicals has traditionally relied on data from animal experiments. These experiments are considered cruel, unsustainable and an inefficient way of performing risk assessments for the large number of chemicals to which humans are potentially exposed. Besides this, it is possible that substantial differences in toxicity exist between rats and humans, further incentivizing the search for alternatives to animal testing (103). Recently, there has been a push towards replacement, reduction and refinement of animal experiments (104,105,105–107,255). Next generation risk assessment aims to reduce the reliance on toxicity tests with animals and integrate data from a battery of *in vitro* assays and in silico tools. This approach aims to translate estimated bioactive concentrations from *in vitro* assays to bioequivalent *in vivo* exposures (105–107). Translating *in vitro* data to the *in vivo* situation is called quantitative *in vitro* to *in vivo* extrapolation (QIVIVE), which can be performed using physiologically based kinetic (PBK) models. PBK models are computational tools that describe the body and compound kinetics using mathematical equations, enabling prediction of internal concentrations of a compound after exposure (108,256). In QIVIVE, *in vitro* concentration-effect data is translated to *in vivo* dose-effect data, by predicting what external dose is needed to reach internal concentrations at the levels used in the *in vitro* experiments.

According to next generation risk assessment principles, this manuscript describes an approach for deriving points of departure of eight organophosphate pesticides, without relying on animal experiments. In this approach, a previously published physiologically based kinetic model (257) will be used to translate *in vitro* determined AChE concentration-inhibition curves to *in vivo* dose response curves for eight organophosphate pesticides. These dose response curves, in turn, will be used to predict a point of departure (POD) using benchmark dose modelling (BMD) and compared to reported *in vivo* points of departure.

2. Materials and methods

2.1 Chemicals

Chlorpyrifos, diazinon, diazinon-oxon, methyl-parathion, methyl-paraoxon, ethyl-parathion, ethyl paraoxon, dimethoate, omethoate, chlorfenvinphos, profenofos, 5,5'-dithiobis (2-nitrobenzoic acid)

(DTNB; >98%), acetylthiocholine iodide (ATC; >98%), ethopropazine hydrocholoride (>98%) and Triton X-100 reduced (>99%) were ordered at Merck Life Sciences N.V. (Amsterdam, the Netherlands). Chlorpyrifos-oxon, was ordered from LGC standards (Teddington, United Kingdom). Bovine serum albumin (BSA) and recombinant human AChE (rhAChE) were ordered from Sigma Aldrich (St. Louis, USA). Pooled Sprague Dawley rat whole blood with K2EDTA (assumed 5 mM) as anti-coagulant was ordered from Innovative Research (Novi, USA). Human whole blood was donated by human volunteers (2 female, 1 male) and was drawn by a professional.

2.2 AChE isolation

Isolation of AChE from rat whole blood was performed based on the protocols by Zhao et al. and Meek et al. (130,157). Two milliliters of rat whole blood was centrifuged (4°C; 3000g) for 15 minutes and plasma was removed. The erythrocytes were resuspended in 9 mL of phosphate buffer (20mM; pH 7.4) and stored at -80°C for 24 hours. Next, the cells were thawed and centrifuged (4°C; 4000 g) for 15 minutes and supernatant was removed. The cells were washed three times using 9 mL of phosphate buffer (20mM; pH 7.4), centrifuging each time (4°C; 4000 g) and removing the supernatant. After washing three times, the pellet was resuspended in 500 uL of phosphate buffer (100 mM; pH 7.4) centrifuged one more time and the supernatant was aliquoted and stored at -80°C. One aliquot of isolated rat AChE was used to determine the enzyme activity by creating a calibration curve using recombinant human AChE. The activity was found to be 0.4-0.6 U/mL. In preliminary studies, activity of the resuspended pellet was about 12-fold higher than that of the supernatant (1.8 vs 0.15 U/ml, respectively). However, the supernatant was used since it would give less interference of hemoglobin and cell debris, which could lower the free fraction of compound. Furthermore, the half maximal inhibitory concentrations (IC_{50}s) for chlorpyrifos-oxon were very similar for supernatant and pellet: 15.29 and 17.45 nM, respectively.

2.3 Whole blood AChE inhibition assay

Whole blood AChE inhibition assay was based on the method by Ellman et al. (138), modified by Kasteel et al. (12) for whole blood. Pesticide stock solutions (13 different concentrations) were prepared in ethanol, which was found to have low influence on AChE at final concentrations (0.1%) (258). These were diluted 100 times in phosphate buffer (100 mM; pH 7.4), after which 10 µL was added to 90 µL whole blood in a 48 wells plate. For the negative and vehicle controls, 10 µL of phosphate buffer and 1% ethanol in phosphate buffer was added instead, respectively. The plate was incubated on a shaker (room temperature, 600 rpm) for 30 minutes, after which 50uL of each of the incubation mixtures was added to 950 µL of 0.3% triton-X solution and mixed well. Triton-X was found to have minimal effects on AChE but an inhibitory effect on BuChE (10,259). In a new 48-wells plate, 460uL of DTNB solution (1.3 mM), 20 µL of ethopropazine solution (3 mM), a specific BuChE inhibitor (260), and 20 µL of the triton-X diluted blood-pesticide mixtures were added to each well, except for the blanks, to which only 480 µL of DTNB solution (1.3 mM) and 20 µL ethopropazine was (3 mM) added. The plate was incubated on a shaker (room temperature; 600 rpm) for 20 minutes, after which 100 µL of ATC solution (6 mM) was added to each well except for the blanks, to which 100 µL of phosphate buffer (100 mM; pH 7.4) was added. Immediately after,

the absorbance was measured every 2 minutes for 1 hour at 436 nm (to minimize absorption from hemoglobin at 412 nm (259)) with a final volume of 600 µL/well. For each compound the assay was performed three times with three technical replicates per plate. Preliminary experiments showed that a prolonged incubation time did not change the inhibition curve. Using this protocol, the uninhibited AChE activity ranges of human and rat whole blood experiments were 3-4 U/ml and 0.5-0.6 U/ml, respectively.

2.4 AChE enzyme inhibition assay

Recombinant human/isolated rat AChE inhibition assay was based on the method by Ellman et al. (138) modified by Zhao et al. (157). Pesticide stock solutions (10 different concentrations) were prepared in ethanol and were diluted 100 times using buffer A (phosphate buffer 100 mM at pH 7.4 containing 0.1 mg/mL BSA). In case of the negative and positive controls, 5 µL of the solvent and chlorpyrifos-oxon solution were used instead of the pesticide stock solutions, respectively. In a 96 wells plate, 40 µL of buffer A and 5 µL of the pesticide working solutions were added to each well. For the negative and positive controls, 5uL of the respective 2% ethanol and 100 µM chlorpyrifos-oxon (prepared in buffer B) were added instead. Next, 5 µL of enzyme solution was added to each well, after which the plate was incubated on a shaker (room temperature; 600 rpm) for 15 minutes. After incubation, 150 µL of a solution containing 0.4 mM ATC and 0.05 mM DTNB in buffer A was added to each well and absorbance was measured every minute for 20 minutes at 412nm at room temperature. For the quantification of background signal, the same incubations were performed, but instead of enzyme solution, phosphate buffer (100 mM; pH 7.4) containing 1 mg/mL BSA was added. For each compound the assay was performed three times with three technical replicates per assay. Using this protocol, the activity ranges of uninhibited human recombinant and rat isolated AChE were 0.6-0.8 U/ml and 0.4-0.6 U/ml, respectively.

2.5 Fraction unbound estimation

The fraction unbound of organophosphate-oxons was estimated by comparing the IC_{50}s for AChE inhibition in whole blood and in recombinant human/isolated rat enzyme, assuming an unbound fraction of 1 in the enzyme-based AChE inhibition assays. This method assumes that the difference in IC_{50} between these assays is solely due to nonspecific binding of the organophosphate pesticides to different components of the blood, which are considered absent in the enzyme-based AChE inhibition assay.

$$fu_b = \frac{IC_{50-enzyme}}{IC_{50-blood}} \quad (1) \qquad fu_p = \frac{fu_b \times BPR}{1 - Hct} \quad (2)$$

Since BPR values are unavailable for the pesticides under investigation, the BPR was assumed to be 1, since all compounds of concern in this study are neutral compounds (261). The estimated fu_p were not used in the physiologically based kinetic model, since the model was not validated using these values.

2.6 Quantitative *in vitro* to *in vivo* extrapolation and BMD modelling

A previously published physiologically based kinetic model was used to predict internal concentrations for eight organophosphate pesticides. QIVIVE was performed for a 0.25 kg rat and a 70 kg human. The parameters used are stated in a previously published study on the development of the physiologically based kinetic model of Moerenhout et al. (209,257). It is assumed that desalkylated organophosphates do not sufficiently inhibit AChE as long as the molecule does not contain an amine group (253), and that di-methyl- or di-ethyl-phosphates (without the rest group) do not sufficiently inhibit AChE with respect to organophosphate-oxons (262). Absorption rate constants (k_as) for organophosphate pesticides in humans were calculated using the same method as was used for rats by Moerenhout et al. (209). In short, k_as were scaled based on the k_as of 0.1 and 0.6 for chlorpyrifos, which were found when fitting the k_a (209) to data from Timchalk et al. (131) and Nolan et al. (175) in humans (see **SI Absorption rate constant calculation**). Since blood AChE inhibition is considered an adequate surrogate endpoint for neuronal AChE inhibition (263,264), blood AChE inhibition is used to predict the point of departure. Therefore, the C_{max} in blood and the C_{max} of the free unbound fraction in blood of the physiologically based kinetic model predictions was used to translate concentrations in the *in vitro* determined concentration-inhibition curves to the associated dose for the whole blood AChE and recombinant human/isolated rat enzyme experiments respectively. The predicted dose-inhibition curve was used for BMD modelling using the online tool provided by the Dutch National Institute for Public Health and the Environment (RIVM; https://proastweb.rivm.nl/, version 71.1). The benchmark response (BMR) was set to 10% with a lower 95% confidence limit. Continuous model fitting was used to get a weighted average model fit.

2.7 Data analysis

GraphPad Prism (version 5.04) was used to derive concentration-inhibition curve and the IC_{50} using the 'log(inhibitor) vs. response -- Variable slope (four parameters)' model. R (version 4.4.2), Rstudio (version 2024.09.1 build 394) and the RxODE2 package (version 4.02) were used to run the physiologically based kinetic model for QIVIVE.

3. Results

3.1 AChE inhibition assays

Figure 1 and table 1 show that organophosphate-oxons were stronger inhibitors of AChE compared to their parent (organothiophosphate) compounds in experiments using rat and human whole blood and isolated rat and recombinant human enzyme. Furthermore, recombinant human and isolated rat AChE were more strongly inhibited compared to AChE in whole blood. An exception is omethoate, where inhibition of AChE in blood was stronger than isolated rat and recombinant human AChE (8.9 vs 16.7 and 19.7 vs 34.7 µM, respectively). Profenofos and fenitrothion were not able to fully inhibit AChE activity in both rat and human blood. Furthermore, species differences were observed for omethoate and methyl-paraoxon, which fully inhibited AChE activity at high

concentrations in rat blood, but not in human blood. Other species differences were found where humans were 10-fold more sensitive to than rats to AChE inhibition by ethyl-paraoxon in whole blood, but not when using recombinant human and isolated rat enzyme. Furthermore, differences in enzyme incubations, but not whole blood incubations were observed. Compared to humans, rats were five and eight times more sensitive to AChE inhibition by methyl parathion and fenitrothion, respectively. In turn, humans were four times more sensitive to AChE inhibition by profenofos compared to rats. All other compounds generally differed not more than 2- and 5-fold in enzyme and blood IC_{50}s respectively. Overall, IC_{50} values determined in this study were not more than 2-fold different from those reported in literature, except for ethyl-paraoxon in rats, which was at most three times lower (see **SI table S1**).

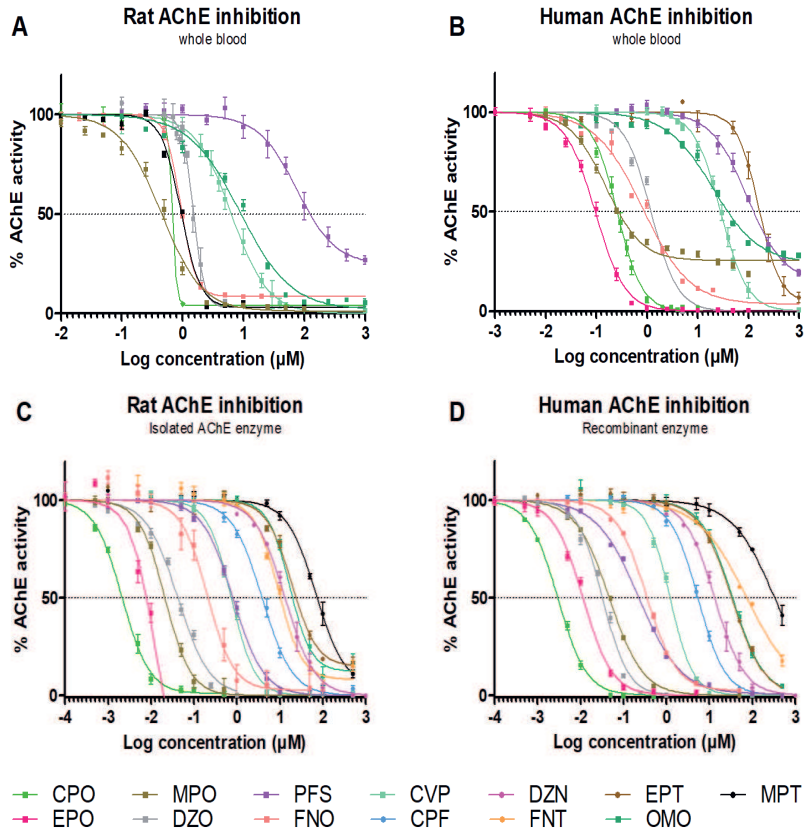


Figure 1: AChE inhibition of human and rat whole blood and recombinant human/isolated rat enzyme by organophosphate pesticides. AChE inhibition of rat and human whole blood are shown in panel A and B, respectively. Inhibition of isolated rat and human recombinant AChE are shown in panel C and D, respectively. AChE was inhibited by methyl-parathion (MPT), omethoate (OMO), ethyl-parathion (EPT), diazinon (DZN), fenitrothion (FNT), chlorpyrifos (CPF), chlorfenvinphos (CVP), profenofos (PFS), fenitro-oxon (FNO), methyl-paraoxon (MPO), diazinon-oxon (DZO), chlorpyrifos-oxon (CPO) and ethyl-paraoxon (EPO). Chlorpyrifos-oxon was used as positive control to define 0% AChE activity. Circle (organothiophosphates) and square (organophosphate-oxons) shapes represent the mean ± SEM for 3 separate determinations. Human and rat blood data for fenitrothion and fenitro-oxon were obtained from Chen et al. (152); Human blood data for diazinon from Kasteel et al. (12) and human blood data for diazinon-oxon were obtained from Chen et al. (265); Rat enzyme data for diazinon were obtained from Zhao et al. (157). All other data was measured in this study.

Table 1: IC_{50} values for human and rat whole blood and recombinant human/isolated rat enzyme AChE inhibition by organophosphate pesticides.

Pesticide / metabolite	Rat IC_{50} (µM)		Human IC_{50} (µM)	
	Blood	Enzyme	Blood	Enzyme
Chlorpyrifos	NI	3.8521 ± 0.2962	NI	5.3976 ± 0.2173
Chlorpyrifos-oxon	0.6767 ± 0.1472	0.0021 ± 0.0002	0.2557 ± 0.0092	0.0030 ± 0.0001
Diazinon*	>1000	13.459 ± 0.5534	>10	13.152 ± 0.7156
Diazinon-oxon*	1.5018 ± 0.0478	0.0423 ± 0.0034	1.1964 ± 0.1820	0.034 ± 0.0017
Fenitrothion*	489.78 ± 84.430	9.1706 ± 1.0833	>1000	74.302 ± 17.525
Fenitro-oxon*	0.9333 ± 0.0249	0.2027 ± 0.0443	0.8232 ± 0.1104	0.3414 ± 0.0106
Methyl-parathion	NI	68.549 ± 6.3319	>1000	331.13 ± 374.54
Methyl-paraoxon	0.4467 ± 0.0306	0.0212 ± 0.0017	0.1537 ± 0.0081	0.0468 ± 0.0017
Ethyl-parathion	NI	18.750 ± 2.2699	159.22 ± 15.040	32.659 ± 2.7295
Ethyl-paraoxon	0.9390 ± 0.0326	0.0125 ± 0.0010	0.0953 ± 0.0036	0.0115 ± 0.0007
Dimethoate	NI	NI	NI	NI
Omethoate	8.8614 ± 0.7878	16.749 ± 2.2404	19.678 ± 1.7190	34.674 ± 3.9933
Chlorfenvinphos	6.3929 ± 0.5642	0.7408 ± 0.0325	28.379 ± 1.5559	1.2134 ± 0.0425
Profenofos	75.509 ± 13.172	0.8046 ± 0.0455	94.406 ± 10.928	0.2253 ± 0.0083

NI: No inhibition up until 1000 µM. *Some or all concentration-response data obtained from other studies: Blood data for fenitrothion and fenitro-oxon were obtained from Chen et al. (152); Human blood data for diazinon from Kasteel et al. (12) and human blood data for diazinon-oxon were obtained from Chen et al. (265); Rat enzyme data for diazinon were obtained from Zhao et al. (157). Data is presented as mean ± SE.

3.2 Fraction unbound in blood and plasma

Fractions unbound in blood were estimated based on blood and enzyme IC_{50}s, using equation 1 (see **table 2**). The fraction unbound in blood was lower in rat for chlorpyrifos-oxon, fenitro-oxon, methyl paraoxon and ethyl paraoxon, while omethoate, chlorfenvinphos and profenofos had a higher fraction unbound in rats compared to humans. This suggests differential binding to blood components in rats and humans. The estimated fraction unbound of diazinon-oxon was very similar in rat and human blood. For organothiophosphates, the data allowed only estimations of fractions unbound for fenitrothion in rats and ethyl-parathion in humans. The estimated fraction unbound of fenitrothion in rat blood was lower compared to that of its oxon, fentro-oxon (0.042 vs 0.483, respectively). Furthermore, the estimated fraction unbound in human blood of ethyl-parathion was higher compared to its oxon, ethyl-paraoxon (0.267 vs 0.456, respectively), suggesting the presence of alternative binding sites or increased binding affinity for ethyl-paraoxon in human blood (see also **SI figure S1**). The indication of alternative binding sites is also shown in **SI figure S2**, where ethyl-paraoxon inhibited AChE to a larger extend than the positive control (chlorpyrifos-oxon). Estimation of the fraction unbound in blood of omethoate was higher than 1 for both rats and humans (1.89 and 1.76, respectively). Consequently, estimated fractions unbound in plasma for omethoate were even higher, surpassing the maximum value of 1. This suggests that either the assumption of a BPR of 1 is not correct for omethoate, or that something is else is happening to the compound during incubations. When comparing the estimated fu_p of diazinon-oxon to its in silico predicted values based on algorithm of Lobell & Sivarajah (119), a 5-fold difference was found for both humans and rats. For many other organophosphates, the in silico predicted fu_p was often close to the estimated fraction unbound of one of the two species.

Table 2: Comparison of fraction unbound in blood (fu_b) and plasma (fu_p) estimated from human and rat whole blood and recombinant human/isolated rat enzyme IC_{50}s with in silico QSPR predictions.

Pesticide / metabolite	*In vitro* estimated fu_b		*In vitro* estimated fu_p		In silico predicted fu_p
	Rat	Human	Rat	Human	
Chlorpyrifos-oxon	0.0031	0.0115	0.007	0.026	0.051
Diazinon-oxon	0.0281	0.0284	0.063	0.063	0.262
Fenitrothion	0.0187	NP	0.042	NP	0.091
Fenitro-oxon	0.2172	0.4147	0.483	0.922	0.344
Methyl-paraoxon	0.0474	0.3043	0.105	0.676	0.453
Ethyl-parathion	NP	0.2051	NP	0.456	0.054
Ethyl-paraoxon	0.0133	0.1202	0.030	0.267	0.28
Omethoate	*1.8902*	*1.7619*	*4.200*	*3.916*	0.866
Chlorfenvinphos	0.1159	0.0428	0.258	0.095	0.056
Profenofos	0.0107	0.0024	0.024	0.005	0.023

Unbound fraction in blood was calculated for rat and human whole blood and recombinant human/isolated rat enzyme IC_{50}s. The estimated fu_ps were derived from IC_{50}s in blood and recombinant human/isolated rat enzyme using equations 1 and 2 assuming a BPR of 1 (see methods section). In silico predictions were predicted by the QSPR of Lobell & Sivarajah (119). NP: not possible due to missing IC_{50}.

3.3 Quantitative *in vitro* to *in vivo* extrapolation

A previously published physiologically based kinetic model (257) was used to translate concentrations from *in vitro* AChE inhibition-concentration curves to the oral doses required to reach

those concentrations *in vivo* in blood or plasma. Next, the estimated dose-response data was used for BMD modeling to derive $BMDL_{10}$ values as points of departure for hazard characterization (see **SI figures S3-S17**). Generally, point of departure predictions using the blood derived AChE inhibition curves resulted in higher predicted $BMDL_{10}$ values for all compounds (**table 3**), except for chlorfenvinphos in rats and humans, and fenitrothion and methyl-parathion in humans. Predicted $BMDL_{10}$ values were compared to *in vivo* determined no- and low-observable-adverse-effect levels (NOAEL and LOAEL), respectively.

Predicted $BMDL_{10}$ values for blood-based AChE inhibition in rats by fenitrothion, methyl-parathion, dimethoate, chlorfenvinphos and profenofos are all within 4-fold from *in vivo* LOAEL values and above the NOAEL values. Blood-based predictions for chlorpyrifos and diazinon in rats were not possible since translation of *in vitro* concentrations to *in vivo* doses resulted in doses over 10000 mg/kg body weight. Rat $BMDL_{10}$ predictions for chlorpyrifos and diazinon were possible with enzyme-based data and were more than 10-fold and less than 2-fold higher, respectively, from *in vivo* LOAEL values, while *in vivo* $BMDL_{10}$ values are significantly lower. Furthermore, enzyme-based $BMDL_{10}$ for rats were within 4-fold for fenitrothion, dimethoate, chlorfenvinphos and profenofos. However, rat $BMDL_{10}$ predictions for methyl- and ethyl-parathion were below the NOAEL value. *In vivo* determined $BMDL_{10}$ values for rats generally did not correspond with LOAEL values nor predicted $BMDL_{10}$ values.

In humans, both blood- and enzyme-based $BMDL_{10}$ predictions for fenitrothion, methyl-parathion and dimethoate were higher than reported NOAEL values. No LOAEL values were reported for human exposures to these compounds. Similar to blood-based predictions in rats, blood-based $BMDL_{10}$ predictions for humans were not possible for diazinon since translation of *in vitro* concentrations to *in vivo* doses resulted in doses over 10000 mg/kg body weight. However, enzyme-based $BMDL_{10}$ predictions for diazinon in humans were higher than reported NOAEL values, but were also more than 50-fold higher than reported LOAEL values. For chlorpyrifos, blood-based $BMDL_{10}$ predictions in humans were more than 2-fold below the NOAEL, while enzyme-based predictions were in the overlapping NOAEL and LOAEL ranges. Predicted blood-based human $BMDL_{10}$ values for ethyl-parathion were 4-fold lower than *in vivo* LOAEL values, but also lower than the reported NOAEL values. The enzyme predicted $BMDL_{10}$ values for ethyl-parathion were about 7-fold lower compared to *in vivo* LOAEL values. For profenofos and chlorfenvinphos, no *in vivo* point of departure data was available for humans.

Table 3: Predicted and *in vivo* determined points of departure (PODs) for human and rat (in mg/kg body weight) for erythrocyte RBC inhibition.

		In vivo				Predicted			
						Blood-based		Enzyme-based	
	Pesticide	NOAEL	LOAEL	$BMDL_{10}$	References	BMD_{10}	$BMDL_{10}$	BMD_{10}	$BMDL_{10}$
Rat	Chlorpyrifos	0.5-1	2	0.36 - 1.3	(223,266–268)	NP	NP	71.4	24.2
	Diazinon	2.5	25	1.8	(269,270)	NP	NP	31.8	23.3
	Fenitrothion	0.125[b]	0.25[b]-3.99[a]		(271,272)	*7.30	5.80	2.70	0.56
	Methyl-parathion	0.25[b]	2.5[b]		(273)	2.49	1.88	0.55	0.22
	Ethyl-parathion	0.025-0.5	0.7-2.5		(274,275)	9.73	8.45	0.01	0.003
	Dimethoate	0.1	0.3		(276)	1.01	0.66	1.67	0.30
	Chlorfenvinphos	1.25-3[a]	0.08 - 6.2		(277)	9.54	2.08	49.7	10.1
	Profenofos	0.243-25	100-400	1.99-11.24	(278,279)	362	272	256	184
Human	Chlorpyrifos	0.01-2	0.01 - 2		(266,280)	2.73	0.004	0.86	0.03
	Diazinon	0.2	(0.21-0.3)°		(281)	NP	NP	18.6	13.2
	Fenitrothion	0.36			(216,282)	1.33	0.96	1.85	1.52
	Methyl-parathion	0.06-0.27			(273)	0.42	0.143	0.73	0.32
	Ethyl-parathion	0.021-0.08	0.047[b]-0.11[b]		(274)	0.09	0.013	0.02	0.007
	Dimethoate	0.13			(283)	11.0	4.81	8.68	4.63
	Chlorfenvinphos	No PODs found				24.8	6.84	27.6	7.01
	Profenofos	No PODs found				128	81.6	25.3	3.23

BMD_{10} values are shown to give an indication of variability. [a]: Points of departure based on subchronic studies. [b]: Points of departure are based on chronic study. NOAEL and LOAEL: No and low observed adverse effect level, respectively. *Bad initial BMD model fit, which was worked around by assuming that at a 10-fold lower concentration than the lowest concentration tested, AChE activity would be 100% and adding this assumption as a datapoint when performing BMD modelling. °Poor data quality according to APVMA document. BMD_{10}: Benchmark dose at 10% AChE inhibition. $BMDL_{10}$: BMD_{10} lower limit. NP: not possible. Predicted points of departure are based on the predicted highest k_a values (see **SI: absorption rate constant calculations**).

4. Discussion

In the current study, points of departure were derived for hazard characterrization of oral exposure in human and rat for eight organophosphate pesticides using solely *in vitro* and in silico methods. Quantitative *in vitro* to *in vivo* extrapolation was used to translate *in vitro* derived concentration-response curves for blood and recombinant human/isolated rat AChE inhibition to dose-response data for humans and rats. In turn, these dose-response data were used for benchmark dose modelling and point of departure predictions. Enzyme-based predicted points of departure for rat exposure to diazinon, fenitrothion, dimethoate, chlorfenvinphos and profenofos were within 4-fold from reported *in vivo* LOAEL values. Similarly, blood-based predictions for fenitrothion, methyl-parathion, dimethoate, chlorfenvinphos and profenofos exposures in rats were within 4-fold difference from *in vivo* LOAEL values as well. For predicted points of departure in humans, enzyme-based predictions for chlorpyrifos, diazinon, fenitrothion, methyl-parathion and dimethoate all were similar or higher than reported *in vivo* NOAEL values. While, for human blood-based predictions, fenitrothion, methyl-parathion, ethyl-parathion and dimethoate were similar or higher than reported *in vivo* NOAEL values as well. For chlorfenvinphos and profenofos, no *in vivo* points of departure for oral exposures in humans were available.

For chlorpyrifos and diazinon, blood-based point of departure predictions were not possible. The in vitro concentrations used in whole blood AChE inhibition assays, could not be reached in vivo based on the predicted whole blood concentrations using the physiologically based kinetic model. For the enzyme-based point of departure predictions, this problem only occurred at the highest *in vitro* concentrations in predictions using rat isolated AChE inhibition data. Furthermore, for the enzyme-based point of departure predictions for chlorpyrifos and diazinon in rats, predicted points of departure were much higher than *in vivo* reported NOAEL and LOAEL values, while this difference was lower in human enzyme-based point of departure predictions. These results suggests that components present in whole blood interfere with the AChE inhibition by organophosphate pesticides, and that this component is more present/active in rats compared to humans.

Organophosphates are known to interact not only with AChE, but also with other esterases in blood like paraoxonase-1 (PON1), butyrylcholinesterase (BuChE) and carboxylesterase (CaE) (35,36). Many organophosphates are known to bind to CaE, PON1 or other esterases with higher affinity than to AChE. Furthermore, some of these esterases are also capable of metabolizing organophosphates (37,162,284–286). In the current investigation, PON1 activity was inhibited by chelating its cofactor calcium with EDTA (234), and BuChE activity was inhibited by using the specific BuChE inhibitor ethopropazine (259,260). However, the influence of CaE was not considered in our studies and is also often ignored in AChE inhibition assays performed by others (12,157). While carboxylesterases are only present in minute amounts in human blood (35,36), CaE is present in high amounts in rat blood (35,36). Since this enzyme is not inhibited by ethopropazine (287), it was available for binding to and potentially metabolizing the organophosphate pesticides in our studies using rat whole blood. Consequently, in vitro measured IC_{50}s, and therefore predicted $BMDL_{10}$ values, will be higher for compounds that bind to or are metabolized by CaE, compared to when CaE is not present or able to bind/metabolize.

The effect of CaE binding and/or metabolism in whole blood assays were highest for chlorpyrifos and diazinon. Therefore, only for these two compounds no high enough in vivo blood concentrations

could be predicted using the physiologically based kinetic model, whereas blood concentrations corresponding to concentrations inhibiting the (pure) enzyme could be predicted. This is supported by the high metabolic clearance rates in rat plasma for these two pesticides, compared to other organophosphate pesticides (see supplementary data of Moerenhout et al. (209)), as well as the low IC_{50}, and therefore affinity, of chlorpyrifos-oxon for CaE activity in rat plasma (37). CaE might very well be also present in the isolated enzyme mixture used for rat AChE inhibition assay, since the isolation of rat AChE from rat blood was very aspecific. It is therefore advised to use a CaE specific inhibitor, like benzil (288), in AChE inhibition assays using whole blood or isolated AChE enzyme, especially in species, like rodents, with high CaE activity in blood and plasma (35,36).

Our findings suggest that enzyme-based AChE inhibition assays should be preferred over blood-based AChE inhibition assays for use in QIVIVE approaches. Data obtained using blood-based assays can only be properly interpreted when the effects of all blood components are understood. As Mortensen et al. showed, tissue and plasma components can increase measured IC_{50}s (289), likely due to nonspecific binding of the inhibiting compound to the other components in the tissue or plasma. Also suggesting that tissue incubations are less reliable for IC_{50} determinations compared to pure protein. An IC_{50} value, as well as all other datapoints in a concentration-effect assay, is system specific, meaning there is not one IC_{50} for a compound and that IC_{50}s measured in a system containing pure protein, cannot be directly compared to IC_{50}s measured using whole blood assays. To investigate species differences in whole blood AChE inhibition, it is of interest to include the effects of all the blood components in the measurement. However, for QIVIVE it is more accurate to determine concentration-effect relations based on pure enzyme, since aspects like binding to blood components and metabolism in blood should be accounted for in the physiologically based kinetic model used in the QIVIVE predictions. In the current study, binding to/clearance by CaE is possibly accounted for twice when blood-based concentration-effect data is used for QIVIVE: first binding/clearance is happening in the in vitro experiment, altering the measured IC50, and second metabolism in plasma is included in the physiologically based kinetic model. This would result in higher predicted $BMDL_{10}$s, compared to predictions using enzyme-based data.

In the current study, predicted $BMDL_{10}$ values for rats and humans were compared to both NOAEL and LOAEL values for the respective species, with predicted values considered accurate being at least equal or above the NOAEL or close to the LOAEL. However, currently there does not seem to be a scientific consensus about what predicted $BMDL_{10}$ values should be compared to: NOAEL or LOAEL values. Both NOAEL and LOAEL have an inherent uncertainty to them. The NOAEL is defined as the highest dose tested where no adverse effects were observed. So if only a few, widely spread out doses are tested, the determined NOAEL might still be very conservative, since the 'true' NOAEL dose was never tested. Similarly, the LOAEL is also affected by the study design and lacks a strict definition of what numerical value should be attached to the 'low' observed adverse effect level. For example, the referenced points of departure in **table 3** contain LOAELs based on anything from 3 to 36% of erythrocyte AChE inhibition. At the same time, for many of the reported LOAEL values in **table 3**, no quantitative amount of AChE inhibition was reported. In addition, both the NOAEL and LOAEL do not give any information about the statistical variability of the data. The European food and safety authority (EFSA) suggests $BMDL_{10}$ data are closest to NOAEL values, but this seems to be based on evaluations of endpoints like carcinogenicity and developmental toxicity (290). For more transient effects like AChE inhibition due to acute exposure to organophosphates, where

higher inherent variability in the endpoint is present, comparison to LOAEL might be more appropriate, especially if the effect value is close to 10% erythrocyte AChE inhibition.

In traditional chemical risk assessment, points of departure like NOAELs and LOAELs are often translated to safe exposure values by incorporating uncertainty factors for species differences as well as for interindividual differences. However, for point of departure data derived from animal-free methods no standardized use of uncertainty factors has been reported. A QIVIVE case study on imazalil by the Dutch national institute for public health and the environment (RIVM) suggested to use extrapolation factors for species differences in case non-human *in vitro* material was used, for interindividual differences, and for exposure duration extrapolation in case risk assessment concerns (sub)chronic exposures (291). If a similar approach is to be used for risk assessment of acute organophosphate pesticide exposure in humans based on the predicted points of departure in this study, an uncertainty factor of 10 should be used for interspecies differences (i.e. variability in the human population). This uncertainty factor would correct for the use of a deterministic physiologically based kinetic model and the small (n=3) human sample size for *in vitro* AChE inhibition assays. However, due to lacking data and experience, more research is needed to define what uncertainty factors are required for animal free QIVIVE-based risk assessment.

Overall, the use of physiologically based kinetic modelling in combination with *in vitro* toxicity assays was shown to be a viable strategy for organophosphate point of departure derivation for AChE inhibition endpoints, since nearly all QIVIVE-derived $BMDL_{10}$s were higher than the NOAEL and within 4-fold difference from the LOAEL. This approach supports hazard/risk assessments using novel assessment methodology and next generation risk assessment approaches and shows that when all important kinetic processes are fully investigated, points of departure can be determined without the use data obtained using animal experiments.

Supporting information

Absorption rate constant calculation

The absorption rate constant (k_a) was estimated using a method that was introduced by Moerenhout et al. (209), which was based on the method proposed by Punt et al. (112).

In the modelling study of Moerenhout et al. (209), k_a values were predicted for rats and humans. While the calculated values for rats worked very well, when these extrapolated to humans it resulted in poor predictions for human simulations. Furthermore, human absorption was found to be highly variable for the same compound (chlorpyrifos) between different studies. It was speculated that this might depend on the fasted/fed state and the effect of bile acids, which help solubilize lipophilic compounds. Eventually Moerenhout et al. used the same k_a value for all organophosphates in the human model. Here it was attempted to get compound specific k_a values for humans, based on the same ratio, but instead of extrapolating from rat ka values, they were extrapolated from fitted k_a values for chlorpyrifos.

The values were calculated as follows:

- First, k_a values were calculated for each organophosphate using the method of (112).
- Next, a ratio was calculated between the k_a of each organophosphate and the calculated k_a value of chlorpyrifos.
- These ratios were used to extrapolate the fitted k_a values for minimum and maximum absorption (assumed to be fasted and fed situations, respectively) in chlorpyrifos studies (which had the most human data available), to minimum and maximum values for all other organophosphate pesticides studied here.
- Associated fraction absorbed (f_a) values were calculated according to Yu and Amidon (114).

Calculated k_a (/h) and f_a values using the described method:

	Minimum absorption (fasted state)		Maximum absorption (fed state)		Average absorption	
Pesticide	**k_a**	**f_a**	**k_a**	**f_a**	**k_a**	**f_a**
CPF	0.10	0.28	0.60	0.83	0.35	0.66
DZN	0.09	0.24	0.52	0.79	0.30	0.61
FNT	0.07	0.20	0.41	0.71	0.24	0.53
PFS	0.11	0.29	0.64	0.84	0.37	0.68
MPT	0.07	0.20	0.41	0.71	0.24	0.53
CVP	0.10	0.27	0.57	0.81	0.33	0.64
EPT	0.07	0.21	0.43	0.72	0.25	0.54
DMO	0.09	0.26	0.55	0.80	0.32	0.63

Supplementary tables

Table S1: Comparison of IC_{50}s with other studies

Compound	Type	Organism	IC_{50} (µM)	Reference
CPF	hAChE	Human	5.397	This study
	hAChE	Human	0.12	Das et al. 2006
	hAChE	Human	40.17	Li et al. 2019
	Isolated hAChE	Human	21.42	Linhares et al. 2023
	Isolated rAChE	Rat	3.852	This study
	Whole blood	Human	NI	This study
	Whole blood	Rat	NI	This study
CPO	hAChE	Human	0.0030	This study
	hAChE	Human	0.0035	Moser and Padilla 2011
	hAChE	Human	0.0040	Moser and Padilla 2011
	hAChE	Human	0.00189	Zhao et al. 2022
	Isolated rAChE	Rat	0.0021	This study
	Whole blood	Human	0.256	This study
	Whole blood	Human	0.27	Kasteel et al. 2020
	Whole blood	Rat	0.677	This study
DZN	hAChE	Human	14.26	Zhao et al. 2021
	hAChE	Human	37.99	Li et al. 2019
	hAChE	Human	30.10	Li et al. 2019
	Isolated rAChE	Rat	14.66	Zhao et al. 2021
	Whole blood	Human	>10	Kasteel et al. 2020
DZO	hAChE	Human	0.0440	Zhao et al. 2021
	hAChE	Human	1.33	Li et al. 2019
	hAChE	Human	0.50	Li et al. 2019
	Isolated rAChE	Rat	0.0515	Zhao et al. 2021
	Whole blood	Human	1.20	Chen et al. 2025
FNT	hAChE	Human	74.3	This study
	Isolated rAChE	Rat	9.17	This study
	Whole blood	Human	>1000	This study
	Whole blood	Rat	489.8	This study
FNO	hAChE	Human	0.34	This study
	Isolated rAChE	Rat	0.20	This study
	Whole blood	Human	0.82	Chen et al. 2023
	Whole blood	Rat	0.93	Chen et al. 2023
MPT	hAChE	Human	331	This study
	Isolated rAChE	Rat	68.5	This study
	Whole blood	Human	>1000	This study
	Whole blood	Rat	NI	This study
MPO	hAChE	Human	0.0468	This study
	hAChE	Human	0.0744	Moser and Padilla 2011
	Isolated rAChE	Rat	0.0212	This study
	Whole blood	Human	0.1527	This study
	Whole blood	Rat	0.4467	This study
EPT	hAChE	Human	32.657	This study
	Isolated rAChE	Rat	18.750	This study
	Whole blood	Human	159.22	This study
	Whole blood	Rat	NI	This study
EPO	hAChE	Human	0.0115	This study
	hAChE	Human	0.0204	Chapleau et al. 2015
	hAChE	Human	0.0355	Moser and Padilla 2011
	hAChE	Human	0.024	Lock 2020
	Diluted whole blood	Human	0.013	Petroianu et al. 2003
	Isolated rAChE	Rat	0.0125	This study
	Isolated rAChE	Rat	0.032	Cohen et al. 1985
	Isolated rAChE	Rat	0.036	Cohen et al. 1985
	Whole blood	Human	0.095	This study
	Whole blood	Rat	0.939	This study
DMO	hAChE	Human	NI	This study

	Isolated rAChE	Rat	NI	This study
	Whole blood	Human	NI	This study
	Whole blood	Human	93000	Rios et al. 2005
	Whole blood	Rat	NI	This study
OMO	hAChE	Human	34.67	This study
	hAChE	Human	68.95	Li et al. 2019
	Isolated rAChE	Rat	16.75	This study
	Whole blood	Human	19.68	This study
	Whole blood	Rat	8.861	This study
CVP	hAChE	Human	1.213	This study
	hAChE	Human	1.962	Moser and Padilla 2011
	Isolated rAChE	Rat	0.741	This study
	Whole blood	Human	28.38	This study
	Whole blood	Rat	6.393	This study
PFS	hAChE	Human	0.225	This study
	hAChE	Human	0.302	Omwenga et al. 2021
	hAChE	Human	12.15	Li et al. 2019
	hAChE	Human	1.89	Li et al. 2019
	Isolated rAChE	Rat	0.805	This study
	Isolated rAChE	Rat	0.312	Omwenga et al. 2021
	Whole blood	Human	94.41	This study
	Whole blood	Rat	75.51	This study

NI: No inhibition up until 1000 µM. >10 or >1000 mean AChE was slightly inhibited at a concentration of 10 or 1000µM, respectively, but it did not reach 50% inhibition at the highest concentrations tested.

Supplementary figures

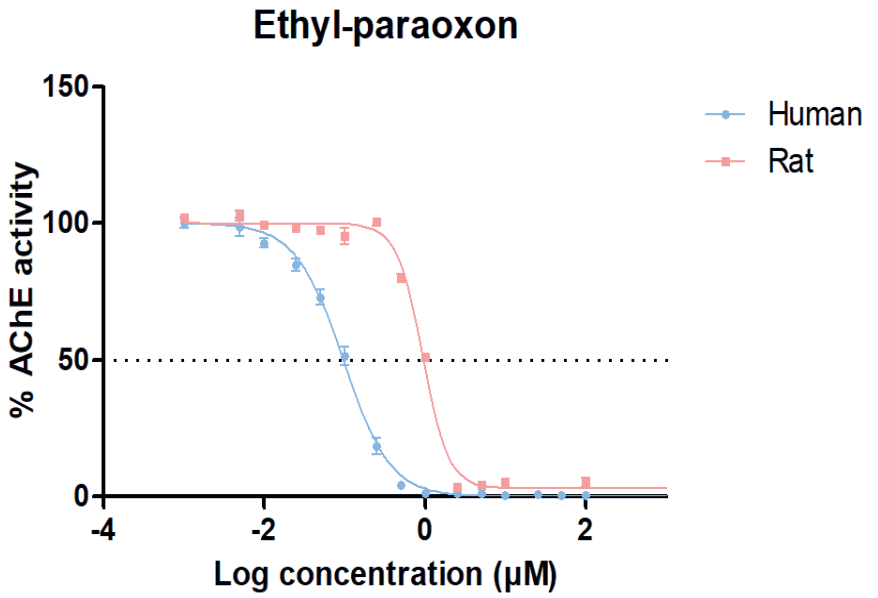


Figure S1: Inhibition of AChE in human and rat whole blood. Chlorpyrifos-oxon was used as positive control to define 0% AChE activity.

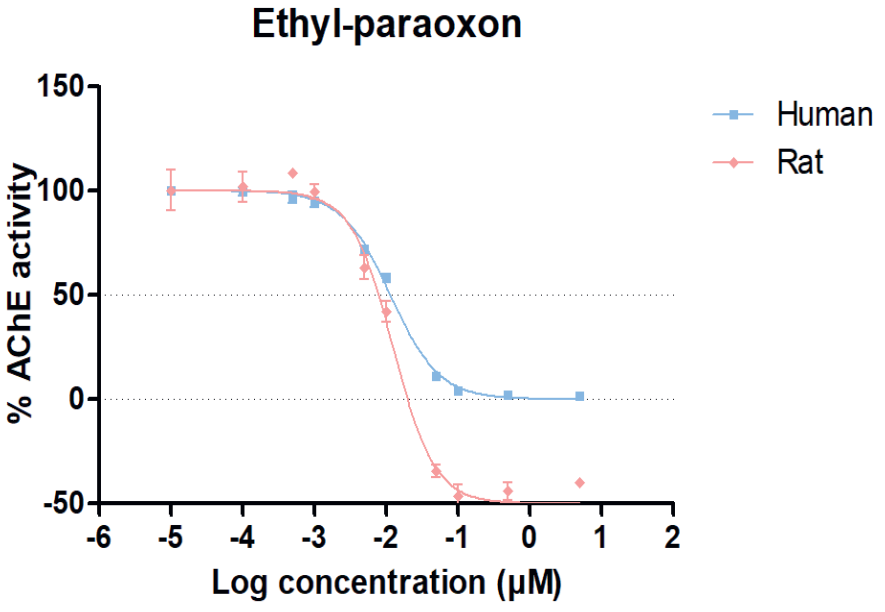


Figure S2: Inhibition of human recombinant and isolated rat AChE by ethyl paraoxon. Chlorpyrifos-oxon was used as positive control to define 0% AChE activity.

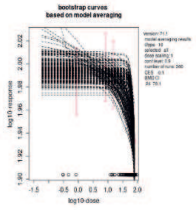
This report was generated by **Anonymous** on **2/20/2026 5:08:50 PM (CET)**. PROAST version 71.1

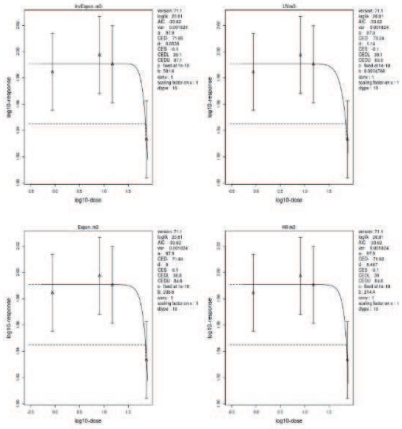
Input values

Removed data	No
Type of response data	Continuous, summary data
Dose column(s)	dose
Response column(s)	response
Dispersion measure column(s)	SD
Relating to	Standard deviation
Group size column(s)	n
Covariate column	*none*
Litter effect	No
BMR (CES)	0.1
Model averaging	Yes
Number of bootstrap runs	200
AIC criterion	2

Graphical output

Note that the plotted means and/or fitted curves relate to geometric means, which are lower than the arithme





Fitted models

model	converged	loglik	npar	AIC
full model	1	21.19	5	-32.38
null model	1	14.63	2	-25.26
Expon. m3-	1	20.81	4	-33.62
Expon. m5-	1	20.81	5	-31.62
Hill m3-	1	20.81	4	-33.62
Hill m5-	1	20.81	5	-31.62
Inv.Expon. m3-	1	20.81	4	-33.62
Inv.Expon. m5-	1	20.81	5	-31.62
LN m3-	1	20.81	4	-33.62
LN m5-	0	20.81	5	-31.62

Model weights

model	weight
EXP	0.25
HILL	0.25
INVEXP	0.25
LOGN	0.25

BMD confidence interval based on model averaging

subgroup	BMDlower.ma	BMDupper.ma
all	24.2	78.1

Figure S3: PROAST benchmark modelling output for AChE inhibition after oral exposure to chlorpyrifos in rats. Enzyme-based predictions

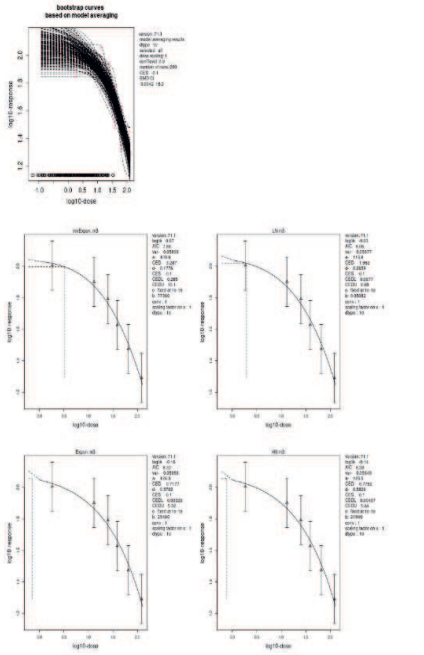
This report was generated by **Anonymous** on **2/20/2026 5:14:51 PM (CET)**. PROAST version 71.1

Input values

Removed data	No
Type of response data	Continuous, summary data
Dose column(s)	dose
Response column(s)	response
Dispersion measure column(s)	SD
Relating to	Standard deviation
Group size column(s)	n
Covariate column	*none*
Litter effect	No
BMR (CES)	0.1
Model averaging	Yes
Number of bootstrap runs	200
AIC criterion	2

Graphical output

Note that the plotted means and/or fitted curves relate to geometric means, which are lower than the arithm



Fitted models

model	converged	loglik	npar	AIC
full model	1	0.67	7	12.66
null model	1	-16.67	2	37.34
Expon. m3-	1	-0.16	4	8.32
Expon. m5-	1	0.58	5	8.84
Hill m3-	1	-0.14	4	8.28
Hill m5-	1	0.6	5	8.8
Inv.Expon. m3-	1	0.07	4	7.86
Inv.Expon. m5-	1	0.56	5	8.88
LN m3-	1	-0.03	4	8.06
LN m5-	1	0.59	5	8.82

Model weights

model	weight
EXP	0.2264
HILL	0.2309
INVEXP	0.2849
LOGN	0.2578

BMD confidence interval based on model averaging

subgroup	BMDlower.ma	BMDupper.ma
all	0.0042	18.3

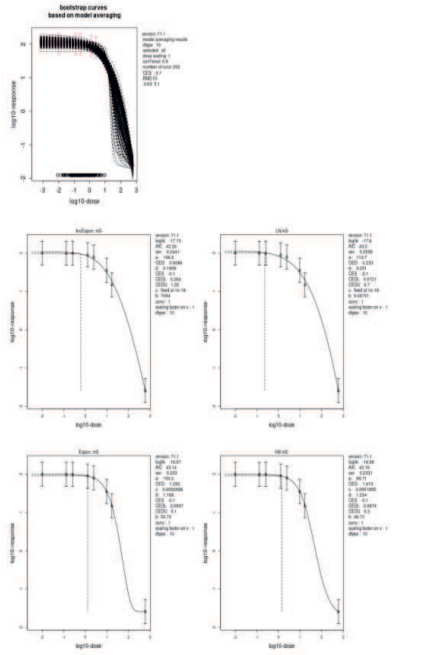
This report was generated by **Anonymous** on **2/20/2026 5:15:59 PM (CET)**. PROAST version 71.1

Input values

Removed data	No
Type of response data	Continuous, summary data
Dose column(s)	dose
Response column(s)	response
Dispersion measure column(s)	SD
Relating to	Standard deviation
Group size column(s)	n
Covariate column	*none*
Litter effect	No
BMR (CES)	0.1
Model averaging	Yes
Number of bootstrap runs	200
AIC criterion	2

Graphical output

Note that the plotted means and/or fitted curves relate to geometric means, which are lower than the arithm



Fitted models

model	converged	loglik	npar	AIC
full model	1	-16.57	9	51.14
null model	1	-57.86	2	119.72
Expon. m3-	1	-18.25	4	44.5
Expon. m5-	1	-16.57	5	43.14
Hill m3-	1	-18.13	4	44.26
Hill m5-	1	-16.58	5	43.16
Inv.Expon. m3-	1	-17.13	4	42.26
Inv.Expon. m5-	0	-48.53	5	107.06
LN m3-	1	-17.6	4	43.2
LN m5-	1	-16.61	5	43.22

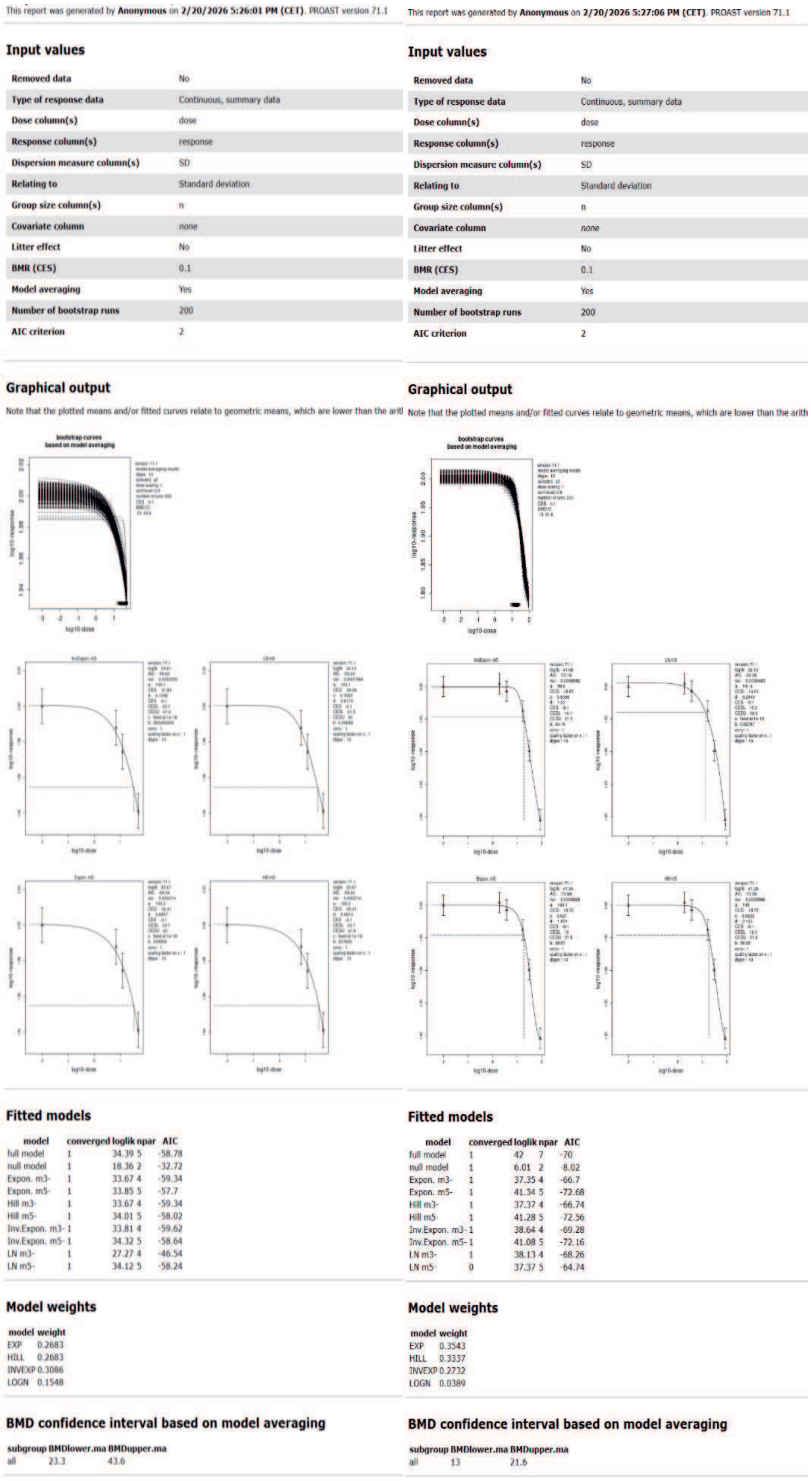
Model weights

model	weight
EXP	0.2216
HILL	0.2194
INVEXP	0.344
LOGN	0.215

BMD confidence interval based on model averaging

subgroup	BMDlower.ma	BMDupper.ma
all	0.0302	3.1

Figure S4: PROAST benchmark modelling output for AChE inhibition after oral exposure to chlorpyrifos in humans. Blood-based predictions on the left, enzyme-based predictions on the right.



This report was generated by **Anonymous** on **2/20/2026 5:26:01 PM (CET)**. PROAST version 71.1

Input values

Removed data	No
Type of response data	Continuous, summary data
Dose column(s)	dose
Response column(s)	response
Dispersion measure column(s)	SD
Relating to	Standard deviation
Group size column(s)	n
Covariate column	*none*
Litter effect	No
BMR (CES)	0.1
Model averaging	Yes
Number of bootstrap runs	200
AIC criterion	2

Graphical output

Note that the plotted means and/or fitted curves relate to geometric means, which are lower than the arit

Fitted models

model	converged	loglik	npar	AIC
full model	1	34.39	5	-58.78
null model	1	18.36	2	-32.72
Expon. m3-	1	33.67	4	-59.34
Expon. m5-	1	33.85	5	-57.7
Hill m3-	1	33.67	4	-59.34
Hill m5-	1	34.01	5	-58.02
Inv.Expon. m3-	1	33.81	4	-59.62
Inv.Expon. m5-	1	34.32	5	-58.64
LN m3-	1	27.27	4	-46.54
LN m5-	1	34.12	5	-58.24

Model weights

model	weight
EXP	0.2683
HILL	0.2683
INVEXP	0.3086
LOGN	0.1548

BMD confidence interval based on model averaging

subgroup	BMDlower.ma	BMDupper.ma
all	23.3	43.6

This report was generated by **Anonymous** on **2/20/2026 5:27:06 PM (CET)**. PROAST version 71.1

Input values

Removed data	No
Type of response data	Continuous, summary data
Dose column(s)	dose
Response column(s)	response
Dispersion measure column(s)	SD
Relating to	Standard deviation
Group size column(s)	n
Covariate column	*none*
Litter effect	No
BMR (CES)	0.1
Model averaging	Yes
Number of bootstrap runs	200
AIC criterion	2

Graphical output

Note that the plotted means and/or fitted curves relate to geometric means, which are lower than the arith

Fitted models

model	converged	loglik	npar	AIC
full model	1	42	7	-70
null model	1	6.01	2	-8.02
Expon. m3-	1	37.35	4	-66.7
Expon. m5-	1	41.34	5	-72.68
Hill m3-	1	37.37	4	-66.74
Hill m5-	1	41.28	5	-72.56
Inv.Expon. m3-	1	38.64	4	-69.28
Inv.Expon. m5-	1	41.08	5	-72.16
LN m3-	1	38.13	4	-68.26
LN m5-	0	37.37	5	-64.74

Model weights

model	weight
EXP	0.3543
HILL	0.3337
INVEXP	0.2732
LOGN	0.0389

BMD confidence interval based on model averaging

subgroup	BMDlower.ma	BMDupper.ma
all	13	21.6

Figure S5: PROAST benchmark modelling output for AChE inhibition after oral exposure to diazinon in rats (left) and humans (right). Predictions are based on enzyme inhibition data.

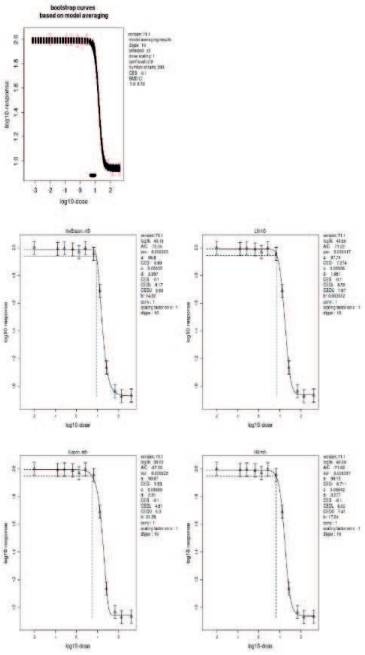
This report was generated by **Anonymous** on **2/23/2026 10:17:54 AM (CET)**. PROAST version 71.1

Input values

Removed data	No
Type of response data	Continuous, summary data
Dose column(s)	dose
Response column(s)	response
Dispersion measure column(s)	SD
Relating to	Standard deviation
Group size column(s)	n
Covariate column	*none*
Litter effect	No
BMR (CES)	0.1
Model averaging	Yes
Number of bootstrap runs	200
AIC criterion	2

Graphical output

Note that the plotted means and/or fitted curves relate to geometric means, which are lower than the ari



Fitted models

model	converged	loglik	npar	AIC
full model	1	42.35	13	-58.7
null model	1	-53.33	2	110.66
Expon. m3-	1	-20.73	4	49.46
Expon. m5-	1	38.69	5	-67.38
Hill m3-	0	-48.03	4	104.06
Hill m5-	1	40.84	5	-71.68
Inv.Expon. m3-	1	-18.77	4	45.54
Inv.Expon. m5-	1	40.18	5	38.12
LN m3-	1	-19.75	4	47.5
LN m5-	1	40.66	5	-71.32

Model weights

model	weight
EXP	0.0472
HILL	0.4051
INVEXP	0.2094
LOGN	0.3384

BMD confidence interval based on model averaging

subgroup	BMDlower.ma	BMDupper.ma
all	5.84	8.58

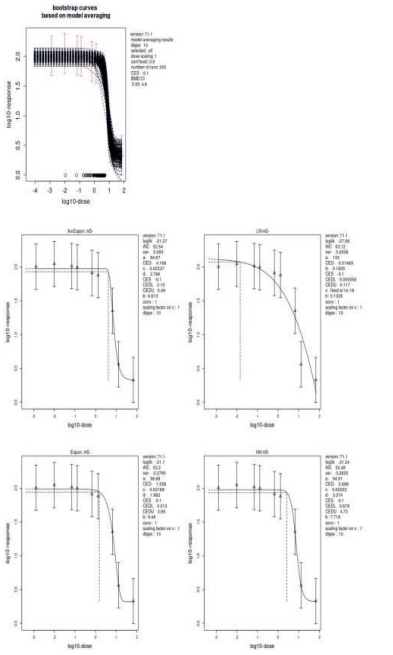
This report was generated by **Anonymous** on **2/23/2026 10:12:49 AM (CET)**. PROAST version 71.1

Input values

Removed data	No
Type of response data	Continuous, summary data
Dose column(s)	dose
Response column(s)	response
Dispersion measure column(s)	SD
Relating to	Standard deviation
Group size column(s)	n
Covariate column	*none*
Litter effect	No
BMR (CES)	0.1
Model averaging	Yes
Number of bootstrap runs	200
AIC criterion	2

Graphical output

Note that the plotted means and/or fitted curves relate to geometric means, which are lower than the ari



Fitted models

model	converged	loglik	npar	AIC
full model	1	-20.65	10	61.3
null model	1	-50.14	2	104.28
Expon. m3-	1	-28.19	4	64.38
Expon. m5-	1	-21.1	5	52.2
Hill m3-	1	-28.08	4	64.16
Hill m5-	1	-21.24	5	52.48
Inv.Expon. m3-	1	-27.01	4	62.02
Inv.Expon. m5-	1	-21.27	5	52.54
LN m3-	1	-27.56	4	63.12
LN m5-	0	-39.92	5	89.84

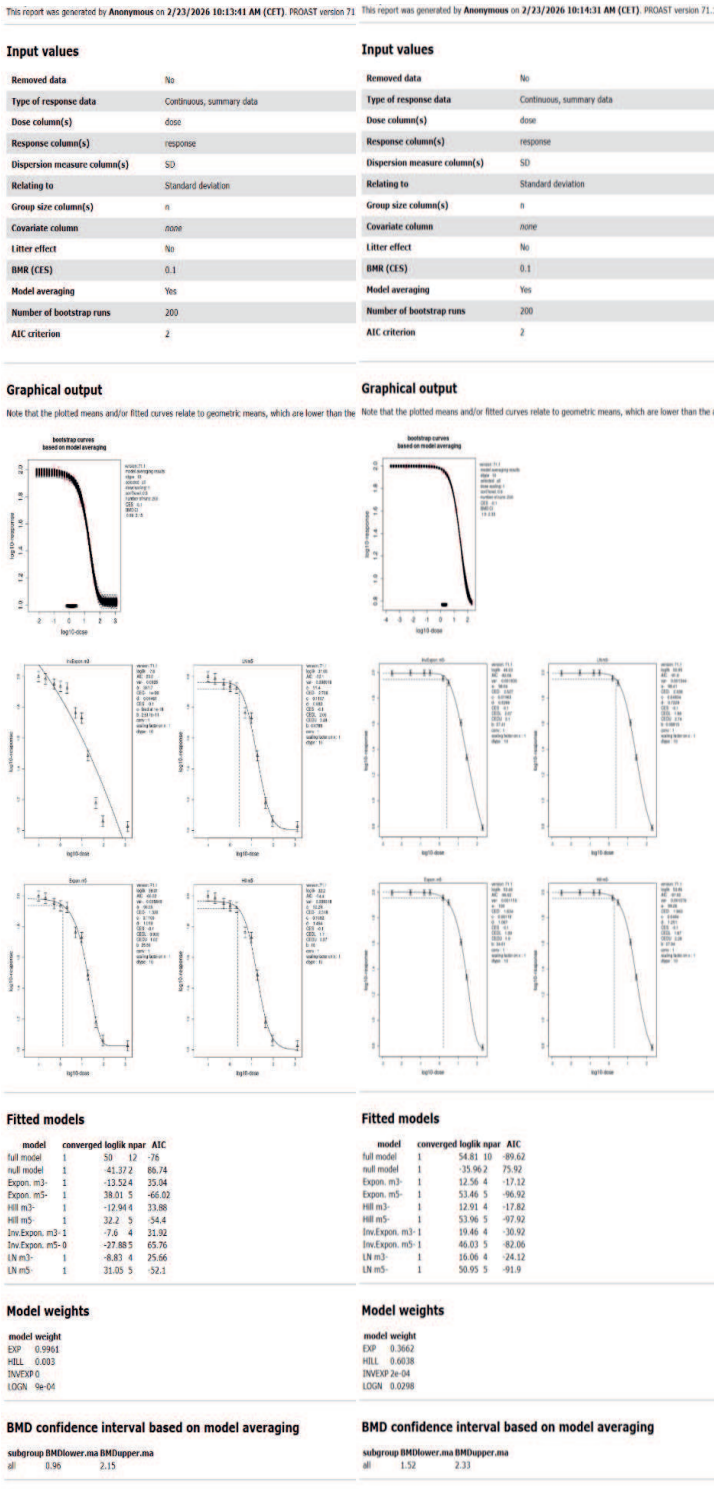
Model weights

model	weight
EXP	0.368
HILL	0.3199
INVEXP	0.3105
LOGN	0.0016

BMD confidence interval based on model averaging

subgroup	BMDlower.ma	BMDupper.ma
all	0.551	4.6

Figure S6: PROAST benchmark modelling output for AChE inhibition after oral exposure to fenitrothion in rats. Blood-based predictions on the left, enzyme-based predictions on the right.



This report was generated by **Anonymous** on **2/23/2026 10:13:41 AM (CET)**. PROAST version 71

Input values

Removed data	No
Type of response data	Continuous, summary data
Dose column(s)	dose
Response column(s)	response
Dispersion measure column(s)	SD
Relating to	Standard deviation
Group size column(s)	n
Covariate column	*none*
Litter effect	No
BMR (CES)	0.1
Model averaging	Yes
Number of bootstrap runs	200
AIC criterion	2

Graphical output

Note that the plotted means and/or fitted curves relate to geometric means, which are lower than the

bootstrap curves based on model averaging

log10-response

log10-dose

Fitted models

model	converged	loglik	npar	AIC
full model	1	50	12	-76
null model	1	-41.37	2	86.74
Expon. m3-	1	-13.52	4	35.04
Expon. m5-	1	38.01	5	-66.02
Hill m3-	1	-12.94	4	33.88
Hill m5-	1	32.2	5	-54.4
Inv.Expon. m3-	1	-7.6	4	31.92
Inv.Expon. m5-	0	-27.88	5	65.76
LN m3-	1	-8.83	4	25.66
LN m5-	1	31.05	5	-52.1

Model weights

model	weight
EXP	0.9961
HILL	0.003
INVEXP	0
LOGN	9e-04

BMD confidence interval based on model averaging

subgroup	BMDlower.ma	BMDupper.ma
all	0.96	2.15

This report was generated by **Anonymous** on **2/23/2026 10:14:31 AM (CET)**. PROAST version 71.

Input values

Removed data	No
Type of response data	Continuous, summary data
Dose column(s)	dose
Response column(s)	response
Dispersion measure column(s)	SD
Relating to	Standard deviation
Group size column(s)	n
Covariate column	*none*
Litter effect	No
BMR (CES)	0.1
Model averaging	Yes
Number of bootstrap runs	200
AIC criterion	2

Graphical output

Note that the plotted means and/or fitted curves relate to geometric means, which are lower than the

bootstrap curves based on model averaging

log10-response

log10-dose

Fitted models

model	converged	loglik	npar	AIC
full model	1	54.81	10	-89.62
null model	1	-35.96	2	75.92
Expon. m3-	1	12.56	4	-17.12
Expon. m5-	1	53.46	5	-96.92
Hill m3-	1	12.91	4	-17.82
Hill m5-	1	53.96	5	-97.92
Inv.Expon. m3-	1	19.46	4	-30.92
Inv.Expon. m5-	1	46.03	5	-82.06
LN m3-	1	16.06	4	-24.12
LN m5-	1	50.95	5	-91.9

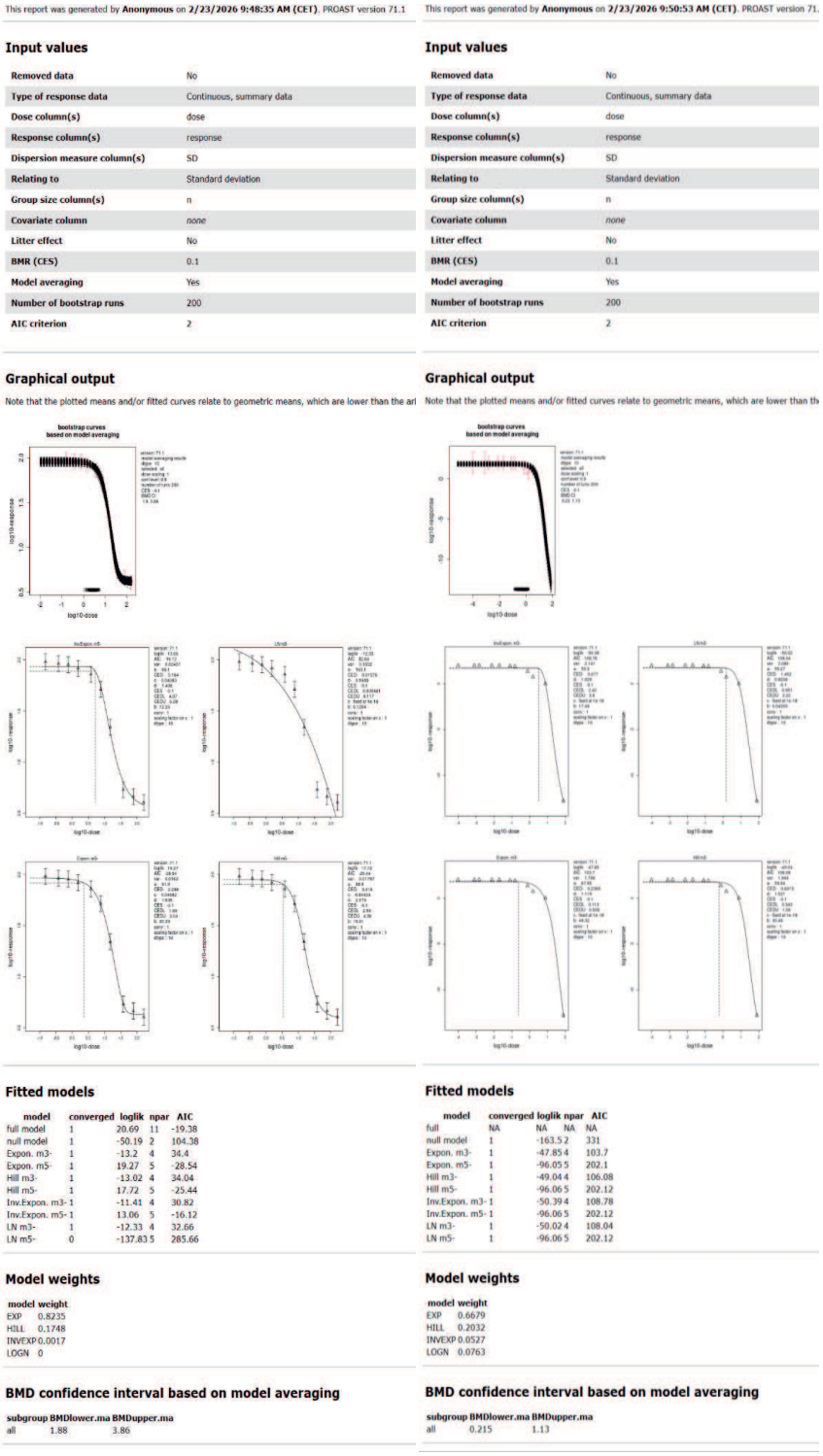
Model weights

model	weight
EXP	0.3662
HILL	0.6038
INVEXP	2e-04
LOGN	0.0298

BMD confidence interval based on model averaging

subgroup	BMDlower.ma	BMDupper.ma
all	1.52	2.33

Figure S7: PROAST benchmark modelling output for AChE inhibition after oral exposure to fenitrothion in humans. Blood-based predictions on the left, enzyme-based predictions on the right.



This report was generated by **Anonymous** on **2/23/2026 9:48:35 AM (CET)**. PROAST version 71.1

Input values

Removed data	No
Type of response data	Continuous, summary data
Dose column(s)	dose
Response column(s)	response
Dispersion measure column(s)	SD
Relating to	Standard deviation
Group size column(s)	n
Covariate column	*none*
Litter effect	No
BMR (CES)	0.1
Model averaging	Yes
Number of bootstrap runs	200
AIC criterion	2

Graphical output

Note that the plotted means and/or fitted curves relate to geometric means, which are lower than the ari

bootstrap curves based on model averaging

log10-response

log10-dose

Fitted models

model	converged	loglik	npar	AIC
full model	1	20.69	11	-19.38
null model	1	-50.19	2	104.38
Expon. m3-	1	-13.2	4	34.4
Expon. m5-	1	19.27	5	-28.54
Hill m3-	1	-13.02	4	34.04
Hill m5-	1	17.72	5	-25.44
Inv.Expon. m3-	1	-11.41	4	30.82
Inv.Expon. m5-	1	13.06	5	-16.12
LN m3-	1	-12.33	4	32.66
LN m5-	0	-137.83	5	285.66

Model weights

model	weight
EXP	0.8235
HILL	0.1748
INVEXP	0.0017
LOGN	0

BMD confidence interval based on model averaging

subgroup	BMDlower.ma	BMDupper.ma
all	1.88	3.86

This report was generated by **Anonymous** on **2/23/2026 9:50:53 AM (CET)**. PROAST version 71.

Input values

Removed data	No
Type of response data	Continuous, summary data
Dose column(s)	dose
Response column(s)	response
Dispersion measure column(s)	SD
Relating to	Standard deviation
Group size column(s)	n
Covariate column	*none*
Litter effect	No
BMR (CES)	0.1
Model averaging	Yes
Number of bootstrap runs	200
AIC criterion	2

Graphical output

Note that the plotted means and/or fitted curves relate to geometric means, which are lower than th

bootstrap curves based on model averaging

log10-response

log10-dose

Fitted models

model	converged	loglik	npar	AIC
full	NA	NA	NA	NA
null model	1	-163.52	2	331
Expon. m3-	1	-47.854	4	103.7
Expon. m5-	1	-96.055	5	202.1
Hill m3-	1	-49.044	4	106.08
Hill m5-	1	-96.065	5	202.12
Inv.Expon. m3-	1	-50.394	4	108.78
Inv.Expon. m5-	1	-96.065	5	202.12
LN m3-	1	-50.024	4	108.04
LN m5-	1	-96.065	5	202.12

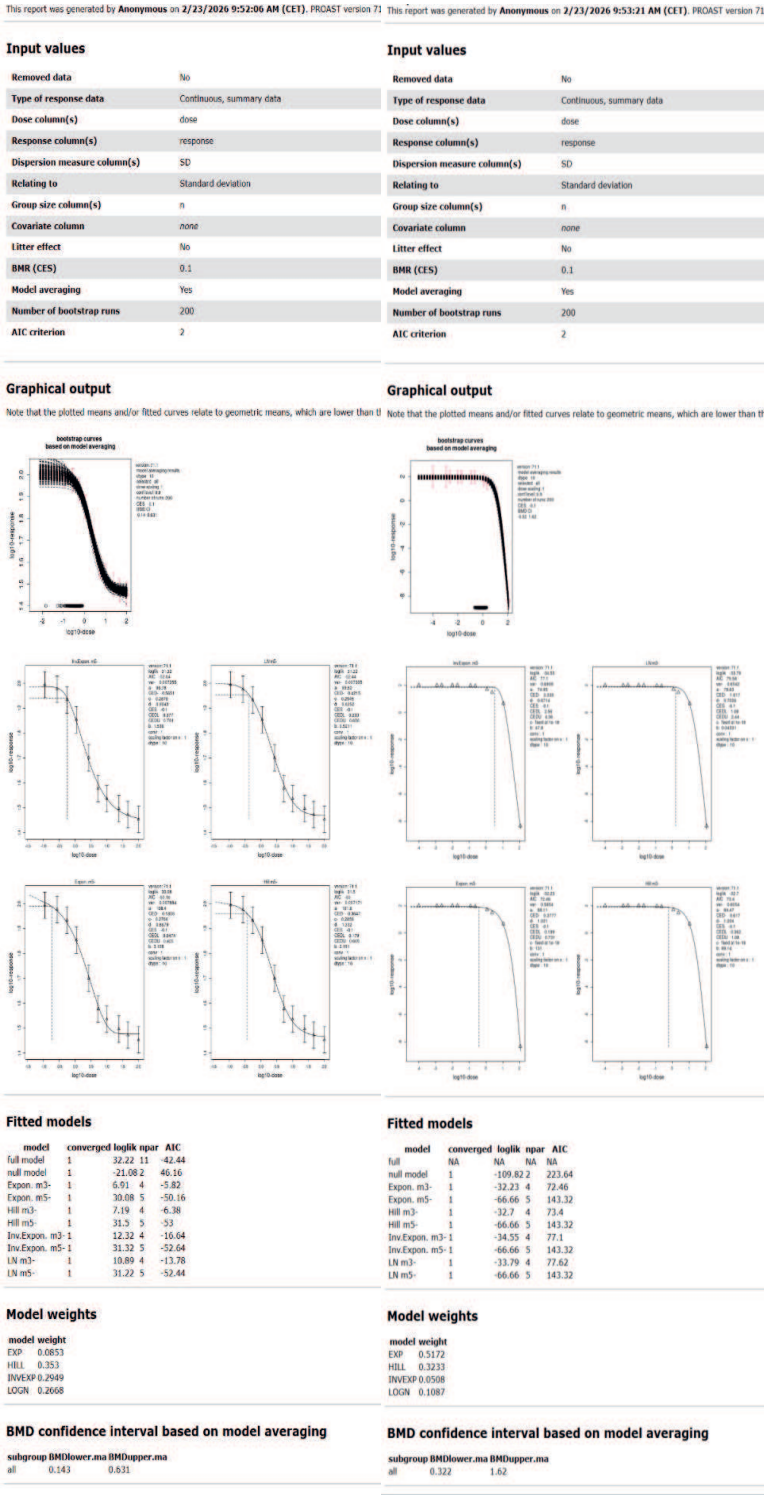
Model weights

model	weight
EXP	0.6679
HILL	0.2032
INVEXP	0.0527
LOGN	0.0763

BMD confidence interval based on model averaging

subgroup	BMDlower.ma	BMDupper.ma
all	0.215	1.13

Figure S8: PROAST benchmark modelling output for AChE inhibition after oral exposure to methyl-parathion in rats. Blood-based predictions on the left, enzyme-based predictions on the right.



This report was generated by **Anonymous** on **2/23/2026 9:52:06 AM (CET)**. PROAST version 71

Input values

Removed data	No
Type of response data	Continuous, summary data
Dose column(s)	dose
Response column(s)	response
Dispersion measure column(s)	SD
Relating to	Standard deviation
Group size column(s)	n
Covariate column	*none*
Litter effect	No
BMR (CES)	0.1
Model averaging	Yes
Number of bootstrap runs	200
AIC criterion	2

Graphical output

Note that the plotted means and/or fitted curves relate to geometric means, which are lower than th

bootstrap curves based on model averaging

log10-response

log10-dose

Fitted models

model	converged	loglik	npar	AIC
full model	1	32.22	11	-42.44
null model	1	-21.08	2	46.16
Expon. m3-	1	6.91	4	-5.82
Expon. m5-	1	30.08	5	-50.16
Hill m3-	1	7.19	4	-6.38
Hill m5-	1	31.5	5	-53
Inv.Expon. m3-	1	12.32	4	-16.64
Inv.Expon. m5-	1	31.32	5	-52.64
LN m3-	1	10.89	4	-13.78
LN m5-	1	31.22	5	-52.44

Model weights

model	weight
EXP	0.0853
HILL	0.353
INVEXP	0.2949
LOGN	0.2668

BMD confidence interval based on model averaging

subgroup	BMDlower.ma	BMDupper.ma
all	0.143	0.631

This report was generated by **Anonymous** on **2/23/2026 9:53:21 AM (CET)**. PROAST version 71

Input values

Removed data	No
Type of response data	Continuous, summary data
Dose column(s)	dose
Response column(s)	response
Dispersion measure column(s)	SD
Relating to	Standard deviation
Group size column(s)	n
Covariate column	*none*
Litter effect	No
BMR (CES)	0.1
Model averaging	Yes
Number of bootstrap runs	200
AIC criterion	2

Graphical output

Note that the plotted means and/or fitted curves relate to geometric means, which are lower than th

bootstrap curves based on model averaging

log10-response

log10-dose

Fitted models

model	converged	loglik	npar	AIC
full	NA	NA	NA	NA
null model	1	-109.82	2	223.64
Expon. m3-	1	-32.23	4	72.46
Expon. m5-	1	-66.66	5	143.32
Hill m3-	1	-32.7	4	73.4
Hill m5-	1	-66.66	5	143.32
Inv.Expon. m3-	1	-34.55	4	77.1
Inv.Expon. m5-	1	-66.66	5	143.32
LN m3-	1	-33.79	4	77.62
LN m5-	1	-66.66	5	143.32

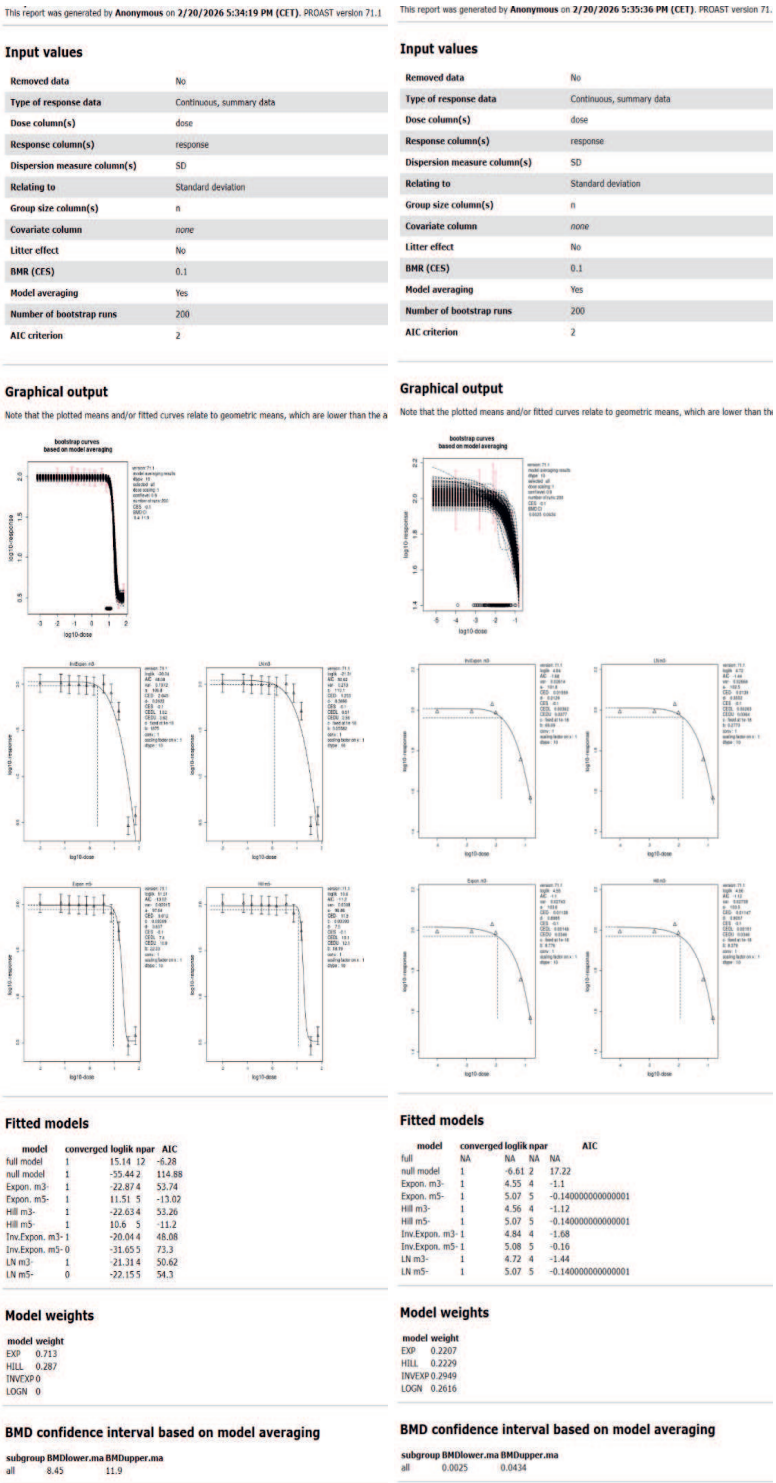
Model weights

model	weight
EXP	0.5172
HILL	0.3233
INVEXP	0.0508
LOGN	0.1087

BMD confidence interval based on model averaging

subgroup	BMDlower.ma	BMDupper.ma
all	0.322	1.62

Figure S9: PROAST benchmark modelling output for AChE inhibition after oral exposure to methyl-parathion in humans. Blood-based predictions on the left, enzyme-based predictions on the right.



This report was generated by **Anonymous** on **2/20/2026 5:34:19 PM (CET)**. PROAST version 71.1

Input values

Removed data	No
Type of response data	Continuous, summary data
Dose column(s)	dose
Response column(s)	response
Dispersion measure column(s)	SD
Relating to	Standard deviation
Group size column(s)	n
Covariate column	*none*
Litter effect	No
BMR (CES)	0.1
Model averaging	Yes
Number of bootstrap runs	200
AIC criterion	2

Graphical output

Note that the plotted means and/or fitted curves relate to geometric means, which are lower than the a

bootstrap curves based on model averaging

log10-response

log10-dose

Fitted models

model	converged	loglik	npar	AIC
full model	1	15.14	12	-6.28
null model	1	-55.44	2	114.88
Expon. m3-	1	-22.87	4	53.74
Expon. m5-	1	11.51	5	-13.02
Hill m3-	1	-22.63	4	53.26
Hill m5-	1	10.6	5	-11.2
Inv.Expon. m3-	1	-20.04	4	48.08
Inv.Expon. m5-	0	-31.65	5	73.3
LN m3-	1	-21.31	4	50.62
LN m5-	0	-22.15	5	54.3

Model weights

model	weight
EXP	0.713
HILL	0.287
INVEXP	0
LOGN	0

BMD confidence interval based on model averaging

subgroup	BMDlower.ma	BMDupper.ma
all	8.45	11.9

This report was generated by **Anonymous** on **2/20/2026 5:35:36 PM (CET)**. PROAST version 71.

Input values

Removed data	No
Type of response data	Continuous, summary data
Dose column(s)	dose
Response column(s)	response
Dispersion measure column(s)	SD
Relating to	Standard deviation
Group size column(s)	n
Covariate column	*none*
Litter effect	No
BMR (CES)	0.1
Model averaging	Yes
Number of bootstrap runs	200
AIC criterion	2

Graphical output

Note that the plotted means and/or fitted curves relate to geometric means, which are lower than th

bootstrap curves based on model averaging

log10-response

log10-dose

Fitted models

model	converged	loglik	npar	AIC
full	NA	NA	NA	NA
null model	1	-6.61	2	17.22
Expon. m3-	1	4.55	4	-1.1
Expon. m5-	1	5.07	5	-0.140000000000001
Hill m3-	1	4.56	4	-1.12
Hill m5-	1	5.07	5	-0.140000000000001
Inv.Expon. m3-	1	4.84	4	-1.68
Inv.Expon. m5-	1	5.08	5	-0.16
LN m3-	1	4.72	4	-1.44
LN m5-	1	5.07	5	-0.140000000000001

Model weights

model	weight
EXP	0.2207
HILL	0.2229
INVEXP	0.2949
LOGN	0.2616

BMD confidence interval based on model averaging

subgroup	BMDlower.ma	BMDupper.ma
all	0.0025	0.0434

Figure S10: PROAST benchmark modelling output for AChE inhibition after oral exposure to ethyl-parathion in rats. Blood-based predictions on the left, enzyme-based predictions on the right.

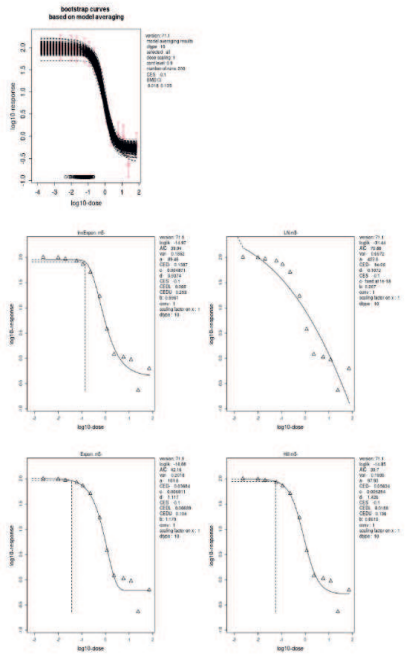
This report was generated by **Anonymous** on **2/20/2026 5:43:05 PM (CET)**. PROAST version 71

Input values

Removed data	No
Type of response data	Continuous, summary data
Dose column(s)	dose
Response column(s)	response
Dispersion measure column(s)	SD
Relating to	Standard deviation
Group size column(s)	n
Covariate column	*none*
Litter effect	No
BMR (CES)	0.1
Model averaging	Yes
Number of bootstrap runs	200
AIC criterion	2

Graphical output

Note that the plotted means and/or fitted curves relate to geometric means, which are lower than th



Fitted models

model	converged	loglik	npar	AIC
full	NA	NA	NA	NA
null model	1	-58.02	2	120.04
Expon. m3-	1	-34.96	4	77.92
Expon. m5-	1	-16.08	5	42.16
Hill m3-	1	-34.14	4	76.28
Hill m5-	1	-14.85	5	39.7
Inv.Expon. m3-	0	-38.28	4	84.56
Inv.Expon. m5-	1	-14.97	5	39.94
LN m3-	1	-31.44	4	70.88
LN m5-	0	-65.56	5	141.12

Model weights

model	weight
EXP	0.1341
HILL	0.4589
INVEXP	0.407
LOGN	0

BMD confidence interval based on model averaging

subgroup	BMDlower.ma	BMDupper.ma
all	0.0181	0.135

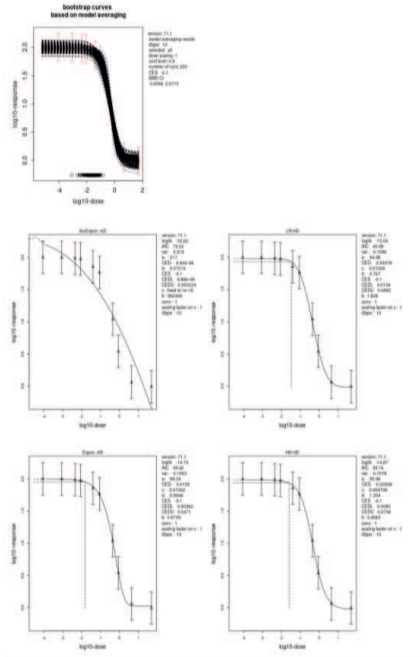
This report was generated by **Anonymous** on **2/20/2026 5:43:57 PM (CET)**. PROAST version 71.

Input values

Removed data	No
Type of response data	Continuous, summary data
Dose column(s)	dose
Response column(s)	response
Dispersion measure column(s)	SD
Relating to	Standard deviation
Group size column(s)	n
Covariate column	*none*
Litter effect	No
BMR (CES)	0.1
Model averaging	Yes
Number of bootstrap runs	200
AIC criterion	2

Graphical output

Note that the plotted means and/or fitted curves relate to geometric means, which are lower than the



Fitted models

model	converged	loglik	npar	AIC
full model	1	-14.56	11	51.12
null model	1	-61.38	2	126.76
Expon. m3-	1	-37.07	4	82.14
Expon. m5-	1	-14.73	5	39.46
Hill m3-	1	-36.42	4	80.84
Hill m5-	1	-14.87	5	39.74
Inv.Expon. m3-	1	-32.62	4	73.24
Inv.Expon. m5-	0	-53.14	5	116.28
LN m3-	0	-51.95	4	111.9
LN m5-	1	-15.04	5	40.08

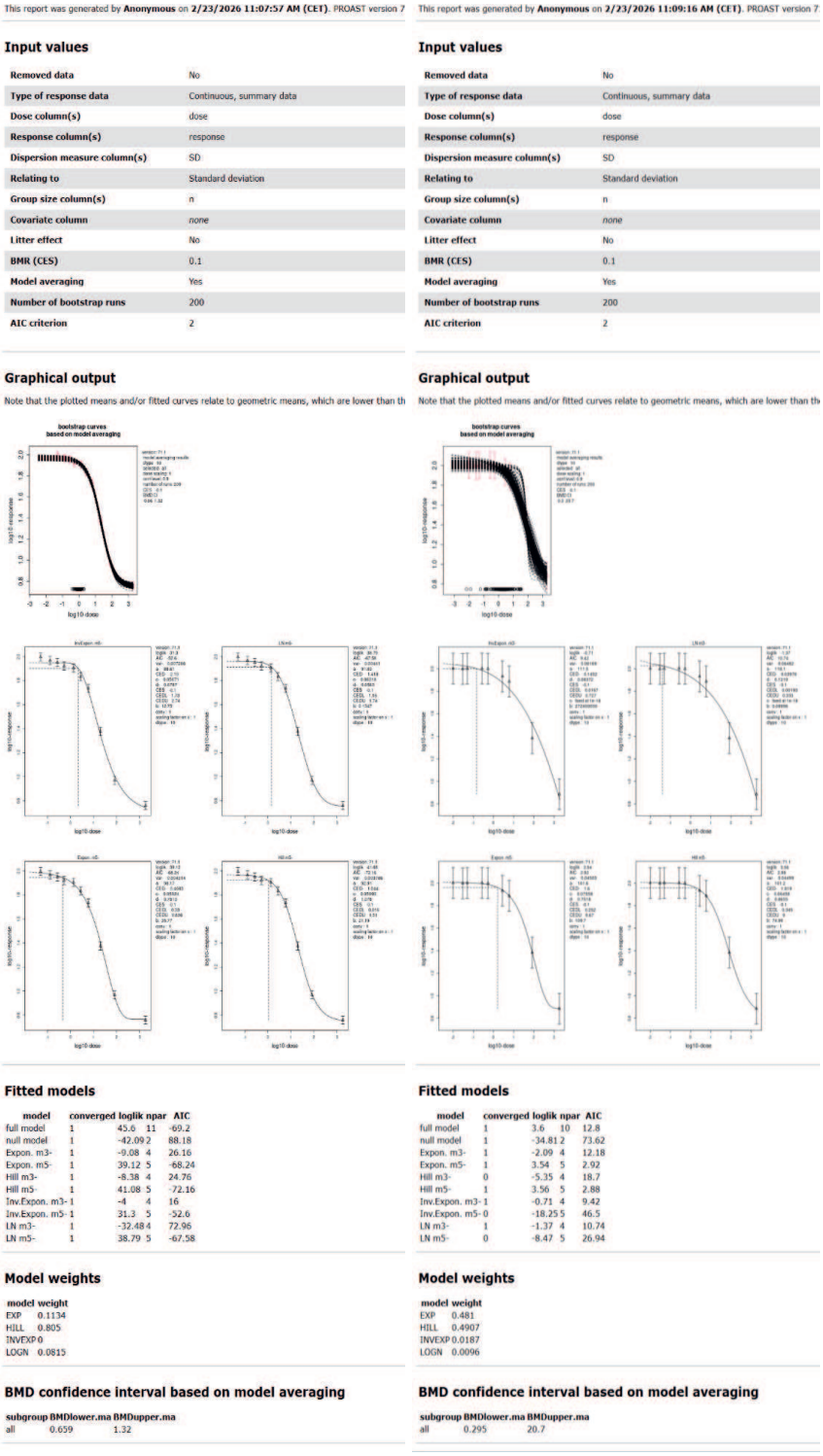
Model weights

model	weight
EXP	0.3842
HILL	0.334
INVEXP	0
LOGN	0.2818

BMD confidence interval based on model averaging

subgroup	BMDlower.ma	BMDupper.ma
all	0.00657	0.0715

Figure S11: PROAST benchmark modelling output for AChE inhibition after oral exposure to ethyl-parathion in humans. Blood-based predictions on the left, enzyme-based predictions on the right.



This report was generated by **Anonymous** on **2/23/2026 11:07:57 AM (CET)**. PROAST version 7

Input values

Removed data	No
Type of response data	Continuous, summary data
Dose column(s)	dose
Response column(s)	response
Dispersion measure column(s)	SD
Relating to	Standard deviation
Group size column(s)	n
Covariate column	*none*
Litter effect	No
BMR (CES)	0.1
Model averaging	Yes
Number of bootstrap runs	200
AIC criterion	2

Graphical output

Note that the plotted means and/or fitted curves relate to geometric means, which are lower than th

bootstrap curves based on model averaging

log10-response

log10-dose

Fitted models

model	converged	loglik	npar	AIC
full model	1	45.6	11	-69.2
null model	1	-42.09	2	88.18
Expon. m3-	1	-9.08	4	26.16
Expon. m5-	1	39.12	5	-68.24
Hill m3-	1	-8.38	4	24.76
Hill m5-	1	41.08	5	-72.16
Inv.Expon. m3-	1	-4	4	16
Inv.Expon. m5-	1	31.3	5	-52.6
LN m3-	1	-32.48	4	72.96
LN m5-	1	38.79	5	-67.58

Model weights

model	weight
EXP	0.1134
HILL	0.805
INVEXP	0
LOGN	0.0815

BMD confidence interval based on model averaging

subgroup	BMDlower.ma	BMDupper.ma
all	0.659	1.32

This report was generated by **Anonymous** on **2/23/2026 11:09:16 AM (CET)**. PROAST version 7

Input values

Removed data	No
Type of response data	Continuous, summary data
Dose column(s)	dose
Response column(s)	response
Dispersion measure column(s)	SD
Relating to	Standard deviation
Group size column(s)	n
Covariate column	*none*
Litter effect	No
BMR (CES)	0.1
Model averaging	Yes
Number of bootstrap runs	200
AIC criterion	2

Graphical output

Note that the plotted means and/or fitted curves relate to geometric means, which are lower than th

bootstrap curves based on model averaging

log10-response

log10-dose

Fitted models

model	converged	loglik	npar	AIC
full model	1	3.6	10	12.8
null model	1	-34.81	2	73.62
Expon. m3-	1	-2.09	4	12.18
Expon. m5-	1	3.54	5	2.92
Hill m3-	0	-5.35	4	18.7
Hill m5-	1	3.56	5	2.88
Inv.Expon. m3-	1	-0.71	4	9.42
Inv.Expon. m5-	0	-18.25	5	46.5
LN m3-	1	-1.37	4	10.74
LN m5-	0	-8.47	5	26.94

Model weights

model	weight
EXP	0.481
HILL	0.4907
INVEXP	0.0187
LOGN	0.0096

BMD confidence interval based on model averaging

subgroup	BMDlower.ma	BMDupper.ma
all	0.295	20.7

Figure S12: PROAST benchmark modelling output for AChE inhibition after oral exposure to dimethoate in rats. Blood-based predictions on the left, enzyme-based predictions on the right.

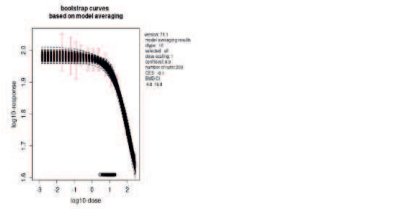
This report was generated by **Anonymous** on **2/23/2026 11:10:14 AM (CET)**. PROAST version 71

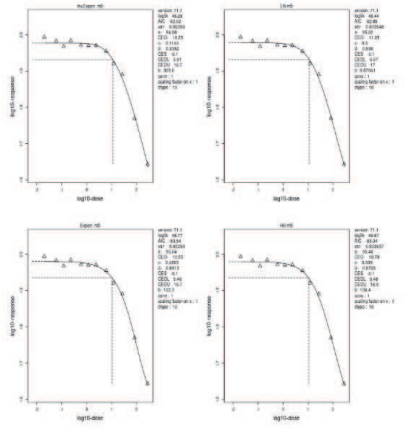
Input values

Removed data	No
Type of response data	Continuous, summary data
Dose column(s)	dose
Response column(s)	response
Dispersion measure column(s)	SD
Relating to	Standard deviation
Group size column(s)	n
Covariate column	*none*
Litter effect	No
BMR (CES)	0.1
Model averaging	Yes
Number of bootstrap runs	200
AIC criterion	2

Graphical output

Note that the plotted means and/or fitted curves relate to geometric means, which are lower than the





Fitted models

model	converged	loglik	npar	AIC
full	NA	NA	NA	NA
null model	1	-1.21	2	6.42
Expon. m3-	1	43.9	4	-79.8
Expon. m5-	1	46.77	5	-83.54
Hill m3-	1	43.94	4	-79.88
Hill m5-	1	46.67	5	-83.34
Inv.Expon. m3-	1	45.12	4	-82.24
Inv.Expon. m5-	1	46.26	5	-82.52
LN m3-	1	44.62	4	-81.24
LN m5-	1	46.44	5	-82.88

Model weights

model	weight
EXP	0.3101
HILL	0.2806
INVEXP	0.1862
LOGN	0.223

BMD confidence interval based on model averaging

subgroup	BMDlower.ma	BMDupper.ma
all	4.81	16.8

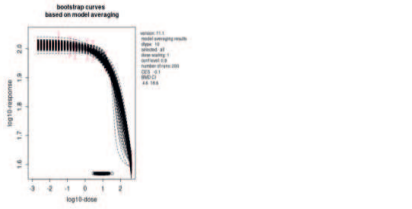
This report was generated by **Anonymous** on **2/23/2026 11:11:18 AM (CET)**. PROAST version 71

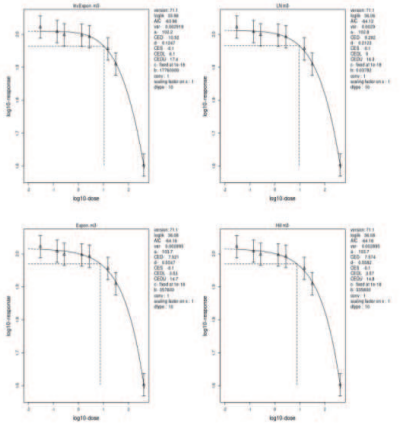
Input values

Removed data	No
Type of response data	Continuous, summary data
Dose column(s)	dose
Response column(s)	response
Dispersion measure column(s)	SD
Relating to	Standard deviation
Group size column(s)	n
Covariate column	*none*
Litter effect	No
BMR (CES)	0.1
Model averaging	Yes
Number of bootstrap runs	200
AIC criterion	2

Graphical output

Note that the plotted means and/or fitted curves relate to geometric means, which are lower than the





Fitted models

model	converged	loglik	npar	AIC
full model	1	36.86	9	-55.72
null model	1	-5.47	2	14.94
Expon. m3-	1	36.08	4	-64.16
Expon. m5-	1	36.12	5	-62.24
Hill m3-	1	36.08	4	-64.16
Hill m5-	1	36.12	5	-62.24
Inv.Expon. m3-	1	35.98	4	-63.96
Inv.Expon. m5-	1	35.92	5	-61.84
LN m3-	1	36.06	4	-64.12
LN m5-	1	36.04	5	-62.08

Model weights

model	weight
EXP	0.2574
HILL	0.2574
INVEXP	0.2329
LOGN	0.2523

BMD confidence interval based on model averaging

subgroup	BMDlower.ma	BMDupper.ma
all	4.63	18.6

Figure S13: PROAST benchmark modelling output for AChE inhibition after oral exposure to dimethoate in humans. Blood-based predictions on the left, enzyme-based predictions on the right.

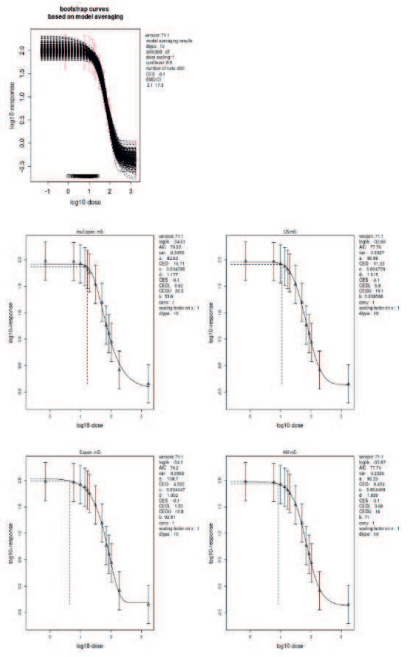
This report was generated by **Anonymous** on **2/23/2026 2:22:13 PM (CET)**. PROAST version 71

Input values

Removed data	No
Type of response data	Continuous, summary data
Dose column(s)	dose
Response column(s)	response
Dispersion measure column(s)	SD
Relating to	Standard deviation
Group size column(s)	n
Covariate column	*none*
Litter effect	No
BMR (CES)	0.1
Model averaging	Yes
Number of bootstrap runs	200
AIC criterion	2

Graphical output

Note that the plotted means and/or fitted curves relate to geometric means, which are lower than t



Fitted models

model	converged	loglik	npar	AIC
full model	1	-33.64	14	95.28
null model	1	-80.57	2	165.14
Expon. m3-	1	-53.02	4	114.04
Expon. m5-	1	-34.1	5	78.2
Hill m3-	1	-52.48	4	112.96
Hill m5-	1	-33.87	5	77.74
Inv.Expon. m3-	1	-51.45	4	110.9
Inv.Expon. m5-	1	-34.61	5	79.22
LN m3-	1	-52.01	4	112.02
LN m5-	1	-33.88	5	77.76

Model weights

model	weight
EXP	0.2436
HILL	0.3066
INVEXP	0.1463
LOGN	0.3035

BMD confidence interval based on model averaging

subgroup	BMDlower.ma	BMDupper.ma
all	2.08	17.3

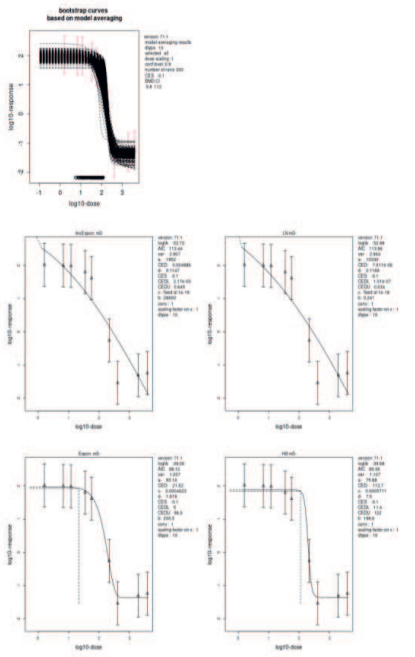
This report was generated by **Anonymous** on **2/23/2026 1:54:05 PM (CET)**. PROAST version 71.

Input values

Removed data	No
Type of response data	Continuous, summary data
Dose column(s)	dose
Response column(s)	response
Dispersion measure column(s)	SD
Relating to	Standard deviation
Group size column(s)	n
Covariate column	*none*
Litter effect	No
BMR (CES)	0.1
Model averaging	Yes
Number of bootstrap runs	200
AIC criterion	2

Graphical output

Note that the plotted means and/or fitted curves relate to geometric means, which are lower than th



Fitted models

model	converged	loglik	npar	AIC
full model	1	-38.38	10	96.76
null model	1	-73.64	2	151.28
Expon. m3-	1	-53.96	4	115.92
Expon. m5-	1	-39.06	5	88.12
Hill m3-	1	-53.41	4	114.82
Hill m5-	1	-39.68	5	89.36
Inv.Expon. m3-	1	-52.72	4	113.44
Inv.Expon. m5-	0	-59.79	5	129.58
LN m3-	1	-52.98	4	113.96
LN m5-	0	-68.83	5	147.66

Model weights

model	weight
EXP	0.6502
HILL	0.3498
INVEXP	0
LOGN	0

BMD confidence interval based on model averaging

subgroup	BMDlower.ma	BMDupper.ma
all	9.77	112

Figure S14: PROAST benchmark modelling output for AChE inhibition after oral exposure to chlorfenvinphos in rats. Blood-based predictions on the left, enzyme-based predictions on the right.

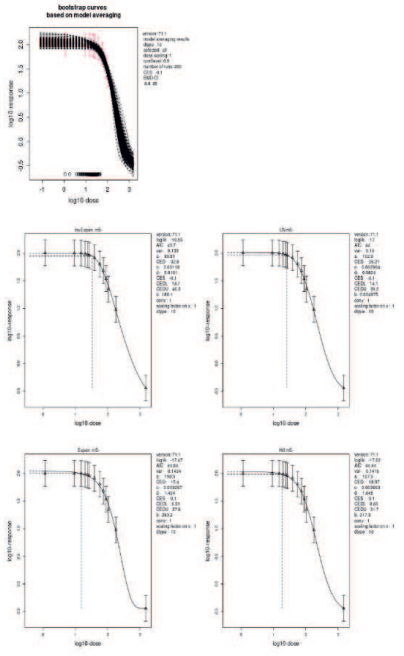
This report was generated by **Anonymous** on **2/23/2026 11:29:57 AM (CET)**. PROAST version 71

Input values

Removed data	No
Type of response data	Continuous, summary data
Dose column(s)	dose
Response column(s)	response
Dispersion measure column(s)	SD
Relating to	Standard deviation
Group size column(s)	n
Covariate column	*none*
Litter effect	No
BMR (CES)	0.1
Model averaging	Yes
Number of bootstrap runs	200
AIC criterion	2

Graphical output

Note that the plotted means and/or fitted curves relate to geometric means, which are lower than the



Fitted models

model	converged	loglik	npar	AIC
full model	1	-10.49	14	60.98
null model	1	-72.84	2	149.68
Expon. m3-	1	-25.19	4	58.38
Expon. m5-	1	-17.47	5	44.94
Hill m3-	1	-24.92	4	57.84
Hill m5-	1	-17.22	5	44.44
Inv.Expon. m3-	1	-22.35	4	52.7
Inv.Expon. m5-	1	-16.85	5	43.7
LN m3-	1	-23.73	4	55.46
LN m5-	1	-17	5	44

Model weights

model	weight
EXP	0.1741
HILL	0.2236
INVEXP	0.3237
LOGN	0.2786

BMD confidence interval based on model averaging

subgroup	BMDlower.ma	BMDupper.ma
all	6.84	35

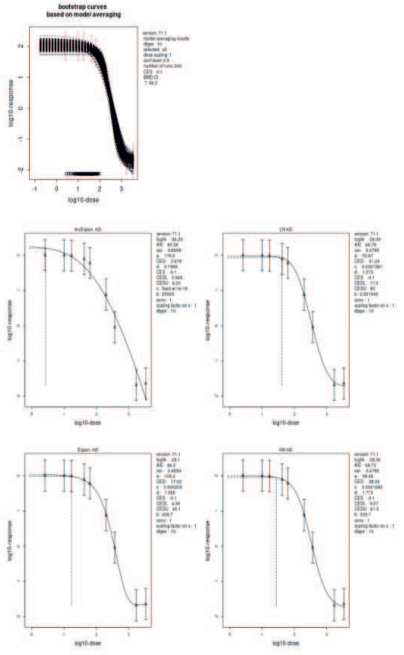
This report was generated by **Anonymous** on **2/23/2026 12:15:08 PM (CET)**. PROAST version 7

Input values

Removed data	No
Type of response data	Continuous, summary data
Dose column(s)	dose
Response column(s)	response
Dispersion measure column(s)	SD
Relating to	Standard deviation
Group size column(s)	n
Covariate column	*none*
Litter effect	No
BMR (CES)	0.1
Model averaging	Yes
Number of bootstrap runs	200
AIC criterion	2

Graphical output

Note that the plotted means and/or fitted curves relate to geometric means, which are lower than th



Fitted models

model	converged	loglik	npar	AIC
full model	1	-28.05	10	76.1
null model	1	-71.85	2	147.7
Expon. m3-	1	-38.54	4	85.08
Expon. m5-	1	-28.1	5	66.2
Hill m3-	1	-38.11	4	84.22
Hill m5-	1	-28.36	5	66.72
Inv.Expon. m3-	1	-36.29	4	80.58
Inv.Expon. m5-	0	-64.63	5	139.26
LN m3-	1	-37.47	4	82.94
LN m5-	1	-28.39	5	66.78

Model weights

model	weight
EXP	0.3968
HILL	0.306
INVEXP	3e-04
LOGN	0.2969

BMD confidence interval based on model averaging

subgroup	BMDlower.ma	BMDupper.ma
all	7.01	66.2

Figure S15: PROAST benchmark modelling output for AChE inhibition after oral exposure to chlorfenvinphos in humans. Blood-based predictions on the left, enzyme-based predictions on the right.

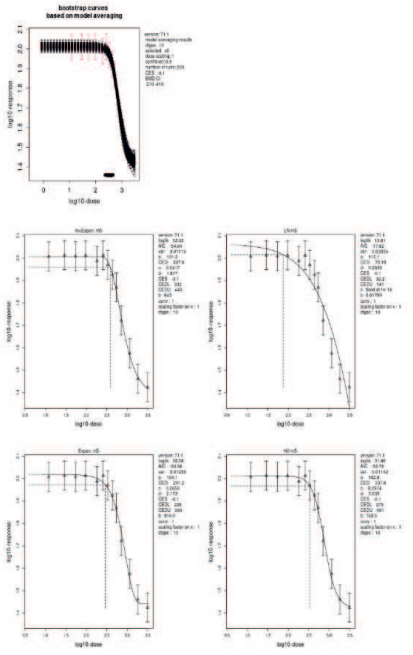
This report was generated by **Anonymous** on **2/23/2026 1:19:54 PM (CET)**. PROAST version 71

Input values

Removed data	No
Type of response data	Continuous, summary data
Dose column(s)	dose
Response column(s)	response
Dispersion measure column(s)	SD
Relating to	Standard deviation
Group size column(s)	n
Covariate column	*none*
Litter effect	No
BMR (CES)	0.1
Model averaging	Yes
Number of bootstrap runs	200
AIC criterion	2

Graphical output

Note that the plotted means and/or fitted curves relate to geometric means, which are lower than th



Fitted models

model	converged	loglik	npar	AIC
full model	1	33.47	14	-38.94
null model	1	-28.48	2	60.96
Expon. m3-	1	11.49	4	-14.98
Expon. m5-	1	30.28	5	-50.56
Hill m3-	1	11.6	4	-15.2
Hill m5-	1	31.88	5	-53.76
Inv.Expon. m3-	1	13.99	4	-19.98
Inv.Expon. m5-	1	32.32	5	-54.64
LN m3-	1	12.81	4	-17.62
LN m5-	0	-9.39	5	28.78

Model weights

model	weight
EXP	0.0733
HILL	0.363
INVEXP	0.5637
LOGN	0

BMD confidence interval based on model averaging

subgroup	BMDlower.ma	BMDupper.ma
all	272	410

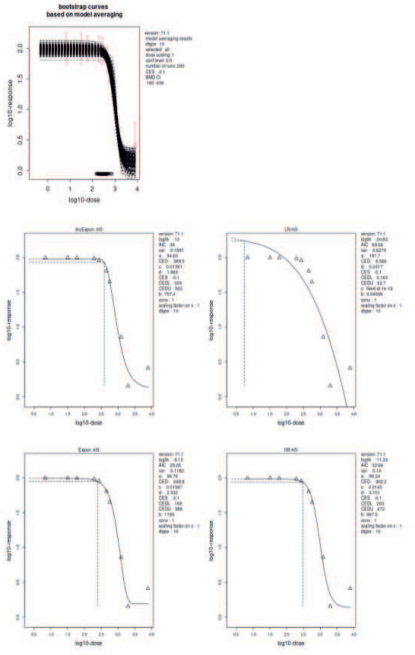
This report was generated by **Anonymous** on **2/23/2026 1:21:03 PM (CET)**. PROAST version 71.

Input values

Removed data	No
Type of response data	Continuous, summary data
Dose column(s)	dose
Response column(s)	response
Dispersion measure column(s)	SD
Relating to	Standard deviation
Group size column(s)	n
Covariate column	*none*
Litter effect	No
BMR (CES)	0.1
Model averaging	Yes
Number of bootstrap runs	200
AIC criterion	2

Graphical output

Note that the plotted means and/or fitted curves relate to geometric means, which are lower than the



Fitted models

model	converged	loglik	npar	AIC
full	NA	NA	NA	NA
null model	1	-48.2	2	100.4
Expon. m3-	1	-31.67	4	71.34
Expon. m5-	1	-9.13	5	28.26
Hill m3-	1	-31.47	4	70.94
Hill m5-	1	-11.33	5	48.68
Inv.Expon. m3-	1	-29.93	4	67.86
Inv.Expon. m5-	1	-13	5	36
LN m3-	1	-30.83	4	69.66
LN m5-	0	-30.88	5	71.76

Model weights

model	weight
EXP	0.8837
HILL	0.0979
INVEXP	0.0184
LOGN	0

BMD confidence interval based on model averaging

subgroup	BMDlower.ma	BMDupper.ma
all	184	436

Figure S16: PROAST benchmark modelling output for AChE inhibition after oral exposure to profenofos in rats. Blood-based predictions on the left, enzyme-based predictions on the right.

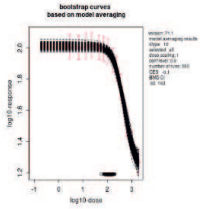
This report was generated by **Anonymous** on **2/23/2026 1:22:09 PM (CET)**. PROAST version 71.

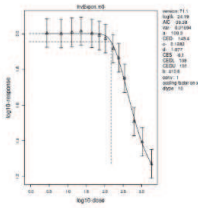
Input values

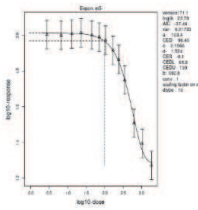
Removed data	No
Type of response data	Continuous, summary data
Dose column(s)	dose
Response column(s)	response
Dispersion measure column(s)	SD
Relating to	Standard deviation
Group size column(s)	n
Covariate column	*none*
Litter effect	No
BMR (CES)	0.1
Model averaging	Yes
Number of bootstrap runs	200
AIC criterion	2

Graphical output

Note that the plotted means and/or fitted curves relate to geometric means, which are lower than the







Fitted models

model	converged	loglik	npar	AIC
full model	1	25.24	14	-22.48
null model	1	-34.97	2	73.94
Expon. m3-	1	12.37	4	-16.74
Expon. m5-	1	23.73	5	-37.46
Hill m3-	1	12.51	4	-17.02
Hill m5-	1	24.6	5	-39.2
Inv.Expon. m3-	1	15.4	4	-22.8
Inv.Expon. m5-	1	24.19	5	-38.38
LN m3-	1	14.01	4	-20.02
LN m5-	1	24.49	5	-38.98

Model weights

model	weight
EXP	0.1407
HILL	0.3357
INVEXP	0.2228
LOGN	0.3008

BMD confidence interval based on model averaging

subgroup	BMDlower.ma	BMDupper.ma
all	81.6	163

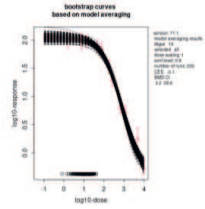
This report was generated by **Anonymous** on **2/23/2026 1:23:40 PM (CET)**. PROAST version 71.

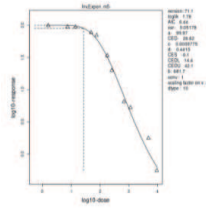
Input values

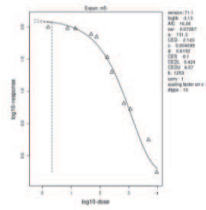
Removed data	No
Type of response data	Continuous, summary data
Dose column(s)	dose
Response column(s)	response
Dispersion measure column(s)	SD
Relating to	Standard deviation
Group size column(s)	n
Covariate column	*none*
Litter effect	No
BMR (CES)	0.1
Model averaging	Yes
Number of bootstrap runs	200
AIC criterion	2

Graphical output

Note that the plotted means and/or fitted curves relate to geometric means, which are lower than the







Fitted models

model	converged	loglik	npar	AIC
full	NA	NA	NA	NA
null model	1	-56.35	2	116.7
Expon. m3-	1	-10.05	4	28.1
Expon. m5-	1	-3.13	5	16.26
Hill m3-	1	-9.7	4	27.4
Hill m5-	1	-1	5	12
Inv.Expon. m3-	1	-7.03	4	22.06
Inv.Expon. m5-	1	1.78	5	6.44
LN m3-	0	-8.61	4	25.22
LN m5-	0	-140.77	5	291.54

Model weights

model	weight
EXP	0.0069
HILL	0.058
INVEXP	0.935
LOGN	1e-04

BMD confidence interval based on model averaging

subgroup	BMDlower.ma	BMDupper.ma
all	3.23	28.6

Figure S17: PROAST benchmark modelling output for AChE inhibition after oral exposure to profenofos in humans. Blood-based predictions on the left, enzyme-based predictions on the right.

6

General discussion

1. Overview of results

Each year, the safety of many old and new chemicals needs to be assessed. This is a huge task for both the companies producing these chemicals as well as agencies tasked with defining the safety of chemical exposures. Most current day chemical safety regulations still rely heavily on animal testing, which often requires hundreds of animals for various experiments focusing on specific toxicities and endpoints. These experiments would be needed for thousands of substances, being drugs, compounds in our food or in our environment, killing millions of animals each year (102). While the number of animals needed raises ethical questions, the time and financial costs are also immense. More importantly, scientific scrutiny of the current animal centered approach to risk assessment based on the notion that humans and animals can respond differently to the same chemical exposure, leads many to think that animal experiments might not provide accurate data needed for human centric risk assessment. Therefore, for ethical, scientific and economic reasons, it is clear that change is needed in the way chemical risk assessment is performed.

The aim of this thesis was to evaluate animal-free approaches for application in next generation risk assessment of organophosphate pesticides. The approach was based on in silico and in vitro methods, and was evaluated for predicting points of departure (PODs) of acetylcholinesterase (AChE) inhibition by organophosphate pesticides. This approach consisted of development of a generic physiologically based kinetic (PBK) model for organophosphate pesticides (**chapter 2 and 4**), in vitro quantification of AChE inhibition by various organophosphate pesticides (**chapter 3 and 5**), exposure safety evaluation using the dietary comparator ratio (DCR) method (**chapter 3**), and point of departure prediction for hazard characterization using quantitative in vitro to in vivo extrapolation (QIVIVE) of in vitro AChE inhibition to the in vivo situation (**chapter 5**). The experimental approaches and findings of each chapter are briefly summarized below.

In **chapter 2**, a PBK model was developed to predict blood/plasma concentrations of eight organophosphate pesticides and their metabolites in humans. A rat model was developed as well, allowing for validation of the modelling approach using rat data as well. The developed PBK model predicts how organophosphates are absorbed, distributed, metabolized and excreted in/from the body, based on in vitro or in silico derived parameters. The implementation of metabolism was essential, since organothiophosphate pesticides are both bioactivated to their oxon metabolites as well as detoxified to metabolites that are excreted in urine. Validation of the PBK model was done using literature derived blood or plasma concentration-time data from in vivo exposure studies. Reported human in vivo data showed that blood/plasma concentrations could vary significantly between studies (up to 6-fold) for the same doses. This was assumed to be caused by food effects on absorption and was taken along for validation of the human PBK model. When validating the model, blood/plasma concentrations of most of the organophosphate pesticides can be predicted within 5-fold difference from in vivo values. Those pesticides that were less well predicted were all found to be in the dimethyl-organophosphate pesticide subclass.

The use of the DCR method for safety evaluation of organophosphate pesticides was investigated in **chapter 3**. Six organophosphate pesticides were used to evaluate the DCR method for organophosphate pesticides: chlorpyrifos, fenitrothion, profenofos, diazinon, methyl-parathion and chlorfenvinphos. For these compounds, concentration-effect data were derived from in vitro AChE inhibition assays using human blood. Furthermore, for each pesticide, reported in vivo human

exposures where both dose and adverse effects were mentioned were collected from literature. Chlorpyrifos was selected as the comparator compound for the DCR method. A safe exposure-activity ratio for the comparator compound was calculated as the ratio between the 5% lower limit benchmark concentration ($BMCL_5$) and the IC_{50}. Next, the PBK model developed in **chapter 2** was used to predict the maximum blood concentration for each exposure found in literature. The exposure-activity ratio for each exposure scenario was calculated by dividing the maximum blood concentration for that scenario by the IC_{50} for the compound to which a human was exposed in that scenario. Next, for each exposure scenario, the DCR was determined as the ratio between the exposure-activity ratio for the exposure to the test compound and the exposure-activity ratio of the comparator compound. A DCR below 1 indicates a safe exposure with minimal adverse effects. The DCR method correctly predicted 70 out of 74 exposures to be safe when these were indeed reported to have no adverse effects. Four exposure scenarios were predicted to be dangerous, while these were reported to be safe. The four false positives were all for dimethyl-organophosphates. Since the DCR method was shown to accurately predict the occurrence of adverse effects after exposure to organophosphate pesticides, it can be used for safety evaluation of exposures to these pesticides in the future.

Looking at the findings in **chapters 2 and 3**, it was hypothesized that the lower accuracy of predictions for the dimethyl-organophosphates fenitro-oxon, methyl-paraoxon and omethoate could be due to a metabolic pathway not incorporated in the PBK model. This hypothesis was further investigated in **chapter 4**, where in vitro metabolism studies were performed to see if dimethyl-organophosphate pesticides could be metabolized by an understudied metabolic pathway. Incubations of methyl-paraoxon and omethoate with human and rat liver S9 protein, showed that both pesticides were metabolized via a glutathione-mediated pathway. It was also shown that omethoate is metabolized by a slow chemical reaction with glutathione, while methyl-paraoxon requires an enzyme to facilitate this reaction, but at a much higher rate. Furthermore, species differences were observed for the enzymatic glutathione-mediated metabolism of methyl-paraoxon, since rats were able to metabolize the compound four times faster than humans. The glutathione-mediated metabolic pathway was incorporated in the PBK model developed in **chapter 2** and validated with the three dimethyl-organophosphate pesticides that were previously less well predicted: fenitrothion, methyl-paraoxon and omethoate. For glutathione-mediated metabolism of fenitro-oxon, read-across from methyl-paraoxon was used, since these compounds are nearly identical in molecular structure. PBK model blood/plasma predictions for methyl-paraoxon and fenitro-oxon improved from over 10-fold difference when glutathione-mediated metabolism was not included, to less than 5- and often even 2-fold differences compared to in vivo rat data. For omethoate, no significant changes in predicted blood/plasma concentrations were observed. For humans, predicted maximal concentrations were more than 12-fold lower when glutathione-mediated metabolism was incorporated in the model.

While the DCR method can be used to predict if an exposure to organophosphate pesticides will result in adverse effects, the quantitative in vitro to in vivo extrapolation (QIVIVE) approach is more useful for animal-free hazard characterization and point of departure determination. Therefore, the use of QIVIVE for point of departure determination of AChE inhibition by organophosphate pesticides was explored in **chapter 5**. For eight organophosphate pesticides and their active metabolites, concentration-response curves were derived from in vitro AChE inhibition assays using human and

rat whole blood. To investigate the effect of using whole blood or isolated/recombinant enzyme in AChE inhibition assays on QIVIVE, in vitro AChE inhibition assays were also performed using isolated rat or recombinant human enzyme. For each pesticide, both whole blood and enzyme concentration-response curves were translated to dose-response curves using the adjusted PBK model developed in **chapter 4**. The points of departure were then predicted by determining the 10% lower limit benchmark dose ($BMDL_{10}$) of the dose-response curves with the use of benchmark dose modelling. These predicted points of departure were compared to in vivo determined points of departure reported in literature. All predicted points of departure, for both rats and humans, were within 4-fold from in vivo determined points of departure low-observed-adverse-effect levels (LOAELs) and higher than the reported no-observed-adverse-effect levels (NOAELs). However, prediction of $BMDL_{10}$ values based on whole blood data was not possible for chlorpyrifos and diazinon. It was hypothesized that this was caused by significant metabolism by non-AChE esterases present in whole blood. Therefore, pure AChE enzyme should be used when obtaining concentration-response data for QIVIVE of organophosphate pesticides. Furthermore, in **chapter 5** it was shown that QIVIVE-based point of departure determination can be used for animal-free hazard characterization for organophosphate pesticides.

The findings in this thesis show the applicability of several in vitro and in silico approaches in a next generation safety assessment for organophosphate pesticides. Furthermore, using these approaches side by side also provided valuable insights into species differences between rats and humans. For example, in **chapter 4**, it was shown that dimethyl organophosphate pesticides were metabolized four times faster in rats compared to humans. Moreover, in **chapter 2**, more interspecies differences in the rate of metabolism via other pathways. In **chapter 5**, it was also discussed that rat blood contains an esterase that is not present in humans. All these findings support the thought that animals used in toxicity testing do not always represent humans very well. Therefore, the human centric data provided by animal-free approaches is essential for chemical risk assessment for humans.

2 General discussion and future perspectives

The findings reported in this thesis show that in vitro and in silico methods can be used successfully for next generation risk assessment of organophosphate pesticides. While the current thesis focused on predicting AChE inhibition after acute (single) exposure to organophosphate pesticides, risk assessments for realistic exposure scenarios requires consideration of many more aspects. Furthermore, the risk assessment approaches used here (DCR and QIVIVE) relied heavily on the developed PBK model and therefore show that PBK modelling forms an integral part of animal-free risk assessment. From the conclusions of this thesis, several considerations and recommendations for the future directions of organophosphate pesticide risk assessment and PBK modelling can be derived. Specifically, the following future directions are discussed in detail in the sections below:

- Effects of mixtures and chronic exposures on adverse effects of organophosphate pesticides
- Organophosphate pesticides and neurodegenerative diseases
- Modelling platforms in PBK modelling
- Missing physiological processes in PBK modelling

- Required physiological detail in PBK modelling
- The use of physiological parameters in population and growth modelling
- Reliability of in vitro and in silico derived kinetic parameters
- PBK model validation
- Thoughts on adoption of animal free risk assessment

2.1 Organophosphate pesticides

2.1.1 Effects of mixtures and chronic exposures

In this thesis the focus was on acute (single) exposures to organophosphate pesticides. However, the average person is not exposed to only one type of organophosphate pesticide at a time, but is frequently and repeatedly (chronically) exposed to a combination of pesticides via their daily meals. Therefore, both chronic exposure and exposure to mixtures of organophosphate pesticides would be a more realistic exposure scenarios for the general population.

Compared to acute exposure, chronic exposure can result in accumulation of adverse effects in multiple ways. For example, lipophilic organophosphate pesticides, like chlorpyrifos or profenofos and some of their metabolites, cannot be efficiently expelled from the body by passive clearance processes like glomerular filtration. The clearance of these compounds relies mainly on active processes like metabolism and is limited by accumulation in nonmetabolizing tissues like fat (292,293). It therefore takes more time to clear these lipophilic compounds from the body after an exposure. If repeated exposures are frequent enough, not all of the pesticide is cleared from the body, before a new exposure occurs. This causes lipophilic compounds to accumulate in the body with frequent repeated exposures, for example with multiple meals a day. Besides the direct increase in adverse effects due to bioaccumulation of organophosphate pesticides, their specific mechanism of action could also cause an accumulation of adverse effects due to the time it takes the body to recover the lost function of irreversibly inhibited enzymes. Organophosphate pesticides are known to irreversibly inhibit esterases like AChE, NTE and others. In case of reversible inhibition, the inhibited enzyme can resume it's function once the inhibitor compound is cleared from the body. However, for irreversible inhibited enzyme, its function can only be regained by replacing inhibited protein with newly produced enzyme. Breaking down and synthesizing new enzymes takes time. For example, for irreversibly inhibited AChE, functional recovery can take days in muscle and brain tissue (294), and possibly weeks in blood, since AChE can only be recovered by replacing the erythrocyte to which irreversibly inhibited AChE is attached (265). Frequent repeated exposure could therefore cause incremental depression of esterase activity in the body. Compared to acute exposure, chronic exposure to organophosphate pesticides could therefore result in (bio)accumulation of the pesticide in the body, as well as additional accumulation of its adverse effect intensity like that of inhibition of AChE.

Since different pesticides are used on different crops, the general population is not only exposed to one pesticide at a time. On average, an individual consumes multiple types of fruits and vegetables and is therefore exposed to many different kinds of pesticides. When pesticides, and other compounds, are metabolized or transported by the same proteins, they can alter each others metabolism or excretion (295,296). For example, when metabolism or excretion is inhibited, the amount of pesticides can increase, which could also increase the intensity of adverse effects of those

compounds. In case of organophosphate pesticides, it has been reported that the pesticide atrazine can affect the metabolism of several organophosphate pesticides, increasing their adverse effects (297). Such effects can be highly compound specific and is therefore hard to predict. Furthermore, different pesticides, or other compounds present in foods, can also share the same target enzyme in the body. Altering, and potentially increasing, the effect on that target. For example, plants contain many compounds that are also able to inhibit AChE, the target enzyme of organophosphate pesticides (298). Therefore, exposure to mixtures can alter the toxicokinetics and intensity of adverse effects.

In this thesis, points of departure were predicted for single, acute exposures to organophosphate pesticides. While these are useful for getting an idea of how toxic a single compound would be, both chronic and mixture exposures could significantly change the total toxicity of an exposure. Therefore an exposure analysis is of great importance. Mixture exposures can be characterized using residue data, for example based on different basic diets (299,300). For each diet, one can have an estimated dose per meal for all (organophosphate) pesticides. A PBK model can be used to predict chronic internal exposures for each pesticide in each diet. This PBK model can be expanded upon with mechanistic dynamic models for AChE inhibition (131,265), allowing to model the combined binding/inhibition of a target of all these pesticides. Due to the sheer number of pesticides present in a typical diet, such a model will likely be very computationally heavy to run. However, using such an approach, risk assessment could be performed for more realistic exposure scenarios for the general population.

2.1.2 Organophosphate pesticides and neurodegenerative diseases

While organophosphate pesticides are known for their acute neurotoxic mechanism of action of inhibiting AChE (13,14), epidemiological studies have associated organophosphate pesticide exposure to neurodegenerative diseases (301). However, the direct mechanism of action has not yet been elucidated. Inhibition of red blood cell AChE or secondary target enzymes by organophosphate pesticides might hold the key to finding a mechanism of action for neurodegenerative diseases.

For many years, the physiological function of AChE on red blood cell membranes has been poorly understood, since most acetylcholine research focusses on its neurological functions and effects. However, acetylcholine is known to play a role in the immune system. Some white blood cells have been shown to synthesize and release acetylcholine (302), affecting blood pressure (303,304), and extravasation of, and cytokine release by, white blood cells (302). Red blood cell AChE might therefore manage the inflammatory status of the body. Organophosphate pesticides might therefore alter the inflammatory status, which has been associated with neurodegenerative diseases (305).

While the functions and effects of AChE are reasonably well understood, this is not the case for other esterases inhibited by organophosphate pesticides, like BuChE, CES, PON1 and NTE. All of these esterases are known to have endogenous ligands associated with various aspects of lipid metabolism. For example, BuChE showed lipase activity towards various fatty acids and acyl-ghrelin (306–309), carboxylesterases have been shown to hydrolyze acyl-coenzyme A and cholesteryl esters (310–312), and PON1 metabolizes oxidized fatty acids, estrogen-acyl esters and fatty acid lactones (313–315). Furthermore, NTE is known to hydrolyze (lyso)phosphatidylcholine, an important component of the cell membrane (31,32,316). NTE knock-out in mice or NTE gene

mutations in humans show motor neurodegeneration (317,318). The functions of BuChE, CES, PON1 and NTE are all related to lipid metabolism or membrane homeostasis. It has been speculated that disturbances in lipid metabolism could play a role in protein misfolding and aggregation, which has been associated with many neurodegenerative diseases (319). Furthermore, some preliminary evidence shows a possible correlation of disturbed lipid metabolism with neurodegenerative diseases (320). Lipid metabolism related esterase inhibition by organophosphate pesticides could therefore be related to neurodegenerative diseases.

2.2 Opportunities in physiologically based kinetic modelling

In the last few decades, the idea of personalized medicine has been coined in the field of pharmacology. The idea is that for each patient or person, a virtual version can be made based on their body measurements and/or DNA. Such a virtual version of a person is also known as a digital twin or a virtual human. Virtual humans could accelerate drug development and risk assessment, as well as personalize dosing regimens (321). Projects like the Virtual Human Platform for Safety (VHP4S), of which this thesis is part of, aim to apply such an approach for chemical risk assessment for humans. PBK modeling forms a corner stone in the use of virtual humans, since PBK models provide an in silico approach for predicting internal kinetics of compounds. While PBK modelling is a promising tool, there are still many limitations and opportunities for further development and it's use for virtual humans.

2.2.1 Modelling platforms

Many modelling platforms (software) are available for PBK modelling these days. While these platforms all have their strengths and weaknesses, some limit further development and usability of PBK models. For example, some of the best and user friendly modelling platforms are behind a paywall, limiting the shareability and usability of the developed models (Simcyp (322), GastroPlus (323)). Other paid platforms allow for unlimited flexibility by enabling users to write their own custom model code (MATLAB (324), Berkeley Madonna (325)). While this flexibility is very useful for developing new modelling approaches, it is hard to standardize such approaches. Moreover, it limits user friendliness since these platforms focus on writing model code instead of (toxico)kinetic processes. The PKsim and MoBi modelling platforms of Open Systems Pharmacology are free and open source (326), increasing accessibility and usability. Both of these software's have a reasonably user friendly interface and MoBi allows for flexibility in making custom models with no coding knowledge required. Lastly, as programming languages, modelling in R or python allow for easy integration in data or workflow pipelines, and are free and open source, making them accessible for others to work with. However, as is the case for MATLAB and Berkeley Madonna, R and Python allow for the flexibility of writing custom model code, making it hard to standardize models on these platforms.

All of the discussed modelling platforms have their strengths and weaknesses. While some of the discussed modelling platforms allow for open sharing and using of developed PBK models, non of them allow for easy reusability of custom model components (reusing detailed tissue or absorption submodels in a new PBK model, for example). Here, programming languages could be used to develop web apps and packages/libraries to standardize modelling methods, and improve user

friendliness, flexibility, accessibility and (re)usability. Furthermore, academic and governmental PBK modelling projects should be encouraged to use free (and open source) modelling platforms like programming languages or the Open Systems Pharmacology suite to save taxpayer money and to increase model transparency, accessibility and (re)usability.

2.2.2 Missing physiological processes in PBK models

The body is immensely complex, with a multitude of processes and structures interacting with one another. PBK models try to describe some of these complexities. Most models incorporate the overall internal structure of the body as well as processes, like various kinds of absorption, circulation, metabolism and excretion. Such PBK models are very helpful for describing the interactions between the body and many compounds. However, some compounds are affected by processes that are not well understood. Incorporating and standardizing the implementation of such processes could improve reliability and accuracy of PBK model predictions. Some processes that provide opportunities for PBK modelling are discussed here. These concern the effects of food on the oral absorption process, and of lymph transport on the internal exposure of a compound.

2.2.2.1 The effect of food on oral absorption

The effect of food on compound absorption is generally observed in drugs (327). For this reason, drug labels often state if the respective drug should be taken with a meal or not. However, the effect of food on compound absorption is not limited to drugs. For example, in the current thesis the effect of food on pesticide absorption was also encountered: in human oral exposure studies where the organophosphate pesticide chlorpyrifos was dosed with food, the pesticide was absorbed to a much higher extend (6-fold) compared to exposure studies without food (see **chapter 2**). If a compound is ingested without any food, its absorption relies mainly on how fast it can reach the small intestine and how well it can dissolve in the small intestinal water. Such scenarios can be modelled fairly well by incorporating physiological processes like gastric emptying and intestinal transit, as well as kinetic processes like dissolution intestinal lumen and permeation across the intestinal wall (328–331). However, incorporation of mechanistic models in PBK models for predicting food effects are currently in their infancy. A major mechanism by which food alters the absorption profile of a compound is due to changes in solubility due to bile release (327).

Fatty- and amino-acids present in food can trigger bile release in the small intestine (332). Bile consists of bile acids and various enzymes. Among these enzymes are lipases, which break down triglycerides into fatty acids. Bile acids and fatty acids are able to form micelles, which improve the solubility (333,334) and mucus layer penetration (335) of poorly soluble or lipophilic compounds. Next, bile acids on the surface of the micelles can likely interact with (proteins on) the membrane of intestinal endothelium cells (mainly enterocytes), improving their uptake (336).

Complete mechanistic in silico modelling of bile release or its effects on absorption is currently not possible. However, combinations of in vitro and in silico methods can improve predictions of food effects. For example, solubility differences in fasted and fed state intestinal fluids can be estimated with in vitro fasted and fed state simulated intestinal fluids (FaSSIF and FeSSIF) solubility studies (337). Alternatively, in vitro digestion combined with caco-2 permeability assays can be used to estimate food effects on absorption as well (338). In vitro derived solubilities and permeabilities specific for fasted or fed states can be used in PBK models to investigate food effects on absorption. While this approach has been slowly developed over the years, it is not yet widely adopted for PBK

models. Since many chemicals we are exposed to reside in our food, it is essential to investigate the effect food has on absorption of compounds in chemical risk assessment. Implementing in vitro intestinal fluid solubility and digestion methods, or developing new mechanistic in silico models will allow PBK models to better predict food effects and increase PBK accuracy for risk assessment.

2.2.2.2 The effect of lymph transport on internal exposure

Many orally absorbed compounds are immediately transported through the portal vein to the liver. Most of these compounds can therefore be metabolized before reaching the rest of the body. However, fats and some lipophilic compounds diffuse poorly into blood. To prevent accumulation in the intestinal tissue, fats and some lipophilic compounds are released into intestinal lymph as lipoprotein particles called chylomicrons (339,340). As opposed to blood flowing from the intestinal tissues directly to the liver (where metabolism might occur), lymph does not flow directly to the liver, but joins the vascular system near the heart. Compounds and chylomicrons travelling via lymph therefore evade the liver and, once in the blood stream, can distribute throughout the whole body. Compounds that associate with chylomicrons or travel through intestinal lymph after absorption evade initial metabolism in the liver, increasing internal exposure (341).

Since lymphatic transport can change internal exposure to a compound (341,342), it is of interest for chemical risk assessment to predict if a compound indeed travels through lymph, and if so, to model this lymphatic transport. Attempts have been made to predict lymphatic transport based on molecular properties (343,344). While these attempts were reasonably successful, the parameters used for prediction of lymphatic transport of a compound are not readily available. Alternatively, lymphatic transport can be predicted based on chylomicron association, measured in vitro using plasma or chylomicrons isolated from blood (345,346). Such experiments might be more reliable and accessible. However, for all mentioned lymphatic transport prediction studies goes that in vivo validation data is very limited. A similar problem plagues further incorporation of lymphatic transport in PBK models, which is limited by intestinal lymph flow data availability and uncertainty. While there are some studies reporting tissue specific lymph flow rates, associated data on age, sex, body weight, fasted/fed state and meal composition, are often lacking or limited. Especially for the intestine, both lymphatic and blood flow rates can change based on fed/fasted state and meal composition (347,348). With the availability of more high quality intestinal lymph flow data and in vivo validation data, the effect of lymphatic transport on internal exposure can be more reliably modelled in PBK models.

2.2.3 Physiological detail in PBK modelling

Due to their modular nature, PBK models could theoretically include most physiological complexities of the body. While this is impossible in reality due to knowledge and computational limitations, it is also important to strike a balance between model simplicity and functional effectivity. For different substances different physiological detail might be needed. Chemical substances usually require the least physiological detail. Most PBK models for small molecules describe tissues as single (homogenous) compartments, while for particulate substances tissues are described by multiple subcompartments. PBK models often describe tissues as single, homogenous compartments. In reality, tissues are vastly more complex, containing multiple subcompartments divided by membranes and cells. Generally, tissues can be subdivided into the vascular space, interstitial space and the (intra)cellular space (with further subcompartments for cell organelles).

2.2.3.1 Vascular space

The vascular space, consisting of the blood present in the tissue, is separated from the interstitial space by the vascular endothelium. The vascular endothelium functions as a size filter, based on what type of vasculature is present in the tissue. Most tissues have either continuous of fenestrated vasculature (349), which contain small pores between the endothelial cells. The liver has a discontinuous or sinusoid vasculature (349), containing larger holes, and spleen capillaries are open ended (350), enabling even red blood cells to leave the capillaries. Depending on the type of vasculature present in a tissue, different sizes of particles can leave the blood and enter the interstitial space.

The size filter functionality of the vascular endothelium is of importance for modelling the passive distribution of exogenous particles and endogenous (lipoprotein) particles. For example, as part of lipid metabolism (351), most classes and sizes of lipoprotein particles are only able to leave the vasculature in the liver and spleen (190,352,353), since the pores in the vasculature of other tissues are too small to fit through (349,354). Chylomicrons, being the largest of lipoproteins by far (354), can only leave the vasculature in the liver once they released their lipid content (355) and became smaller chylomicron remnant particles. This way, (lipoprotein) particles are directed to the spleen and the liver. Similar trends are also seen for exogenous particles, where particles smaller than the capillary diameter ended up in the liver and spleen (and particles larger than the capillary diameter get stuck in lung capillaries) (356,357). The size filter functionality of the vascular endothelium makes separate modelling of the tissue vascular compartment essential for distribution modelling of exogenous particles as well as chemical substances that strongly associate with lipoprotein particles. Contrary to particulate substances, vascular space does not need to be modelled for small molecules, which easily fit through pores in the vascular endothelium to reach the interstitial space.

2.2.3.2 Interstitial and cellular spaces

The interstitial space is separates the vascular space and the (non-vascular) cells of the tissue. It is separated from the intracellular space by the phospholipid bilayer of the cell membrane. Due to the lipophilic core of the phospholipid bilayer, only neutral, relatively apolar molecules can diffuse across the cell membrane. On the other hand, charged or very polar (hydrophilic) compounds cannot passively diffuse through the phospholipid bilayer and require the help of channel or transporter proteins to gain entry into the cellular space. Therefore, the membrane functions as a charge/polarity filter. For most drugs and compounds, the molecular targets reside inside a cell. This makes it important to model separate interstitial and cellular spaces for charged and highly polar substances, especially if a compound is known to be actively transported.

Due to the complexities of predicting specific compound-protein interactions, it is currently not possible to mechanistically predict if a compound is a transporter substrate, aside from using computationally expensive molecular dynamics approaches. However, rules of thumb can be used to make an educated guess. For example, many glucuronic acid, sulfonic acid and glutathione conjugates are known to be actively transported (358–360). Alternatively, to get an idea of if a compound could be a transporter substrate, it might help to compare it to it's endogenous substrate, in terms of (geometric, 3D) structure, chemical properties and localization in the cell. Endogenous substrates are known for the more well known transporters. For example, P-glycoprotein transports compounds associated with the (core of the) cell membrane, like phospholipids, oxidized lipids and

steroids (361–364). Breast cancer resistance protein and multidrug transporters transport amphiphilic compounds associated with the surface part of the cell membrane (365,366). Organic cation and anion transporters transport mostly soluble polar or charged compounds, with preferences for specific moieties (367–369). While comparing compound properties, structure and cell location with endogenous substrates does not provide quantitative data that can be used in a PBK model, it could help by narrowing down what transporters should be investigated in silico and in vitro methods.

2.2.4 PBK model parameters

2.2.4.1 Physiological growth and variation

In PBK models, the body is described by physiological parameters, which generally consist of tissue/organ volumes and blood flows for an average adult individual (human, or any other animal). Since the larger part of a population usually consists of adults, PBK models for average adult individuals work quite well for predicting and investigating toxico- and pharmacokinetic profiles. However, such models will not suffice when investigating lifelong exposures, for example in case of chronic exposure to persistent pollutants or medication usage. Furthermore, determining how safe the most sensitive individuals are is important in chemical risk assessments. In such cases, modelling an average adult individual will not be sufficient either. In these cases it is important to incorporate body growth and variation in a population in PBK models.

When modelling lifelong exposure scenarios, physical growth and changes in tissue/organ sizes are often scaled based on age (370,371). However, the use of age for internal growth, does not exclude confounding factors like ethnicity, cultural and environmental influences. In contrast, when predicting tissue/organ growth based on body weight, there seems to be no statistical differences for individuals of different ethnicity (372). Theoretically, body weight seems to be a better predictor of internal growth, since it relates internal tissue/organ growth to external growth and seemingly excludes external confounding factors to a bigger extend. Therefore, internal growth could likely be more accurately modelled by incorporating an age based growth model for external growth (body weight), while internal growth is modelled based on body weight.

In population models, body weight, cardiac output and tissue/organ volumes and blood flows are often generated independently from one another using Monte-Carlo sampling (265,370,371). For organ volumes, this is fine if they are expressed in the model as a percentage of body weight, since bigger bodies will result in bigger organs proportional to the whole body size. However, if absolute organ weights are used, unreasonably large or small organs can be generated for a specific body weight, since body weight and tissue/organ weights are often generated independently in population models. On the other hand, tissue/organ blood flows are often modelled based on a percentage of the cardiac output, while the cardiac output in itself is based on the body weight or height (371). When the physiological parameters are generated for a virtual population, the cardiac output and tissue blood flows are generated independently. Consequently, the generated tissue volume can be on the large side, while the randomly generated tissue blood flow can be on the low side. This creates unrealistic extremes in the populations, wherein overlapping uncertainties/variations are stacked (370). Therefore, it would be more useful to generate organ blood flows based on the size of the organ instead of the cardiac output. Besides enabling the generation of more realistic populations, this also allows for more flexibility in modelling non-standard or patient populations.

For example, a kidney donor can be modelled more easily with one kidney, when the blood flow depends on the total kidney size, instead of the need to adjust the fraction of cardiac output for all tissues. Furthermore, during growth, relative tissue/organ sizes change and their specific blood flows should reflect those changes in size (370). To generate realistic populations, tissue/organ sizes and blood flows should therefore be related to body weight and tissue/organ size, respectively.

2.2.4.2 Reliability of in vitro derived kinetic parameters

In vitro models can be used to derive kinetic parameters describing absorption, distribution or metabolism. Such models capture many of the in vivo complexities of the cellular microenvironment. For example, when determining absorption or metabolic parameters in (caco-2, hepatocyte) cell models, active transport in and out of the cell as well as (non)specific binding to cell proteins and membranes are included. On the other hand, while many of the in vitro models do contain most important enzymes, the expression of these proteins is often different from the in vivo situation (373,374). The use of some types of stem cell models could bring improvements in these aspects, but easy and high throughput application of these models is not yet possible. While in vitro models represent the in vivo situation quite well, this can also become a problem, since different kinetic reactions cannot always be separated. For example, during permeability measurements using a barrier of intestinal cells, these cells could also metabolize the compound of interest. Or when measuring metabolism in hepatocytes, active transport of the compound of interest out of the cell could influence concentration dependent metabolic parameters. Alternatively, chemical interactions can also alter the perceived measurement. For example, a compound could evaporate, or bind to the plastic of the container used for the experiment (wells plates, Eppendorf, etc.) (375,376). The reliability of in vitro methods can therefore be affected due to biochemical and chemical interactions altering the concentration that is available to undergo the intended process.

The effects of nonspecific binding, metabolism and evaporation can be accounted for to determine the actual concentration available for interaction with the process of interest. For example, a mass balance can be used to check how much of a compound is associated with various components or compartments in the in vitro (cell) model. In case of a transwell plate, concentrations can be measured in apical and basolateral medium, compound can be extracted from the cell layer and the plastic in the well plate. In case of a compound that is rapidly metabolized, the metabolites can also be measured in all these compartments. Knowing how much of a compound is metabolized, or associated with plastics or cells, allows correction of the assumed average (nominal) concentration of the whole system to the real (actual) concentration available for interaction with the process of interest. Alternative to the mass balance approach, chemical distribution models for in vitro systems can be used to estimate evaporation, as well as plastic, protein and membrane binding (377). These in silico models also enable prediction of the concentration available to interact with the process of interest. The use of either mass balance and chemical distribution models for in vitro experiments can account for the effect of evaporation and binding to secondary model components, improving reliability of the measured endpoints in in vitro models.

2.2.4.3 In silico prediction of kinetic parameters

Three types of in silico methods can be used to predict kinetic parameters: molecular dynamics, mechanistic algorithms and regression based quantitative property structure relationships (QSPRs). Molecular dynamics can be used to predict some parameters based on quantum mechanical

parameters and interactions. Currently some kinetic parameters, like membrane permeability (378), can be predicted based on molecular dynamic simulations. Potentially such approaches could be used in the future to predict movement of compounds through cytochrome P450 substrate access tunnels (379,380) to predict clearance rates. However, such simulations require immense computing power, limiting the use of molecular dynamics simulations to those with access to powerful computers as well as limiting its use for high throughput predictions. Next, mechanistic algorithms predict kinetic parameters based on readily available chemical properties. Currently, these methods are used to predict the distribution between blood/plasma and tissues (75,115,118,381), however mechanistic algorithms are not available for predicting many other kinetic parameters. Lastly, QSPRs are widely available for many kinetic parameters. However, since these models are essentially regression models, they rely heavily on in vitro or in vivo data. This data potentially has the same uncertainties and problems as were discussed in the previous section. Furthermore, since regression based models are not mechanistic, it can be uncertain if the compound of interest fits within the chemical domain of the QSPR. While QSPRs are easy to use and available for predicting many types of kinetic parameters, the requirement of large amounts of in vivo or in vitro data for QSPR development as well as the uncertainty of its output should steer towards other methods. Therefore, future efforts should focus on developing mechanistic algorithms and/or lowering the required computational power for running molecular dynamics simulations.

2.2.5 Model validation

Physiologically based kinetic models need to be validated with in vivo toxico- or pharmacokinetic data. It is preferred to use human data when available, however this is often not the case. Animal data can be used if human data is not available, however a verifying PBK model for that animal needs to be made as well. This not only beats the purpose of using PBK modelling for animal free risk assessment, but could also still lead to missing processes due to differences in physiology between humans and test animals. However, when a compound is still in development or used to kill, like pesticides, it is not ethical to test such compounds in humans. Microdosing studies could be a solution to this problem. Improvements in analytical techniques, like mass spectrometry, spectroscopy and PET imaging (for radiolabeled test compounds) significantly increased analytical sensitivity, enabling human testing with very low doses (382). Such approaches cannot be used for any compound though. In vitro carcinogenicity and mutagenicity tests should be negative for the compound of interest and main metabolites. Furthermore, the molecular initiation event (and related affinity) should be known for the compound of interest and toxic metabolites in order to estimate safe doses. A significant safety margin should be in place between the lowest expected effect dose and the actual dose applied to volunteers. Furthermore, internal concentrations should still be measurable and allow for different dose levels to be tested. Further requirements and guidelines for microdosing studies are published by the ICH (383), supporting animal free, human centric dosing studies for chemical risk assessment.

2.2.6 Future application of PBK models

In the current day and age, PBK modelling is already very useful, but held back by limitations in mechanistic modelling of some physiological processes and structures, parameterization and validation. With advances in knowledge and data acquisition these limitations can be overcome, enabling the use of PBK models for virtual humans. In chemical risk assessment, PBK models can be expanded by further incorporating systems toxicology/pharmacology approaches, like

quantitative adverse outcome pathway (qAOP) modelling, which would enable predictions of chronic and mixture effects. To get there, reliance on regression and estimation methods introducing high uncertainties should be phased out, and more mechanistic approaches need be developed and made accessible.

2.3 Thoughts on adoption of animal free risk assessment

Transitioning to animal free methods in chemical risk assessment is currently progressing at a steady, but slow pace. This seems to be partially related to the reliability of, and regulatory trust in new approach methodologies (NAMs). To speed up adoption and increase trust in NAMs, companies should be encouraged or required to deliver side by side animal and animal-free risk assessment for (re)registration of their compounds. A few properly designed animal studies can provide a large amount of data to compare with results of various NAMs at the same time. This gives the opportunity to improve and validate NAMs, increase knowledge and expertise at companies and regulatory institutions about these methods and potentially increase trust in using these methods for risk assessment. Data produced at companies will likely be highly reliable and give a better understanding on the variability and reproducibility of these methods due to strictly adhered GLP standards. Governmental institutions could meet those companies in the middle with subsidies for those companies to perform side by side animal- and NAM-based risk assessment, and with increased subsidies if the (anonymized) data and NAM experience is shared publicly with governmental and academic researchers. In turn academic researchers could focus more on improving existing NAMs or developing new ones, looking more into molecular mechanisms of these systems and how they can be used optimally. The downside will be that companies likely don't want to perform more tests than needed, since each extra test performed could reveal some kind of toxicity, potentially falsely at that. Therefore this approach could focus on preclinical experiments, since if at this stage the extra data shows a new toxicity mechanism, it will likely be cheaper for companies to find out where this toxicity arises from than to find out later in human trials or when full production is being set up.

2.4 Conclusion

For animal welfare, saving chemical development time, or for plain scientific accuracy; in the last few decades the fields of toxicology and chemical risk assessment have expressed a large sentiment for replacement of animal testing in human risk assessment. Such an endeavor requires thorough mechanistic understanding of complex chemical and physiological systems. While there are still opportunities for improvement, the combination of PBK modelling with in vitro experiments is already able to take many of such complexities into account. In this thesis, such in silico and in vitro approaches were combined to predict in vivo organophosphate pesticide toxicity. While more trust and knowledge in such methods needs to be build in the coming years, the findings reported here show the applicability of animal-free methods in next generation safety assessment.

References

1. Ritchie H, Rodés-Guirao L, Mathieu E, Gerber M, Ortiz-Ospina E, Hasell J, et al. Population Growth. Our World in Data [Internet]. 2023 Jul 11 [cited 2025 Aug 5]. Available from: https://ourworldindata.org/population-growth

2. Epstein L. Fifty Years Since Silent Spring. Annual Review of Phytopathology. 2014 Aug 4;52(Volume 52, 2014):377–402. doi:10.1146/annurev-phyto-102313-045900

3. Zhang W. Global pesticide use: Profile, trend, cost / benefit and more. Proceedings of the International Academy of Ecology and Environmental Sciences. 2018 Mar;8(1):1–27.

4. Casida JE, Quistad GB. Golden Age of Insecticide Research: Past, Present, or Future? Annual Review of Entomology. 1998 Jan 1;43(Volume 43, 1998):1–16. doi:10.1146/annurev.ento.43.1.1

5. Balali-Mood B. Chemistry and Classification of OP Compounds. In: Balali-Mood M, Abdollahi M, editors. Basic and Clinical Toxicology of Organophosphorus Compounds [Internet]. London: Springer; 2014 [cited 2025 Jul 22]. p. 1–23. Available from: https://doi.org/10.1007/978-1-4471-5625-3_1 doi:10.1007/978-1-4471-5625-3_1

6. Cao Y, Herrero-Nogareda L, Cedergreen N. A comparative study of acetylcholinesterase and general-esterase activity assays using different substrates, *in vitro* and *in vivo* exposures and model organisms. Ecotoxicology and Environmental Safety. 2020 Feb 1;189:109954. doi:10.1016/j.ecoenv.2019.109954

7. Chuiko GM, Podgornaya VA, Zhelnin YY. Acetylcholinesterase and butyrylcholinesterase activities in brain and plasma of freshwater teleosts: cross-species and cross-family differences. Comparative Biochemistry and Physiology Part B: Biochemistry and Molecular Biology. 2003 May 1;135(1):55–61. doi:10.1016/S1096-4959(03)00048-4

8. Fildes K, Szabo JK, Hooper MJ, Buttemer WA, Astheimer LB. Plasma Cholinesterase characteristics in native Australian birds: significance for monitoring avian species for pesticide exposure. Emu - Austral Ornithology. 2009 Mar 1;109(1):41–7. doi:10.1071/MU08027

9. Jbilo O, Bartels CF, Chatonnet A, Toutant JP, Lockridge O. Tissue distribution of human acetylcholinesterase and butyrylcholinesterase messenger RNA. Toxicon. 1994 Nov 1;32(11):1445–57. doi:10.1016/0041-0101(94)90416-2

10. Li B, Stribley JA, Ticu A, Xie W, Schopfer LM, Hammond P, et al. Abundant Tissue Butyrylcholinesterase and Its Possible Function in the Acetylcholinesterase Knockout Mouse. Journal of Neurochemistry. 2000;75(3):1320–31. doi:10.1046/j.1471-4159.2000.751320.x

11. Ord MG, Thompson RHS. The distribution of cholinesterase types in mammalian tissues. Biochem J. 1950 Mar;46(3):346–52. doi:10.1042/bj0460346 PubMed PMID: 16748688; PubMed Central PMCID: PMC1275143.

12. Kasteel EEJ, Nijmeijer SM, Darney K, Lautz LS, Dorne JLCM, Kramer NI, et al. Acetylcholinesterase inhibition in electric eel and human donor blood: an in vitro approach to investigate interspecies differences and human variability in toxicodynamics. Arch Toxicol. 2020;94(12):4055–65. doi:10.1007/s00204-020-02927-8 PubMed PMID: 33037899; PubMed Central PMCID: PMC7655571.

13. Fukuto TR. Mechanism of action of organophosphorus and carbamate insecticides. Environ Health Perspect. 1990 Jul;87:245–54. doi:https://doi.org/10.1289%2Fehp.9087245 PubMed PMID: 2176588; PubMed Central PMCID: PMC1567830.

14. Sultatos LG. Mammalian toxicology of organophosphorus pesticides. Journal of Toxicology and Environmental Health. 1994 Nov 1;43(3):271–89. doi:10.1080/15287399409531921 PubMed PMID: 7966438.

15. Carr RL, Chambers JE. Kinetic Analysis of the in Vitro Inhibition, Aging, and Reactivation of Brain Acetylcholinesterase from Rat and Channel Catfish by Paraoxon and Chlorpyrifos-oxon. Toxicology and Applied Pharmacology. 1996 Aug 1;139(2):365–73. doi:10.1006/taap.1996.0177

16. Matsubara T, Horikoshi I. Spontaneous Reactivation of Mouse Plasma Cholinesterase After Inhibition by Various Organophosphorus Compounds. Journal of Pharmacobio-Dynamics. 1984;7(5):322–8. doi:10.1248/bpb1978.7.322

17. Gao M, Ni Z, Li G, Wu G, Huang B. Study on Spontaneous Reactivation and Aging of Acetylcholinesterase Inhibited by Paraoxon and Malaoxon in Ten Species. International Journal of Molecular Sciences. 2023 Jan;24(18):18. doi:10.3390/ijms241814213

18. Tang X, Zhu L, Chen J, Hu J, Zhang Q, Wang W. Reaction pathway for reactivation and aging of paraoxon-inhibited-acetylcholinesterase: A QM/MM study. Computational and Theoretical Chemistry. 2014 May 1;1035:44–50. doi:10.1016/j.comptc.2014.02.018

19. Worek F, Eyer P, Szinicz L. Inhibition, reactivation and aging kinetics of cyclohexylmethylphosphonofluoridate-inhibited human cholinesterases. Arch Toxicol. 1998 Sep 1;72(9):580–7. doi:10.1007/s002040050546

20. Masson P, Fortier PL, Albaret C, Fromen MT, Bartels FC, Lockridge O. Aging of di-isopropyl-phosphorylated human butyrylcholinesterase. Biochemical Journal. 1997 Oct 15;327(2):601–7. doi:10.1042/bj3270601

21. Maxwell DM, Brecht KM. Carboxylesterase: specificity and spontaneous reactivation of an endogenous scavenger for organophosphorus compounds. Journal of Applied Toxicology. 2001;21(S1):S103–7. doi:10.1002/jat.833

22. Singh AK. QSAR for the Organophosphate-Induced Inhibition and ‚Aging‘ of the Enzyme Neuropathy Target Esterase (NTE). SAR and QSAR in Environmental Research. 2001 Jun 1;12(3):275–95. doi:10.1080/10629360108032917 PubMed PMID: 11696925.

23. Sogorb MA, González-González I, Pamies D, Vilanova E. An alternative *in vitro* method for detecting neuropathic compounds based on acetylcholinesterase inhibition and on inhibition and aging of neuropathy target esterase (NTE). Toxicology in Vitro. 2010 Apr 1;24(3):942–52. doi:10.1016/j.tiv.2010.01.008

24. Eddleston M, Szinicz L, Eyer P, Buckley N. Oximes in acute organophosphorus pesticide poisoning: a systematic review of clinical trials. QJM. 2002 May 1;95(5):275–83. doi:10.1093/qjmed/95.5.275

25. Kutty KM, Huang SN, Kean KT. Pseudocholinesterase in obesity: Hypercaloric diet induced changes in experimental obese mice. Experientia. 1981 Nov 1;37(11):1141–2. doi:10.1007/BF01989883

26. Chu MI, Fontaine P, Kutty KM, Murphy D, Redheendran R. Cholinesterase in serum and low density lipoprotein of hyperlipidemic patients. Clinica Chimica Acta. 1978 Apr 3;85(1):55–9. doi:10.1016/0009-8981(78)90100-6

27. Furtado-Alle L, Tureck LV, de Oliveira CS, Hortega JVM, Souza RLR. Butyrylcholinesterase and lipid metabolism: Possible dual role in metabolic disorders. Chemico-Biological Interactions. 2023 Sep 25;383:110680. doi:10.1016/j.cbi.2023.110680

28. Clitherow JW, Mitchard M, Harper NJ. The Possible Biological Function of Pseudo-cholinesterase. Nature. 1963 Sep;199(4897):1000–1. doi:10.1038/1991000a0

29. Šisková K, Bilka F, Adameová A, Balážová A, Mydla M, Pauliková I. Influence of lipid imbalance on butyrylcholinesterase activity and biotransformation efficiency [Internet]. 2012 Apr. doi:10.1691/ph.2012.1653

30. Li Y, Dinsdale D, Glynn P. Protein Domains, Catalytic Activity, and Subcellular Distribution of Neuropathy Target Esterase in Mammalian Cells *. Journal of Biological Chemistry. 2003 Mar 7;278(10):8820–5. doi:10.1074/jbc.M210743200 PubMed PMID: 12514188.

31. van Tienhoven M, Atkins J, Li Y, Glynn P. Human Neuropathy Target Esterase Catalyzes Hydrolysis of Membrane Lipids*. Journal of Biological Chemistry. 2002 Jun 7;277(23):20942–8. doi:10.1074/jbc.M200330200

32. Zaccheo O, Dinsdale D, Meacock PA, Glynn P. Neuropathy Target Esterase and Its Yeast Homologue Degrade Phosphatidylcholine to Glycerophosphocholine in Living Cells *. Journal of Biological Chemistry. 2004 Jun 4;279(23):24024–33. doi:10.1074/jbc.M400830200 PubMed PMID: 15044461.

33. Akassoglou K, Malester B, Xu J, Tessarollo L, Rosenbluth J, Chao MV. Brain-specific deletion of neuropathy target esterase/swisscheese results in neurodegeneration. Proceedings of the National Academy of Sciences. 2004 Apr 6;101(14):5075–80. doi:10.1073/pnas.0401030101

34. Basit A, Fan PW, Khojasteh SC, Murray BP, Smith BJ, Heyward S, et al. Comparison of Tissue Abundance of Non-Cytochrome P450 Drug-Metabolizing Enzymes by Quantitative Proteomics between Humans and Laboratory Animal Species. Drug Metab Dispos. 2022 Mar 1;50(3):197–203. doi:10.1124/dmd.121.000774 PubMed PMID: 34969659.

35. Li B, Sedlacek M, Manoharan I, Boopathy R, Duysen EG, Masson P, et al. Butyrylcholinesterase, paraoxonase, and albumin esterase, but not carboxylesterase, are present in human plasma. Biochemical Pharmacology. 2005 Nov 25;70(11):1673–84. doi:10.1016/j.bcp.2005.09.002

36. Rudakova EV, Boltneva NP, Makhaeva GF. Comparative Analysis of Esterase Activities of Human, Mouse, and Rat Blood. Bull Exp Biol Med. 2011 Nov 1;152(1):73–5. doi:10.1007/s10517-011-1457-y

37. Chanda SM, Mortensen SR, Moser VC, Padilla S. Tissue-Specific Effects of Chlorpyrifos on Carboxylesterase and Cholinesterase Activity in Adult Rats: An in Vitro and in Vivo Comparison. Fundamental and Applied Toxicology. 1997 Aug 1;38(2):148–57. doi:10.1006/faat.1997.2329

38. Ecobichon DJ, Zelt D. The acute toxicity of fenitrothion in weanling rats and effects on tissue esterases and mono-oxygenases. Toxicology. 1979 Jan 1;13:287–96. doi:10.1016/S0300-483X(79)80032-3

39. Wang D, Kamijima M, Okamura A, Ito Y, Yanagiba Y, Jia X fang, et al. Evidence for diazinon-mediated inhibition of cis-permethrin metabolism and its effects on reproductive toxicity in adult male mice. Reproductive Toxicology. 2012 Dec 1;34(4):489–97. doi:10.1016/j.reprotox.2012.07.007

40. Crow JA, Middleton BL, Borazjani A, Hatfield MJ, Potter PM, Ross MK. Inhibition of carboxylesterase 1 is associated with cholesteryl ester retention in human THP-1 monocyte/macrophages. Biochimica et Biophysica Acta (BBA) - Molecular and Cell Biology of Lipids. 2008 Oct 1;1781(10):643–54. doi:10.1016/j.bbalip.2008.07.005

41. Hayden KM, Norton MC, Darcey D, Østbye T, Zandi PP, Breitner JCS, et al. Occupational exposure to pesticides increases the risk of incident AD. Neurology. 2010 May 11;74(19):1524–30. doi:10.1212/WNL.0b013e3181dd4423

42. Dhillon AS, Tarbutton GL, Levin JL, Plotkin GM, Lowry LK, Nalbone JT, et al. Pesticide/Environmental Exposures and Parkinson's Disease in East Texas. Journal of Agromedicine. 2008 Jun 27;13(1):37–48. doi:10.1080/10599240801986215 PubMed PMID: 19042691.

43. Gatto NM, Cockburn M, Bronstein J, Manthripragada AD, Ritz B. Well-Water Consumption and Parkinson's Disease in Rural California. Environmental Health Perspectives. 2009 Dec;117(12):1912–8. doi:10.1289/ehp.0900852

44. Manthripragada AD, Costello S, Cockburn MG, Bronstein JM, Ritz B. Paraoxonase 1, Agricultural Organophosphate Exposure, and Parkinson Disease. Epidemiology. 2010 Jan;21(1):87. doi:10.1097/EDE.0b013e3181c15ec6

45. Narayan S, Liew Z, Paul K, Lee PC, Sinsheimer JS, Bronstein JM, et al. Household organophosphorus pesticide use and Parkinson's disease. International Journal of Epidemiology. 2013 Oct 1;42(5):1476–85. doi:10.1093/ije/dyt170

46. Paul KC, Sinsheimer JS, Cockburn M, Bronstein JM, Bordelon Y, Ritz B. Organophosphate pesticides and *PON1* L55M in Parkinson's disease progression. Environment International. 2017 Oct 1;107:75–81. doi:10.1016/j.envint.2017.06.018

47. Aardema H, Meertens JHJM, Ligtenberg JJM, Peters-Polman OM, Tulleken JE, Zijlstra JG. Organophosphorus pesticide poisoning: cases and developments. Neth J Med. 2008 Apr;66(4):149–53. PubMed PMID: 18424861.

48. Aygun D. Diagnosis in an acute organophosphate poisoning: report of three interesting cases and review of the literature. European Journal of Emergency Medicine. 2004 Feb;11(1):55.

49. Lee P, Tai DYH. Clinical features of patients with acute organophosphate poisoning requiring intensive care. Intensive Care Med. 2001 Apr 1;27(4):694–9. doi:10.1007/s001340100895

50. Baker D, Sedgwick EM. Single fibre electromyographic changes in man after organophosphate exposure. Hum Exp Toxicol. 1996 May 1;15(5):369–75. doi:10.1177/096032719601500501

51. Bleecker JD, Den Neucker KV, Colardyn F. Intermediate syndrome in organophosphorus poisoning: A prospective study. Critical Care Medicine. 1993 Nov;21(11):1706.

52. Dandapani M, Zachariah A, Kavitha MR, Jeyaseelan L, Oommen A. Oxidative damage in intermediate syndrome of acute organophosphorous poisoning. [Internet]. 2003 [cited 2025 Jul 21]. Available from: http://imsear.searo.who.int/handle/123456789/23617

53. John M, Oommen A, Zachariah A. Muscle Injury in Organophosphorous Poisoning and Its Role in the Development of Intermediate Syndrome. NeuroToxicology. 2003 Jan 1;24(1):43–53. doi:10.1016/S0161-813X(02)00111-0

54. Khan S, Hemalatha R, Jeyaseelan L, Oommen A, Zachariah A. Neuroparalysis and oxime efficacy in organophosphate poisoning: a study of butyryicholinesterase. Hum Exp Toxicol. 2001 Apr 1;20(4):169–74. doi:10.1191/096032701678766796

55. Lotti M, Moretto A. Organophosphate-Induced Delayed Polyneuropathy. Toxicol Rev. 2005 Mar 1;24(1):37–49. doi:10.2165/00139709-200524010-00003

56. Chuang CC, Lin TS, Tsai MC. Delayed Neuropathy and Myelopathy after Organophosphate Intoxication. New England Journal of Medicine. 2002 Oct 3;347(14):1119–21. doi:10.1056/NEJM200210033471421

57. Jędrzejowska H, Rowińska-Marcińska K, Hoppe B. Neuropathy due to phytosol (Agritox). Acta Neuropathol. 1980 Jan 1;49(2):163–8. doi:10.1007/BF00690757

58. Johnson MK. Organophosphates and delayed neuropathy—Is NTE alive and well? Toxicology and Applied Pharmacology. 1990 Mar 1;102(3):385–99. doi:10.1016/0041-008X(90)90036-T

59. Lotti M, Moretto A, Capodicasa E, Bertolazzi M, Peraica M, Scapellato ML. Interactions between Neuropathy Target Esterase and Its Inhibitors and the Development of Polyneuropathy. Toxicology and Applied Pharmacology. 1993 Oct 1;122(2):165–71. doi:10.1006/taap.1993.1184

60. McConnell R, Delgado-Téllez E, Cuadra R, Tórres E, Keifer M, Almendárez J, et al. Organophosphate neuropathy due to methamidophos: biochemical and neurophysiological markers. Arch Toxicol. 1999 Aug 1;73(6):296–300. doi:10.1007/s002040050621

61. Sarin S, Gill KD. Biochemical Characterization of Dichlorvos-Induced Delayed Neurotoxicity in Rat. IUBMB Life. 2000;49(2):125–30. doi:10.1080/15216540050022449

62. Senanayake N, Johnson MK. Acute Polyneuropathy after Poisoning by a New Organophosphate Insecticide. New England Journal of Medicine. 1982 Jan 21;306(3):155–7. doi:10.1056/NEJM198201213060306

63. Sevim S, Aktekin M, Dogu O, Ozturk H, Ertas M. Late Onset Polyneuropathy due to Organophosphate (DDVP) Intoxication. Canadian Journal of Neurological Sciences. 2003 Feb;30(1):75–8. doi:10.1017/S0317167100002493

64. Susser M, Stein Z. An Outbreak of Tri-ortho-cresyl Phosphate (T.O.C.P.) Poisoning in Durban. Br J Ind Med. 1957 Apr;14(2):111–20. doi:10.1136/oem.14.2.111 PubMed PMID: 13426434; PubMed Central PMCID: PMC1037779.

65. Vasilescu C, Alexianu M, Dan A. Delayed neuropathy after organophosphorus insecticide (Dipterex) poisoning: a clinical, electrophysiological and nerve biopsy study. Journal of Neurology, Neurosurgery & Psychiatry. 1984 May 1;47(5):543–8. doi:10.1136/jnnp.47.5.543 PubMed PMID: 6736986.

66. Muñoz-Quezada MT, Lucero BA, Iglesias VP, Muñoz MP, Cornejo CA, Achu E, et al. Chronic exposure to organophosphate (OP) pesticides and neuropsychological functioning in farm workers: a review. International

Journal of Occupational and Environmental Health. 2016 Jan 2;22(1):68–79. doi:10.1080/10773525.2015.1123848 PubMed PMID: 27128815.

67. Rohlman DS, Anger WK, Lein PJ. Correlating neurobehavioral performance with biomarkers of organophosphorous pesticide exposure. NeuroToxicology. 2011 Mar 1;32(2):268–76. doi:10.1016/j.neuro.2010.12.008

68. Rosenstock L, Keifer M, Daniell WE, McConnell R, Claypoole K. Chronic central nervous system effects of acute organophosphate pesticide intoxication. The Lancet. 1991 Jul 27;Originally published as Volume 2, Issue 8761338(8761):223–7. doi:10.1016/0140-6736(91)90356-T

69. Ross SM, McManus IC, Harrison V, Mason O. Neurobehavioral problems following low-level exposure to organophosphate pesticides: a systematic and meta-analytic review. Critical Reviews in Toxicology. 2013 Jan 1;43(1):21–44. doi:10.3109/10408444.2012.738645 PubMed PMID: 23163581.

70. Rothlein J, Rohlman D, Lasarev M, Phillips J, Muniz J, McCauley L. Organophosphate Pesticide Exposure and Neurobehavioral Performance in Agricultural and Nonagricultural Hispanic Workers. Environmental Health Perspectives. 2006 May;114(5):691–6. doi:10.1289/ehp.8182

71. Starks SE, Gerr F, Kamel F, Lynch CF, Jones MP, Alavanja MC, et al. Neurobehavioral function and organophosphate insecticide use among pesticide applicators in the Agricultural Health Study. Neurotoxicology and Teratology. 2012 Jan 1;34(1):168–76. doi:10.1016/j.ntt.2011.08.014

72. Carrasco Cabrera L, Di Piazza G, Dujardin B, Marchese E, Medina Pastor P, European Food Safety Agency (EFSA). The 2022 European Union report on pesticide residues in food. EFSA Journal. 2024;22(4):e8753. doi:10.2903/j.efsa.2024.8753

73. Jaga K, Dharmani C. Sources of exposure to and public health implications of organophosphate pesticides. Rev Panam Salud Publica. 2003 Sep;14(3):171–85. doi:10.1590/s1020-49892003000800004 PubMed PMID: 14653904.

74. Poulin P, Theil F. Prediction of Pharmacokinetics Prior to In Vivo Studies. 1. Mechanism-Based Prediction of Volume of Distribution. Journal of Pharmaceutical Sciences. 2002 Jan 1;91(1):129–56. doi:10.1002/jps.10005

75. Rodgers T, Rowland M. Physiologically based pharmacokinetic modelling 2: Predicting the tissue distribution of acids, very weak bases, neutrals and zwitterions. Journal of Pharmaceutical Sciences. 2006 Jun 1;95(6):1238–57. doi:10.1002/jps.20502

76. Buratti FM, Volpe MT, Meneguz A, Vittozzi L, Testai E. CYP-specific bioactivation of four organophosphorothioate pesticides by human liver microsomes. Toxicology and Applied Pharmacology. 2003 Feb 1;186(3):143–54. doi:10.1016/S0041-008X(02)00027-3

77. Ellison CA, Tian Y, Knaak JB, Kostyniak PJ, Olson JR. Human Hepatic Cytochrome P450-Specific Metabolism of the Organophosphorus Pesticides Methyl Parathion and Diazinon. Drug Metabolism and Disposition. 2012 Jan 1;40(1):1–5. doi:10.1124/dmd.111.042572

78. Foxenberg RJ, McGarrigle BP, Knaak JB, Kostyniak PJ, Olson JR. Human Hepatic Cytochrome P450-Specific Metabolism of Parathion and Chlorpyrifos. Drug Metabolism and Disposition. 2007 Feb 1;35(2):189–93. doi:10.1124/dmd.106.012427

79. Nallani G, Chandrasekaran A, Kassahun K, Shen L, Reiss R, Whatling P. Determination of enzymatic kinetics of metabolism of dimethoate and omethoate in rats and humans. Xenobiotica. 2023 Apr 3;53(4):279–87. doi:10.1080/00498254.2023.2228904 PubMed PMID: 37347282.

80. Poet TS, Wu H, Kousba AA, Timchalk C. In Vitro Rat Hepatic and Intestinal Metabolism of the Organophosphate Pesticides Chlorpyrifos and Diazinon. Toxicological Sciences. 2003 Apr 1;72(2):193–200. doi:10.1093/toxsci/kfg035

81. Vitarius JA, Sultatos LG. Kinetic mechanism of the detoxification of the organophosphate paraoxon by human serum A-esterase. Drug Metabolism and Disposition. 1994 May 1;22(3):472–8. doi:10.1016/S0090-9556(25)08400-4 PubMed PMID: 8070326.

82. Chambers JE. PON1 multitasks to protect health. Proceedings of the National Academy of Sciences. 2008 Sep 2;105(35):12639–40. doi:10.1073/pnas.0807062105

83. Costa LG, Li WF, Richter RJ, Shih DM, Lusis A, Furlong CE. The role of paraoxonase (PON1) in the detoxication of organophosphates and its human polymorphism. Chemico-Biological Interactions. 1999 May 14;119–120:429–38. doi:10.1016/S0009-2797(99)00055-1

84. Li WF, Costa LG, Richter RJ, Hagen T, Shih DM, Tward A, et al. Catalytic efficiency determines the in-vivo efficacy of PON1 for detoxifying organophosphorus compounds. Pharmacogenetics and Genomics. 2000 Dec;10(9):767.

85. Abel EL, Bammler TK, Eaton DL. Biotransformation of Methyl Parathion by Glutathione S-Transferases 1TKB and ELA contributed equally to this study.2Current address: Department of Molecular Carcinogenesis, MD Anderson Cancer Center, Smithville, TX 78957. Toxicological Sciences. 2004 Jun 1;79(2):224–32. doi:10.1093/toxsci/kfh118

86. Benke GM, Murphy SD. The influence of age on the toxicity and metabolism of methyl parathion and parathion in male and female rats. Toxicology and Applied Pharmacology. 1975 Feb 1;31(2):254–69. doi:10.1016/0041-008X(75)90161-1

87. Crawford MJ, Hutson DH, King PA. Metabolic Demethylation of the Insecticide Dimethyl-vinphos in Rats, in Dogs, and in vitro. Xenobiotica. 1976 Jan 1;6(12):745–62. doi:10.3109/00498257609151391

88. Fujioka K, Casida JE. Glutathione S-Transferase Conjugation of Organophosphorus Pesticides Yields S-Phospho-, S-Aryl-, and S-Alkylglutathione Derivatives. Chem Res Toxicol. 2007 Aug 1;20(8):1211–7. doi:10.1021/tx700133c

89. Fukami J ichi, Shishido T 1st. Nature of a Soluble, Glutathione-Dependent Enzyme System Active in Cleavage of Methyl Parathion to Desmethyl Parathion. Journal of Economic Entomology. 1966 Dec 1;59(6):1338–46. doi:10.1093/jee/59.6.1338

90. Fukunaga K, Fukami J ichi, Shishido T. The in vitro metabolism of organophosphorus insecticides by tissue homogenates from mammal and insect. In: Gunther FA, editor. Residues of Pesticides and Other Foreign Chemicals in Foods and Feeds / Rückstände von Pesticiden und anderen Fremdstoffen in Nahrungs- und Futtermitteln. New York, NY: Springer; 1969. p. 223–49. (Residue Reviews / Rückstands-Berichte). doi:10.1007/978-1-4615-8443-8_18

91. Hollingworth RM. Dealkylation of organophosphorus esters by mouse liver enzymes in vitro and invivo. J Agric Food Chem. 1969 Sep 1;17(5):987–96. doi:10.1021/jf60165a044

92. Hutson DH, Pickering BA, Donninger C. Phosphoric acid triester–glutathione alkyltransferase. A mechanism for the detoxification of dimethyl phosphate triesters. Biochemical Journal. 1972 Mar 1;127(1):285–93. doi:10.1042/bj1270285

93. Morello A, Vardanis A, Spencer EY. Differential glutathione-dependent detoxication of two geometrical vinyl organophosphorus (mevinphos) isomers. Biochemical and Biophysical Research Communications. 1967 Oct 16;29(2):241–5. doi:10.1016/0006-291X(67)90594-3

94. Nakatsugawa T, Tolman NM, Dahm PA. Degradation of parathion in the rat. Biochemical Pharmacology. 1969 May 1;18(5):1103–14. doi:10.1016/0006-2952(69)90114-2

95. Shishido T, Usui K, Sato M, Fukami J ichi. Enzymatic conjugation of diazinon with glutathione in rat and American cockroach. Pesticide Biochemistry and Physiology. 1972 Mar 1;2(1):51–63. doi:10.1016/0048-3575(72)90006-5

96. Stenersen J. Demethylation of the Insecticide Bromophos by a Glutathione-Dependent Liver Enzyme and by Alkaline Buffers1. Journal of Economic Entomology. 1969 Oct 1;62(5):1043–5. doi:10.1093/jee/62.5.1043

97. Yamamoto T, Egashira T, Yoshida T, Kuroiwa Y. Comparative Metabolism of Fenitrothion and Methylparathion in Male Rats. Acta Pharmacologica et Toxicologica. 1983;53(2):96–102. doi:10.1111/j.1600-0773.1983.tb01875.x

98. Filipsson AF, Sand S, Nilsson J, Victorin K. The Benchmark Dose Method—Review of Available Models, and Recommendations for Application in Health Risk Assessment. Critical Reviews in Toxicology. 2003 Jan 1;33(5):505–42. doi:10.1080/10408440390242360 PubMed PMID: 14594105.

99. Schroeder K, Bremm KD, Alépée N, Bessems JGM, Blaauboer B, Boehn SN, et al. Report from the EPAA workshop: *In vitro* ADME in safety testing used by EPAA industry sectors. Toxicology in Vitro. 2011 Apr 1;25(3):589–604. doi:10.1016/j.tiv.2010.12.005

100. Dourson ML, Felter SP, Robinson D. Evolution of Science-Based Uncertainty Factors in Noncancer Risk Assessment. Regulatory Toxicology and Pharmacology. 1996 Oct 1;24(2):108–20. doi:10.1006/rtph.1996.0116

101. Nair RS, Sherman JH, Stevens MW, Johannsen FR. Selecting a more realistic uncertainty factor: Reducing compounding effects of multiple uncertainties. Human and Ecological Risk Assessment: An International Journal. 1995 Dec 1;1(5):576–89. doi:10.1080/10807039509380048

102. Knight J, Hartung T, Rovida C. 4.2 million and counting… The animal toll for REACH systemic toxicity studies. ALTEX - Alternatives to animal experimentation. 2023 Jul 20;40(3):3. doi:10.14573/altex.2303201

103. Akhtar A. The Flaws and Human Harms of Animal Experimentation. Camb Q Healthc Ethics. 2015 Oct;24(4):407–19. doi:10.1017/S0963180115000079 PubMed PMID: 26364776; PubMed Central PMCID: PMC4594046.

104. Russell WMS, Burch RL. The Principles of Humane Experimental Technique. Methuen; 1959. 260 p.

105. Pallocca G, Moné MJ, Kamp H, Luijten M, Water B van de, Leist M. Next-generation risk assessment of chemicals – Rolling out a human-centric testing strategy to drive 3R implementation: The RISK-HUNT3R project perspective. ALTEX - Alternatives to animal experimentation. 2022 Jul 20;39(3):3. doi:10.14573/altex.2204051

106. Sewell F, Alexander-White C, Brescia S, Currie RA, Roberts R, Roper C, et al. New approach methodologies (NAMs): identifying and overcoming hurdles to accelerated adoption. Toxicol Res (Camb). 2024 Mar 25;13(2):tfae044. doi:10.1093/toxres/tfae044 PubMed PMID: 38533179; PubMed Central PMCID: PMC10964841.

107. US EPA. Next Generation Risk Assessment: Incorporation Of Recent Advances In Molecular, Computational, And Systems Biology (Final Report) [Reports & Assessments] [Internet]. 2014 [cited 2022 Dec 7]. Available from: https://cfpub.epa.gov/ncea/risk/recordisplay.cfm?deid=286690

108. Rietjens IMCM, Louisse J, Punt A. Tutorial on physiologically based kinetic modeling in molecular nutrition and food research. Molecular Nutrition & Food Research. 2011;55(6):941–56. doi:10.1002/mnfr.201000655

109. Jones H, Rowland-Yeo K. Basic Concepts in Physiologically Based Pharmacokinetic Modeling in Drug Discovery and Development. CPT: Pharmacometrics & Systems Pharmacology. 2013;2(8):63. doi:10.1038/psp.2013.41

110. Brown RP, Delp MD, Lindstedt SL, Rhomberg LR, Beliles RP. Physiological Parameter Values for Physiologically Based Pharmacokinetic Models. Toxicol Ind Health. 1997 Jul 1;13(4):407–84. doi:10.1177/074823379701300401

111. Hou TJ, Zhang W, Xia K, Qiao XB, Xu XJ. ADME Evaluation in Drug Discovery. 5. Correlation of Caco-2 Permeation with Simple Molecular Properties. J Chem Inf Comput Sci. 2004 Sep 1;44(5):1585–600. doi:10.1021/ci049884m

112. Punt A, Louisse J, Pinckaers N, Fabian E, van Ravenzwaay B. Predictive Performance of Next Generation Physiologically Based Kinetic (PBK) Model Predictions in Rats Based on In Vitro and In Silico Input Data. Toxicological Sciences. 2022 Mar 1;186(1):18–28. doi:10.1093/toxsci/kfab150

113. Sun D, Lennernas H, Welage LS, Barnett JL, Landowski CP, Foster D, et al. Comparison of Human Duodenum and Caco-2 Gene Expression Profiles for 12,000 Gene Sequences Tags and Correlation with Permeability of 26 Drugs. Pharm Res. 2002 Oct 1;19(10):1400–16. doi:10.1023/A:1020483911355

114. Yu LX, Amidon GL. A compartmental absorption and transit model for estimating oral drug absorption. International Journal of Pharmaceutics. 1999 Sep 20;186(2):119–25. doi:10.1016/S0378-5173(99)00147-7

115. Peyret T, Poulin P, Krishnan K. A unified algorithm for predicting partition coefficients for PBPK modeling of drugs and environmental chemicals. Toxicology and Applied Pharmacology. 2010 Dec 15;249(3):197–207. doi:10.1016/j.taap.2010.09.010

116. Rodgers T, Leahy D, Rowland M. Physiologically Based Pharmacokinetic Modeling 1: Predicting the Tissue Distribution of Moderate-to-Strong Bases. Journal of Pharmaceutical Sciences. 2005 Jun 1;94(6):1259–76. doi:10.1002/jps.20322

117. Ruark CD, Hack CE, Robinson PJ, Mahle DA, Gearhart JM. Predicting Passive and Active Tissue:Plasma Partition Coefficients: Interindividual and Interspecies Variability. Journal of Pharmaceutical Sciences. 2014 Jul 1;103(7):2189–98. doi:10.1002/jps.24011

118. Schmitt W. General approach for the calculation of tissue to plasma partition coefficients. Toxicology in Vitro. 2008 Mar 1;22(2):457–67. doi:10.1016/j.tiv.2007.09.010

119. Lobell M, Sivarajah V. In silico prediction of aqueous solubility, human plasma protein binding and volume of distribution of compounds from calculated pKa and AlogP98 values. Mol Divers. 2003 Mar 1;7(1):69–87. doi:10.1023/B:MODI.0000006562.93049.36

120. Uchimura T, Kato M, Saito T, Kinoshita H. Prediction of human blood-to-plasma drug concentration ratio. Biopharmaceutics & Drug Disposition. 2010;31(5–6):286–97. doi:10.1002/bdd.711

121. Volpe DA, Faustino PJ, Ciavarella AB, Asafu-Adjaye EB, Ellison CD, Yu LX, et al. Classification of Drug Permeability with a Caco-2 Cell Monolayer Assay. Clinical Research and Regulatory Affairs. 2007 Jan 1;24(1):39–47. doi:10.1080/10601330701273669

122. Zhu C, Jiang L, Chen TM, Hwang KK. A comparative study of artificial membrane permeability assay for high throughput profiling of drug absorption potential. European Journal of Medicinal Chemistry. 2002 May 1;37(5):399–407. doi:10.1016/S0223-5234(02)01360-0

123. Waters NJ, Jones R, Williams G, Sohal B. Validation of a Rapid Equilibrium Dialysis Approach for the Measurement of Plasma Protein Binding. Journal of Pharmaceutical Sciences. 2008 Oct 1;97(10):4586–95. doi:10.1002/jps.21317

124. Musteata FM, Pawliszyn J, Qian MG, Wu JT, Miwa GT. Determination of drug plasma protein binding by solid phase microextraction. Journal of Pharmaceutical Sciences. 2006 Aug 1;95(8):1712–22. doi:10.1002/jps.20558

125. Asha S, Vidyavathi M. Role of Human Liver Microsomes in In Vitro Metabolism of Drugs—A Review. Appl Biochem Biotechnol. 2010 Mar 1;160(6):1699–722. doi:10.1007/s12010-009-8689-6

126. Jia L, Liu X. The Conduct of Drug Metabolism Studies Considered Good Practice (II): In Vitro Experiments. Current Drug Metabolism. 2007 Dec 1;8(8):822–9. doi:10.2174/138920007782798207

127. Seibert E, Tracy TS. Fundamentals of Enzyme Kinetics. In: Nagar S, Argikar UA, Tweedie DJ, editors. Enzyme Kinetics in Drug Metabolism: Fundamentals and Applications [Internet]. Totowa, NJ: Humana Press; 2014 [cited 2023 May 23]. p. 9–22. (Methods in Molecular Biology). Available from: https://doi.org/10.1007/978-1-62703-758-7_2 doi:10.1007/978-1-62703-758-7_2

128. Lautz LS, Hendriks AJ, Dorne JLCM, Louisse J, Kramer NI. Establishing allometric relationships between microsomal protein and cytochrome P450 content with body weight in vertebrate species. Toxicology. 2023 Jan 12;153429. doi:10.1016/j.tox.2023.153429

129. Zimmer AA, Collier AC. Scaling factors to inform in vitro-in vivo extrapolation from preclinical and livestock animals: state of the field and recommendations for development of missing data. Drug Metabolism Reviews. 2025 Apr 3;57(2):91–114. doi:10.1080/03602532.2025.2462527 PubMed PMID: 39898873.

130. Meek EC, Reiss R, Crow JA, Chambers JE. Inhibition Kinetics of 16 Organophosphorus Pesticides or Their Active Metabolites on Erythrocyte Acetylcholinesterase From Humans and Rats. Toxicological Sciences. 2021 Oct 1;183(2):404–14. doi:10.1093/toxsci/kfab031

131. Timchalk C, Nolan RJ, Mendrala AL, Dittenber DA, Brzak KA, Mattsson JL. A Physiologically Based Pharmacokinetic and Pharmacodynamic (PBPK/PD) Model for the Organophosphate Insecticide Chlorpyrifos in Rats and Humans. Toxicological Sciences. 2002 Mar 1;66(1):34–53. doi:10.1093/toxsci/66.1.34

132. Bellman R, Jacquez JA, Kalaba R. Some mathematical aspects of chemotherapy: I. One-organ models. Bulletin of Mathematical Biophysics. 1960 Jun 1;22(2):181–98. doi:10.1007/BF02478005

133. WHO. Characterization and application of physiologically based pharmacokinetic models in risk assessment [Internet]. 2010 [cited 2024 Aug 22]. Available from: https://www.who.int/publications/i/item/9789241500906

134. Kamiloglu S, Sari G, Ozdal T, Capanoglu E. Guidelines for cell viability assays. Food Frontiers. 2020 Sep;1(3):332–49. doi:10.1002/fft2.44

135. Hajibabaie F, Abedpoor N, Mohamadynejad P. Types of Cell Death from a Molecular Perspective. Biology. 2023 Nov;12(11):1426. doi:10.3390/biology12111426

136. Nguyen N, Jennen D, Kleinjans J. Omics technologies to understand drug toxicity mechanisms. Drug Discovery Today. 2022 Nov 1;27(11):103348. doi:10.1016/j.drudis.2022.103348

137. van der Burg B, Winter R, Weimer M, Berckmans P, Suzuki G, Gijsbers L, et al. Optimization and prevalidation of the *in vitro* ERα CALUX method to test estrogenic and antiestrogenic activity of compounds. Reproductive Toxicology. 2010 Aug 1;ReProTect Special Issue30(1):73–80. doi:10.1016/j.reprotox.2010.04.007

138. Ellman GL, Courtney KD, Andres V, Featherstone RM. A new and rapid colorimetric determination of acetylcholinesterase activity. Biochemical Pharmacology. 1961 Jul 1;7(2):88–95. doi:10.1016/0006-2952(61)90145-9

139. Izadi H, Grundy JE, Bose R. Evaluation of the Benchmark Dose for Point of Departure Determination for a Variety of Chemical Classes in Applied Regulatory Settings. Risk Analysis. 2012;32(5):830–5. doi:10.1111/j.1539-6924.2011.01732.x

140. More SJ, Benford D, Bragard C, Halldorsson TI, Hernández-Jerez AF, Bennekou SH, et al. Guidance on the use of the benchmark dose approach in risk assessment. EFSA Journal. 2022;20(10):e07584. doi:10.2903/j.efsa.2022.7584

141. Becker RA, Friedman KP, Simon TW, Marty MS, Patlewicz G, Rowlands JC. An exposure:activity profiling method for interpreting high-throughput screening data for estrogenic activity—Proof of concept. Regulatory Toxicology and Pharmacology. 2015 Apr 1;71(3):398–408. doi:10.1016/j.yrtph.2015.01.008

142. Donley N. The USA lags behind other agricultural nations in banning harmful pesticides. Environmental Health. 2019 Jun 7;18(1):44. doi:10.1186/s12940-019-0488-0

143. Food and Agriculture Organization of the United Nations. Pesticides Use FAOSTAT. [Internet]. 2020 [cited 2022 Dec 12]. Available from: https://www.fao.org/faostat/en/#data/RP

144. Canbay HS, Ögüt S, Yilmazer M, Ünsal RS. Pesticide Residues Analysis in Human Milk Samples in Isparta Region (Turkey). Asian J Chem. 2013;25(7):3931–6. doi:10.14233/ajchem.2013.13849

145. Dalmolin SP, Dreon DB, Thiesen FV, Dallegrave E. Biomarkers of occupational exposure to pesticides: Systematic review of insecticides. Environmental Toxicology and Pharmacology. 2020 Apr 1;75:103304. doi:10.1016/j.etap.2019.103304

146. Katsikantami I, Colosio C, Alegakis A, Tzatzarakis MN, Vakonaki E, Rizos AK, et al. Estimation of daily intake and risk assessment of organophosphorus pesticides based on biomonitoring data – The internal exposure approach. Food and Chemical Toxicology. 2019 Jan 1;123:57–71. doi:10.1016/j.fct.2018.10.047

147. Kavvalakis MP, Tsatsakis AM. The atlas of dialkylphosphates; assessment of cumulative human organophosphorus pesticides' exposure. Forensic Science International. 2012 May 10;Proceedings of the Society of Hair Testing (SoHT) annual meeting in Chamonix (21-26 March 2011).218(1):111–22. doi:10.1016/j.forsciint.2011.10.019

148. Naksen W, Prapamontol T, Mangklabruks A, Chantara S, Thavornyutikarn P, Robson MG, et al. A single method for detecting 11 organophosphate pesticides in human plasma and breastmilk using GC-FPD. Journal of Chromatography B. 2016 Jul 1;1025:92–104. doi:10.1016/j.jchromb.2016.04.045

149. Jokanović M. Neurotoxic effects of organophosphorus pesticides and possible association with neurodegenerative diseases in man: A review. Toxicology. 2018 Dec 1;410:125–31. doi:10.1016/j.tox.2018.09.009

150. Sánchez-Santed F, Colomina MT, Herrero Hernández E. Organophosphate pesticide exposure and neurodegeneration. Cortex. 2016 Jan 1;What's your poison? Neurobehavioural consequences of exposure to industrial, agricultural and environmental chemicals74:417–26. doi:10.1016/j.cortex.2015.10.003

151. EU EFSA. Building a European Partnership for next generation, systems-based Environmental Risk Assessment (PERA) | EFSA [Internet]. 2022 [cited 2022 Dec 7]. Available from: https://www.efsa.europa.eu/en/supporting/pub/en-7546

152. Chen J, Zhao S, Wesseling S, Kramer NI, Rietjens IMCM, Bouwmeester H. Acetylcholinesterase Inhibition in Rats and Humans Following Acute Fenitrothion Exposure Predicted by Physiologically Based Kinetic Modeling-Facilitated Quantitative In Vitro to In Vivo Extrapolation. Environ Sci Technol. 2023 Nov 26. doi:10.1021/acs.est.3c07077

153. Gearhart JM, Jepson GW, Clewell HJ, Andersen ME, Conolly RB. Physiologically based pharmacokinetic model for the inhibition of acetylcholinesterase by organophosphate esters. Environmental Health Perspectives. 1994 Dec;102(suppl 11):51–60. doi:10.1289/ehp.94102s1151

154. Omwenga I, Zhao S, Kanja L, Mol H, Rietjens IMCM, Louisse J. Prediction of dose-dependent in vivo acetylcholinesterase inhibition by profenofos in rats and humans using physiologically based kinetic (PBK) modeling-facilitated reverse dosimetry. Arch Toxicol. 2021;95(4):1287–301. doi:10.1007/s00204-021-03004-4 PubMed PMID: 33651127; PubMed Central PMCID: PMC8032624.

155. Poet TS, Kousba AA, Dennison SL, Timchalk C. Physiologically Based Pharmacokinetic/Pharmacodynamic Model for the Organophosphorus Pesticide Diazinon. NeuroToxicology. 2004 Dec 1;25(6):1013–30. doi:10.1016/j.neuro.2004.03.002

156. Zhao S, Wesseling S, Rietjens IvonneMCM, Strikwold M. Inter-individual variation in chlorpyrifos toxicokinetics characterized by physiologically based kinetic (PBK) and Monte Carlo simulation comparing human liver microsome and Supersome™ cytochromes P450 (CYP)-specific kinetic data as model input. Arch Toxicol. 2022 May 1;96(5):1387–409. doi:10.1007/s00204-022-03251-z

157. Zhao S, Wesseling S, Spenkelink B, Rietjens IMCM. Physiologically based kinetic modelling based prediction of in vivo rat and human acetylcholinesterase (AChE) inhibition upon exposure to diazinon. Arch Toxicol. 2021;95(5):1573–93. doi:10.1007/s00204-021-03015-1 PubMed PMID: 33715020; PubMed Central PMCID: PMC8113213.

158. Zhao S, Kamelia L, Boonpawa R, Wesseling S, Spenkelink B, Rietjens IMCM. Physiologically Based Kinetic Modeling-Facilitated Reverse Dosimetry to Predict In Vivo Red Blood Cell Acetylcholinesterase Inhibition Following Exposure to Chlorpyrifos in the Caucasian and Chinese Population. Toxicol Sci. 2019 Sep;171(1):69–83. doi:10.1093/toxsci/kfz134 PubMed PMID: 31214721; PubMed Central PMCID: PMC6736452.

159. Yu LX, Crison JR, Amidon GL. Compartmental transit and dispersion model analysis of small intestinal transit flow in humans. International Journal of Pharmaceutics. 1996 Aug 16;140(1):111–8. doi:10.1016/0378-5173(96)04592-9

160. Chen M jun, Liu C, Wan Y, Yang L, Jiang S, Qian D wei, et al. Enterohepatic circulation of bile acids and their emerging roles on glucolipid metabolism. Steroids. 2021 Jan 1;165:108757. doi:10.1016/j.steroids.2020.108757

161. Brzak KA, Harms DW, Bartels MJ, Nolan RJ. Determination of Chlorpyrifos, Chlorpyrifos Oxon, and 3,5,6-Trichloro-2-Pyridinol in Rat and Human Blood. Journal of Analytical Toxicology. 1998 May 1;22(3):203–10. doi:10.1093/jat/22.3.203

162. Sams C, Mason HJ. Detoxification of organophosphates by A-esterases in human serum. Hum Exp Toxicol. 1999 Nov 1;18(11):653–8. doi:10.1191/096032799678839581

163. Grandoni S, Cesari N, Brogin G, Puccini P, Magni P. Building in-house PBPK modelling tools for oral drug administration from literature information. ADMET DMPK. 2019 Feb 23;7(1):4–21. doi:10.5599/admet.638 PubMed PMID: 35350741; PubMed Central PMCID: PMC8957249.

164. Walton K, Dorne JLCM, Renwick AG. Species-specific uncertainty factors for compounds eliminated principally by renal excretion in humans. Food and Chemical Toxicology. 2004 Feb 1;42(2):261–74. doi:10.1016/j.fct.2003.09.001

165. Berezhkovskiy LM. Volume of Distribution at Steady State for a Linear Pharmacokinetic System with Peripheral Elimination. Journal of Pharmaceutical Sciences. 2004 Jun 1;93(6):1628–40. doi:10.1002/jps.20073

166. DeJongh J, Verhaar HJM, Hermens JLM. A quantitative property-property relationship (QPPR) approach to estimate in vitro tissue-blood partition coefficients of organic chemicals in rats and humans. Arch Toxicol. 1997 Dec 1;72(1):17–25. doi:10.1007/s002040050463

167. Rodgers T, Rowland M. Mechanistic Approaches to Volume of Distribution Predictions: Understanding the Processes. Pharm Res. 2007 May 1;24(5):918–33. doi:10.1007/s11095-006-9210-3

168. Chan R, De Bruyn T, Wright M, Broccatelli F. Comparing Mechanistic and Preclinical Predictions of Volume of Distribution on a Large Set of Drugs. Pharm Res. 2018 Mar 8;35(4):87. doi:10.1007/s11095-018-2360-2

169. Utsey K, Gastonguay MS, Russell S, Freling R, Riggs MM, Elmokadem A. Quantification of the Impact of Partition Coefficient Prediction Methods on Physiologically Based Pharmacokinetic Model Output Using a Standardized Tissue Composition. Drug Metab Dispos. 2020 Oct 1;48(10):903–16. doi:10.1124/dmd.120.090498 PubMed PMID: 32665416.

170. Ikeda T, Tsuda S, Shirasu Y. Metabolic Induction of the Hepatic Cytochrome P450 System by Chlorfenvinphos in Rats. Toxicological Sciences. 1991 Aug 1;17(2):361–7. doi:10.1093/toxsci/17.2.361

171. von der Wellen J, Bierwisch A, Worek F, Thiermann H, Wille T. Kinetics of pesticide degradation by human fresh frozen plasma (FFP) in vitro. Toxicology Letters. 2016 Feb 26;Impact of chemical warfare agents and highly toxic chemicals on the respiratory system244:124–8. doi:10.1016/j.toxlet.2015.07.014

172. Cook TJ, Shenoy SS. Intestinal permeability of chlorpyrifos using the single-pass intestinal perfusion method in the rat. Toxicology. 2003 Mar 3;184(2):125–33. doi:10.1016/S0300-483X(02)00555-3

173. EPA. Data Evaluation Record for Chlorpyrifos [Internet]. 2009 May [cited 2024 Mar 28]. Report No. Available from: https://archive.epa.gov/osa/hsrb/web/pdf/1d5-science-rvw-kisicki-052709.pdf

174. Timchalk C, Poet TS, Hinman MN, Busby AL, Kousba AA. Pharmacokinetic and pharmacodynamic interaction for a binary mixture of chlorpyrifos and diazinon in the rat. Toxicology and Applied Pharmacology. 2005 May 15;205(1):31–42. doi:10.1016/j.taap.2004.09.004

175. Nolan RJ, Rick DL, Freshour NL, Saunders JH. Chlorpyrifos: Pharmacokinetics in human volunteers. Toxicology and Applied Pharmacology. 1984 Mar 30;73(1):8–15. doi:10.1016/0041-008X(84)90046-2

176. Ikeda T, Tsuda S, Shirasu Y. Pharmacokinetic analysis of protection by an organophosphorus insecticide, chlorfenvinphos, against the toxicity of its succeeding dosage in rats. Fundamental and Applied Toxicology. 1992 Feb 1;18(2):299–306. doi:10.1016/0272-0590(92)90059-Q

177. Ikeda T, Kojima T, Yoshida M, Takahashi H, Tsuda S, Shirasu Y. Pretreatment of rats with an organophosphorus insecticide, chlorfenvinphos, protects against subsequent challenge with the same compound. Fundamental and Applied Toxicology. 1990 Apr 1;14(3):560–7. doi:10.1016/0272-0590(90)90260-Q

178. Hutson DH, Hathway DE. Toxic effects of chlorfenvinphos in dogs and rats. Biochemical Pharmacology. 1967 Jun 1;16(6):949–62. doi:10.1016/0006-2952(67)90267-5

179. Boyer AC. Vinyl phosphate insecticide sorption to proteins and its effect on cholinesterase I50 values. J Agric Food Chem. 1967 Mar 1;15(2):282–6. doi:10.1021/jf60150a031

180. McKim JM, Kolanczyk RC, Lien GJ, Hoffman AD. Dynamics of renal excretion of phenol and major metabolites in the rainbow trout (Oncorhynchus mykiss). Aquatic Toxicology. 1999 May 1;45(4):265–77. doi:10.1016/S0166-445X(98)00105-2

181. WHO. Characterization and application of physiologically based pharmacokinetic models in risk assessment [Internet]. 2010 [cited 2024 Jan 2]. Available from: https://www.who.int/publications-detail-redirect/9789241500906

182. Abduljalil K, Cain T, Humphries H, Rostami-Hodjegan A. Deciding on Success Criteria for Predictability of Pharmacokinetic Parameters from In Vitro Studies: An Analysis Based on In Vivo Observations. Drug Metab Dispos. 2014 Sep 1;42(9):1478–84. doi:10.1124/dmd.114.058099 PubMed PMID: 24989891.

183. Soetaert K, Petzoldt T. Inverse Modelling, Sensitivity and Monte Carlo Analysis in R Using Package FME. Journal of Statistical Software. 2010 Feb 2;33:1–28. doi:10.18637/jss.v033.i03

184. Wang W, Hallow K, James D. A Tutorial on RxODE: Simulating Differential Equation Pharmacometric Models in R. CPT: Pharmacometrics & Systems Pharmacology. 2016;5(1):3–10. doi:10.1002/psp4.12052

185. Gärtner K. The forestomach of rats and mice, an effective device supporting digestive metabolism in muridae (review). Journal of Experimental Animal Science. 2002 Jan 1;42(1):1–20. doi:10.1016/S0939-8600(02)80002-5

186. Kararli TT. Comparison of the gastrointestinal anatomy, physiology, and biochemistry of humans and commonly used laboratory animals. Biopharmaceutics & Drug Disposition. 1995;16(5):351–80. doi:10.1002/bdd.2510160502

187. Vonk RJ, van Doorn ABD, Strubbe JH. Bile Secretion and Bile Composition in the Freely Moving, Unanaesthetized Rat with a Permanent Biliary Drainage: Influence of Food Intake on Bile Flow. Clinical Science and Molecular Medicine. 1978 Sep 1;55(3):253–9. doi:10.1042/cs0550253

188. Ginsberg HN. Lipoprotein physiology. Endocrinology and Metabolism Clinics. 1998 Sep 1;27(3):503–19. doi:10.1016/S0889-8529(05)70023-2 PubMed PMID: 9785050.

189. Cooper AD. Hepatic uptake of chylomicron remnants. Journal of Lipid Research. 1997 Nov 1;38(11):2173–92. doi:10.1016/S0022-2275(20)34932-4

190. Hildebrand S, Löwa N, Paysen H, Fratila RM, Reverte-Salisa L, Trakoolwilaiwan T, et al. Quantification of Lipoprotein Uptake in Vivo Using Magnetic Particle Imaging and Spectroscopy. ACS Nano. 2021 Jan 26;15(1):434–46. doi:10.1021/acsnano.0c03229

191. Tudi M, Li H, Li H, Wang L, Lyu J, Yang L, et al. Exposure Routes and Health Risks Associated with Pesticide Application. Toxics. 2022 Jun;10(6):335. doi:10.3390/toxics10060335

192. Authority (EFSA) EFS, Carrasco Cabrera L, Di Piazza G, Dujardin B, Medina Pastor P. The 2021 European Union report on pesticide residues in food. EFSA Journal. 2023;21(4):e07939. doi:10.2903/j.efsa.2023.7939

193. Mali H, Shah C, Raghunandan BH, Prajapati AS, Patel DH, Trivedi U, et al. Organophosphate pesticides an emerging environmental contaminant: Pollution, toxicity, bioremediation progress, and remaining challenges. Journal of Environmental Sciences. 2023 May 1;127:234–50. doi:10.1016/j.jes.2022.04.023

194. Pesticide Action Network (PAN). PAN International Consolidated List of Banned Pesticides [Internet]. 2022 [cited 2026 Mar 13]. Available from: https://pan-international.org/pan-international-consolidated-list-of-banned-pesticides/

195. Jardim ANO, Brito AP, van Donkersgoed G, Boon PE, Caldas ED. Dietary cumulative acute risk assessment of organophosphorus, carbamates and pyrethroids insecticides for the Brazilian population. Food and Chemical Toxicology. 2018 Feb 1;112:108–17. doi:10.1016/j.fct.2017.12.010

196. Ottenbros I, Lebret E, Huber C, Lommen A, Antignac JP, Čupr P, et al. Assessment of exposure to pesticide mixtures in five European countries by a harmonized urinary suspect screening approach. International Journal of Hygiene and Environmental Health. 2023 Mar 1;248:114105. doi:10.1016/j.ijheh.2022.114105

197. Zhang X, Driver JH, Li Y, Ross JH, Krieger RI. Dialkylphosphates (DAPs) in Fruits and Vegetables May Confound Biomonitoring in Organophosphorus Insecticide Exposure and Risk Assessment. J Agric Food Chem. 2008 Nov 26;56(22):10638–45. doi:10.1021/jf8018084

198. Dhanarisi J, Tzotzolaki TM, Vasileva AMD, Kjellberg MA, Hakulinen H, Vanninen P, et al. Osmolal and anion gaps after acute self-poisoning with agricultural formulations of the organophosphorus insecticides profenofos and diazinon: A pilot study. Basic & Clinical Pharmacology & Toxicology. 2022;130(2):320–7. doi:10.1111/bcpt.13686

199. World Health Organization (WHO). Harmonized studies on organophosphorous pesticide poisonings [Internet]. 2000 [cited 2026 Mar 13]. Available from: https://iris.who.int/server/api/core/bitstreams/ee3c073e-9aca-479c-a2c9-e5d61e5d3e44/content

200. Jokanović M. Biotransformation of organophosphorus compounds. Toxicology. 2001 Sep 25;166(3):139–60. doi:10.1016/S0300-483X(01)00463-2

201. Henretig FM, Kirk MA, McKay CA. Hazardous Chemical Emergencies and Poisonings. New England Journal of Medicine. 2019 Apr 25;380(17):1638–55. doi:10.1056/NEJMra1504690

202. Dent MP, Vaillancourt E, Thomas RS, Carmichael PL, Ouedraogo G, Kojima H, et al. Paving the way for application of next generation risk assessment to safety decision-making for cosmetic ingredients. Regulatory Toxicology and Pharmacology. 2021 Oct 1;125:105026. doi:10.1016/j.yrtph.2021.105026

203. Stucki AO, Barton-Maclaren TS, Bhuller Y, Henriquez JE, Henry TR, Hirn C, et al. Use of new approach methodologies (NAMs) to meet regulatory requirements for the assessment of industrial chemicals and pesticides for effects on human health. Front Toxicol. 2022 Sep 1;4. doi:10.3389/ftox.2022.964553

204. Roggen EL. In vitro Toxicity Testing in the Twenty-First Century. Front Pharmacol. 2011 Feb 7;2. doi:10.3389/fphar.2011.00003

205. Dent MP, Li H, Carmichael PL, Martin FL. Employing Dietary Comparators to Perform Risk Assessments for Anti-Androgens Without Using Animal Data. Toxicol Sci. 2019 Feb 1;167(2):375–84. doi:10.1093/toxsci/kfy245

206. van Tongeren TCA, Moxon TE, Dent MP, Li H, Carmichael PL, Rietjens IMCM. Next generation risk assessment of human exposure to anti-androgens using newly defined comparator compound values. Toxicology in Vitro. 2021 Jun 1;73:105132. doi:10.1016/j.tiv.2021.105132

207. van Tongeren TCA, Wang S, Carmichael PL, Rietjens IMCM, Li H. Next generation risk assessment of human exposure to estrogens using safe comparator compound values based on in vitro bioactivity assays. Arch Toxicol. 2023 Jun 1;97(6):1547–75. doi:10.1007/s00204-023-03480-w

208. van Gemert M, Dourson M, Moretto A, Watson M. Use of Human Data for the Derivation of a Reference Dose for Chlorpyrifos. Regulatory Toxicology and Pharmacology. 2001 Apr 1;33(2):110–6. doi:10.1006/rtph.2000.1447

209. Moerenhout T, Chen J, Bouwmeester H, Rietjens IMCM, Kramer NI. Development of a Generic Physiologically Based Kinetic Model for the Prediction of Internal Exposure to Organophosphate Pesticides. Environ Sci Technol. 2024 Oct 7. doi:10.1021/acs.est.4c06534

210. European Food Safety Authority. Conclusion on the peer review of the pesticide human health risk assessment of the active substance chlorpyrifos. EFSA Journal. 2014;12(4):3640. doi:10.2903/j.efsa.2014.3640

211. US Environmental Protection Agency. Chlorpyrifos: Revised human health risk assessment [Internet]. 2016 [cited 2026 Mar 13]. Available from: https://www.regulations.gov/document/EPA-HQ-OPP-2015-0653-0454

212. Rietjens IMCM, Ning J, Chen L, Wesseling S, Strikwold M, Louisse J. Selecting the dose metric in reverse dosimetry based QIVIVE. Arch Toxicol. 2019 May 1;93(5):1467–9. doi:10.1007/s00204-019-02438-1

213. Drevenkar V, Vasilić Ž, Štengl B, Fröbe Z, Rumenjak V. Chlorpyrifos metabolites in serum and urine of poisoned persons. Chemico-Biological Interactions. 1993 Jun 1;The Second International Meeting on Esterases Interacting with Organophosphorus Compounds87(1):315–22. doi:10.1016/0009-2797(93)90059-8

214. Inoue S, Saito T, Suzuki Y, Iizuka S, Takazawa K, Akieda K, et al. Prognostic factors and toxicokinetics in acute fenitrothion self-poisoning requiring intensive care. Clinical Toxicology. 2008 Jan 1;46(6):528–33. doi:10.1080/15563650701666280

215. Lotti M. Clinical Toxicology of Anticholinesterase Agents in Humans. In: Hayes' Handbook of Pesticide Toxicology [Internet]. Academic Press; 2010 [cited 2026 Mar 13]. p. 1543–89. Available from: https://www.sciencedirect.com/science/chapter/edited-volume/abs/pii/B9780123743671000720 doi:10.1016/B978-0-12-374367-1.00072-0

216. Nosál' M, Hladká A. Determination of the exposure to fenitrothion (0,0-dimethyl-0/3-methyl-4-nitrophenyl/thiophosphate) on the basis of the excretion of p-nitro-m-cresol by the urine of the persons tested. Int Arch Gewerbepath Gewerbehyg. 1968 Mar 1;25(1):28–38. doi:10.1007/BF00404665

217. Brown VKH. Interim review of Chlorfenvinphos - Evaluation of the Mammalian Toxicology and Metabolism Toxicokinetics: The effect of chlorfenvinphos (SD 7859) on two human volunteers [Internet]. 1966 [cited 2026 Mar 13]. Available from: https://www.apvma.gov.au/sites/default/files/publication/14716-chlorfenvinphos-irr-toxicology.pdf

218. Australian Pesticides and Veterinary Medicines Authority. Diazinon: Human health risk assessment, part 2: Toxicological hazard assessment [Internet]. 2011 [cited 2026 Mar 13]. Available from: https://sk.sagepub.com/reference/nanoscience/n22.xml doi:10.4135/9781412972093.n22

219. US Environmental Protection Agency. Diazinon: Review of a single dose and a 28-day dosing studies with diazinon in human volunteers [Internet]. 2001 [cited 2026 Mar 13]. Available from: https://www3.epa.gov/pesticides/chem_search/cleared_reviews/csr_PC-057801_8-Nov-01_114.pdf

220. Boyeson MG. A randomized, double-blind, ascending, acute, oral dose study of diazinon to determine the no effect level (NOEL) for plasma and RBC cholinesterase activity in normal, healthy subjects (study no. NCP-8373, Part A); Unpublished report (Novartis no. 587-98). 2000.

221. Kisicki JC, Seip CW. A rising dose toxicology study to determine the no-observable-effect-levels (NOEL) for erythrocyte acetylcholinesterase (AChE) inhibition and cholinergic signs and symptoms of chlorpyrifos at three dose levels; Unpublished report [Internet]. 1999. Available from: https://doi.org/10.1006/rtph.2000.1447

222. US EPA. The Use of Data on Cholinesterase Inhibition for Risk Assessments of Organophosphorous and Carbamate Pesticides [Internet]. 2000 [cited 2026 Mar 13]. Available from: https://www.epa.gov/sites/default/files/2015-07/documents/cholin.pdf

223. Reiss R, Neal B, Lamb JC, Juberg DR. Acetylcholinesterase inhibition dose–response modeling for chlorpyrifos and chlorpyrifos-oxon. Regulatory Toxicology and Pharmacology. 2012 Jun 1;63(1):124–31. doi:10.1016/j.yrtph.2012.03.008

224. US Environmental Protection Agency. Chlorpyrifos: Special Non-Guideline Assessment for RBC Cholinesterase in Humans [Internet]. 2009 [cited 2026 Mar 13]. Available from: https://archive.epa.gov/osa/hsrb/web/pdf/1d5-science-rvw-kisicki-052709.pdf

225. Lockridge O, Norgren RBJr, Johnson RC, Blake TA. Naturally Occurring Genetic Variants of Human Acetylcholinesterase and Butyrylcholinesterase and Their Potential Impact on the Risk of Toxicity from Cholinesterase Inhibitors. Chem Res Toxicol. 2016 Sep 19;29(9):1381–92. doi:10.1021/acs.chemrestox.6b00228

226. Mangas I, Estevez J, Vilanova E, França TCC. New insights on molecular interactions of organophosphorus pesticides with esterases. Toxicology. 2017 Feb 1;9TH Congress of Toxicology in Developing Countries and XIX Brazilian Congress of Toxicology376:30–43. doi:10.1016/j.tox.2016.06.006

227. Ross MK, Streit TM, Herring KL, Xie S. Carboxylesterases: dual roles in lipid and pesticide metabolism. Journal of Pesticide Science. 2010;35(3):257–64. doi:10.1584/jpestics.R10-07

228. Smith JN, Timchalk C, Bartels MJ, Poet TS. In Vitro Age-Dependent Enzymatic Metabolism of Chlorpyrifos and Chlorpyrifos-Oxon in Human Hepatic Microsomes and Chlorpyrifos-Oxon in Plasma. Drug Metab Dispos. 2011 Aug 1;39(8):1353–62. doi:10.1124/dmd.111.038745 PubMed PMID: 21521795.

229. Chedik L, Bruyere A, Fardel O. Interactions of organophosphorus pesticides with solute carrier (SLC) drug transporters. Xenobiotica. 2019 Mar 4;49(3):363–74. doi:10.1080/00498254.2018.1442030 PubMed PMID: 29448871.

230. Leung MCK, Meyer JN. Mitochondria as a target of organophosphate and carbamate pesticides: Revisiting common mechanisms of action with new approach methodologies. Reprod Toxicol. 2019 Oct;89:83–92. doi:10.1016/j.reprotox.2019.07.007 PubMed PMID: 31315019; PubMed Central PMCID: PMC6766410.

231. Clarke ED, Greenhow DT, Adams D. Metabolism-related assays and their application to agrochemical research: reactivity of pesticides with glutathione and glutathione transferases. Pesticide Science. 1998;54(4):385–93. doi:10.1002/(SICI)1096-9063(199812)54:4<385::AID-PS842>3.0.CO;2-C

232. Hayes PC, Harrison DJ, Bouchier IA, McLellan LI, Hayes JD. Cytosolic and microsomal glutathione S-transferase isoenzymes in normal human liver and intestinal epithelium. Gut. 1989 Jun 1;30(6):854–9. doi:10.1136/gut.30.6.854 PubMed PMID: 2753409.

233. Peters MA, Fouts JR. A study of some possible mechanisms by which magnesium activates hepatic microsomal drug metabolism in vitro. The Journal of Pharmacology and Experimental Therapeutics. 1970 Jun 1;173(2):233–41. doi:10.1016/S0022-3565(25)28560-3 PubMed PMID: 4393573.

234. Pla A, Rodrigo L, Hernández AF, Gil F, Lopez O. Effect of metal ions and calcium on purified PON1 and PON3 from rat liver. Chemico-Biological Interactions. 2007 Apr 5;167(1):63–70. doi:10.1016/j.cbi.2007.01.006

235. Paolini M, Tonelli F, Bauer C, Bronzetti G, Corsi C, Cantelli-Forti G. EDTA affects cytochrome *P*450-dependent biotransformation reactions during incubations for the liver microsomal assay. Mutation Research Letters. 1988 Jul 1;208(3):189–94. doi:10.1016/0165-7992(88)90059-0

236. Koelle GB, Davis R, Diliberto EJ, Koelle WA. Selective, near-total, irreversible inactivation of peripheral pseudocholin-esterase and acetylcholinesterase in cats *In vivo*. Biochemical Pharmacology. 1974 Jan 15;23(2):175–88. doi:10.1016/0006-2952(74)90408-0

237. Plapp FW, Casida JE. Animal Metabolism of Insecticides, Bovine Metabolism of Organophosphorus Insecticides. Metabolic Fate of O,O-Dimethyl O-(2,4,5-trichlorophenyl) Phosphorothioate in Rats and a Cow. J Agric Food Chem. 1958 Sep 1;6(9):662–7. doi:10.1021/jf60091a002

238. Silva VB, Campos RB, Pavez P, Medeiros M, Orth ES. Nucleophilic Neutralization of Organophosphates: Lack of Selectivity or Plenty of Versatility? The Chemical Record. 2021;21(10):2638–65. doi:10.1002/tcr.202100123

239. Silva VB, Orth ES. Structure-Reactivity Insights on the Alkaline Hydrolysis of Organophosphates: Non-Leaving and Leaving Group Effects in a Bilinear Brønsted-Like Relationship. ChemPhysChem. 2023;24(6):e202200612. doi:10.1002/cphc.202200612

240. Abass K, Reponen P, Jalonen J, Pelkonen O. In vitro metabolism and interaction of profenofos by human, mouse and rat liver preparations. Pesticide Biochemistry and Physiology. 2007 Mar 1;87(3):238–47. doi:10.1016/j.pestbp.2006.08.002

241. EURL. Analysis of Dimethoate and Omethoate Metabolites – Method Development and Pilot Monitoring [Internet]. 2019 [cited 2025 Jun 11]. Available from: https://www.eurl-pesticides.eu/docs/public/tmplt_article.asp?LabID=200&CntID=1124&Theme_ID=1&Pdf=False&Lang=EN

242. Aw TY, Wierzbicka G, Jones DP. Oral glutathione increases tissue glutathione in vivo. Chemico-Biological Interactions. 1991 Jan 1;80(1):89–97. doi:10.1016/0009-2797(91)90033-4

243. Favilli F, Marraccini P, Iantomasi T, Vincenzini MT. Effect of orally administered glutathione on glutathione levels in some organs of rats: role of specific transporters. British Journal of Nutrition. 1997 Aug;78(2):293–300. doi:10.1079/BJN19970147

244. Giustarini D, Dalle-Donne I, Milzani A, Rossi R. Low molecular mass thiols, disulfides and protein mixed disulfides in rat tissues: Influence of sample manipulation, oxidative stress and ageing. Mechanisms of Ageing and Development. 2011 Apr 1;132(4):141–8. doi:10.1016/j.mad.2011.02.001

245. Hazelton GA, Lang CA. Glutathione contents of tissues in the aging mouse. Biochemical Journal. 1980 Apr 15;188(1):25–30. doi:10.1042/bj1880025

246. Hissin PJ, Hilf R. A fluorometric method for determination of oxidized and reduced glutathione in tissues. Analytical Biochemistry. 1976 Jul;74(1):214–26. doi:10.1016/0003-2697(76)90326-2

247. Potter DW, Tran TB. Apparent Rates of Glutathione Turnover in Rat Tissues. Toxicology and Applied Pharmacology. 1993 Jun 1;120(2):186–92. doi:10.1006/taap.1993.1102

248. Barter ZE, Bayliss MK, Beaune PH, Boobis AR, Carlile DJ, Edwards RJ, et al. Scaling Factors for the Extrapolation of In Vivo Metabolic Drug Clearance From In Vitro Data: Reaching a Consensus on Values of Human Micro-somal Protein and Hepatocellularity Per Gram of Liver. Current Drug Metabolism. 2007;8(1):33–45. doi:10.2174/138920007779315053

249. Cubitt HE, Houston JB, Galetin A. Prediction of Human Drug Clearance by Multiple Metabolic Pathways: Integration of Hepatic and Intestinal Microsomal and Cytosolic Data. Drug Metab Dispos. 2011 May 1;39(5):864–73. doi:10.1124/dmd.110.036566 PubMed PMID: 21303923.

250. Medinsky MA, Leavens TL, Csanády GA, Gargas ML, Bond JA. In vivo metabolism of butadiene by mice and rats: a comparison of physiological model predictions and experimental data. Carcinogenesis. 1994 Jul 1;15(7):1329–40. doi:10.1093/carcin/15.7.1329

251. Becker JM, Nakatsugawa T. Significance of hepatic breakthrough thresholds in fenitrothion toxicity in male rats and female mice. Pesticide Biochemistry and Physiology. 1990 Sep 1;38(1):34–40. doi:10.1016/0048-3575(90)90145-R

252. Miyamoto J. Studies on the Mode of Action of Organophosphorus Compounds. Agricultural and Biological Chemistry. 1964 Jul 1;28(7):411–30. doi:10.1080/00021369.1964.10858259

253. Aharoni AH, O'Brien RD. Inhibition of acetylcholinesterases by anionic organophosphorus compounds. Biochemistry. 1968 Apr 1;7(4):1538–45. doi:10.1021/bi00844a042

254. Costa LG. Organophosphorus Compounds at 80: Some Old and New Issues. Toxicol Sci. 2018 Mar;162(1):24–35. doi:10.1093/toxsci/kfx266 PubMed PMID: 29228398; PubMed Central PMCID: PMC6693380.

255. EU. DIRECTIVE 2010/63/EU OF THE EUROPEAN PARLIAMENT AND OF THE COUNCIL on the protection of animals used for scientific purposes [Internet]. 2010 [cited 2026 Mar 16]. Available from: https://eur-lex.europa.eu/eli/dir/2010/63/oj/eng

256. Jones H, Rowland-Yeo K. Basic Concepts in Physiologically Based Pharmacokinetic Modeling in Drug Discovery and Development. CPT Pharmacometrics Syst Pharmacol. 2013 Aug;2(8):e63. doi:10.1038/psp.2013.41 PubMed PMID: 23945604; PubMed Central PMCID: PMC3828005.

257. Moerenhout T, Bakker W, Bouwmeester H, Kramer NI. The effect of glutathione-mediated metabolism of organophosphate pesticides on rat and human in vivo toxicokinetics investigated using physiologically based kinetic modelling. 2026.

258. Sands D, Davis A, Banfield S, Pottie IR, Darvesh S. Solvents and detergents compatible with enzyme kinetic studies of cholinesterases. Chemico-Biological Interactions. 2023 Sep 25;383:110667. doi:10.1016/j.cbi.2023.110667

259. Worek F, Mast U, Kiderlen D, Diepold C, Eyer P. Improved determination of acetylcholinesterase activity in human whole blood. Clinica Chimica Acta. 1999 Oct 1;288(1):73–90. doi:10.1016/S0009-8981(99)00144-8

260. Simeon-Rudolf V, Šinko G, Štuglin A, Reiner E. Inhibition of Human Blood Acetylcholinesterase and Butyrylcholinesterase by Ethopropazine. Croatica Chemica Acta. 2001 Feb 1;74(1):173–82.

261. Cubitt HE, Houston JB, Galetin A. Relative Importance of Intestinal and Hepatic Glucuronidation—Impact on the Prediction of Drug Clearance. Pharm Res. 2009 May 1;26(5):1073–83. doi:10.1007/s11095-008-9823-9

262. Yang F, Li J, Pang G, Ren F, Fang B. Effects of Diethyl Phosphate, a Non-Specific Metabolite of Organophosphorus Pesticides, on Serum Lipid, Hormones, Inflammation, and Gut Microbiota. Molecules. 2019 May 24;24(10):2003. doi:10.3390/molecules24102003 PubMed PMID: 31137755; PubMed Central PMCID: PMC6572208.

263. Chen WL, Sheets JJ, Nolan RJ, Mattsson JL. Human Red Blood Cell Acetylcholinesterase Inhibition as the Appropriate and Conservative Surrogate Endpoint for Establishing Chlorpyrifos Reference Dose. Regulatory Toxicology and Pharmacology. 1999 Feb 1;29(1):15–22. doi:10.1006/rtph.1998.1256

264. EPA. The Use of Data on Cholinesterase Inhibition for Risk Assessments of Organophosphorous and Carbamate Pesticides [Internet]. 2000 [cited 2025 Jul 1]. Available from: https://www.epa.gov/sites/default/files/2015-07/documents/cholin.pdf

265. Chen, Chen B, Wesseling S, Bouwmeester H, Rietjens IMCM, Kramer NI. A population physiologically based kinetic and toxicodynamic model for acute diazinon exposure. Ecotoxicology and Environmental Safety. 2025 Apr 1;294:118083. doi:10.1016/j.ecoenv.2025.118083

266. EFSA EFS. Statement on the available outcomes of the human health assessment in the context of the pesticides peer review of the active substance chlorpyrifos. EFSA Journal. 2019;17(8):e05809. doi:10.2903/j.efsa.2019.5809

267. Marty MS, Andrus AK, Bell MP, Passage JK, Perala AW, Brzak KA, et al. Cholinesterase inhibition and toxicokinetics in immature and adult rats after acute or repeated exposures to chlorpyrifos or chlorpyrifos–oxon. Regulatory Toxicology and Pharmacology. 2012 Jul 1;63(2):209–24. doi:10.1016/j.yrtph.2012.03.015

268. US EPA. Chlorpyrifos: Review of the comparative cholinesterase (including chlorpyrifos oxon), special acute inhalation sutdy and immunotoxicity studies. [Internet]. 2011 [cited 2025 Jul 17]. Available from: https://www3.epa.gov/pesticides/chem_search/cleared_reviews/csr_PC-059101_20-May-11_a.pdf

269. US ATSDR. Toxicological profile for diazinon. 2008.

270. US EPA. Diazinon Draft Human Health Risk Assessment for Registration Review [Internet]. 2016 [cited 2025 Jul 9]. Available from: https://www.regulations.gov/document/EPA-HQ-OPP-2008-0351-0093

271. EFSA. Conclusion regarding the peer review of the pesticide risk assessment of the active substance fenitrothion. EFSA Journal. 2006;4(2):59r. doi:10.2903/j.efsa.2006.59r

272. US EPA. Fenitrothion. Risk Assessment to Support Final Registration Review Decision [Internet]. 2010 [cited 2025 Jul 14]. Available from: https://www.regulations.gov/document/EPA-HQ-OPP-2009-0172-0016

273. US ATSDR. Methyl Parathion | Toxicological Profile | ATSDR [Internet]. 2001 [cited 2024 Aug 21]. Available from: https://wwwn.cdc.gov/TSP/ToxProfiles/ToxProfiles.aspx?id=636&tid=117

274. US ATSDR. Parathion | Toxicological Profile | ATSDR [Internet]. 2017 [cited 2024 Aug 21]. Available from: https://wwwn.cdc.gov/TSP/ToxProfiles/ToxProfiles.aspx?id=1425&tid=246

275. US EPA. Ethyl Parathion: Revised humanhealth risk assessment [Internet]. 2000 [cited 2025 Jul 17]. Available from: https://www.epa.gov/system/files/documents/2022-07/ethyl-parathion-memo-1999.pdf

276. US EPA. Dimethoate: Human Health Risk Assessment for Registration Review. 2015.

277. US ATSDR. Chlorfenvinphos | Toxicological Profile | ATSDR [Internet]. 1997 [cited 2024 Aug 21]. Available from: https://wwwn.cdc.gov/TSP/ToxProfiles/ToxProfiles.aspx?id=932&tid=193

278. US EPA. Profenofos: Human Health Draft Risk Assessment (DRA) for Registration Review. 2016.

279. FAO. Pesticide residues in food - 2007: toxicological evaluations [Internet]. 2007 [cited 2022 Jul 6]. Available from: https://www.who.int/publications-detail-redirect/9789241665230

280. Griffin P, Mason H, Heywood K, Cocker J. Oral and dermal absorption of chlorpyrifos: a human volunteer study. Occupational and Environmental Medicine. 1999 Jan 1;56(1):10–3. doi:10.1136/oem.56.1.10 PubMed PMID: 10341740.

281. APVMA. The reconsideration of approvals of the active constituent diazinon, registrations of products containing diazinon and approval of their associated labels. Australian Pesticides & Veterinary Medicines Authority; 2006.

282. JMPR. Fenitrothion [Internet]. 2000 [cited 2025 Jul 14]. Available from: https://www.fao.org/fileadmin/templates/agphome/documents/Pests_Pesticides/JMPR/Report07/Fenitrothion.pdf

283. Krieger RI, Thongsinthusak T. Metabolism and excretion of dimethoate following ingestion of overtolerance peas and a bolus dose. Food and Chemical Toxicology. 1993 Mar 1;31(3):177–82. doi:10.1016/0278-6915(93)90091-C

284. Moser VC, Padilla S. Esterase metabolism of cholinesterase inhibitors using rat liver in vitro. Toxicology. 2011 Mar 15;281(1):56–62. doi:10.1016/j.tox.2011.01.002

285. Su MQ, Kinoshita FK, Frawley JP, DuBois KP. Comparative inhibition of aliesterases and cholinesterase in rats fed eighteen organophosphorus insecticides. Toxicology and Applied Pharmacology. 1971 Oct 1;20(2):241–9. doi:10.1016/0041-008X(71)90050-0

286. Tang J, Chambers JE. Detoxication of paraoxon by rat liver homogenate and serum carboxylesterases and A-esterases*. Journal of Biochemical and Molecular Toxicology. 1999;13(5):261–8. doi:10.1002/(SICI)1099-0461(1999)13:5<261::AID-JBT6>3.0.CO;2-0

287. Imai T, Takase Y, Iwase H, Hashimoto M. Involvement of Carboxylesterase in Hydrolysis of Propranolol Prodrug during Permeation across Rat Skin. Pharmaceutics. 2013 Sep;5(3):3. doi:10.3390/pharmaceutics5030371

288. Wadkins RM, Hyatt JL, Wei X, Yoon KJP, Wierdl M, Edwards CC, et al. Identification and Characterization of Novel Benzil (Diphenylethane-1,2-dione) Analogues as Inhibitors of Mammalian Carboxylesterases. J Med Chem. 2005 Apr 21;48(8):2906–15. doi:10.1021/jm049011j

289. Mortensen SR, Brimijoin S, Hooper MJ, Padilla S. Comparison of the in Vitro Sensitivity of Rat Acetylcholinesterase to Chlorpyrifos-oxon: What Do Tissue IC50 Values Represent? Toxicology and Applied Pharmacology. 1998 Jan 1;148(1):46–9. doi:10.1006/taap.1997.8287

290. More SJ, Bampidis V, Benford D, Bragard C, Halldorsson TI, Hernández-Jerez AF, et al. Guidance on the use of the benchmark dose approach in risk assessment. EFSA Journal. 2022;20(10):e07584. doi:10.2903/j.efsa.2022.7584

291. Zwartsen A, Zeilmaker M, de Boer WJ, Rorije E, van der Voet H. Uncertainties in the Extrapolation of In Vitro Data in Human Risk Assessment: A Case Study of qIVIVE for Imazalil Using the Monte Carlo Risk Assessment Platform. Chem Res Toxicol. 2025 Jun 16;38(6):1006–18. doi:10.1021/acs.chemrestox.4c00287

292. Freed VH, Haque R, Schmedding D, Kohnert R. Physicochemical properties of some organophosphates in relation to their chronic toxicity. Environ Health Perspect. 1976 Feb;13:77–81. doi:10.1289/ehp.761377 PubMed PMID: 1269510; PubMed Central PMCID: PMC1474991.

293. Karalliedde LD, Edwards P, Marrs TC. Variables influencing the toxic response to organophosphates in humans. Food and Chemical Toxicology. 2003 Jan 1;41(1):1–13. doi:10.1016/S0278-6915(02)00232-6

294. Grubić Z, Sketelj J, Klinar B, Brzin M. Recovery of Acetylcholinesterase in the Diaphragm, Brain, and Plasma of the Rat After Irreversible Inhibition by Soman: A Study of Cytochemical Localization and Molecular Forms of the Enzyme in the Motor End Plate. Journal of Neurochemistry. 1981;37(4):909–16. doi:10.1111/j.1471-4159.1981.tb04478.x

295. Leucuta SE, Vlase L. Pharmacokinetics and Metabolic Drug Interactions. Current Clinical Pharmacology. 2006;5-20(16)1(1). doi:10.2174/157488406775268183

296. Müller F, Fromm MF. Transporter-Mediated Drug–Drug Interactions. Pharmacogenomics. 2011 Jul 1;12(7):1017–37. doi:10.2217/pgs.11.44 PubMed PMID: 21787191.

297. Belden JB, Lydy MJ. Impact of atrazine on organophosphate insecticide toxicity. Environmental Toxicology and Chemistry. 2000 Sep 1;19(9):2266–74. doi:10.1002/etc.5620190917

298. Mukherjee PK, Kumar V, Mal M, Houghton PJ. Acetylcholinesterase inhibitors from plants. Phytomedicine. 2007 Apr 10;14(4):289–300. doi:10.1016/j.phymed.2007.02.002

299. Paoli GM, Hartnett E, Price PS. Use of probabilistic exposure models in the assessment of dietary exposure to chemicals. Food Additives & Contaminants: Part A. 2025 Jul 3;42(7):819–48. doi:10.1080/19440049.2025.2506104 PubMed PMID: 40587777.

300. Witczak A, Pohoryło A, Abdel-Gawad H, Cybulski J. Residues of some organophosphorus pesticides on and in fruits and vegetables available in Poland, an assessment based on the European union regulations and health assessment for human populations. Phosphorus, Sulfur, and Silicon and the Related Elements. 2018 Nov 2;193(11):711–20. doi:10.1080/10426507.2018.1492921

301. Jokanović M. Neurotoxic effects of organophosphorus pesticides and possible association with neurodegenerative diseases in man: A review. Toxicology. 2018 Dec 1;410:125–31. doi:10.1016/j.tox.2018.09.009

302. Malin SG, Shavva VS, Tarnawski L, Olofsson PS. Functions of acetylcholine-producing lymphocytes in immunobiology. Current Opinion in Neurobiology. 2020 Jun 1;Brain, gut, and immune system interactions62:115–21. doi:10.1016/j.conb.2020.01.017

303. Furchgott RF, Zawadzki JV. The obligatory role of endothelial cells in the relaxation of arterial smooth muscle by acetylcholine. Nature. 1980 Nov;288(5789):373–6. doi:10.1038/288373a0

304. Tarnawski L, Shavva VS, Kort EJ, Zhuge Z, Nilsson I, Gallina AL, et al. Cholinergic regulation of vascular endothelial function by human ChAT+ T cells. Proceedings of the National Academy of Sciences. 2023 Apr 4;120(14):e2212476120. doi:10.1073/pnas.2212476120

305. Fakhoury M. Role of Immunity and Inflammation in the Pathophysiology of Neurodegenerative Diseases. Neurodegener Dis. 2015 Jan 15;15(2):63–9. doi:10.1159/000369933

306. Barricklow J, Blatnik M. 2-Arachidonoylglycerol is a substrate for butyrylcholinesterase: A potential mechanism for extracellular endocannabinoid regulation. Archives of Biochemistry and Biophysics. 2013 Aug 1;536(1):1–5. doi:10.1016/j.abb.2013.05.003

307. Gok M, Cicek C, Sari S, Bodur E. Novel activity of human BChE: Lipid hydrolysis. Biochimie. 2023 Jan 1;204:127–35. doi:10.1016/j.biochi.2022.09.008

308. Gok M, Cicek C, Sari S, Bodur E. The role of unsaturated fatty acids in modulating human butyrylcholinesterase activity: insights from kinetics and molecular docking. Naunyn-Schmiedeberg's Arch Pharmacol. 2025 Sep 1;398(9):12253–65. doi:10.1007/s00210-025-04065-3

309. Schopfer LM, Lockridge O, Brimijoin S. Pure human butyrylcholinesterase hydrolyzes octanoyl ghrelin to desacyl ghrelin. General and Comparative Endocrinology. 2015 Dec 1;224:61–8. doi:10.1016/j.ygcen.2015.05.017

310. Becker A, Böttcher A, Lackner KJ, Fehringer P, Notka F, Aslanidis C, et al. Purification, cloning, and expression of a human enzyme with acyl coenzyme A: cholesterol acyltransferase activity, which is identical to liver carboxylesterase. Arteriosclerosis and Thrombosis: A Journal of Vascular Biology. 1994 Aug;14(8):1346–55. doi:10.1161/01.ATV.14.8.1346

311. Mukherjee JJ, Jay FT, Choy PC. Purification, characterization and modulation of a microsomal carboxylesterase in rat liver for the hydrolysis of acyl-CoA. Biochem J. 1993 Oct 1;295(1):81–6. doi:10.1042/bj2950081

312. Tsujita T, Okuda H. Palmitoyl-coenzyme A hydrolyzing activity in rat kidney and its relationship to carboxylesterase. Journal of Lipid Research. 1993 Oct 1;34(10):1773–81. doi:10.1016/S0022-2275(20)35740-0

313. Draganov DI, Teiber JF, Speelman A, Osawa Y, Sunahara R, Du BNL. Human paraoxonases (PON1, PON2, and PON3) are lactonases with overlapping and distinct substrate specificities. Journal of Lipid Research. 2005 Jun 1;46(6):1239–47. doi:10.1194/jlr.M400511-JLR200

314. Teiber JF, Billecke SS, La Du BN, Draganov DI. Estrogen esters as substrates for human paraoxonases. Archives of Biochemistry and Biophysics. 2007 May 1;461(1):24–9. doi:10.1016/j.abb.2007.02.015

315. Teiber JF, Xiao J, Kramer GL, Ogawa S, Ebner C, Wolleb H, et al. Identification of biologically active δ-lactone eicosanoids as paraoxonase substrates. Biochemical and Biophysical Research Communications. 2018 Oct 20;505(1):87–92. doi:10.1016/j.bbrc.2018.09.083

316. Quistad GB, Barlow C, Winrow CJ, Sparks SE, Casida JE. Evidence that mouse brain neuropathy target esterase is a lysophospholipase. Proceedings of the National Academy of Sciences. 2003 Jun 24;100(13):7983–7. doi:10.1073/pnas.1232473100

317. Rainier S, Bui M, Mark E, Thomas D, Tokarz D, Ming L, et al. Neuropathy Target Esterase Gene Mutations Cause Motor Neuron Disease. The American Journal of Human Genetics. 2008 Mar 3;82(3):780–5. doi:10.1016/j.ajhg.2007.12.018

318. Read DJ, Li Y, Chao MV, Cavanagh JB, Glynn P. Neuropathy Target Esterase Is Required for Adult Vertebrate Axon Maintenance. J Neurosci. 2009 Sep 16;29(37):11594–600. doi:10.1523/JNEUROSCI.3007-09.2009 PubMed PMID: 19759306.

319. Piccinini M, Scandroglio F, Prioni S, Buccinnà B, Loberto N, Aureli M, et al. Deregulated Sphingolipid Metabolism and Membrane Organization in Neurodegenerative Disorders. Mol Neurobiol. 2010 Jun 1;41(2):314–40. doi:10.1007/s12035-009-8096-6

320. Wang Z, Yin Z, Sun G, Zhang D, Zhang J. Genetic evidence for the liver-brain axis: lipid metabolism and neurodegenerative disease risk. Lipids Health Dis. 2025 Feb 8;24(1):41. doi:10.1186/s12944-025-02455-3

321. Venkatapurapu SP, Clegg L, Nowojewski A, Kimko H, Olabode D, Sawant-Basak A, et al. Digital twins for accelerating drug discovery and development: opportunities and challenges. Drug Discovery Today. 2026 Feb 2;104617. doi:10.1016/j.drudis.2026.104617

322. Certara. Certara [Internet]. 2026 [cited 2026 Jan 27]. Simcyp PBPK. Available from: https://www.certara.com/software/simcyp-pbpk/

323. Simulations Plus. Simulations Plus [Internet]. 2026 [cited 2026 Jan 27]. GastroPlus® PBPK & PBBM Software | Simulate Drug Absorption. Available from: https://www.simulations-plus.com/software/gastroplus/

324. MathWorks. MATLAB [Internet]. 2026 [cited 2026 Feb 10]. Available from: https://nl.mathworks.com/products/matlab.html

325. Berkeley Madonna. Berkeley Madonna [Internet]. 2026 [cited 2026 Feb 10]. Berkeley Madonna. Available from: https://berkeley-madonna.myshopify.com/

326. Open Systems Pharmacology. PKsim [Internet]. 2026 [cited 2026 Jan 27]. Available from: https://www.open-systems-pharmacology.org/

327. Singh BN. Effects of Food on Clinical Pharmacokinetics. Clin Pharmacokinet. 1999 Sep 1;37(3):213–55. doi:10.2165/00003088-199937030-00003

328. Agoram B, Woltosz WS, Bolger MB. Predicting the impact of physiological and biochemical processes on oral drug bioavailability. Advanced Drug Delivery Reviews. 2001 Oct 1;Supplement: Oral Drug Absorption: A Renaissance50:S41–67. doi:10.1016/S0169-409X(01)00179-X

329. Jamei M, Turner D, Yang J, Neuhoff S, Polak S, Rostami-Hodjegan A, et al. Population-Based Mechanistic Prediction of Oral Drug Absorption. AAPS J. 2009 Apr 21;11(2):225–37. doi:10.1208/s12248-009-9099-y PubMed PMID: 19381840; PubMed Central PMCID: PMC2691459.

330. Willmann S, Schmitt W, Keldenich J, Dressman JB. A Physiologic Model for Simulating Gastrointestinal Flow and Drug Absorption in Rats. Pharm Res. 2003 Nov 1;20(11):1766–71. doi:10.1023/B:PHAM.0000003373.72652.c0

331. Yu LX. An Integrated Model for Determining Causes of Poor Oral Drug Absorption. Pharm Res. 1999 Dec 1;16(12):1883–7. doi:10.1023/A:1018911728161

332. Liddle R. Regulation of cholecystokinin secretion by intraluminal releasing factors. American Journal of Physiology-Gastrointestinal and Liver Physiology. 1995. doi:https://doi.org/10.1152/ajpgi.1995.269.3.G319

333. Carrière F. Impact of gastrointestinal lipolysis on oral lipid-based formulations and bioavailability of lipophilic drugs. Biochimie. 2016 Jun 1;125:297–305. doi:10.1016/j.biochi.2015.11.016

334. Simmonds W. The role of micellar solubilization in lipid absorption. Immunol Cell Biol. 1972 Aug;50(4):403–21. doi:10.1038/icb.1972.35

335. Macierzanka A, M. Rigby N, P. Corfield A, Wellner N, Böttger F, Clare Mills EN, et al. Adsorption of bile salts to particles allows penetration of intestinal mucus. Soft Matter. 2011;7(18):8077–84. doi:10.1039/C1SM05888F

336. Drover VA, Nguyen DV, Bastie CC, Darlington YF, Abumrad NA, Pessin JE, et al. CD36 Mediates Both Cellular Uptake of Very Long Chain Fatty Acids and Their Intestinal Absorption in Mice*. Journal of Biological Chemistry. 2008 May 9;283(19):13108–15. doi:10.1074/jbc.M708086200

337. Clarysse S, Brouwers J, Tack J, Annaert P, Augustijns P. Intestinal drug solubility estimation based on simulated intestinal fluids: Comparison with solubility in human intestinal fluids. European Journal of Pharmaceutical Sciences. 2011 Jul 17;43(4):260–9. doi:10.1016/j.ejps.2011.04.016

338. Garrett DA, Failla ML, Sarama RJ. Estimation of carotenoid bioavailability from fresh stir-fried vegetables using an in vitro digestion/Caco-2 cell culture model. The Journal of Nutritional Biochemistry. 2000 Nov 1;11(11):574–80. doi:10.1016/S0955-2863(00)00122-4

339. Beilstein F, Carrière V, Leturque A, Demignot S. Characteristics and functions of lipid droplets and associated proteins in enterocytes. Experimental Cell Research. 2016 Jan 15;The Biology of Lipid Droplets340(2):172–9. doi:10.1016/j.yexcr.2015.09.018

340. Gugliucci A. The chylomicron saga: time to focus on postprandial metabolism. Front Endocrinol. 2024 Jan 18;14. doi:10.3389/fendo.2023.1322869

341. Brocks DR, Davies NM. Lymphatic Drug Absorption via the Enterocytes: Pharmacokinetic Simulation, Modeling, and Considerations for Optimal Drug Development. Journal of Pharmacy & Pharmaceutical Sciences. 2018 Oct 23;21(1s):1s. doi:10.18433/jpps30217

342. Caliph SM, Cao E, Bulitta JB, Hu L, Han S, Porter CJH, et al. The Impact of Lymphatic Transport on the Systemic Disposition of Lipophilic Drugs. Journal of Pharmaceutical Sciences. 2013 Jul 1;102(7):2395–408. doi:10.1002/jps.23597

343. Holm R, Hoest J. Successful in silico predicting of intestinal lymphatic transfer. International Journal of Pharmaceutics. 2004 Mar 19;272(1):189–93. doi:10.1016/j.ijpharm.2003.12.017

344. Ichihashi T, Nagasaki T, Takagishi Y, Yamada H. A Quantitative Concept of the Mechanism of Intestinal Lymphatic Transfer of Lipophilic Molecules. Pharm Res. 1994 Apr 1;11(4):508–12. doi:10.1023/A:1018954213469

345. Brockman AH, Oller HR, Moreau B, Kriksciukaite K, Bilodeau MT. Simple Method Provides Resolution of Albumin, Lipoprotein, Free Fraction, and Chylomicron To Enhance the Utility of Protein Binding Assays. J Med Chem. 2015 Feb 12;58(3):1420–5. doi:10.1021/jm501748h

346. Gershkovich P, Hoffman A. Uptake of lipophilic drugs by plasma derived isolated chylomicrons: Linear correlation with intestinal lymphatic bioavailability. European Journal of Pharmaceutical Sciences. 2005 Dec 1;26(5):394–404. doi:10.1016/j.ejps.2005.07.011

347. Kassis T, Yarlagadda SC, Kohan AB, Tso P, Breedveld V, Dixon JB. Postprandial lymphatic pump function after a high-fat meal: a characterization of contractility, flow, and viscosity. American Journal of Physiology-Gastrointestinal and Liver Physiology. 2015. doi:10.1152/ajpgi.00318.2015

348. Sieber C, Beglinger C, Jäger K, Stalder GA. Intestinal phase of superior mesenteric artery blood flow in man. [Internet]. 1992 Apr 1. doi:10.1136/gut.33.4.497

349. Sarin H. Physiologic upper limits of pore size of different blood capillary types and another perspective on the dual pore theory of microvascular permeability. Vasc Cell. 2010 Aug 11;2(1):14. doi:10.1186/2040-2384-2-14

350. Steiniger BS, Pfeffer H, Gaffling S, Lobachev O. The human splenic microcirculation is entirely open as shown by 3D models in virtual reality. Sci Rep. 2022 Oct 1;12(1):16487. doi:10.1038/s41598-022-19885-z

351. Havel RJ, Hamilton RL. Hepatocytic lipoprotein receptors and intracellular lipoprotein catabolism. Hepatology. 1988;8(6):1689–704. doi:10.1002/hep.1840080637

352. Bruns OT, Ittrich H, Peldschus K, Kaul MG, Tromsdorf UI, Lauterwasser J, et al. Real-time magnetic resonance imaging and quantification of lipoprotein metabolism in vivo using nanocrystals. Nature Nanotech. 2009 Mar;4(3):3. doi:10.1038/nnano.2008.405

353. Freund B, Tromsdorf UI, Bruns OT, Heine M, Giemsa A, Bartelt A, et al. A Simple and Widely Applicable Method to 59Fe-Radiolabel Monodisperse Superparamagnetic Iron Oxide Nanoparticles for In Vivo Quantification Studies. ACS Nano. 2012 Aug 28;6(8):7318–25. doi:10.1021/nn3024267

354. German JB, Smilowitz JT, Zivkovic AM. Lipoproteins: When size really matters. Current Opinion in Colloid & Interface Science. 2006 Jun 1;11(2):171–83. doi:10.1016/j.cocis.2005.11.006

355. Higgins JM, Fielding CJ. Lipoprotein lipase. Mechanism of formation of triglyceride-rich remnant particles from very low density lipoproteins and chylomicrons. Biochemistry. 1975 Jun 1;14(11):2288–93. doi:10.1021/bi00682a002

356. De Jong WH, Hagens WI, Krystek P, Burger MC, Sips AJAM, Geertsma RE. Particle size-dependent organ distribution of gold nanoparticles after intravenous administration. Biomaterials. 2008 Apr 1;29(12):1912–9. doi:10.1016/j.biomaterials.2007.12.037

357. Ilium L, Davis SS, Wilson CG, Thomas NW, Frier M, Hardy JG. Blood clearance and organ deposition of intravenously administered colloidal particles. The effects of particle size, nature and shape. International Journal of Pharmaceutics. 1982 Oct 1;12(2):135–46. doi:10.1016/0378-5173(82)90113-2

358. Brechbuhl HM, Gould N, Kachadourian R, Riekhof WR, Voelker DR, Day BJ. Glutathione Transport Is a Unique Function of the ATP-binding Cassette Protein ABCG2 *. Journal of Biological Chemistry. 2010 May 28;285(22):16582–7. doi:10.1074/jbc.M109.090506 PubMed PMID: 20332504.

359. Järvinen E, Deng F, Kiander W, Sinokki A, Kidron H, Sjöstedt N. The Role of Uptake and Efflux Transporters in the Disposition of Glucuronide and Sulfate Conjugates. Frontiers in Pharmacology. 2022;12. doi:10.3389/fphar.2021.802539

360. Yang G, Ge S, Singh R, Basu S, Shatzer K, Zen M, et al. Glucuronidation: Driving Factors and Their Impact on Glucuronide Disposition. Drug Metab Rev. 2017 May;49(2):105–38. doi:10.1080/03602532.2017.1293682 PubMed PMID: 28266877; PubMed Central PMCID: PMC7660525.

361. Masuda M, Nakai E, Mizutani T. Study of Oxidized Lipids as Endogenous Substrates of P-gp (ABCB1) [Internet]. 2008. doi:10.2174/187231208786734139

362. Romsicki Y, Sharom FJ. Phospholipid Flippase Activity of the Reconstituted P-Glycoprotein Multidrug Transporter. Biochemistry. 2001 Jun 1;40(23):6937–47. doi:10.1021/bi0024456

363. Ueda K, Okamura N, Hirai M, Tanigawara Y, Saeki T, Kioka N, et al. Human P-glycoprotein transports cortisol, aldosterone, and dexamethasone, but not progesterone. Journal of Biological Chemistry. 1992 Dec 5;267(34):24248–52. doi:10.1016/S0021-9258(18)35757-0

364. Yano K, Seto S, Kamioka H, Mizoi K, Ogihara T. Testosterone and androstenedione are endogenous substrates of P-glycoprotein. Biochemical and Biophysical Research Communications. 2019 Nov 26;520(1):166–70. doi:10.1016/j.bbrc.2019.09.067

365. Borst P, de Wolf C, van de Wetering K. Multidrug resistance-associated proteins 3, 4, and 5. Pflugers Arch - Eur J Physiol. 2007 Feb 1;453(5):661–73. doi:10.1007/s00424-006-0054-9

366. Järvinen E, Deng F, Kidron H, Finel M. Efflux transport of estrogen glucuronides by human MRP2, MRP3, MRP4 and BCRP. The Journal of Steroid Biochemistry and Molecular Biology. 2018 Apr 1;178:99–107. doi:10.1016/j.jsbmb.2017.11.007

367. Gebauer L, Jensen O, Brockmöller J, Dücker C. Substrates and Inhibitors of the Organic Cation Transporter 3 and Comparison with OCT1 and OCT2. J Med Chem. 2022 Sep 22;65(18):12403–16. doi:10.1021/acs.jmedchem.2c01075

368. Koepsell H, Lips K, Volk C. Polyspecific Organic Cation Transporters: Structure, Function, Physiological Roles, and Biopharmaceutical Implications. Pharm Res. 2007 Jul 1;24(7):1227–51. doi:10.1007/s11095-007-9254-z

369. Nigam SK, Bush KT, Martovetsky G, Ahn SY, Liu HC, Richard E, et al. The Organic Anion Transporter (OAT) Family: A Systems Biology Perspective. Physiol Rev. 2015 Jan;95(1):83–123. doi:10.1152/physrev.00025.2013 PubMed PMID: 25540139; PubMed Central PMCID: PMC4281586.

370. Bosgra S, van Eijkeren J, Bos P, Zeilmaker M, Slob W. An improved model to predict physiologically based model parameters and their inter-individual variability from anthropometry. Critical Reviews in Toxicology. 2012 Oct 1;42(9):751–67. doi:10.3109/10408444.2012.709225 PubMed PMID: 22954170.

371. McNally K, Cotton R, Hogg A, Loizou G. PopGen: A virtual human population generator. Toxicology. 2014 Jan 6;315:70–85. doi:10.1016/j.tox.2013.07.009

372. Young JF, Luecke RH, Pearce BA, Lee T, Ahn H, Baek S, et al. Human Organ/Tissue Growth Algorithms that Include Obese Individuals and Black/White Population Organ Weight Similarities from Autopsy Data. Journal of Toxicology and Environmental Health, Part A. 2009 Mar 16;72(8):527–40. doi:10.1080/15287390802647203 PubMed PMID: 19267313.

373. Brück S, Strohmeier J, Busch D, Drozdzik M, Oswald S. Caco-2 cells – expression, regulation and function of drug transporters compared with human jejunal tissue. Biopharmaceutics & Drug Disposition. 2017;38(2):115–26. doi:10.1002/bdd.2025

374. Guo L, Dial S, Shi L, Branham W, Liu J, Fang JL, et al. Similarities and Differences in the Expression of Drug-Metabolizing Enzymes between Human Hepatic Cell Lines and Primary Human Hepatocytes. Drug Metabolism and Disposition. 2011 Mar 1;39(3):528–38. doi:10.1124/dmd.110.035873

375. Fukazawa T, Yamazaki Y, Miyamoto Y. Reduction of non-specific adsorption of drugs to plastic containers used in bioassays or analyses. Journal of Pharmacological and Toxicological Methods. 2010 May 1;61(3):329–33. doi:10.1016/j.vascn.2009.12.005

376. Palmgrén JJ, Mönkkönen J, Korjamo T, Hassinen A, Auriola S. Drug adsorption to plastic containers and retention of drugs in cultured cells under *in vitro* conditions. European Journal of Pharmaceutics and Biopharmaceutics. 2006 Nov 1;64(3):369–78. doi:10.1016/j.ejpb.2006.06.005

377. Proença S, Escher BI, Fischer FC, Fisher C, Grégoire S, Hewitt NJ, et al. Effective exposure of chemicals in in vitro cell systems: A review of chemical distribution models. Toxicology in Vitro. 2021 Jun 1;73:105133. doi:10.1016/j.tiv.2021.105133

378. Menichetti R, Kanekal KH, Bereau T. Drug–Membrane Permeability across Chemical Space. ACS Cent Sci. 2019 Feb 27;5(2):290–8. doi:10.1021/acscentsci.8b00718

379. Berka K, Paloncýová M, Anzenbacher P, Otyepka M. Behavior of Human Cytochromes P450 on Lipid Membranes. J Phys Chem B. 2013 Oct 3;117(39):11556–64. doi:10.1021/jp4059559

380. Urban P, Lautier T, Pompon D, Truan G. Ligand Access Channels in Cytochrome P450 Enzymes: A Review. Int J Mol Sci. 2018 May 30;19(6):1617. doi:10.3390/ijms19061617 PubMed PMID: 29848998; PubMed Central PMCID: PMC6032366.

381. Berezhkovskiy LM. Determination of volume of distribution at steady state with complete consideration of the kinetics of protein and tissue binding in linear pharmacokinetics. J Pharm Sci. 2004 Feb;93(2):364–74. doi:10.1002/jps.10539 PubMed PMID: 14705193.

382. Burt T, Vuong LT, Baker E, Young GC, McCartt AD, Bergstrom M, et al. Phase 0, Including Microdosing Approaches: Applying the Three Rs and Increasing the Efficiency of Human Drug Development. Altern Lab Anim. 2018 Dec;46(6):335–46. doi:10.1177/026119291804600603

383. EMA. https://www.ema.europa.eu/en/ich-m3-r2-non-clinical-safety-studies-conduct-human-clinical-trials-pharmaceuticals-scientific-guideline [Internet]. 2013 [cited 2026 Feb 10]. ICH M3 (R2) Non-clinical safety studies for the conduct of human clinical trials for pharmaceuticals - Scientific guideline. Available from: https://www.ema.europa.eu/en/documents/scientific-guideline/ich-guideline-m3r2-non-clinical-safety-studies-conduct-human-clinical-trials-and-marketing-authorisation-pharmaceuticals-step-5_en.pdf

Summary

In this thesis animal-free methods for next generation risk assessment of organophosphate pesticides were evaluated. These approaches are based on in silico and in vitro methods, and were evaluated for predicting the safety of human exposures, as well as points of departure for acetylcholinesterase (AChE) inhibition by organophosphate pesticides. This was achieved by the development of a generic physiologically based kinetic (PBK) model for organophosphate pesticides, in vitro quantification of AChE inhibition by various organophosphate pesticides, exposure safety evaluation using the dietary comparator ratio (DCR) method, and point of departure prediction for hazard characterization using quantitative in vitro to in vivo extrapolation (QIVIVE) of in vitro AChE inhibition to the in vivo situation.

Chapter 1 introduces essential information of organophosphate pesticides on their use, chemistry, kinetics and effects. It is also explained how traditional risk assessment is performed and how animal-free in vitro and in silico methods can be used to perform risk assessment without animal testing. Lastly, the aim of the thesis is presented.

In **chapter 2**, a PBK model was developed to predict blood concentrations of eight organophosphate pesticides and their metabolites in rats and humans. The developed PBK model predicts how organophosphates are absorbed, distributed, metabolized and excreted in/from the body, based on in vitro or in silico derived parameters. The PBK model was validated using literature derived blood concentration-time data from in vivo exposure studies data. When validating the model, blood concentrations of most of the organophosphate pesticides were predicted within 5-fold difference from in vivo values. Those pesticides that were less well predicted were all found to be in the dimethyl-organophosphate pesticide subclass.

The developed PBK model was used in **chapter 3**, to investigate if the DCR method can be reliably used for safety evaluation of organophosphate pesticides. Six organophosphate pesticides were used to evaluate the DCR method for organophosphate pesticides. The DCR method correctly predicted 70 out of 74 exposures to be safe when these were indeed reported to have no adverse effects. Four exposure scenarios were predicted to be dangerous, while in literature these were reported to be safe. The four false positives were all for dimethyl-organophosphates. It was concluded that in the future the DCR method can be used for safety evaluation of exposures to organophosphate pesticides, since it was shown to accurately predict the occurrence of adverse effects after exposure to these pesticides.

In **chapter 4**, it was investigated if the overprediction of the dimethyl-organophosphates fenitro-oxon, methyl-paraoxon and omethoate could be due to a metabolic pathway not incorporating in the PBK model. In vitro metabolism studies showed that methyl-paraoxon and omethoate were metabolized via a glutathione-mediated pathway. Furthermore, rats were found to metabolize methyl-paraoxon four times faster than humans via this pathway. When the glutathione-mediated metabolic pathway was incorporated in the PBK model, blood predictions for methyl-paraoxon and fenitro-oxon improved from over 10-fold difference when glutathione-mediated metabolism was not included, to less than 5- and often even 2-fold differences compared to in vivo rat data. For omethoate, no significant changes in predicted blood concentrations were observed. For humans,

predicted maximum concentrations for methyl-parathion and fenitrothion exposures were more than 12-fold lower when glutathione-mediated metabolism was incorporated in the model.

The quantitative in vitro to in vivo extrapolation approach was used for point of departure determination of AChE inhibition by organophosphate pesticides in **chapter 5**. For eight organophosphate pesticides and their active metabolites, concentration-response curves derived from in vitro AChE inhibition assays using blood or pure enzyme. For each pesticide, both whole blood and enzyme concentration-response curves were translated to dose-response curves using the adjusted PBK model developed in **chapter 4**. Benchmark dose modelling was used on the dose-response curves to predict points of departure, which were then compared to in vivo determined points of departure reported in literature. All predicted points of departure, for both rats and humans, were within 4-fold from in vivo determined points of departure low-observed-adverse-effect levels (LOAELs) and higher than the reported no-observed-adverse-effect levels (NOAELs). For some organophosphate pesticides it was not possible to a point of departure based on whole blood data, possibly due to non-AChE esterases present in whole blood. It was shown that QIVIVE-based point of departure determination can be used for animal-free hazard characterization for organophosphate pesticides when pure enzyme is used for AChE inhibition assays.

In **chapter 6**, the results of each experimental chapter are summarized. Considerations with regard to chronic and mixture exposures are discussed and the association of organophosphate pesticides with neurodegenerative diseases briefly touched upon. For PBK modelling some opportunities are discussed in detail, focusing food effects on oral absorption, lymphatic transport, the required physiological detail that is needed in a PBK model, growth and population modelling and limitations of and solutions for in vitro and in silico derivation of kinetic parameters. Lastly, model validation and adoption of animal-free risk assessment were discussed.

The findings in this thesis show how several in vitro and in silico approaches can be used for next generation safety assessment for organophosphate pesticides. Using these approaches for both rats and humans also provided valuable insights into species differences. All these findings support the thought that animals used in toxicity testing do not always represent humans very well. Therefore the human centric data provided by animal-free approaches is essential for chemical risk assessment for humans.

Acknowledgements

After more than four years, my PhD journey finally came to an end. I was lucky enough to get to know and work with many amazing people along the way. I would not have been able to finish my PhD without the support of my supervisors, colleagues, friends and family.

I would like to thank my supervisors Nynke, Ivonne and Hans for their guidance during the past four(-ish) years. I am very grateful to have had the opportunity to do my PhD at the toxicology department with such passionate and experienced people.

Nynke, from the very beginning of my PhD journey we've worked closely together. Your kind and accepting attitude made every meeting a joy, and your experience on all things kinetics made you the person to go to when I got new ideas or got stuck when developing a PBK model. I am amazed by how you manage to take time to listen everyone proposing a meeting or walking into your office. Even though you are very busy, you always made time for, and were enthusiastic about my random theories, ideas and findings. I also fondly remember our more personal chats in the car, when you kindly offered a ride if we were both leaving late from Wageningen. While my PhD is over, I still look forward to working together on the projects that we have yet to finish. Thank you for all the guidance, enthusiasm and opportunities Nynke!

Hans, during the past years I feel like you went beyond project supervision. Since I am not a big fan of having a lot of meetings, you made sure to check in every so often, to see if I did not get stuck in the project, or with myself. I really appreciate that you took the time to keep checking up on me and also give advice when things did not seem to work and I was losing hope. This happened a couple of times and you always had ideas to look into or to simplify experiments. When setting up the blood experiments, your help with the MEC administration and connections with the right people to get the fresh blood was invaluable. You were also very supportive when you heard that I was to undergo surgery, thinking along in how to approach this. Once recovered, you provided me with the opportunity to help with a project as a Postdoc. Hans, thank you for your patience, your guidance and the opportunities you have given me.

Ivonne, we frequently met in the beginning of the project. During this time I was a bit overwhelmed by the different opinions on the project of three supervisors. I highly appreciated that you kept order in the chaos during these times. You helped me to think about my planning and about what I actually wanted from each meeting. I really enjoyed our in depth scientific discussions about the chemistry and metabolism of organophosphate pesticides. While in the last year you have been going through challenging times, know that you are deeply missed at the department.

Much of the work I did would not have been possible without the help of the technicians and staff at the tox department. **Wouter**, we spent a lot of time working together, and even though I caused many LCMS errors and missing compounds along the way, I enjoyed every moment of it. No matter how busy you were, your help always came with a smile, and at least one dad joke. Thank you for your help, patience and teaching me so much about the LCMS. It was really a treat to work with you in the past years and I'll make sure you get a copy of the PBK game when it releases. **Sebas**, I appreciate your help when getting started with the analytical equipment in the lab and when we puzzled together to get the microTOF working. I could also always come to you to discuss some in

depth chemical questions I had. Thank you for your support and brightening the mood with your jokes and puns, which often caught me off-guard. I would also like to thank **Nico**, **Samantha**, **Alexandros**, **Naomi**, **David** and **Mathias** for the fun and often insightful conversations we've had during practicals, in the lab or at the lunch table. **Carla** and **Gerda**, I could always count on you when I got lost in administration, or when something I ordered got lost on me. Thank you for all the help and energizing conversations in the past years.

Besides the supervision team and department staff, I've worked closely with **Jiaqi** and with **Germaine** on different projects. Your amazing insights and enthusiasm made it both inspiring and fun to work with you. **Jiaqi**, our cooperation on organophosphate pesticides made us the unstoppable OP sisters. Like a big sister, you were there right from the start. Not only did I feel like you knew literally everything in the lab, but you also helped me get started. Your humor and kindness immediately made me feel at home at the department and you were always ready to help me, or other colleagues. Thank you for all your help, kindness and amazing terrible jokes. **Germaine**, you always bring the right kind of energy. If someone is excited you are excited with/for them, and if they are tired, you tone down your nearly inexhaustible enthusiasm about science, movies and musicals. This makes it a joy to work with you, which I'm lucky enough to have done in the PhD trip committee, in the chylomates project and for my defense as a paranymph. Thank you for brightening up all the long and dark lab days with your musical vocalizations and random 'would you rather' questions, and your genuine interest in the lives of everyone setting foot in the cell lab.

My project was part of the Virtual Human Platform 4 Safety (VHP4S) consortium, which allowed me to get in touch and exchange ideas with many experts in the field of toxicology. Thank you to all those who helped make the VHP4S designathons and hackathons possible. I specifically would like to thank **Daan** and **Victor** for the pleasant collaboration and all the work they have put in the pKa predictor project. Also the collaboration with **Fabian**, **Ellen** and **Lianne** on the silychristin developmental neurotoxicity project, and **Mark**, **Ozan** and **Egon** for the enthusiasm for, and help with, all things programming and data.

Working alongside my fellow PhD students and PostDocs at the tox department was a true delight. **Merel**, **Hugo**, **Qiuhui**, **Xiyu**, **Gijs**, **Rizal**, **Thitirat**, **Elise**, **Feihan**, my fellow inhabitants of office 4039. To me our office felt like a second home. We were all there for one another, having a laugh together and listening to each others opinions, complaints, and weekend and life stories. Thank you for all the support and the good times we've had together. I also liked the slightly awkward congratulations-videos we made for the PhD defenses of our colleagues. While arguably I was the one making these more awkward, I hope you guys make an awkward video this time as well. **Gijs**, I still don't know how you do it, but you manage to chat with everyone of the department for seemingly every moment of the day and go on vacation for half of the year, while still having the most organized and well planned work I've seen of any PhD student. Your directness and original worldview is very refreshing, and your small talk is god-tier. I highly respect that you can hold up a mirror to others and while that truth might sometimes be painful in the moment, it will often help them/me in the long run. I also really appreciate that I could always bounce some ideas off of you, or that we could have an energizing conversation about something random, like how blue spruces are not actually blue. Thank you for being my paranymph, and for all the laughs and support in the past years. **Hugo**, I propose a new law of nature, stating that your optimism, interests and energy cannot be depleted. In the office, this lead to both incredibly fun conversations, as well as many

distractions for us both. Outside of our office, you could be summoned at any time or place in the department with the words 'diving' and 'coffee break'. Once there, many ideas for activities and events were proposed, resulting the organization of game nights, spicy tox, PhD trips and much more. Hugo, thank you for your enthusiasm, interest in your colleagues, and making so many fun events possible. **Elise**, when you joined our office, I was so focused on finishing my PhD, I thought I would not really get to know you that well. However, little did I know how social and interested you are in the lives of others. While we've had many fun surface level talks and deep conversations, I liked how most of them sooner or later turned into conversations about food, or music. Thank you for the chitchat, your enthusiasm and cheerfulness when I was writing my thesis. Our talks really kept me afloat during that time.

Chrysanthi, you have a happy and cheerful vibe around you. Talking with you therefore always felt energizing, which, for a tired person like me, was very helpful. We could have insightful, in-depth discussions about PBK modelling at TOX, while in the train back home we were chatting about (non-TOX) Nico, Luna and Djaroui, or discuss politics. Thank youyou're your enthusiasm and cheerfulness, and for the insightful chats had over the years. **Katharina**, you have always been there for anyone that needed your help. I really look up to you for your proactive attitude and how you are able to manage groups of people without being bossy. This made organizing the PhD trip with you and the rest of the PhD trip committee an amazing experience. I also would like to thank you for the good times we had during the vacation in Canada and the board game nights, where we could take off our professional scientist hats and just have fun. Thank you for all your help, good times and often catching me off-guard with your unique humour. **Kiri**, I always enjoyed our silly conversations: yelling some questionable quotes from *de sluipschutters* at the lunch table, or trying to get me to like Italian TikTok AI memes (bombardino crocodilo is slowly growing on me). Thank you for the random talks and the good company at the VHP4S meetings. **Sylvia**, you are the biggest mystery of the toxicology department to me. I still don't know if on purpose or not, but your sarcastic way of talking made our conversations very fun and unexpected, since I never knew what you really meant. Especially on busy lab days, you often offered to help with the LCMS and our conversations really brightened my mood. **Susannah** I really appreciated your help when I got stuck with compound detection. Thank you for taking the time to sit down with me to talk analytical science with me, despite being very busy yourself. **Tom**, as a fellow croissant connoisseur, you are one of the few people I can share my love for half-baked ham and cheese croissants with at the lunch table. Your humour and original view on the things around you always cheered up your colleagues. Thank you for all the delightful talks and I hope by the time you read this, we have had the chance to finally have the game night together with Merel and Jet. **Ghaliya**, **Nick** and **Rebeka**, I really enjoy the vibe and energy you guys bring. Our week together for the PET course in Maastricht was refreshing and fun. While we studied during the day, in the evenings it truly felt like having a minivacation with friends: Good food, sporting, drinking, celebrating, and watching movies on the couch together. And also thank you guys for letting me have the princess/castle bed!

I've also been very lucky that, during my PhD adventure, I got to know **Aafke**, **Annelies**, **Barbara**, **Danlei**, **Donovan**, **Edith**, **Frances**, **Haomiao**, **Jingxuan**, **Liang**, **Matteo**, **Mirena**, **Shivani**, **Tanne**, **Veronique**, **Wisse**, **Xupeng**, **Xuan**, **Xukun**, **Yasser** and **Yiming**. You were always in for a fun chat or ready to help your colleagues. Thank you for all the good moments and fun conversations we've had together. It was really a treat to be your colleague.

I would also would like to thank all the students that I supervised. **Sinchana**, **Jeroen**, **Sofie**, **Bibi**, **Wenxiao**, **Lydia**, **Junhui** and **Aletta**. You all did amazing work during your time at the department, which colleagues often corroborated. Thank you for your enthusiasm, curiosity, insights, patience, and all you have thought me. **Sofie**, I was amazed by how involved you were with everyone around you. Besides doing an a lot of work for your thesis, you also made sure those around you were doing okay and organized *borrels* for the department. I also really like that we still stay in touch. Thank you for the good times, all your work and effort, and for teaching me a lot about supervision and managing expectations.

Besides all the amazing people I worked with in the past years, this PhD would not have been possible with the support of friends and family. **Jan**, **Martin**, **Perry**, **Roeland**, **Tinus** and **Wesley**, the farmacunts, for quite a while you've dealt with zombie Thijs on a weekly basis. When we meet up, our biggest worries are usually: where do we meet, and what do we eat (brains for zombie Thijs of course)? Our laid-back chillings, where we have minimum expectations of one another, are perfect for tired people on a workday. Thank you guys for all the good times. You always cheered me up and gave me some energy to get through the last few days of the week. **Oscar**, **Carmen**, **Igor**, **Julia** and **Livia**, we have had so many DnD sessions and boardgame nights. Our times together always were the perfect escape when work or life was a bit too much. Thank you for all the amazing adventures and snack fests we've had. **Oscar**, you are someone I look up to. After all the years we've been studying, sporting and chilling together, I always secretly hoped your people skills, and interest and enthusiasm for nearly anything would rub off on me. I also thoroughly enjoy our world conquering gaming sessions, and exploring the amazing DnD worlds you've crafted. Thank you for all the good times. **Kelvin**, **Jeroen**, **Marco** and **Rob**, while I think I miss quite a few gaming sessions with the Flippo's for Life (FLL) gaming gang, I enjoy the carefully selected and ranked *pareltjes* we're playing together every time. However, to me any game is a *pareltje* as long as I play it with you guys. Thank you for the good times and organizing the Mario Karty Parties and gaming sessions, despite me always responding too late to the *datumprikkers*. **Oscar**, **Jan** and **Sandermander**, in our wine group, the (mostly) red liquid flows abundantly. And even though I'm often tired and tell myself I will leave on time, eventually I always end up staying longer than intended, because we're deeply invested into one of Jan's crazy stories or some other conversation. Thank you for all the wine trips and *gezellige* evenings we've had together, and cheers to some more of those. I also would like to thank **Maurice** and het Urkermannenkoor (**Martijn**, **Robbert**, **Quinte** en **Perry**) for our *gezellige* get togethers in the past years and before.

Ma, Pa, **Niels, Remi** and **co-siblings**, my sweet, sweet family. I feel like I have not visited you often enough since I moved to Utrecht. But when I take the trip down to Braboland, despite me often arriving either tired or grumpy at your doorstep, your care, love and support helps me unwind and decompress. Thank you for the many years of support throughout my studies and beyond, and for always being there for me. I also would like to thank the other family, the **van den Dijsseltjes**. There were times during which I visited you more than my own family, and it always felt like coming home. When Jet was working in Australia for half a year, I was welcome for a cup of tea or to celebrate Christmas together. Thank you for all the support and *gezelligheid*.

Last but certainly not least, **Jet** (aka **dr. Jetski de Piedelipetski**), you are my sunshine and you make me happy when skies are grey. For years you have been listening to my poorly explained ideas and theories, and to my whining about all the societal inefficiencies I am annoyed by. Your

love, care and support, is what keeps me going. You always laugh at my terrible jokes and listen to my ridiculous serenades, which I sing for you about every two minutes when we are at home. I would have expected those to become old or annoying very quickly, but you always sing along happily. Also thank you for pushing for me to go on vacations together. I am terrible at taking vacations and generally rather stay at home. Despite the lack of enthusiasm from my side, you dragged me with you from Sweden to Australia, giving me time to clear my head and reflect. Thank you for being my enthusiastic and lively better half. I could not be more grateful for having you in my life.

Biography

Thijs Moerenhout was born in 1994 in a village close to Breda and followed his secondary education in Oosterhout. He attended a undergraduate program in pharmacy at Utrecht university and obtained his bachelor degree in 2017, after which Thijs followed a graduate study of pharmaceutical sciences at the same university. During his studies he performed research on bacterial glycobiology at the university medical center in Utrecht and surfactant based vaccine formulation at MSD in Boxmeer. After obtaining his graduate degree in 2020, Thijs worked as a coordinator at a diagnostic laboratory during the corona pandemic. In 2021 he started as a PhD candidate at the department of toxicology at Wageningen university. During this time, Thijs took several courses of the post-graduate education in toxicology as part of the training to be registered as an European registered toxicologist.

List of Publications

Published

Moerenhout, T. M. J. A.; Chen, J.; Bouwmeester, H.; Rietjens, I. M. C. M.; Kramer, N. I. Development of a Generic Physiologically Based Kinetic Model for the Prediction of Internal Exposure to Organophosphate Pesticides. Environ. Sci. Technol. 2024. https://doi.org/10.1021/acs.est.4c06534.

Chen, J.; Moerenhout, T. M. J. A.; Kramer, N. I.; Rietjens, I. M. C. M. Next Generation Risk Assessment of Acute Neurotoxicity from Organophosphate Exposures Using the In Vitro–In Silico Derived Dietary Comparator Ratio. Environ. Sci. Technol. 2025, 59 (12), 6106–6114. https://doi.org/10.1021/acs.est.5c00220.

Submitted

Thijs M.J.A. Moerenhout, Wouter Bakker, Hans Bouwmeester, Nynke I. Kramer. The effect of glutathione-mediated metabolism of organophosphate pesticides on rat and human in vivo toxicokinetics investigated using physiologically based kinetic modelling.

Thijs M.J.A. Moerenhout, Wouter Bakker, Hans Bouwmeester, Nynke I. Kramer Application of new approach methodologies for point of departure prediction in organophosphate pesticide hazard assessment.

Overview of completed training activities

Discipline specific activities

General toxicology (TOX-20303) (WUR, 2022)
PET organ toxicity (online; Radboud University, 2022)
PET Molecular toxicology (Vrije Universiteit Amsterdam, 2022)
PET neurotoxicity (Utrecht University, 2022)
PET epidemiology (Vrije Universiteit Amsterdam, 2022)
PET pathobiology and toxicological pathology (Utrecht University, 2022)

PET Laboratory Animal Science (Utrecht University, 2023)
Food toxicology (TOX-30306) (WUR, 2023)
Environental toxicology (TOX-30806) (WUR, 2023)
PET cellular toxicity (Leiden University, 2023)

PET systems toxicology (Maastricht University, 2025)
Food safety risk assessment (FHM-30306) (WUR, 2025)

General Courses

VLAG PhD week (WUR, 2022)
Essentials of scientific writing and presenting (WUR, 2022)
Supervising BSc & MSc thesis students, WGS (WUR, 2023)
VLAG Big data analysis in life sciences (WUR, 2023)
Writing grant proposals (WUR, 2025)

Optional courses and other activities

Preparation of research proposal (WUR, 2022)
Scientific presentation at Toxicology Division
PhD Trip Committee (2022-2023)
PhD Trip to the UK (2023)
PhD Trip to Canada (2025)

Conferences and meetings

ESTIV conference (Prague, Czechia, 2024)
NVT conference (Ede, 2024)

Funding

The research described in this thesis is part of the VHP4Safety project and funded is funded by the Netherlands Research Council (NWO; NWA-ORC 1292.19.272). Through the contribution of H.B. and N.I.K. to this research, this research was co-funded by the European Union through Horizon Europe project "European Partnership for the Assessment of Risk from Chemicals (PARC) under grant agreement No. 101057014. This publication reflects only the authors' view and does not necessarily reflect those of the funding bodies. The European Union is not responsible for any use that may be made of the information it contains.

Financial support from Wageningen University and for printing this thesis is gratefully acknowledged.

Cover design by T.M.J.A. Moerenhout

Printed by on FSC-certified paper